ELECTRON TRANSFER IN TWO AND THREE DIMENSIONS

By

Darren A. Walsh B.Sc (Hons) M.Sc

A Thesis presented at Dublin City University for the Degree of Doctor of Philosophy

Supervisor Prof Robert J Forster

School of Chemical Sciences

Dublin City University
August 2002

DECLARATION

I hereby certify that the material, which I now submit for assessment on the programme of study leading to the award of doctor of philosophy, is entirely of my own work and has not been taken from the work of others, save and to the extent that such work has been cited and acknowledged within the text of my work

Signed Darren Walsh

I D 95169199

Date 16/9/02

ACKNOWLEDGMENTS

First and foremost, I wish to express my sincere gratitude to my supervisor, Prof Robert Forster, for his advice and enthusiasm during the past three years Without his guidance, the years spent in the laboratories of DCU would have been a much less enjoyable and an infinitely less productive period I am also very grateful to Dr Tia Keyes for the help that she gave me A big thank you also to the technical staff at DCU, Vinnie, Mick, Maurice, Damien, Veronica, Ann, Ambrose and John for their help over the years

A special thanks to the members of the Forster research group, Lorraine, Mary, Richard, Edna, Darragh, Lynn, and Sonia A special thank you to Jenni and Johan, for the many times that they patiently answered my questions Without their insightful help, completing my work in the laboratory would have been a much more difficult task I'd also like to thank previous members Conor and Dominic who were there from the very start

Thanks to the chemistry postgrads and postdocs whom I've had the pleasure of knowing, Rob, Ray, Karl, Jonnie, Shane, Ian, John, Kieran, Peter, Marco, Mairead, Carol, Helen, Dec, Claire, Colm, Ben, Shaggy (biology), Deborah (biology) Also a special thank you, and apologies, to anyone I've forgotten

Finally, thanks to my family, for their support during all the years

TABLE OF CONTENTS

"ELECTRON TRANSFER IN TWO AND THREE DIMENSIONS"

DARREN A WALSH, B Sc , M Sc

A number of osmium bipyridyl complexes have been synthesised and characterised using spectroscopic, chromatographic and electrochemical techniques The complexes formed are $[Os(bpy)_2$ 4-tet Cl$]ClO_4$, $[Os(bpy)_2$ 4-bpt Cl$]PF_6$ and $[Os(bpy)_2$ Cl 4-bpt Os$(bpy)_2$ Cl$](PF_6)_2$, where bpy is 2,2'-bipyridyl, 4-tet is 3,6-bis(4-pyridyl)-1,2,4,5-tetrazine and 4-bpt is 3,5-bis(pyridin-4-yl)-1,2,4-triazole Monolayers of $[Os(bpy)_2$ 4-tet Cl$]ClO_4$ have been formed by spontaneous adsorption onto clean gold microelectrodes The tetrazine bridge between the $[Os(bpy)_2Cl]^+$ head group and the metal electrode surface undergoes a reversible protonation/deprotonation reaction depending on the pH of the contacting electrolyte solution High speed cyclic voltammetry reveals that the redox switching mechanism is best described as a non-adiabatic, through-bond tunnelling mechanism Significantly, while protonating the bridging ligand does not influence the free energy of activation, 10 3±1 1 kJ mol ^{1}, k^o decreases by 1 order of magnitude from $1\ 1 \times 10^4$ s ^{1} to $1\ 2 \times 10^3$ s ^{1} upon going from a deprotonated to a protonated bridge These observations are interpreted in terms of a through-bond tunnelling mechanism in which protonation decreases the electron density on the bridge and reduces the strength of electronic coupling between the redox centre and the electrode

Solid deposits of the dimeric complex $[Os(bpy)_2$ Cl 4-bpt Os$(bpy)_2$ Cl$](PF_6)_2$ have been deposited on platinum microelectrodes by mechanical attachment The electrochemical response exhibited by these deposits is unusually ideal over a wide range of electrolyte compositions and pH values D_{CT}, the charge transport diffusion coefficient, is independent of the electrolyte concentration, indicating that electron self-exchange between adjacent redox centres limits the overall rate of charge transport through the solid In 1 0 M $LiClO_4$ and 1 0 M $HClO_4$, D_{CT} values are 2 0±0 1×10^{10} and 1 7±0 4×10^{10} cm^2 s ^{1}, corresponding to second order electron transfer rate constants of $1\ 8\times10^7$ and 3×10^7 M ^{1} s ^{1} The standard rate of heterogeneous electron transfer across the electrode/deposit interface is 1 08±0 05$\times10^{3}$ cm s ^{1} This value is approximately one order of magnitude lower than that found for a similar monomeric complex in which the bridging ligand is attached directly to the electrode surface, indicating that the 4-bpt ligand does not promote strong electronic communication between the $[Os(bpy)_2Cl]^+$ head group and the electrode surface

Monolayers of $[Os(bpy)_2$ 4-bptCl$]PF_6$ have been formed by spontaneous adsorption onto platinum microelectrodes These monolayers are extremely stable under a wide range of electrolyte compositions and pH values Significantly, the 4-bpt ligand is capable of undergoing a protonation/deprotonation reaction depending on the pH of the contacting electrolyte solution High speed chronoamperometry reveals that protonation of the 4-bpt bridging ligand causes the standard rate of heterogeneous electron transfer to decrease by at least an order of magnitude from $2\ 67 \times 10^6$ to $4\ 5 \times 10^4$ s^{-1} for the oxidation process and from $1\ 60 \times 10^6$ to $1\ 9 \times 10^5$ for the reduction process Consistent with a superexchange mechanism, these observation are interpreted in terms of a hole superexchange process, the rate of which decreases with increasing energy gap between the osmium metal dπ orbitals and the highest occupied molecular orbital of the bridge

CHAPTER 1

THEORETICAL FRAMEWORK
AND
LITERATURE SURVEY

1 1 INTRODUCTION

The study of bridge mediated electron transfer reactions has been the focus of intense research in the past number of years Much of this work has been driven by the desire to synthetically model biological electron transfer events, thereby increasing the understanding of natural phenomena such as photosynthesis [1 2 3] Moreover, electrochemical investigations of electron transfer reactions have aided the development of areas such as molecular electronics, electrochemical sensors and electrocatalysis [4 5,6]

The intervening bridge between an electron donor and acceptor pair plays a critical role in the electron transfer reaction For example, photochemical studies of electron donor-acceptor pairs separated by rigid bridging ligands of increasing length have provided insights into the distance dependence of electron transfer [7 8] Numerous electrochemical investigations of electron donor-acceptor pairs in which either the donor or acceptor is replaced by an electrode surface have allowed an understanding of the effects of parameters such as distance, driving force, temperature and surrounding medium on the electron transfer reaction across molecular bridges [9 10 11]

However, surprisingly few studies have been carried out in which the effect of the nature of the intervening bridge on the electron transfer reaction has been probed Given that the intervening bridge between an electron donor-acceptor pair controls the extent of electronic communication between the electron donor and acceptor, the bridge structure has a crucial role in the electron transfer reaction Only in recent years have chemists begun to examine the effect of, for example, bonding characteristics,[12] substitution[13] and conjugation[14] on electron transfer processes Through these investigations, a thorough understanding of the effect of the bridge structure on electron transfer should emerge

The work described in this thesis is primarily designed to electrochemically probe the effect of the intervening bridge structure on the rate of electron transfer between electron donors and acceptors In this regard, monomolecular films of redox-active species, tethered to an electrode surface via a bridging ligand have proven extremely valuable The electrode surface can then act as either electron donor or acceptor In addition, electron transfer through solid-state films can provide important insights into both electron transfer through solids as well as between donor-acceptor pairs across molecular bridges

The molecular bridges used in this work have been carefully chosen so that not only can the bridge be reduced in an electrochemically accessible potential window, but the bridge is also capable of undergoing a protonation/deprotonation reaction depending on the pH of the contacting electrolyte solution Therefore, these systems provide a convenient means to alter the structure of the bridge by a simple change in the pH of the contacting electrolyte solution The effects of bridge protonation on the dynamics of heterogeneous electron transfer can then be examined, providing an insight into the role of bridge structure in mediated electron transfer processes

In this chapter, the contemporary theories used to describe electron transfer reactions are described The formation and characterisation of monomolecular films and solid-state films at electrode surfaces are then described The electrochemical techniques that are commonly used to characterise the electron transfer activity of redox-active films are then described A review of the relevant literature is then described, providing an insight into the current scientific knowledge regarding the effect of bridge structure on mediated electron transfer

Chapter Two describes the synthesis and characterisation of the complexes used in this study The majority of the work carried out in this study has employed microelectrodes and the construction and characterisation of the microelectrodes are described in Chapter Two In Chapter Three, a novel monolayer system is

described, in which an osmium polypyridyl redox centre is tethered to a gold microelectrode surface Significantly, the bridging ligand employed is capable of undergoing a protonation/deprotonation reaction depending on the pH of the contacting electrolyte solution The effects of bridge protonation on the heterogeneous electron transfer rate between the osmium metal centre and the gold electrode are discussed, providing an insight into the effect of the bridge structure on the electron transfer reaction

Chapter Four describes the electrochemical behaviour of a solid layer of a dimeric osmium polypyridyl complex at platinum electrode surfaces Electrochemical investigations of these films can provide an insight into the factors governing charge transport throughout solid materials The rate of heterogeneous electron transfer across the solid film/electrode interface can also be probed This can allow an insight into how the method of attachment of redox species to electrode surfaces can affect the rate of electron transfer across the electrode surface

In Chapter Five, the effects of bridge protonation on another osmium polypyridyl monolayer system are investigated The bridge employed in this study capable of undergoing a protonation/deprotonation reaction depending on the electrolyte pH In conjunction with the system described in Chapter Three, these studies may allow a deeper understanding of the effects of bridge structure on bridge mediated electron transfer reactions

1 2 THEORIES OF ELECTRON TRANSFER

1 2 1 INTRODUCTION

In order to study the effects of bridge structure on bridge mediated electron transfer, it is important to first describe some of the theoretical models that have been introduced to describe electron transfer processes A number of electron transfer models have been developed to date The oldest of these is the Butler-Volmer model, which is essentially a macroscopic model and is still widely used [15 16] Over the past number of decades a number of microscopic models have been developed, which aim to describe how factors such as the reactant structure, the solvent or the electrode material affect the rate of electron transfer Much of this work has been carried out by Landau, Zener, Marcus and Hush [17 18] In the following sections, the most widely used models assembled to describe electron transfer reactions are described, including the Butler-Volmer formulation of electrode kinetics, the Marcus theory of electron transfer and the semi-classical model of electron transfer

1 2 2 THE BUTLER-VOLMER MODEL

The Butler-Volmer formulation of electrode kinetics is the oldest and simplest model derived to describe heterogeneous electron transfer reactions The model is based on purely classical concepts and has severe limitations It does not account for the known distance dependence of electron transfer It does not account for any changes in the structure of the redox centre or the solvent upon electron transfer The theory also predicts that the rate of electron transfer will increase exponentially with increasing driving force However, this is only true over a limited range of driving forces Nonetheless, the theory does provide a description of experimental electrode kinetics under a variety of conditions and is still widely used in the scientific literature

The rate constant for a reaction can be deduced from activated complex theory[16] and is given by

$$k = Ae^{-E_a/RT} \qquad (1\ 1)$$

where E_a is the activation energy of the reaction This is the energy barrier that must be surmounted before the reaction can proceed The exponential term represents the probability of the reaction surmounting the energy barrier of height E_a The pre-exponential factor, A, is related to the frequency of attempts on the energy barrier Therefore, A is commonly referred to as the frequency factor Upon surmounting the energy barrier the system forms what is known as the activated complex or transition state

To illustrate the effect of activation energy on the path of reactions, the potential energy is usually expressed as a function of a reaction coordinate The reaction coordinate represents the progress of a reaction along the path from reactants to products The reaction coordinate is a multidimensional surface representing all of the independent coordinates of the reactants and the products plus the surrounding medium of each The energy surfaces have minima, corresponding to the most stable configuration of the reactants and the products Typically, as the reaction coordinates change from those of reactants to products the potential energy rises over a maximum, where the two coordinates intersect, and falls into the product configuration The reaction coordinates will only intersect when the reactants and the products have the same energies and configuration The height of the potential energy maximum above which the reaction coordinate must pass in order to reach the products coordinate is identified as the activation energy A representation of the potential energy changes that occur during a reaction is illustrated in Figure 1 1

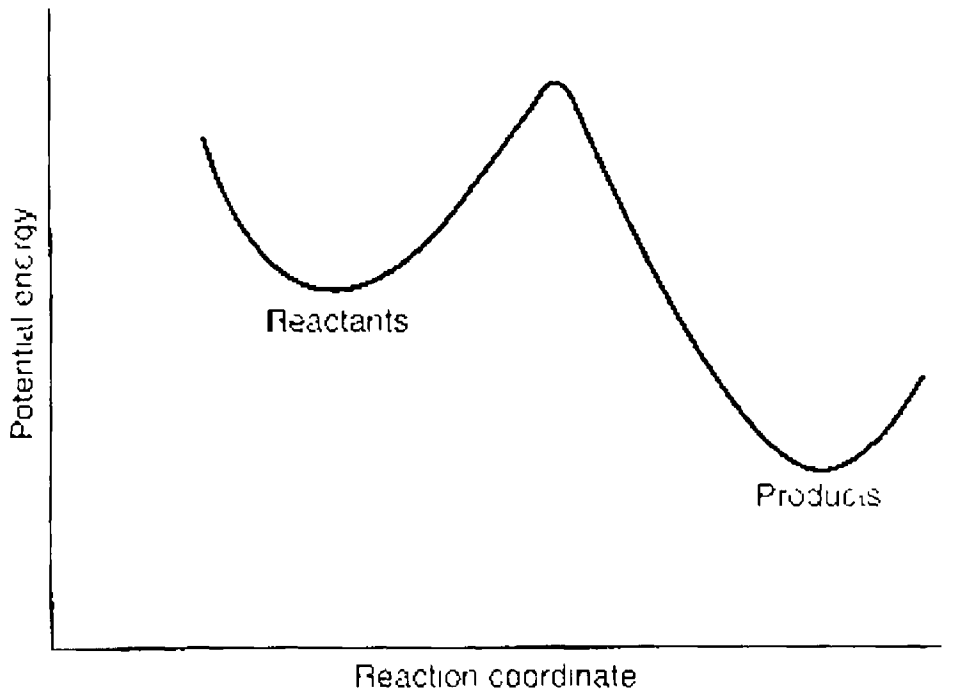

Figure 1 1 Representation of the changes in potential that occur during the course of a reaction

E_a can also be considered as a change in the standard internal energy of the system upon reaching the maximum (intersection) from one of the minima in Figure 1 1 Therefore, it may be called the standard internal energy of activation, $\Delta E^{\neq}$ The standard enthalpy of activation is then given by

$$\Delta H^{\neq} = \Delta E^{\neq} + \Delta(PV)^{\neq} \quad (1\ 2)$$

In condensed phase reactions, $\Delta(PV)^{\neq}$ is usually negligible, therefore

$$\Delta H^{\neq} = \Delta E^{\neq} \quad (1\ 3)$$

Equation 1 1 can then be rewritten as

$$k = Ae^{-\Delta H^{\neq}/RT} \quad (1\ 4)$$

From this, Equation 1 5 can be written as

$$k = A'e^{-\Delta G^{\neq}/RT} \quad (1\ 5)$$

where $\Delta G^{\neq}$ is the standard free energy of activation and A' contains the pre-exponential factor, A, and the exponential term, $\exp(\Delta S^{\neq}/R)$ Because this exponential term is a constant, Equation 1 5 is written simply containing the factor A'

Considering now a one-step, one-electron transfer reaction (e g , in solution, not electrochemically driven) whereby a species, A, is reduced to form the reduced species, B as follows

$$A + e \underset{k_b}{\overset{k_f}{\leftrightarrow}} B \quad (1\ 6)$$

Assuming that the rate constants for the forward reaction, k_f, has an Arrhenius form as in Equation 1 5, k_f can be expressed as

$$k_f = A_f' \exp\left(\frac{-\Delta G^{\neq}}{RT}\right) \qquad (1\ 7)$$

In the case where the reaction is electrochemically driven, i e , the driving force can be controlled externally, the chemical free energy of activation must be replaced with the electrochemical free energy of activation, $\overline{\Delta G^{\neq}}$ The electrochemical rate constant is then

$$k_f = A_f' \exp\left(\frac{-\overline{\Delta G^{\neq}}}{RT}\right) \qquad (1\ 8)$$

The effect of a change in potential on the standard free energies of activation is illustrated in Figure 1 2

If there is a positive shift in potential, ΔE, the energies of the electrons on the electrode shifts by $-F\Delta E$ The parabolic curve representing the reactants coordinates then shifts by that amount The barrier to oxidation (ΔG_a) has now been reduced by a value $1-\alpha$, where α is the transfer coefficient and can have values between zero and one depending on the shape of the free energy curves in the intersection region Upon shifting the potential to a new value by the amount ΔE, the barrier to reduction, (ΔG_c) becomes larger than by the amount αnFE The free energies of activation can be described by

$$\overline{\Delta G_c^{\neq}} = \Delta G_c^{\neq} + \alpha nFE \qquad (1\ 9)$$

$$\overline{\Delta G_a^{\neq}} = \Delta G_a^{\neq} - (1-\alpha)nFE \qquad (1\ 10)$$

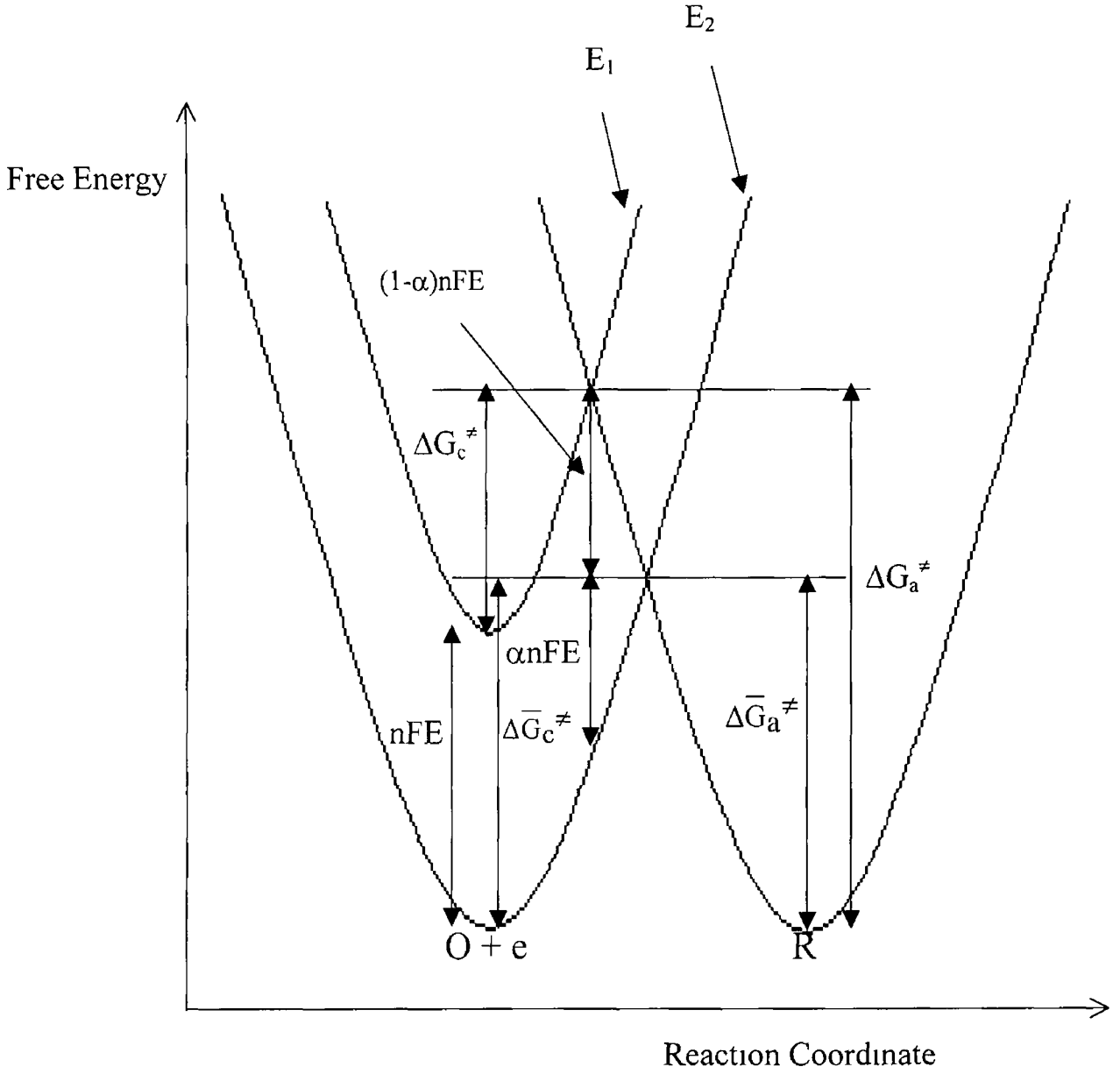

Figure 1 2 Effect of a change in potential (from an initial potential E_1 to E_2) on the standard free energies of activation for oxidation and reduction

The rate constants for the reduction and oxidation reactions have an Arrhenius form (Equation 1 8) and substituting Equations 1 9 and 1 10 into Equation 1 8 yields the rate constants for the reduction and oxidation reactions expressed as a function of potential

$$k_f = A_f' \exp\left(\frac{-\overline{\Delta G_c^{\neq}}}{RT}\right)\exp\left(\frac{-\alpha nFE}{RT}\right) \qquad (1\ 11)$$

$$k_b = A_b' \exp\left(\frac{-\overline{\Delta G_a^{\neq}}}{RT}\right)\exp\left(\frac{(1-\alpha)nFE}{RT}\right) \qquad (1\ 12)$$

The first exponential term in equations 1 11 and 1 12 is independent of the applied potential and represents the rate constants of the reactions at equilibrium, i e at $E = E^{o'}$ However, at equilibrium, the reduction and oxidation reactions occur at the same rate and $k_f = k_b = k^o$ k^o is termed the standard heterogenous electron transfer rate constant The rate constants at potentials other than $E^{o'}$ can then be expressed in terms of k^o according to

$$k_f = k^o \exp\left(\frac{-\alpha nF(E-E^{o'})}{RT}\right) \qquad (1\ 13)$$

$$k_b = k^o \exp\left(\frac{(1-\alpha)nF(E-E^{o'})}{RT}\right) \qquad (1\ 14)$$

The standard heterogenous electron transfer rate constant, k^o, is then a measure of the dynamic facility of a redox couple Redox couples with large k^o values will reach equilibrium rapidly, while couples with small k^o values will exhibit sluggish kinetics Even redox couples which show small k^o values can, however, exhibit

high reaction rate constants if the driving force (i e the potential relative to $E^{o'}$) is high enough

As outlined previously, the Butler-Volmer formulation of electrode kinetics is still widely used in the scientific literature and many systems can be adequately described by this model The model predicts that as the overpotential applied to the system (i e $E - E^{o'}$) is increased, the rate of the reaction will increase exponentially This, however, is only true for a limited range of overpotentials and it is found that at high overpotentials the rate of the reaction becomes independent of the applied potential This model also fails to adequately account for the effect of distance on the rate of electron transfer Thirdly, the model does not describe how the structure of the redox centre or the surrounding solvent can affect the rate of reaction

1 2 3 THE MARCUS THEORY OF HETEROGENOUS ELECTRON TRANSFER

The Marcus theory of electron transfer[19 20] is widely accepted as the most comprehensive description of electron transfer reactions Parabolas are also used in this model as Marcus theory assumes that the reaction coordinates conform to a simple harmonic oscillator model The Franck-Condon Principle states that electron transfer is an instantaneous process Therefore, no nuclear motion occurs during the electron transfer step The first law of thermodynamics which states that energy must be conserved must also be obeyed during the electron transfer step Therefore, electron transfer is an isoenergtic process These two criteria can only be met at the intersection of the two reaction coordinate parabolas Considering the free energy curves illustrated in Figure 1 2, it is apparent that the rate of the forward reaction (reduction) depends on the number of reactant molecules that cross over the intersection region of the two curves and fall into the products configuration

The number of molecules that cross the intersection region depends on the number of molecules that can overcome the energy barrier (i e , E_a) to reach the intersection region (i e , the transition state) However, the number of molecules that cross the intersection also depends on the probability that the molecules reaching the transition state fall into the products configuration and do not fall back into the reactants configuration The heterogeneous electron transfer rate constant, k^o, is given by

$$k^o = K_o \upsilon_n \kappa_{el} \exp\left(\frac{-\Delta G^{\neq}}{RT}\right) \qquad (1\ 15)$$

where υ_n is the nuclear frequency factor, κ_{el} is the electronic transmission coefficient and K_O is a precursor equilibrium constant υ_n represents the frequency of attempts on the energy barrier and is associated with the frequency

at which the molecules achieve the appropriate configuration to form the transition state κ_{el} is the probability that those molecules that achieve the transition state fall into the products configuration and do not fall back into the reactants configuration K_O represents the ratio of reactant molecules in the reactive position for transition state formation For a heterogenous reduction reaction, the precursor state can be envisaged as a molecule that is close to the electrode such that electron transfer from the electrode is possible k^o can then be expressed as

$$k^o = \upsilon_n \sigma \exp\left(\frac{-\Delta G^{\neq}}{RT}\right) \qquad (1\ 16)$$

where σ is an equivalent reaction layer thickness

The activation energy for the reduction reaction, $\Delta G^{\neq}$, is related to the standard free energy change for the reaction, ΔG°, according to

$$\Delta G^{\neq} = \frac{(\Delta G^{\circ} + \lambda)^2}{4\lambda} \qquad (1\ 17)$$

where λ is the total reorganisation energy, which is the energy required to alter the geometry of the reactants and surrounding medium to achieve the configuration of the product state At $E = E^{o\prime}$, where $\Delta G^o = 0$, the free energy of activation is then equal to $\lambda/4$ The reorganisation energy comprises two contributions, the outer sphere component, λ_{out}, is associated with reorganisation of the solvent and surrounding media The inner sphere component, λ_{in}, reflects the contributions from reorganisation of the molecular geometry of the reactant as it reaches the product configuration The total reorganisation energy is described as

$$\lambda = \lambda_{out} + \lambda_{in} \tag{1 18}$$

The inner sphere contribution to the total reorganisation energy is defined as

$$\lambda_{in} = \sum_{j} \frac{f_j^r f_j^p}{f_j^r + f_j^p} (\Delta q_j)^2 \tag{1 19}$$

where f_j^r is the j^{th} normal mode force constant of the reactant species, f_j^p is the j^{th} normal mode force constant of the product and Δq_j is the equilibrium displacement of the j^{th} normal coordinate λ_{in} is difficult to calculate due to the large number of parameters associated with it Knowledge of all of the force constants associated with all molecular vibrations of the reactants and the products is required However, in the majority of systems studied here the bond length changes that accompany redox reactions are small and the major contribution to λ comes from λ_{out} λ_{out} is given by

$$\lambda_{out} = \frac{(\Delta e^2)}{4\pi \in_0} \left[\frac{1}{2r_D} + \frac{1}{2r_A} - \frac{1}{r_{DA}} \right] \left[\frac{1}{\varepsilon_{op}} - \frac{1}{\varepsilon_s} \right] \tag{1 20}$$

where e is the electronic charge, $\in_0$ is the permittivity of free space, ε_{op} and ε_s are the optical and static dielectric constants of the solvent, r_D and r_A are the radii of the reactants, and r_{DA} is the interreactant centre-to-centre distance

Equation 1 17 predicts a parabolic relationship between the free energy of activation and the standard free energy change for the reaction For ΔG^o values less than λ, the rate of the electron transfer reaction increases with increasing ΔG^o values This behaviour is consistent with that described by the Butler-Volmer model of electrode kinetics at low overpotential values However, as ΔG^o becomes equal to λ, $\Delta G^{\neq}$ becomes equal to zero and the reaction becomes activationless In this region, further increases in the driving force do not cause

increases in the rate of the reaction At sufficiently high values of ΔG^{o}, ΔG^{o} becomes greater than λ and any increase in the driving force leads to a decrease in the reaction rate This is known as the Marcus inverted region This behaviour is illustrated in Figure 1 3

The electronic transmission coefficient, κ_{el}, described in equation 1 15 describes the probability of the reactant species achieving the configuration of the products once the transition state has been achieved The transfer of an electron between an electrode and a species held at some distance from the electrode is considered to be a tunnelling process, the probability of which decreases with increasing separation between the electrode and redox species κ_{el} can have values between zero and unity and is dictated by the strength of electronic coupling between the electrode and the redox species

In the case of strong electronic coupling, the probability of products being formed once the transition state has been achieved is close to unity This is reflected in a flattening of the reaction coordinates near the intersection (Figure 1 4 b) However, the probability of initially achieving the transition state is reduced under these conditions This is termed an adiabatic process Electron transfer reactions involving electron transfer over small distances are usually adiabatic If there is weak electronic coupling between the electrode and the redox species, the probability of the reactants crossing over to the products configuration is small and $\kappa_{el} << 1$ This is illustrated in Figure 1 4 a, where the intersection between the two potential energy surfaces appears as a sharp cusp The reactants must cross over onto a new potential energy surface for electron transfer to occur In this case, the process is termed a diabatic (or non-adiabatic) process Electron transfer reactions that involve electron transfer over long distances are usually non-adiabatic

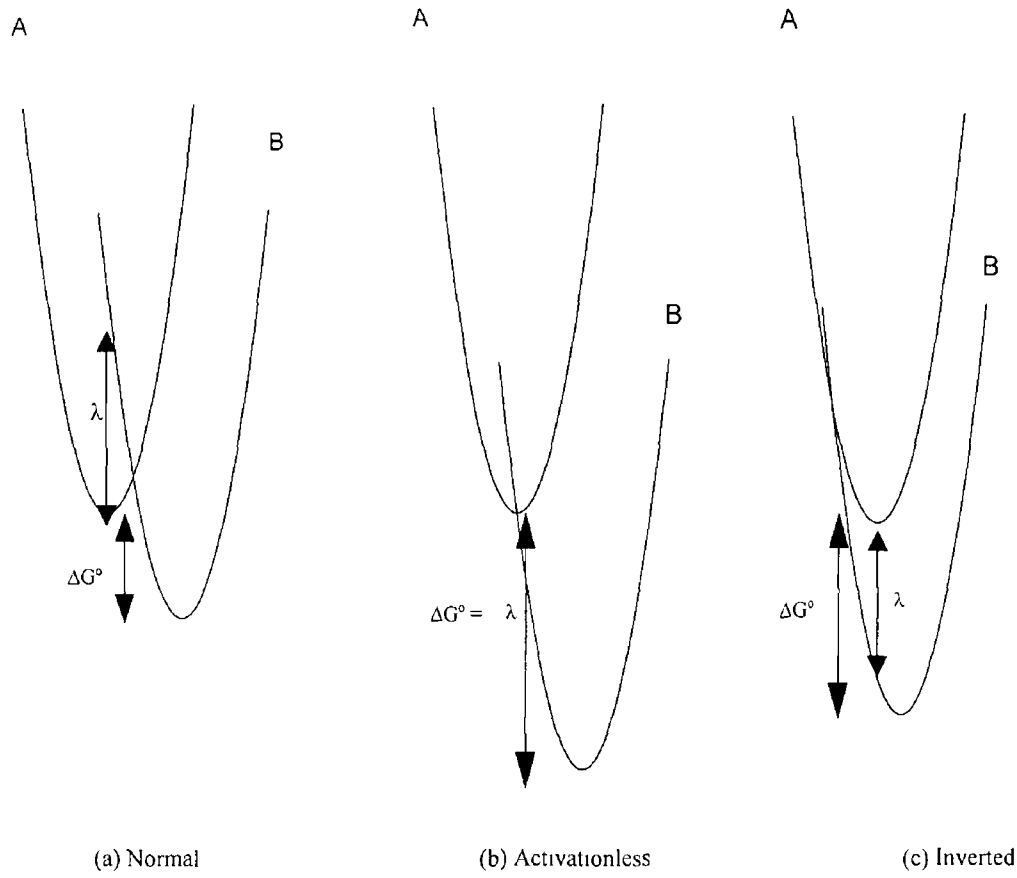

Figure 1 3 Reaction coordinates for a redox reaction illustrating the effect of increasing ΔG^{o} on the reaction rate (a) Normal region where $\Delta G^{o} < \lambda$, (b) Activationless region where $\Delta G^{o} = \lambda$, (c) Inverted region where $\Delta G > \lambda$

Adiabatic electron transfer reactions involving electron transfer to or from electrode surfaces, in which there is strong electronic coupling between the electrode and the redox species generally occurs through the states near the Fermi level of the electrode The potential dependent rate of electron transfer can be expressed for adiabatic systems by

$$k(E) = \upsilon_n D_{Ox} (4\pi\lambda_{Ox} kT)^{-1/2} \exp - \left(\frac{(\lambda_{Ox} - E)^2}{4\lambda_{Ox} kT} \right) \qquad (1\ 21)$$

where D_{Ox} is the density of acceptor states in the molecule

Diabatic systems can involve electron transfer from electronic states other than the Fermi level Therefore, all of the electronic states in the electrode must be considered The Fermi function is used to describe the distribution of occupied states within a metal according to

$$n(E) = \left(\frac{1}{1+\exp[(E-E_F)/kT} \right) \qquad (1\ 22)$$

where E_F is the Fermi level of the metal The potential dependent rate of electron transfer for diabatic systems can then be expressed as

$$k(E) = \upsilon_n D_{OX} (4\pi\lambda_{Ox} kT)^{-1/2} \int_{-\infty}^{+\infty} \frac{e^{-[(\lambda_{Ox} - E)^2 / 4\lambda_{Ox} kT]}}{e^{(E-E_F/kT)}+1} \qquad (1\ 23)$$

Both equations 1 21 and 1 23 predict that at high driving forces (where the overpotential is approximately equal to the reorganisation energy) the rate of electron transfer no longer increases with increasing overpotential At even higher overpotentials, the rate of electron transfer decreases with increasing overpotential This is the "Marcus inverted region" described previously

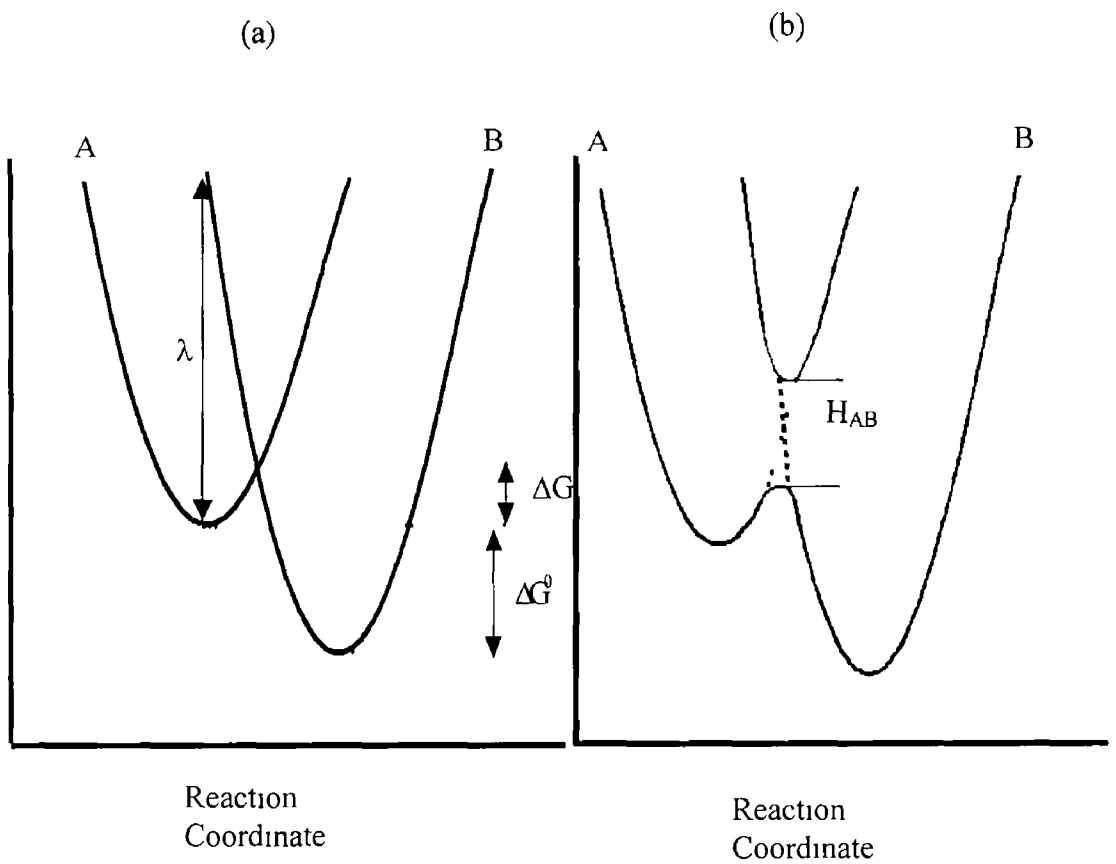

Figure 1 4 Reaction coordinates for (a) non-adiabatic and (b) adiabatic electron transfer reactions H_{AB} is the coupling element between the electron donor (oxidised species) and acceptor (reduced species)

1 2 4 THE SEMI-CLASSICAL MODEL OF ELECTRON TRANSFER

Models described by Landau, Zener, Marcus and Hush[17 18 21] led to the development of the semi-classical model of electron transfer, represented by equation 1 24

$$k_{et} = \upsilon_n \kappa_{el} \exp\left(\frac{-(\Delta G^0 + \lambda)^2}{4k_B T}\right) \qquad (1\ 24)$$

where k_B is the Boltzmann constant For a diabatic electron transfer reaction $\nu_n\kappa_{el}$ is given by

$$\upsilon_n \kappa_{el} = \frac{4\pi^2 |H_{AB}|^2}{h}\left(\frac{1}{4\pi\lambda k_B T}\right)^{\frac{1}{2}} \qquad (1\ 25)$$

The major difference between this model and the models described previously is that the product $\upsilon_n\kappa_{el}$ is proportional to the electronic coupling matrix between the oxidised and reduced species, as well as λ and ΔG^o

1 3 REDOX-ACTIVE LAYERS AT ELECTRODE SURFACES

1 3 1 INTRODUCTION

Monolayers of redox-active species tethered to electrode surfaces via a bridging ligand have been demonstrated to be an extremely valuable tool for the study of electron transfer reactions By using rigid bridging ligands, it is possible to accurately control the distance between the electron donor and acceptor involved in the reaction Through the seminal work of chemists such as Creager, Chidsey and Finklea, alkanethiol monolayers that contain a redox-active head group (e g ferrocene) have been extensively used probe the effects of distance,[22 23,24,25 26] temperature,[27 28] pH and electrolyte[28 29 30] on the dynamics of electron transfer across the electrode/monolayer interface These observations have been instrumental in both furthering the understanding of electron transfer reactions and in testing modern theories of electron transfer

Due to their facile electrochemical responses, stability in a number of oxidation states and ease of adsorption onto inert metal substrates, osmium polypyridyl monolayers have also been used extensively for the study of electron transfer reactions Comprehensive studies by chemists such as Forster and Abruña have employed osmium polypyridyl complexes to probe the adsorption and desorption of these complexes,[31 32 33] and to determine the effects of parameters such as temperature, driving force and solvent on the dynamics of heterogeneous electron transfer [11 34 35]

Solid films of redox-active material mechanically attached to electrode surfaces have also been used to examine the processes that govern electron transfer reactions Since the original experiments that were carried out just over a decade ago by Bond and Scholtz,[36 37] researchers have used solid-state films to probe electron transfer mechanisms both through solid materials and across the solid/electrode interface [38 39 40 41] These studies have provided insights into the

effects of solvent[42 43] and counterion[44 45 46,47 48] on the electron transfer properties of solids

In the following sections, the formation and characterisation of electrodes modified with both monolayers and solid films of redox-active materials are described Upon formation of modified electrode surfaces, it is crucially important that the microscopic structure of the modified electrode surface can be characterised Surface characterisation of modified electrode surfaces can provide insights into the relative perfection of a monolayer or the microcrystalline structure of a solid film This is especially important for the study of electron transfer dynamics, as minute changes in the electron transfer distance can have drastic effects on the rates of electron transfer [22]

For the formation of monolayers at electrodes, thiol compounds are the most frequently used species These compounds form particularly strong bonds with gold and other coinage metal surfaces Therefore, due to the vast body of work that has emerged regarding thiol compounds on gold, some examples of these are described However, for the purposes of this thesis, osmium polypyridyl complexes are of primary interest, therefore the main focus of the examples given in this section shall be on osmium polypyridyl type complexes

1 3 2 FORMATION OF MODIFIED ELECTRODE SURFACES

1 3 2 1 MONOLAYER MODIFIED ELECTRODES

Self-assembly of adsorbates from solution, forming self-assembled monolayers (SAMs), is the most widely used method for forming monolayers at electrode surfaces Typically, low concentration solutions (μM-mM) of the species of interest are used and the electrode surfaces are exposed to the solution at room temperature for a number of hours Non-adsorbed material can be removed by rinsing the electrode with a solvent

In forming monolayers of osmium polypyridyl complexes, a stable bond between the bridging ligand and the metal surface is essential and by probing the adsorption dynamics it is possible to gain an insight into the relative stability of these films In an early report, Acevedo and Abruna[49] described the behaviour of monolayers of $[Os(bpy)_2(dipy)Cl]^+$ at platinum electrodes, where bpy is 2,2'-bipyridine and dipy is 4,4'-trimethylenedipyridine The effect of the solvent on the formal potential of the redox centre were studied in a series of six organic solvents and aqueous solutions Based on the surface activity of Brown and Anson,[50] the anodic and cathodic peak potentials determined from cyclic voltammetry are equal and can be related to the surface coverage of the monolayer by

$$E_{peak} = E^{o} + (RT/nF)(r_R - r_O)\Gamma_T \qquad (1\ 26)$$

where r_R and r_O are interaction parameters representing intermolecular interactions between reduced and oxidised forms respectively The anodic and cathodic peak potentials were not the same and the authors used the average of the two (the formal potential, $E^{o'}$) to represent E_{peak} Therefore, the formal potential can give an insight into the surface coverage as r_R and r_O change with changing surface coverage $E^{o'}$ shifted in a positive direction with increasing surface

coverage, even at low coverage, indicating that a spread submonolayer was formed at low coverages (rather than islands of congregated adsorbates)

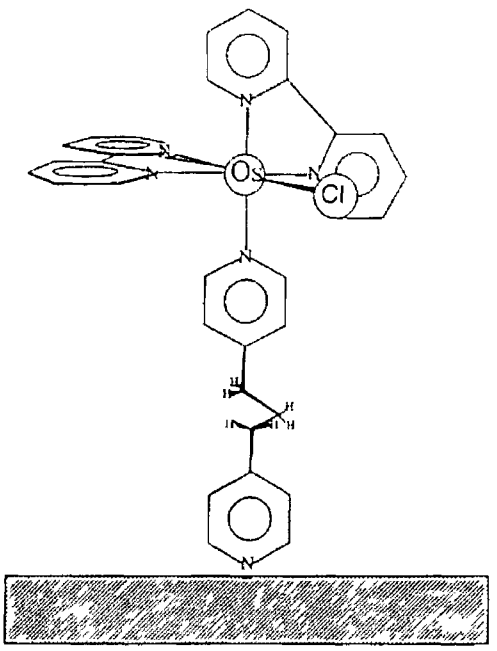

Figure 1 5 Proposed orientation of $[Os(bpy)_2(dipy)Cl]^{+}$ onto a platinum electrode showing the interaction of the pendant nitrogen of the pyridinyl group with the electrode surface [From Reference 49, Acevedo, D , Abruna, H D , *J Phys Chem* , **1991**, *95*, 9590]

The kinetics of adsorption of $[Os(bpy)_2LCl]^+$ complexes onto metal electrodes, where bpy is 2,2'-bipyridine and L are bridging ligands of varying lengths, was studied by Abruna [51] The adsorption behaviour of these complexes was studied as a function of concentration, applied potential and solvent Adsorption of the complexes at the electrode surface appeared to be under kinetic control, rather than by diffusion of the adsorbates to the electrode surface Higher surface coverages of the adsorbates on the electrode surface were observed from aqueous deposition solutions of the complexes than from organic solvent solutions This was due to solubility differences and competitive adsorption of organic solvent molecules at the surface The electrode potential had no appreciable effect on the rate of adsorption, however, the surface coverages were affected by the applied potential Through these investigations, it has been shown that these pyridinyl ligands that contain a pendant nitrogen can strongly adsorb onto metal electrode surfaces

In a later study, Campbell and Anson[52] probed whether the pyridinyl pendant nitrogen of these ligands was necessary for adsorption onto surfaces This was done by examining the factors responsible for the strong adsorption of $[Os(bpy)2(Cl)L]^+$ type complexes, where L is 1,2-bis(pyridyl)ethane and related ligands These complexes adsorbed strongly on graphite electrodes and, with the exception of L = pyridine, onto gold electrodes Significantly, the authors found that the pendant nitrogen of the ligand was not required for strong adsorption The adsorption appeared to be driven by hydrophobic interactions between the organic ligands and the electrode surface and between adjacent ligands Specific, surface-ligand interactions were also formed when the pendant nitrogen was present The dynamics of adsorption and desorption did not fit Langmuirian adsorption (i e , no interactions between adjacent adsorbate molecules), although the concentration dependence of the adsorption could be fit to a Langmuir isotherm It was suggested that the adsorption behaviour of the complexes is due to stabilising interactions between adsorbates, through the aromatic rings of the ligands This produces a surface phase that equilibrates very slowly with the

contacting aqueous solution The most striking result of this work was the fact that the pendant nitrogen of the bridging ligand was not necessary for strong adsorption onto surfaces

1 3 2 2 ELECTRODE SURFACES MODIFIED WITH SOLID FILMS

The monolayers described in the previous section are two-dimensional films and can allow important insights into electron transfer in two dimensions However, another important area of research is to elucidate how electron transfer occurs through solid three-dimensional structures Towards this, crystalline solids attached to electrode surfaces can provide important insights While the macroscopic structure of these materials is highly disordered, highly ordered domains exist within individual crystals Provided that the depletion layer in electrochemical studies of solid crystalline materials remains within individual particles, these deposits offer an attractive means to study charge transport though ordered three-dimensional domains

The process of mechanical attachment of redox-active solid deposits has gained significant interest since the original work carried out over a decade ago [36 37] A novel electrode modification technique was employed involving abrasive transfer of the solid material to the electrode surface By simply attaching some of the redox-active species directly to the electrode surface by mechanical attachment, stable films can be formed The electrode can then be placed in an electrolytic medium, in which the solid is insoluble Solid films of this type has been shown to exhibit unusually ideal electrochemical responses, reminiscent of solution phase responses Previous attempts at immobilising solid materials employed immobilisation of the redox species in, for example, graphite powder at the electrode surface [53] Using such immobilisation methods, poor electrochemical responses were frequently observed, limiting the amount of useful data that could be extracted

Due to the method of attachment, solid films deposited using this method exhibit random structural features at the electrode surface Therefore, characterisation of the modified surface is essential prior to performing any electrochemical investigations In the following section, some of the techniques used to characterise modified electrode surfaces are described

1 3 3 CHARACTERISATION OF MODIFIED ELECTRODE SURFACES

A wide range of instrumental methods is now available for the characterisation of the structure of modified electrodes In this section, some of the major techniques used for characterisation of modified surfaces are described, including scanning electron microscopy, scanning tunnelling microscopy, atomic force microscopy and raman spectroscopy

1 3 3 1 SCANNING ELECTRON MICROSCOPY

Scanning electron microscopy (SEM) has proven extremely useful in the characterisation of mechanically attached solid-state films at electrode surfaces In an early report on mechanically attached films at electrodes,[54] Bond and co-workers used SEM to characterise the surface of a carbon electrode that had been modified with solid layers of *trans*-$[Cr(CO)_2(dpe)_2]BPH_4$ and *cis*-$Cr(CO)_2(dpe)_2$, where dpe = $Ph_2PCH_2CH_2PPH_2$ X-ray electron probe analysis was then used to determine the extent of ion diffusion into the film Upon oxidation of the solid layer, the overall charge of the film will increase In order to maintain electroneutrality, counterions from the electrolyte will diffuse into the interior of the solid from the solution phase Using a $KClO_4$ electrolyte, it was found that oxidative electrolysis of the film caused the influx of ClO_4 into the film The X-ray electron probe microanalysis data obtained are illustrated in Figure 1 6 Figure 1 6a illustrates the response obtained for a solid film of *cis*-$Cr(CO)_2(dpe)_2$ prior to oxidative electrolysis This illustrates the presence of chromium and phosphorous in the theoretically expected ratio of 1 4 Figure 1 6b illustrates the electron probe analysis of the sample depicted in Figure 1 6a, but after oxidative electrolysis of the film This response was observed whether $NaClO_4$ or $KClO_4$ was used as the supporting electrolyte This clearly indicates the presence of Cl in the film after electrolysis X-ray electron probe microanalysis is sensitive to K^+ and the absence of any K^+ in Figure 1 6b suggests that K^+ is not transferred into the solid either as ion-paired $KClO_4$ or as desolvated K^+ Therefore, these results

indicate that the counterion alone is transported into the film to maintain electroneutrality

Forster has demonstrated the ability of SEM to characterise electrode surfaces modified with solid films of osmium polypyridyl complexes [55] The redox behaviour and structural changes that accompanied redox cycling of solid films of $[Os(bpy)_2$ 4-tet Cl$](ClO_4)$ have been studied, where 4-tet is 3,6-bis(4-pyridyl)-1,2,4,5-tetrazine The structure of this complex is shown in Figure 1 7

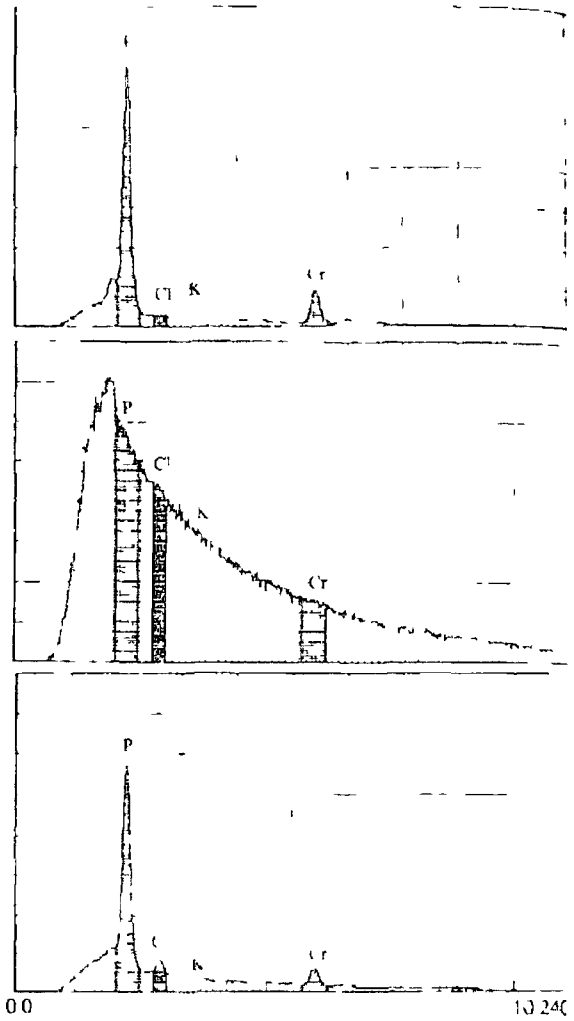

Figure 1 6 X-ray electron probe microanalysis data obtained for solid films of *cis* $-Cr(CO)_2(dpe)_2$ mechanically attached to a pyrolytic graphite electrode surface (a) Before electrolysis showing detection of Cr and P, (b) after electrolysis in $NaClO_4$, showing detection of Cr, P and Cl, but no K, (c) a for (b) but for a bare graphite part of the electrode, showing absence of Cr, P, Cl and K [From Reference 54, Bond, A M , Colton, R , Daniels, F , Fernando, D R , Marken, F , Nagaosa, Y , Van Steveninck, R F M , Walter, J N , *J Am Chem Soc* , **1993**, 115, 9556]

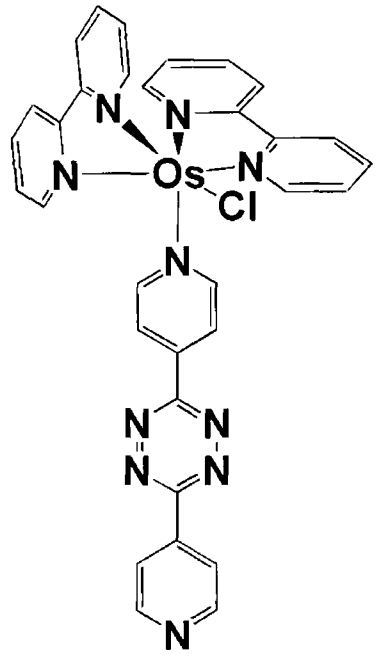

Figure 1 7 Structure of $[Os(bpy)_2\ 4\text{-tet}\ Cl](ClO_4)$ bpy is 2,2'-bipyridyl and 4-tet is 3,6-bis(4-pyridyl)-1,2,4,5-tetrazine, reported by Forster [55]

Using SEM, it was shown that cycling in perchlorate solution caused the films to become more homogenous and to crystallise The structural changes that accompanied cycling in both perchloric acid and sodium perchlorate are shown in Figure 1 8 Electrocrystallisation is not observed in the acidic solution, presumably because of electrostatic repulsion within the solid caused by protonation of the 4-tet ligand

In a subsequent publication,[56] Forster and Keyes described the electrocrystallisation of solid films of $[Os(bpy)_2$ 4-bpt Cl$](ClO_4)$, mechanically attached to platinum microelectrodes, observed using SEM 4-bpt is 3,5-bis(pyridin-4-yl)-1,2,4,-triazole Repetitive cycling of the films caused electrocrystallisation of the microscopically small particles, forming a plate-like semi-crystalline form Electrocrystallisation was found to occur only in $HClO_4$ solution and not in $LiClO_4$ The authors proposed that protonation of the 4-bpt ligand, that causes an increase of the overall charge on the complex to 1+ in the reduced state and 2+ in the oxidised state, results in co-existence of the 1+ and 2+ states in acidic media favoured electrocrystallisation However, unlike their previous report on the electroocrystallisation of $[Os(bpy)_2$ 4-tet Cl$](ClO_4)$,[55] evidence of protonation of the 4-bpt ligand was not provided in this report and the pK_a of the 4-bpt ligand may lie outside the pH range used in this study In this case, electrocrystallisation may not be linked directly to protonation of the bridging ligand

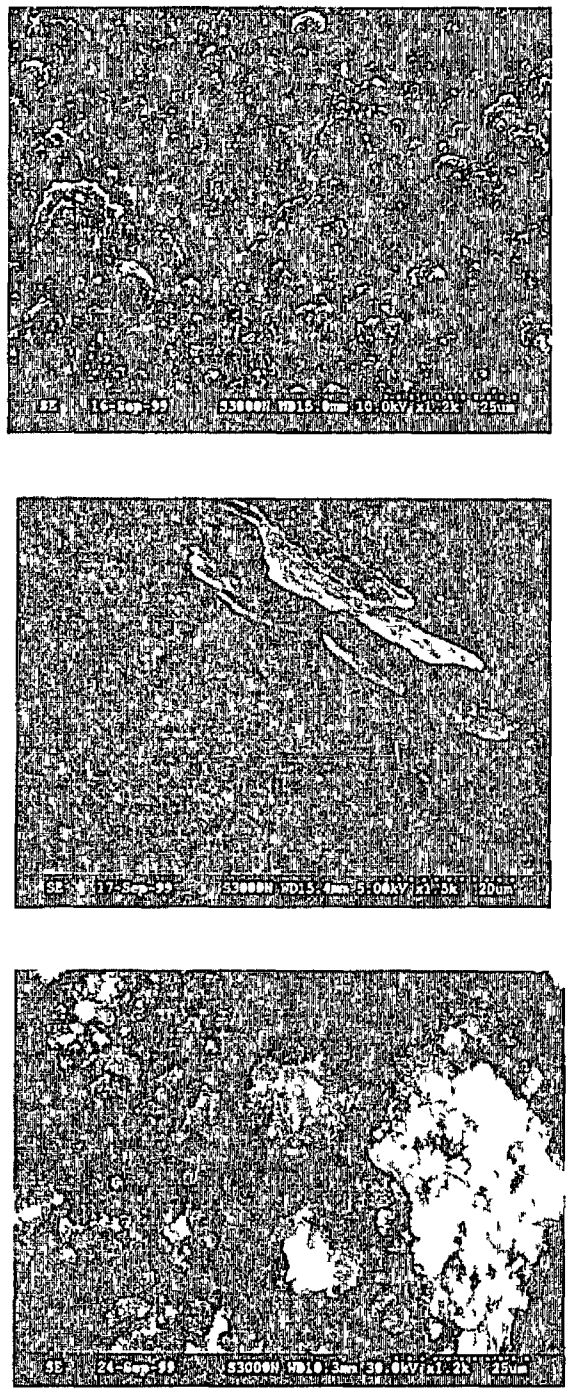

Figure 1 8 Effect of redox cycling on solid films of $[Os(bpy)_2$ 4-tet Cl$](ClO_4)$ The top image is the film after deposition The middle and bottom frame are after cycling in 0 1 M $NaClO_4$ and 0 1 M $HClO_4$ respectively between –0 2 and +0 8 V vs SCE [From Reference 55, Forster, R J , Keyes, T E , Bond, A M , *J Phys Chem , B*, **2000**, *104*, 6839]

1 3 3 2 SCANNING TUNNELLING MICROSCOPY

Developed in 1982,[57] scanning tunnelling microscopy (STM) has become an extremely valuable tool for the characterisation of electrode surfaces modified with monolayers The sub-angstrom resolution of the method means that direct imaging of adsorbates at electrode surfaces may be possible Along with the more recently introduced electrochemical STM (ECSTM), STM and ECSTM have been widely used for the characterisation of monolayer-modified electrode surfaces [58 59 60 61]

Hudson and Abruña have used electrochemical STM to monitor the coverage and the structure of monolayers of $[Os(bpy)_2(dipy)Cl]PF_6$ adsorbed onto a platinum (111) substrate [62] bpy is 2,2'-bipyridine and dipy is trimethylene-4,4'-bipyridine During the initial stages of adsorption, the image obtained was essentially the same as that for the clean platinum surface (Figure 1 9 A) However, the voltammetric response obtained indicated the presence of the adsorbed species on the surface An increased voltammetric response indicated an increased coverage of the adsorbate on the surface and as this was observed small, high contrast regions were observed in the image (Figure 1 9 C) These regions were attributed to clusters of highly mobile adsorbate on the sample surface At coverages of about two-thirds of a monolayer these regions dominated the image (Figure 1 9 D) At this coverage, pits and pinhole defects were observed in the structure, however, at full surface coverage, the monolayer was found to be free of large defects (Figure 1 9 E) Significantly, it was noted that the STM images alone were not sufficient evidence for coverage of the platinum by a monolayer of the complex This is due to the inability of STM to provide any chemical information about the surface under study When considered in conjunction with the electrochemical evidence however, it is clear that the surface was covered by a monolayer of the adsorbates

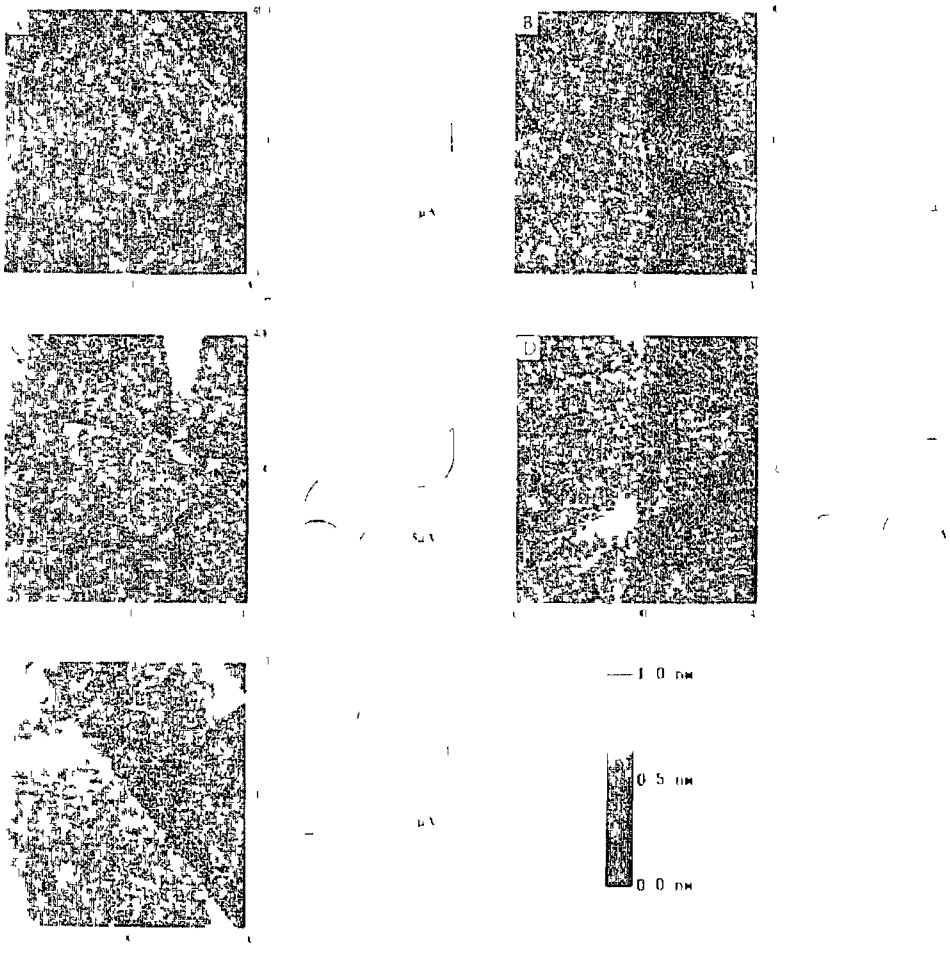

Figure 1 9 ECSTM images of a PT (111) surface at different stages during the deposition of a monolayer of $[Os(bpy)_2(dipy)Cl]PF_6$ from a 0 1 M $KClO_4$ electrolyte solution The cyclic voltammograms were obtained immediately after withdrawing the tip from the surface The electrochemically determined surface coverages are (A) 0%, (B) 25%, (C) 49%, (D) 66%, and (E) 100% The tip bias used for imaging was 50 mV and the tunnelling current was 2 5 nA The scan rate was 8 3 Hz [From reference 62, Hudson, J E , Abruña, H D , *J Phys Chem* , **1996**, *100*, 1036]

Images of this monolayer in air were also described by the authors Upon drying, the monolayers of $[Os(bpy)_2(dipy)Cl]PF_6$ crystallise to form two-dimensional crystals Molecularly resolved images of the crystals were obtained showing molecular scale features in a rectangular close-packed array (Figure 1 10) The molecular corrugation was found to be small (1-2 Å) when compared to the radius of the head group of the adsorbate (5-6 Å) This may have been because the head group only contributed a fraction of the total tunnelling current Tunnelling directly to the platinum surface may have been a major contributory factor to the overall current Assuming that each feature in Figure 1 10 was due to one adsorbate head group a surface coverage of $2\ 3 \times 10^{-10}$ mol cm^{-2} was calculated, significantly higher than the electrochemically determined surface coverage of complexes of this type ($1\ 1 \times 10^{-10}$ mol cm^{-2}) Using molecular modelling calculations, the authors obtained excellent fits of the modelled data with the experimental data The molecular modelling data used a space-filling representations of the head groups, assuming that the head groups align along the dipole of the osmium-chlorine bonds These results suggest that, when in contact with electrolyte solution, the monolayer is less ordered due to the dynamic nature of the monolayer and the presence of solvent molecules

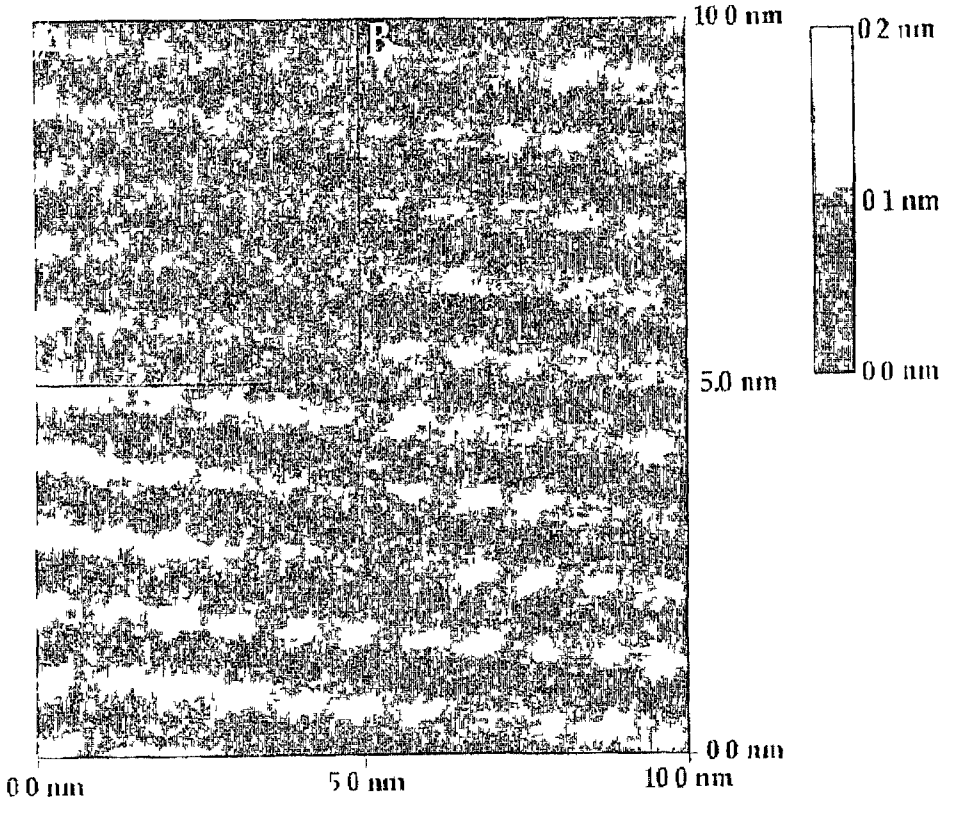

Figure 1 10 Molecularly resolved STM image of a monolayer of $[Os(bpy)_2(dipy)Cl]PF_6$ on a Pt (111) surface Region (A) is Fourier filtered and region (B) is unfiltered The tip bias used was 100 mV producing a tunnelling current of 500 pA The scan rate was 20 Hz [From reference 62, Hudson, J E , Abruña, H D , *J Phys Chem* , **1996**, *100*, 1036]

1 3 3 3 ATOMIC FORCE MICROSCOPY

Atomic force microscopy (AFM) was developed as an alternative to STM,[63] primarily due to the inability of STM to image non-conducting surfaces[64] The ability to provide topographical details about non-conducting surfaces immensely broadened the range of surfaces that could be imaged by scanning probe microscopy As a further development of AFM, tapping mode AFM has been developed in which a stiff cantilever is oscillated at its resonance frequency with a small amplitude (~ 0 5 nm) Interactions of the tip with the surface cause a shift in the frequency of oscillation of the cantilever Piezoelectric drives are then used to control the z-position of the cantilever, maintaining the oscillation frequency at a predetermined value The displacement of the tip provides topographical information about the surface Due to the reduced interactions of the tapping mode AFM tip with the surface, when compared to traditional contact mode AFM, tapping mode AFM can be used for the characterisation of soft surfaces This application has been exploited for the characterisation of monolayer-modified electrodes

There are numerous reports of the use of AFM for the study of self-assembled monolayers on surfaces in the literature[65 66 67] AFM can been used to provide information regarding the dynamics of adsorption on surfaces For example, Crooks has used tapping mode AFM to image the phase segregation of dendrimer/alkylthiol mixed monolayers[68] The use of a mixed dendrimer/alkylthiol monolayer illustrated that although chemical identification of individual adsorbates is impossible using the AFM, large domains of different adsorbates can be identified The effect of parameters such as dendrimer size, solvent and alkylthiol chain length were successfully investigated using the AFM

1 3 3 4 RAMAN SPECTROSCOPY

Spectroscopy can play an important role in the characterisation of modified electrode surfaces Raman spectroscopy has been shown to provide very useful information modified electrode surfaces and insights into the structure of surface-immobilised assemblies can be obtained The area of modified surface characterisation may be particularly suited to raman spectroscopy due to the phenomenon of surface enhanced raman spectroscopy (SERS) Upon adsorption onto surfaces, raman signals can be enhanced by many orders of magnitude It is thought that the increase in the electric field experienced by the molecule due to interaction with surface plasmon waves can increase the raman signal Also, electronic transitions between the metal surface and the adsorbed species can cause charge transfer enhancements of the signal In both mechanisms, microscopic roughening of the surface is critical SERS spectra of adsorbed monolayers are extremely useful as the surface enhancement effect is maximised However, SERS is not only applicable to monolayer applications as it may operate at distances up to tens of nanometers SERS can provide an insight into the structure of films at electrode surfaces For example, the packing density and the adsorbate orientation may be probed using SERS

Kudelski recently demonstrated the usefulness of SERS in characterising structural changes that can accompany protonation of monolayers of 3-mercaptopropionic acid (MPA) [69] Monolayers of MPA were formed at roughened silver surfaces and the structural changes that occurred during adsorption and desorption of the monolayers were studied During self-assembly of the monolayer the portion of a *trans* conformer of MPA at the surface was found to increase and a large portion of the COO groups of MPA were found to be protonated Desorption of the monolayers was accompanied by deprotonation of the COOH groups of the adsorbed MPA and this was observed as an increase in the intensity of the band associated with a vibration of dissociated COO

groups This was found to occur much slower and a reversal of the processes observed during adsorption were observed

Corio and co-workers recently demonstrated the use of potential dependent SERS in the elucidation of the adsorption processes of monolayers of the $[Ru(CN)_5(pyS)]^4$ ion complex [70] This complex is interesting, in that it can adsorb at metallic surfaces either via a CN ligand or the pyS (4-mercaptopyridine) Enhancement of the CN signal in the SERS spectra on gold surfaces indicated that adsorption occurs mainly through the CN group on gold On a silver surface, it was shown that the pyS signal was enhanced over the CN signal, indicating adsorption through the pyS moieties On copper, it was found that both signals were enhanced to the same extent, suggesting interactions of both ligands with the surface By controlling the potential of the surface during adsorption, it was shown that it was possible to choose between the different adsorption sites, thus controlling the properties of the interface The modified electrodes were used to examine the electrochemical response of cytochrome c When the complex was adsorbed through the CN ligands, an electrochemical response for the cytochrome c was not observed However, when adsorbed through the pyS moiety, a reversible response for cytochrome c (corresponding to the Fe(II)/Fe(III) process) was observed These studies indicated that effective interaction between the modifier and the protein could only occur through the CN ligands

Potential controlled SERS of solid films has also been reported by Forster,[55] illustrating the effectiveness of the technique for structures thicker than monolayers As discussed above, maximum surface enhancement can be achieved in monolayer assemblies, although SERS can operate at distances up to tens of nanometers Mechanically attached, solid state films of $[Os(bpy)_2$-4-tet-Cl$](ClO_4)$ were formed at platinum electrodes and the structural changes that accompanied redox switching of the film were monitored The potential controlled raman spectra obtained at gold disk electrodes are illustrated in Figure 1 11 The exciting laser wavelength was pre-resonant with the Os(II)-bpy π^*

MLCT transition and the features present due to the bpy moieties (1604, 1550, 1480, 1320, 1268, 1167 and 1015 cm^{-1}) were enhanced The feature at 373 cm^{-1} is due to the Os-N stretch Intense features due to surface enhanced transitions of the 4-tet ligand were observed at 811 and 934 cm^{-1} By switching the potential from –0 2 to +0 4 V vs SCE, it was possible to examine the effects of oxidising the metal centre Upon oxidation, the Os(II)-N signal is lost, consistent with metal oxidation Oxidation results in a loss of MLCT transitions, however, after oxidation the bpy bands are still observed This is because the exciting laser becomes pre-resonant with the ligand to metal charge transfer (LMCT) transition

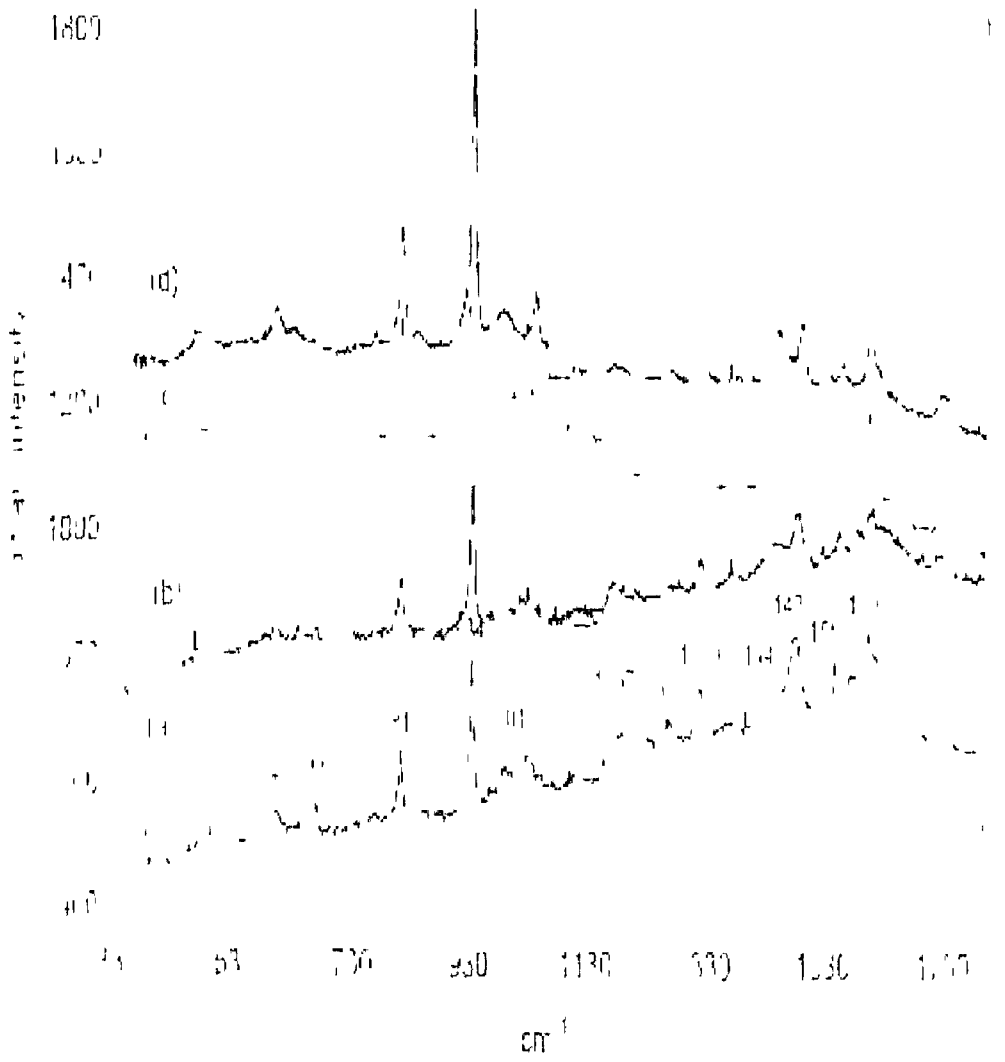

Figure 1 11 Raman spectra obtained for solid state films of $[Os(bpy)_2$ 4-tet Cl], before and after oxidation of the osmium redox centre (a) –0 2 V in 0 1 M $NaClO_4$, (b) 0 4 V in 0 1 M $NaClO_4$, (c) –0 2 V in 0 1 M $HClO_4$ and (d) 0 4 V in 0 1 M $HClO_4$ All potentials are versus the saturated calomel electrode and the wavelength of the exciting He-Ne laser is 632 8 nm [From Reference 55, Forster, R J , Keyes, T E , Bond, A M , *J Phys Chem* , 2000, 6839]

1 3 4 ELECTROCHEMISTRY OF REDOX-ACTIVE FILMS

1 3 4 1 INTRODUCTION

In the preceding sections, the formation and characterisation of electrode surfaces modified with monolayers and solid films of redox-active materials have been discussed The studies can provide important information regarding the structure and orientation of molecular species at electrode surfaces However, in order to extract information about the dynamics of electron transfer across the film/electrode interface or through solids, electrochemical techniques are used In the following sections, the electrochemical responses of ideal redox-active monolayers and solid-state films are discussed These descriptions should provide an insight into some of the parameters of importance, when undertaking a study of electron transfer reactions

1 3 4 2 ELECTROCHEMICAL RESPONSE OF IDEAL REDOX-ACTIVE MONOLAYERS

In the study of the properties of an ideal adsorbed monolayer, it is assumed that the redox couple is adsorbed on the electrode surface and is not present in solution, or its solution concentration is sufficiently low that its contribution to the Faradaic current is negligible Also, it is assumed that all adsorption sites on the electrode surface are equal and that both the oxidised and reduced forms of the redox couple occupy equal areas on the surface It must also be assumed that adsorption and desorption are rapid and do not influence the kinetics of the electrochemical process The free energy of adsorption and maximum surface coverage is assumed to be independent of the applied potential The entire potential drop must occur at the electrode surface and there must be no lateral interaction between adjacent adsorbates

1 3 4 2 1 CYCLIC VOLTAMMETRY

In cyclic voltammetry (CV), the current response of a stationary electrode in an unstirred solution as a function of a triangular potential waveform is monitored The current-potential curve obtained from a cyclic voltammetry experiment of an ideal, surface confined electroactive species under finite diffusion conditions is shown in Figure 1 12 In this voltammogram, the dynamics of heterogenous electron transfer across the electrode/monolayer interface do not influence the observed response In contrast to redox species in solution, which show diffusional tailing in the CV response, the waves observed for a surface confined species are gaussian in shape The reduction wave is a mirror image of the oxidation wave when viewed across the potential axis The peak current, i_p, is given by

$$i_p = \frac{n^2F^2}{4RT} \nu A\Gamma_o \qquad (1\ 27)$$

where n is the number of electrons transferred in the reaction, F is Faradays constant, R is the gas constant, T is the temperature, ν is the scan rate, A is the electrode area and Γ_o is the coverage of electroactive species Other parameters are listed in Figure 1 12 From Equation 1 27, for a surface confined species, i_p is proportional to the scan rate, rather than the $\nu^{1/2}$ dependence observed for a freely diffusing species The area under the reduction wave, when corrected for any background current, represents the charge injected, Q_c, for the full reduction of the monolayer according to

$$Q_C = nFA\Gamma_O \qquad (1\ 28)$$

and for an ideal monolayer of an electroactive species is equal to the charge ejected upon oxidation of the monolayer, Q_a

For an ideal monolayer, under Langmuir isotherm conditions (i e , no interactions between adjacent adsorbates), $E_{pa} = E_{pc}$ and the full width at half maximum (fwhm) of either the reduction or oxidation wave is given by

$$\text{fwhm} = 3\ 53\frac{RT}{nF} = \frac{90\ 6}{n}\text{mV} \qquad (1\ 29)$$

The formal potential, $E^{o'}$, defined as $(E_{p\,a} + E_{p,c})/2$, contains extremely useful information about the ease of oxidation of redox species within the monolayer A shift of $E^{o'}$ to more positive potentials upon immobilisation within a monolayer indicates that it becomes thermodynamically more difficult to oxidise the species, suggesting a lower electron density on the redox centre

$E^{o'}$ can also provide useful information about the movement of charge compensating ions into and out of the monolayer $E^{o'}$ typically shifts in a negative potential direction with increasing electrolyte concentration This shift can be described by the Nernst equation, i e 59/n mV per decade change in the electrolyte ion concentration Ion pairing between redox centres and specific ions from solution can influence the observed response This is described by Equation 1 30

$$(M)^{+}\left(X^{-}\right)_{\zeta} - e^{-} + p\left(X^{-}\right) \Leftrightarrow (M)^{2+}\left(X^{-}\right)_{\zeta+P} \qquad (1\ 30)$$

where M is the redox centre and X is the counterion

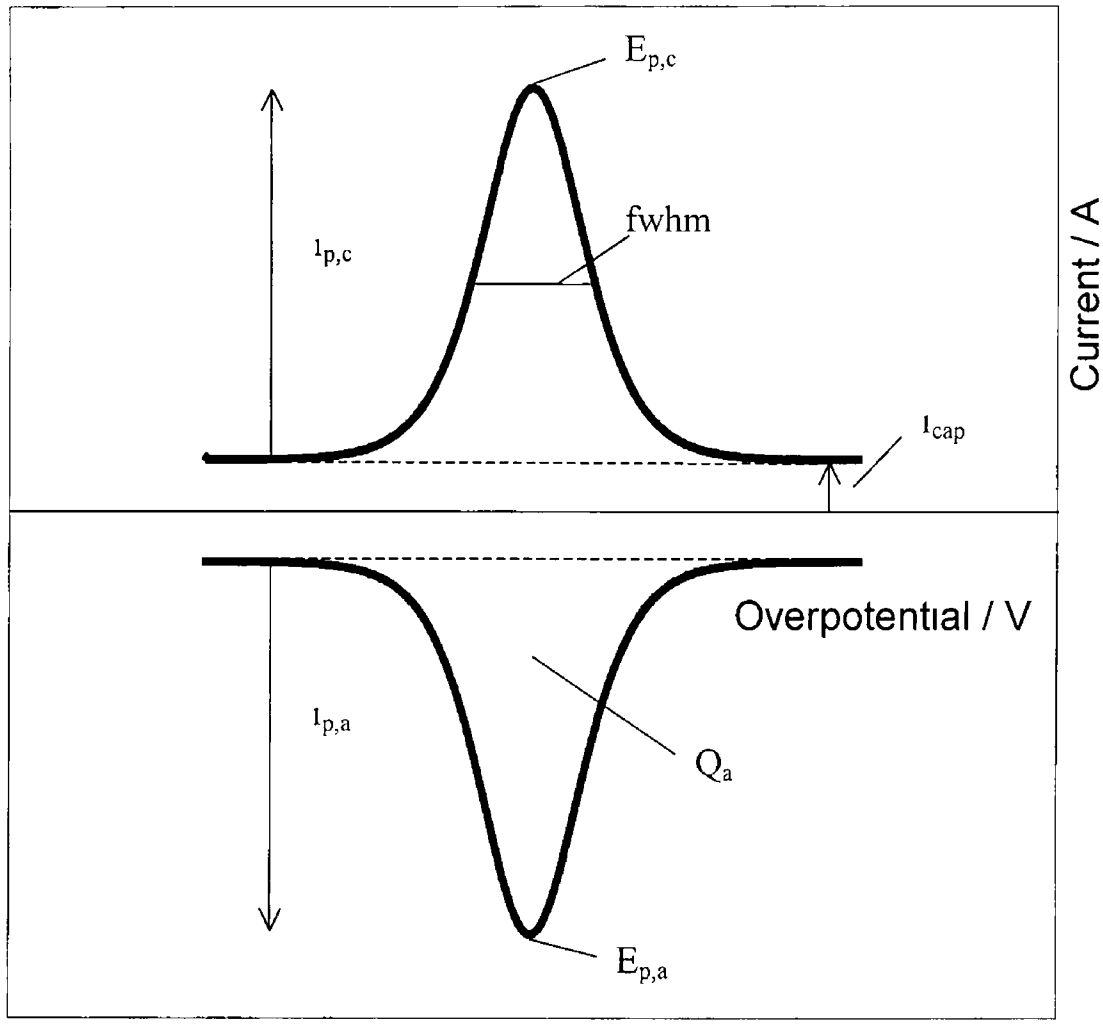

Figure 1 12 Experimental quantities of interest in a cyclic voltammogram for an ideal surface-confined redox active species E = potential, i = current, Q = charge passed, a = anodic, c = cathodic, fwhm = full width at half the maximum peak height, cap = capacitive

The fwhm value may deviate from the ideal value of 90 6/n mV due to intermolecular interactions and double layer effects A distribution of $E^{o'}$ values within the monolayer can also contribute to non-ideal fwhm values A disorganised structure within the monolayer or variations in the electrostatic potential around each redox centre may contribute to the observed behaviour A non-zero ΔE_p value can indicate intermolecular interactions or structural changes within the monolayer upon redox switching of the layer

1 3 4 2 2 CHRONOAMPEROMETRY

After a potential step, charging current, i_c, will flow at the working electrode according to [71]

$$i_C(t) = \frac{\Delta E}{R} \exp\left(\frac{-t}{RC}\right) \qquad (1\ 31)$$

where ΔE is the magnitude of the potential step, R is the cell resistance and C is the total interfacial capacitance A semi-log plot of these transients should be linear and the slope of the plot provides the RC cell time constant For an ideal, reversible, one electron transfer reaction involving a Langmuirian redox active film (i e , there are no interactions between adjacent adsorbates) adsorbed on an electrode surface the Faradaic response observed following a potential step follows a simple exponential decay according to

$$i(t) = kQ\exp(-kt) \qquad (1\ 32)$$

where k is the apparent rate constant for a given overpotential and Q is the total charge passed in the redox reaction After decay of the double layer charging current, a plot of ln i(t) versus *t* is linear and the slope is determined by the rate constant of the reaction

1 3 4 3 ELECTROCHEMICAL RESPONSE OF REDOX-ACTIVE SOLID FILMS

The electrochemical behaviour of redox-active solid films consists of both a heterogeneous electron transfer process across the electrode/film interface, as well as, a homogenous charge transport process within the solid layer As no long-range of the redox-species can occur in solid layers of redox species, charge transport through the solid must occur by electron self-exchange (electron hopping) between adjacent redox moieties Through electron hopping reactions, electrons are shuttled from the electrode to redox species that are located away from the electrode surface This process must be accompanied by counterion movement into and out of the film as the redox composition is changed

1 3 4 3 1 CYCLIC VOLTAMMETRY

The electrochemical behaviour of redox-active, solid-state films is similar to that observed for a solution–phase species under semi-infinite diffusion conditions, provided that the depletion layer remains inside the layer, and that ohmic and migration effects are absent (Figure 1 13) Under these conditions, diffusional peak tailing occurs and a $\upsilon^{1/2}$ dependence on peak current is observed, rather than the υ dependence observed for the surface-confined species described above Under these conditions, the peak-to-peak separation is given by

$$\Delta E_p = 57/n \text{ mV (at } 25°C) \qquad (1\ 33)$$

The diffusion of electrons through the solid can be described by the Dahms-Ruff equation as follows

$$D_{CT} = D_{phys} + k\delta^2 C_{eff} b \qquad (1\ 34)$$

where D_{CT} is the charge transfer diffusion coefficient, D_{phys} is the physical diffusion coefficient, k is the second order rate constant for the reaction, δ is the distance between the redox species, C_{eff} is the effective concentration of the species and b is a constant (usually a value of 1/6 is used for three-dimensional diffusion) Estimates of D_{CT} can be obtained by using the Randles-Sevçik equation

$$i_p = 2.69 \times 10^5 n^{3/2} A D_{CT}^{1/2} C_{eff} \upsilon^{1/2} \quad (1.35)$$

This equation is routinely used for measurement of D_{CT} values using cyclic voltammetry at relatively high scan rates (typically > 50 mV s^{-1}) Although charge transport within solid films occurs by successive electron self-exchange reactions between adjacent redox sites, this may not be rate limiting As the charge on the redox centres change during electron hopping, counterion migration must also occur to maintain electroneutrality The rate limiting process can be either electron self-exchange between redox sites or counterion migration throughout the solid Rapid electron diffusion is promoted at high concentrations of the redox sites due to the close proximity of adjacent redox sites However, sluggish migration of counterions through the film may cause ion migration to be the rate limiting step In films where the free volume is high, rapid ion diffusion through the solid occurs and electron transfer may be the rate limiting step

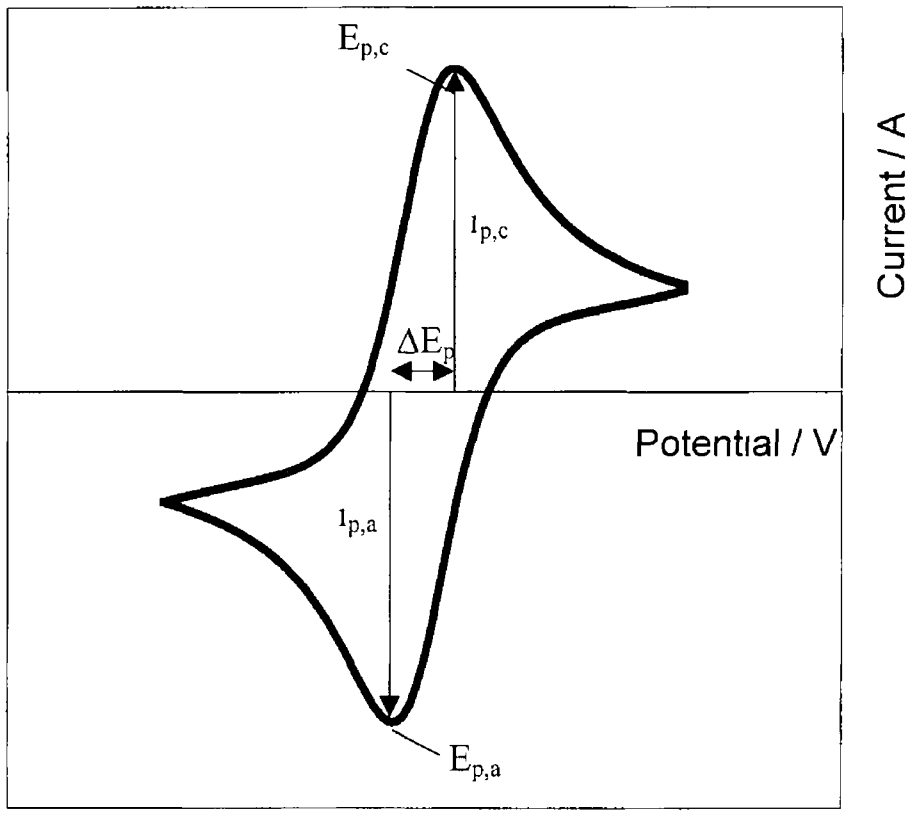

Figure 1 13 Ideal cyclic voltammogram response of an solid film of a redox species at an electrode surface i_p is the peak current, $E_{p\,a}$ and $E_{p\,c}$ are the anodic and cathodic peak potentials respectively and ΔE_p is the peak-to-peak separation

1 4 BRIDGE EFFECTS IN BRIDGE MEDIATED ELECTRON TRANSFER

In this work, the effects of bridge structure on the rate of heterogeneous electron transfer across the electrode/monolayer interface are studied in detail The intervening bridge between an electron donor and acceptor moiety is extremely important For example, if an electroactive bridge is used between the donor and acceptor moieties, there is the possibility of achieving significant virtual coupling (superexchange) [72] This effect is described in detail later Therefore, the structure of the bridge can have a drastic effect on the rate of electron transfer In the following sections, the effects of parameters such as distance, structure and bonding on the rate of electron transfer across molecular bridges are discussed This may provide an insight into some of the approaches that have been taken towards modulating the rate of electron transfer across bridges

1 4 1 DISTANCE DEPENDENCE OF ELECTRON TRANSFER

The bridge or spacer between electron donor and acceptor pairs has a crucially important role in determining the rate of electron transfer between the donor and acceptor As described in the previous sections, $|H_{AB}|$, the electronic coupling matrix between the oxidised and reduced species has a vital role in dictating electron transfer rates $|H_{AB}|$ decreases with increasing distance between electron donor and acceptor states The decay of $|H_{AB}|$ can be represented by Equation 1 36

$$H_{AB}(d) = H_{AB}(d_0)\exp\left(\frac{-\beta(d-d_0)}{2}\right) \qquad (1\ 36)$$

where H_{AB} is the coupling matrix between oxidised and reduced species at Van der Waals distance, d is the centre to centre distance between the donor and acceptor β is the tunnelling parameter, a constant that depends on the height of

the energy barrier and nature of the medium between the donor and acceptor states

$|H_{AB}|$ has been shown to decay exponentially with increasing distance between donor and acceptor moieties The distance dependence of electron transfer, therefore follows an exponential relationship as shown in Equation 1 37

$$k_{et} = \exp(-\beta d) \qquad (1\ 37)$$

As discussed in Section 1 2 1 1, monolayers of electroactive species adsorbed at electrode surfaces have been used extensively to illustrate the exponential decay of the electron transfer rate with increasing distance Typically, a plot of the electron transfer rate constant versus the number of repeating units in the bridging ligand (e g methylene units in an alkane chain) is linear [73] β can be determined from plots of k^{o} versus the number of repeating units in the bridge and for alkanethiol systems is in the range 1 0-1 1 $Å^{-1}$ The β value for electron tunnelling through a vacuum is ~3 $Å^{-1}$ [74] The difference between these values represents the contribution of the molecular bridge to electron tunnelling

1 4 2 MECHANISMS OF BRIDGE MEDIATED ELECTRON TRANSFER

Electron transfer between donor and acceptor pairs can occur by a number of different mechanisms depending on the distance between the donor and acceptor and the nature of the intervening bridge At sufficiently short distances, electron transfer occurs by simple electron or hole transfers Bridge mediated electron transfer occurs when the donor and acceptor are separated by a long distance and can occur by either a hopping or a superexchange mechanism Electronic hopping along the bridge occurs when the bridge electronic states are resonant with the donor states The electron actually occupies the electronic levels of the

bridge and hops sequentially along the bridge to the acceptor moiety This is illustrated in Figure 1 14

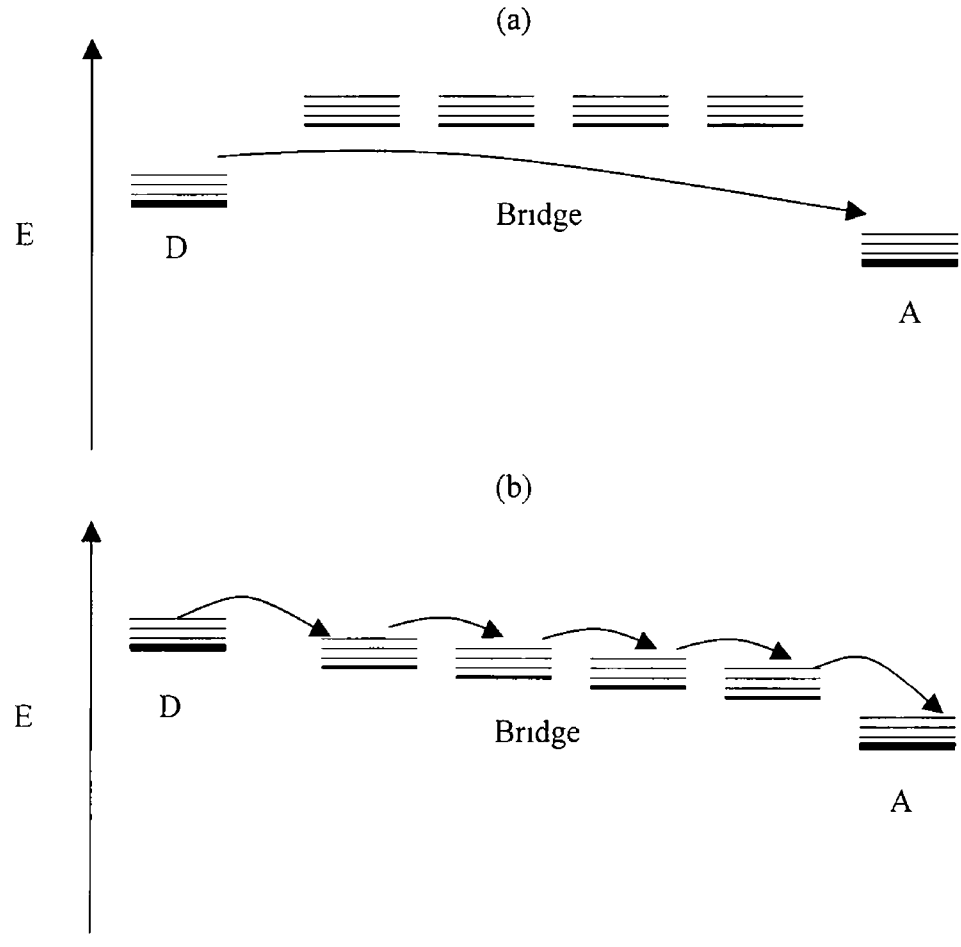

Figure 1 14 Mechanisms of bridge mediated electron transfer (a) Superexchange occurs when the bridge and donor levels are off resonance and is a single step process (b) Electron hopping occurs when the bridge levels are close in energy to that of the donor

Superexchange mechanisms[75] occur when the bridge electronic levels and the donor levels are not resonant with each other (Figure 1 14 a) In this case, the bridge acts to extend the wave functions of the donor and acceptor High energy virtual electron and hole (absence of an electron) states are created within the bridge and the electron transfer occurs in one step Electron transfer via superexchange may be the dominant mechanism if the LUMO of the bridge is similar in energy to the acceptor states of the remote redox centre This pathway predominates because the closeness of the bridge and redox centre energies acts to reduce the activation barrier to electron tunnelling In contrast, if the $Os_{d\pi}$-HOMO separation is relatively smaller, then HOMO mediated hole transfer will contribute significantly to the redox switching mechanism Forster has probed how the proximity of the bridge energy levels to the formal potential of adsorbed redox centres within osmium polypyridyl monolayers can affect the electron tunnelling pathway[76] This system consisted of dense monolayers of $[Os(bpy)_2py(p3p)]^{2+}$, where bpy is 2,2'-bipyridyl, py is pyridine and p3p is 4,4'-trimethylenedipyridine The formal potential of the redox centre and the bridging ligand were separated by at least 2 0 V, whereas the bpy based reduction potentials were within 0 3 V of the half-wave potential for the uncomplexed bridging ligand The electronic transmission coefficient, κ_{el}, describing the probability of electron transfer once the nuclear transition state has been achieved, was considerably less than unity for the metal based redox process and two ligand based reductions However, κ_{el} was larger for the two bipyridyl based reductions ($2\ 4\pm0\ 9 \times 10^{-5}$) than for the metal based reaction ($1\ 5\pm0\ 7 \times 10^{-6}$) Measurement of the potential dependence of the heterogeneous electron transfer rate suggested that for the ligand based reductions electron transfer occurred via a through-bond tunnelling mechanism, whereas electron transfer to the metal centre occurred via a through-space tunnelling mechanism This was consistent with superexchange being important only for the ligand based reactions where the redox potentials of the acceptor states and the bridge were similar The disparity between the metal centre energy levels and the bridging ligand meant that superexchange did not contribute significantly to the electron transfer reaction

This example illustrates the effect that achieving resonance can have on the rate of electron transfer when electron transfer occurs via a superexchange mechanism In this system, electron transfer to the ligands appears to occur via an electron superexchange mechanism as the energy of the LUMO of the bridge is in close proximity to the bridging ligand levels

Therefore, if it is possible to tune the energy of the bridging ligand externally, it may be possible to tune the energy gap between the donor/acceptor moieties and the bridge, thereby allowing control over the rate of heterogeneous electron transfer It is this concept that is one of the main objectives of this work In the following sections, some approaches that have already been taken to modulating the rate of heterogeneous electron transfer are described

1 4 3 EFFECT OF BRIDGE CONJUGATION ON ELECTRON TRANSFER

The production of "molecular wires" that support rapid heterogeneous electron transfer between a remote redox centre and a metal surface is crucial to areas such as molecular electronics In an effort to develop such systems, several studies into the effects of conjugation of the intervening bridge between donor and acceptor have been undertaken For example, Chidsey recently studied the effects of conjugation on the heterogeneous electron transfer dynamics of a series of ferrocene-terminated oligo(phenylenevinylene) methyl thiols attached to gold electrodes [77 78] The oligomers were composed of coplanar phenyl groups linked by vinylene bonds, which imparted a high degree of rigidity to the bridge Oligomers were synthesised containing from 1 to 5 repeating units and for all bridges the standard heterogenous electron transfer rate constant exceeded 10^5 s^{-1} For comparison, k^o for an analogous bridge containing an ethynyl group in place of the vinyl group, containing 4 repeat units was reported to be 6×10^4 s^{-1}, approximately 50 times smaller The difference was because of an increase in the π-conjugation of the bridge in the oligophenylenevinylene, due to the higher

rigidity of the oligophenylenevinylene bridge A higher degree of flexibility in the oligo(phenylene-ethynylene) bridges allowed rotation of the phenyl rings around the ethynylene bonds, reducing the conjugation of the π system Significantly, the prefactor (A_{et}) for electron transfer through these oligo(phenylenevinylene) bridges was found to be independent of bridge length for lengths up to 28 Å The electronic coupling between the donor and acceptor moieties in these complexes was strong enough to allow electron tunnelling occur so rapidly that it did not limit the rate of electron transfer Instead, it was suggested that the electron transfer was rate limited by reorganisation of the redox species

Creager and co-workers described the rates of electron transfer across oligo(phenylethynyl) bridges and compared these rates with those obtained for related monolayers incorporating an aliphatic bridge [79] The bridges used in this study were highly conjugated and a β value of 0 36 $Å^{-1}$ was much lower than the typical value of ~1 0 $Å^{-1}$ for alkanethiol monolayers A low distance dependence of the conjugated system is thought to be due to the extended nature of the electronic orbitals, as compared to aliphatic bridges in which the orbitals are generally localised to small numbers of atoms Similar to the previous examples of conjugated bridging ligands,[77 78] high rates of electron transfer were observed for this system (k^o was 5×10^5 s^{-1}) for the shortest bridge The rate constant extrapolated from plots of k^o versus electron transfer distance was found to be the same for monolayers containing both conjugated and aliphatic bridges (~$6\ 6 \times 10^8$ s^{-1}) This value corresponds to the adiabatic limit, in which nuclear motion governs the rate of electron transfer and not the extent of electronic coupling According to Marcus theory (Section 1 1 3), adiabatic reactions occur when κ_{el}, the electronic transmission coefficient, is close to unity At zero separation between donor and acceptor moieties, the probability of electron transfer occurring once the transition state has been achieved is at a maximum The rate of electron transfer then becomes

$$k^{o} = \upsilon_{n}\exp(-\Delta G^{\neq}/RT) \qquad (1\ 38)$$

Therefore, the maximum reaction rate observed was governed solely by the nuclear frequency factor

The standard heterogenous electron transfer rate constants determined for osmium polypyridyl complexes that were bound to electrode surfaces via *trans*-1,2-bis(4-pyridyl)ethylene and 1,2-bis(4-pyridyl)ethane bridges were examined by Forster [80] Modelling the cyclic voltammetric response of the monolayers using a model describing electron tunnelling through space, assembled by Finklea and Henshaw,[22] indicated that the k^{o} value obtained for the conjugated bridge ($9\ 4 \times 10^{3}\ s^{-1}$) was 30 times smaller than that found for the aliphatic bridge ($30\ 5 \times 10^{4}\ s^{-1}$) The decreased rate constant was observed because the free energy of activation, $\Delta G^{\neq}$, was found to be larger ($11\ 4 \pm 0\ 8$ kJ mol^{-1}) for the conjugated bridge than for the non-conjugated bridge ($8\ 7 \pm 1\ 2$ kJ mol^{-1}) The electron transfer rate, k^{o}, depends on both a frequency factor and Franck-Condon barrier according to

$$k^{o} = A_{et}\exp(-\Delta G^{\neq}/RT) \qquad (1\ 39)$$

where A_{et} is the pre-exponential factor (equal to the product of κ_{el} the electronic transmission coefficient and ν_{n} the nuclear frequency factor) Using the k^{o} and $\Delta G^{\neq}$ values given above yields a pre-exponential factor of $11\ 1 \pm 0\ 5 \times 10^{6}\ s^{-1}$ for the non-conjugated bridge, that is approximately an order of magnitude higher than that found for the conjugated bridge ($0\ 9 \pm 0\ 3 \times 10^{6}\ s^{-1}$) This indicates that the degree of electronic coupling between the osmium centre and the electrode was higher when bridged via the non-conjugated bridge

This is a surprising result, considering that increased bridge conjugation usually results in increased rates of electron transfer However, as these values were

determined using a through space tunnelling model, this indicates that the non-conjugated bridge may be flexible enough to allow the $Os^{2+/3+}$ redox centre to approach the electrode surface closer than the rigid conjugated bridge will allow, resulting in an increased rate of electron transfer Therefore, this increase in the rate of heterogeneous electron transfer is due to the enhanced proximity of the redox centre to the electrode, rather than due to a direct bridge structure effect

1 4 4 CHEMICAL CONTROL OF HETEROGENEOUS ELECTRON TRANSFER

By chemically modifying the structure of a molecular bridge between a remote redox centre and an electrode surface, it may be possible to exert control over the rate of heterogeneous electron transfer The effect of chemically modifying the intervening bridge between an electrode and a remote redox centre has been examined by Cheng and co-workers [81] A series of ω-hydroxyalkanethiol monolayers were formed at gold electrodes and the rate of electron transfer across the bridge between the electrode and $Fe(CN)_6$ and $Os(bpy)_3$ in solution was measured Modification of the alkyl segment of the bridge by the insertion of single ether, olefin and alkyne moieties was found to affect the strength of electronic coupling across the bridge, resulting in reduced rates of heterogenous electron transfer The electronic coupling was found to be highest in the unmodified ω-hydroxyalkanethiol bridge, then reduced by 33 % upon introduction of an ether group, reduced by 65 % upon insertion of an olefin group and reduced by 62 % upon introduction of an alkyne group The decrease in the electronic coupling across was interpreted in terms of a disruption of the electronic coupling across the hydrocarbon bridge The coupling in bridges of this type is thought to be dominated by the overlap of and energy matching of the orbitals of the nearest neighbour atoms [82 83] The introduction of the modification interrupts these interactions, reducing the strength of coupling

The effect of replacing methylene groups of an alkanethiolate monolayer with carboxamide linkages has been reported by Creager and co-workers [13] The rates of electron transfer across unmodified ferrocene-terminated monolayers was compared with those in which the methylene units adjacent to the ferrocene were replaced by a carboxamide group The rates of electron transfer were practically the same for each type of monolayer when the number of bonds between the ferrocene and the electrode was the same This suggested that the contribution to the overall electronic coupling across the bridge from the carboxamide group was essentially the same as that from the methylene units

The authors described an "even-odd" effect on the rates of electron transfer If the number of methylene units in the bridges of the modified bridges was odd the rates of electron transfer were consistently higher than those observed for monolayers containing an even number of methylene units Conversely, for the unmodified monolayers, the rates were higher when the bridges contained an even number of methylene units A number of reasons for this were proposed Firstly, conformational variations in the redox group depending on whether the alkane chain had an odd or even number of bonds were proposed These subtle variations in the conformation of the redox active group could result in variations in the electronic coupling across the monolayer Secondly, it was proposed that the "even-odd" effect may have been due to a quantum interference effect, that results from taking a linear combination of the powers of the positive and negative eigenvalues corresponding to the various electronic states on the bridge This effect can result in weakened electronic coupling across the bridge

Sek and Bilewicz recently reported on the effects of modification of an alkanethiolate monolayer by introduction of amide bonds in place of methylene bonds [84] Three monolayer structures were used in this study Unmodified octadecanethiol monolayers, monolayers where one of the methylene bonds was replaced by an amide bond and monolayers where two of the methylene bonds were replaced by amide bonds In the case of the monolayers containing one

amide bond, the rate of electron transfer across the monolayer was approximately 5 times that observed for the unmodified alkanethiol monolayer This increase was attributed to the ability of the amide bonds to form an internal hydrogen-bonded network within the monolayer, thereby increasing the electronic coupling across the monolayer In the case of the monolayers that contained two amide bonds it was expected that a further increase in the electron transfer rate would be observed due to the presence of two planes of the hydrogen bonded network The electron transfer rate observed in this case was, however, roughly 5 5 times that of the unmodified monolayers This was explained as being due to an "even-odd" effect within the monolayer If the number of methylene units separating the amide linkages was odd, a different orientation of the external amide bonds when compared with the internal bonds This caused a difficulty in forming the hydrogen bonded network It was also noted that the position of the amide bonds with respect to the electrode surface could affect the electronic coupling across the monolayer If the amide plane was too far from the electrode surface, the efficiency of the overlap between the metal and monolayer orbitals was reduced and the hydrogen bond may not contribute to the electron transfer efficiency

1 4 4 1 EFFECT OF BRIDGE CONFORMATION

The effect of ring conformation in substituted alkanethiolate monolayers has been studied by Sumner and Creager [85] Ferrocene-terminated alkanethiolate monolayers were prepared that were unique in that they included a phenyl ring attached directly to one of the cyclopentadiene rings of ferrocene In this work, two different isomers were used, one in which the phenyl ring was substituted at the 1 and 4 positions and one in which the phenyl ring was substituted at the 1 and 3 positions It was found that the rate of electron transfer across the monolayers that included the 1,4 substitution on the phenyl moiety of the bridge were a factor of 10 higher than those for the bridges containing the 1,3 substituted phenyl ring Similar to their earlier work,[13] the authors explained the difference in the electronic coupling across the two bridges as due to a quantum interference

phenomenon involving a cancellation of contributions from two separate electron transfer pathways Coupling depends on both the energy and the sign of the orbitals involved and a cancellation of the coupling is observed if the orbitals have similar energy but different signs In the case of the 1,4 substituted bridge, the orbitals involved have the same energies and sign and their contributions to the coupling are additive and do not cancel This behaviour was observed for monolayers where the number of methylene units in the bridge was large (> 11) When the bridges were shorter than this it was found that the rates of electron transfer were indistinguishable for both bridges This was interpreted as due to the phenylferrocene "bending over" to contact the monolayer surface Tunnelling between the ferrocene and the electrode is then assumed to be predominantly through the adjacent (non-electroactive) alkanethiols

1 4 4 2 HYDROGEN BONDING IN HETEROGENEOUS ELECTRON TRANSFER

Studies on biosystems have revealed that hydrogen-bonding plays a critical role in dictating the efficiency of long distance electron transfer [86] Therefore, studies of electron transfer reactions across hydrogen-bonded molecular bridges is extremely important for understanding biosystems Electron transfer across hydrogen-bonded bridges has been described by Yu and co-workers [87] In this study, both Langmuir-Blodgett films and self-assembled films were used to compare the rates across bilayer bridges that contained ionic bonding and hydrogen bonding A monolayer of either 2-aminoethanethiol or 4-aminothiophenol was formed on a gold electrode by self-assembly Langmuir-Blodgett monolayer films of 4-octyl-4'-(3-carboxy-trimethylene-oxy)-azobenzene (ABD) was then formed on the underlying aminothiol monolayer The interface between the ABD layer and the 4-aminothiophenol is predominantly ionic in nature, whereas the ABD/2-aminoethanethiol interface is predominantly hydrogen-bonded The rate of electron transfer across the ionic bridge was

significantly higher than that observed for electron transfer across the hydrogen-bonded bridge ($k^{o} = 0\ 18\ s^{-1}$ and $0\ 09\ s^{-1}$ respectively)

Electron transfer across hydrogen-bonded bridges had previously been described in a study by De Rege and co-workers [12] In this work, a series of porphyrin donor and acceptor moieties were linked by covalent, π-conjugated, σ-bonded and hydrogen-bonded bridges The rate of electron transfer across the hydrogen-bonded bridge was found to be between that observed for the σ-bonded and π-bonded bridges This illustrated that not only were hydrogen bonds capable of supporting electron transfer but that highly efficient electron transfer can occur across these bridges

1 4 4 3 EFFECT OF PROTONATION ON ELECTRON TRANSFER

In a recent study, Alvarez and co-workers described the irreversible and reversible modulation of electron transfer rates across dinuclear ferrocene compounds linked via the bridging fragment CH_2-N(R)-CH_2 [88] A series of these compounds containing different aliphatic R groups was prepared, with varying degrees of steric bulk A further series of compounds was prepared containing aromatic R groups The extent of electronic communication between the ferrocene moieties was strongest in low polarity solvents and when the attached R group was bulky The electronic communication between the ferrocene moieties was found to be a *through space* mechanism Both methylation and protonation of the bridge was found to practically destroy the electronic coupling between the ferrocene centres The authors suggested that the positive charge induced on the bridge by protonation or methylation may cause increased solvation or ion association with a resultant shielding of the electrostatic interaction between the ferrocene centres Importantly, the modulation of the degree of electronic coupling between the two ferrocene centres was fully reversible for the protonated bridge, illustrating an example of a switchable molecule

Forster and O'Kelly[89] described the modulation of the heterogenous electron transfer rate across metal/monolayers interfaces Monolayers of $[Os(bpy)_2(p3p)_2]^{2+}$ were formed on platinum electrodes, where p3p is 4,4'-trimethylenepyridine Only one of the 4,4'-trimethylenepyridine ligands adsorbed to the platinum surface, leaving the other free to be protonated at the pendant nitrogen The electrochemical response of the monolayers was consistent with electron tunnelling occurring via a through space mechanism The standard heterogenous electron transfer rate constant, k^0, was found to decrease from $6\ 1 \times 10^4\ s^{-1}$ to $1\ 6 \times 10^4\ s^{-1}$ upon protonation of the free ligand Measurement of the free energy of activation, $\Delta G^{\neq}$, indicated that the pH sensitivity of the electron transfer rate was due to changes in the pre-exponential factor, rather than changes in $\Delta G^{\neq}$ Therefore, a weaker electronic coupling between the metallic states of the electrode and the orbitals of the complex was observed upon protonation of the monolayer It was proposed that protonation increased the through space electron transfer distance, either by tilting of the adsorbate with respect to the electrode surface or by extension of the methylene spacer units upon protonation However, in superexchange mechanisms, the rate of electron transfer depends algebraically on the energy difference between the energy levels of the bridge and the donor/acceptor [72] Therefore, in this system, the decrease in the rate of electron transfer upon protonation of the complex may have been due to a shift in energy of either the metal redox centre or the bridge energy levels For example, electron superexchange occurs when the donor/acceptor energy levels are close in energy to the LUMO of the bridge Therefore, if electron transfer in this system occurred via a superexchange mechanism and protonation of the complex causes an increase in this energy difference, a decrease in the rate of electron transfer would be observed

1 5 CONCLUSIONS

As discussed previously, the main objective of this work is to study the effect of structure on electron transfer reactions Towards this, monolayers and solid-state films of redox-active species at electrode surfaces have been employed This chapter has laid out the contemporary models used to describe electron transfer In particular, the Butler-Volmer formulation of electrode kinetics and the Marcus theory of electron transfer have been described Both of the these models are widely used in the literature and are used to describe many experimental observations In later chapters, these theories shall be used in elucidating the heterogeneous electron transfer behaviour of monolayers across the electrode/monolayer interface

The formation and characterisation of modified electrode surfaces is extremely important as electron transfer reactions are exquisitely sensitive to parameters such as distance In this chapter, the main methods of forming and characterising electrode surfaces have been outlined The electrochemical techniques used to characterise the electron transfer behaviour of monolayer and solid-state layers has also been discussed

Finally, the effects of bridge structure on bridge mediated electron transfer has been discussed, based on current knowledge Effects of chemical modification, protonation and bonding on electron transfer dynamics across molecular bridges has been described This should provide an insight into the current scientific knowledge regarding the effects of the bridge on mediated electron transfer

1 6 REFERENCES

1 Kropf, M , van Loyen, D , Schwarz, O , Durr, H , *J Phys Chem A*, **1998**, *102*, 5499

2 Moser, C C , Keske, J M , Warnacke, K , Farid, R S , Dutton, P L , *Nature*, **1992**, *355*, 796

3 Gust, D , Moore, T A , *Science*, **1989**, *244*, 35

4 Murray, R W , Ed , *Molecular Design of Electrode Surfaces*, Vol 22, Wiley, New York, **1992**

5 Wrighton, M S , *Science*, **1986**, *231*, 32

6 Chidsey, C E D , Murray, R W , *Science*, **1986**, *231*, 25

7 Richardson, D E , Taube, H , *J Am Chem Soc* , **1983**, *105*, 40

8 Balzani, V , Juris, A , Venturi, M , *Chem Rev* , **1996**, *96*, 759

9 Chidsey, C E D , *Science*, **1991**, 251, 919

10 Acevedo, D , Abruña, H D , *J Phys Chem* , **1991**, *95*, 9590

11 Forster, R J , Faulkner, L R , *J Am Chem Soc* , **1994**, *116*, 5444

12 de Rege, P J F , Williams, S A , Therien, M J , *Science*, **1995**, *269*, 1409

13 Sumner, J J , Weber, K S , Hockett, L A , Creager, S E , *J Phys Chem B*, **2000**, *104*, 7449

14 Ishida, T , Mizutani, W , Akiba, U , Umemura, K , Inoue, A , Choi, N , Fujihira, M , Tokumoto, H , *J Phys Chem B*, **1999**, *103*, 1686

15 Miller, R J D , McLendon, G L , Nozik, A J , Schmickler, W , Willig, F , *Surface Electron Transfer Processes*, VCH, **1995**

16 Bard, A J , Faulkner, L R , *Electrochemical Methods Fundamentals and Applications*, 2nd Edn , Wiley, **2000**

17 Marcus, R A , *Electrochim Acta* , **1968**, *13*, 955

18 Hush, N S , *Electrochim Acta* , **1968**, *13*, 1005

19 Marcus, R A , *J Chem Phys* , **1965**, *43*, 679

20 Marcus, R A , *Ange Chem Int Ed Eng* , **1993**, *32*, 1111

21 Hush, N S , *Trans Faraday Soc* , **1961**, *57*, 557

22 Finklea, H O , Hanshaw, D D , *J Am Chem Soc* , **1992,** *114,* 3173

23 Finklea, H O , Liu, L , Ravenscroft, M S , Punturi, S , *J Phys Chem* , **1996**, *100*, 18852

24 Weber, K , Hockett, L , Creager, S , *J Phys Chem B*, **1997**, *101*, 8286

25 Song, S , Clark, R A , Bowden, E F , Tarlov, M J , *J Phys Chem* , **1993**, *97*, 6564

26 Feng, Z Q , Imabayashi, S , Kakiuichi, T , Niki, K , *J Chem Soc , Faraday Trans* , **1997**, *93*, 1367

27 Richardson, J N , Peck, S R , Curtin, L S , Tender, L M , Terrill, R H , Carter, M T , Murray, R W , Rowe, G K , Creager, S E , *J Phys Chem* , **1995**, *99*, 766

28 Finklea, H O , Ravenscroft, M S , Snider, D A , *Langmuir*, **1993**, *9*, 223

29 Ravenscroft, M S , Finklea, H O , *J Phys Chem* , **1994**, *98*, 3843

30 Ju, H , Leech, D , *Phys Chem Chem Phys* , **1999**, *1*, 1549

31 Bretz, R L , Abruña, H D , *J Electroanal Chem* , **1995**, *388*, 123

32 Acevedo, D , Bretz, R L , Tirado, J D , Abruña, H , D , *Langmuir*, **1994**, *10*, 1300

33 Tirado, J D , Abruña, H D , *J Phys Chem* , **1996**, *100*, 4556

34 Forster, R J , Faulkner, L R , *J Am Chem Soc* , **1994**, *116*, 5453

35 Forster, R J , Faulkner, L R , *Langmuir*, **1995**, *11*, 1014

36 Bond, A M , Scholz, F , *J Phys Chem* , **1991**, 95, 7460

37 Bond, A M , Scholz, F , *Langmuir*, **1991**, *7*, 3197

38 Kulesza, P J , Faulkner, L R , *J Am Chem Soc* , **1993**, *115*, 11878

39 Dostal, A , Meyer, B , Scholz, F , Schroder, Bond, A , Marken, F , Shaw, S J , *J Phys Chem* , **1995**, *99*, 2096

40 Deuber, R E , Bond, A M , Dickens, P G , *J Electrochem Soc* , **1992**, *139*, 2363

41 Kulesza, P J , Faulkner, L R , Chen, J , Klemperer, W G , *J Am Chem Soc* , **1991**, *113*, 379

42 Bond, A M , Marken, F , *J Electroanal Chem* , **1994**, *372*, 125

43 Bond, A M , Lamprecht, A , Tedesco, V , Marken, F , *Inorg Chim Acta* , **1999**, *291*, 21

44 Shaw, S J , Marken, F , Bond, A M , *J Electroanal Chem* , **1996**, *404*, 227

45 Bond, A M , Cooper, J B , Marken, F , Way, D M , *J Electroanal Chem* , **1995**, *396*, 407

46 Bond, A M , Fletcher, S , Symons, P G , *Analyst*, **1998**, *123*, 1891

47 Bond, A M , Colton, R , Marken, F , Walter, J N , *Organometallics*, **1994**, *13*, 5122

48 Bond, A M , Fletcher, S , Marken, F , Shaw, S J , Symons, P G , *J Chem Soc , Faraday Trans* , **1996**, *92*, 3925

49 Acevedo, D , Abruna, H D , *J Phys Chem* , **1991**, *95*, 9590

50 Brown, A P , Anson, F C , *Anal Chem* , **1977**, *49*, 1589

51 Tirado, J D , Acevedo, D , Bretz, R L , Abruña, H D , *Langmuir*, **1994**, *10*, 1971

52 Campbell, J L E , Anson, F C , *Langmuir*, **1996**, *12*, 4008

53 Gruner, W , Kunath, J , Kalnishevskaja, N , Posokin, J V , Brainina, K Z , *Electroanalysis*, **1993**, *5*, 243

54 Bond, A M , Colton, R , Daniels, F , Fernando, D R , Marken, F , Nagaosa, Y , Van Steveninck, R F M , Walter, J N , *J Am Chem Soc* , **1993**, *115*, 9556

55 Forster, R J , Keyes, T E , Bond, A M , *J Phys Chem , B*, **2000**, *104*, 6389

56 Forster, R J , Keyes, T E , *Phys Chem Chem Phys* , **2001**, *3*, 1336

57 Binnig, G , Rohrer, H , Gerber, C , Weibel, E , *Phys Rev Lett* , **1982**, *49*, 57

58 Poirier, G E , *Chem Rev* , **1997**, *97*, 1117

59 Kobayashi, K, Yamada, H , Horiuchi, T , Matsushige, K , *App Surf Sci* , **1999**, *144*, 435

60 Cavallini, M , Bracali, M , Aloisa, G , Guidelli, R , *Langmuir*, **1999**, *15*, 3003

61 Munakata, H , Kuwabata, S , Ohko, Y , Yoneyama, H , *J Electroanal Chem* , **2001**, *496*, 29

62 Hudson, J E , Abruña, H D , *J Phys Chem* , **1996**, *100*, 1036

63 Binnig, G , Quate, C F , Gerber, C , *Phys Rev Lett* , **1986**, *56*, 930

64 Woodruff, D P , Delchar, T A , *Modern Techniques of Surface Science*, 2nd Edn , Cambridge, 1994

65 Jaschke, M , Schonherr, H , Wolf, H , Butt, H –J , Bamberg, E , Besocke, M K , Ringsdorf, H , *J Phys Chem* , **1996**, *100*, 2290

66 Wolf, H , Ringsdorf, H , Delamarche, E , Takami, T , Kang, H , Michel, B , Gerber, Ch , Jaschke, M , Butt, H –J , Bamberg, E , *J Phys Chem* , **1995**, *99*, 7102

67 Liu, G –Y , Fenter, P , Chidsey, C E D , Ogletree, D F , Eisenberger, P , Salmeron, M , *J Chem Phys* , **1994**, *101*, 4301

68 Lackowski, W M , Campbell, J K , Edwards, G , Chechik, V , Crooks, R M , *Langmuir*, **1999**, *15*, 7632

69 Kudelski, A , *Surf Sci* , **2002**, *502*, 219

70 Corio, P , Andrade, G F S , Diogenes, I C N , Moreira, I S , Nart, F C , Temperini, M L A , *J Electroanal Chem* , **2002**, *520*, 40

71 Wightman, R M , Wipf, D O , in *Electroanalytical Chemistry*, vol 15, Bard, A J , Ed , Marcel Dekker, New York, **1989**

72 Keyes, T E , Forster, R J , Jayaweera, P M , Coates, C G , McGarvey, J J , Vos, J G , *Inorg Chem* , **1998**, *37*, 5925

73 Smalley, J F , Feldberg, S W , Chidsey, C E D , Linford, R , Newton, M R , Liu, Y –P , *J Phys Chem* , **1995**, *99*, 13141

74 Forster, R J , Keyes, T E , Vos, J G , *Interfacial Supramolecular Assemblies Electrochemical and Photophysical Properties*, Wiley, **2002**

75 McConnell, H M , *J Chem Phys* , **1961**, *35*, 508

76 Forster, R J , *Inorg Chem* , **1996**, *35*, 3394

77 Sikes, H D , Smalley, J F , Dudek, S P , Cook, A R , Newton, M D , Chidsey, C E D , Feldberg, S W , *Science*, **2001**, *291*, 1519

78 Dudek, S P , Sikes H D , Chidsey, C E D , *J, Am Chem Soc* , **2001**, *123*, 8033

79 Creager, S , Yu, C J , Bamdad, C , O Connor, S , Maclean, T , Lam, E , Chong, Y , Olsen, G T , Luo, J , Gozin, M , Kayyem, J F , *J Am Chem Soc* , **1999**, *121*, 1059

80 Forster, R J , Loughman, P J , Figgemeier, E , Lees, A C , Hjelm, J , Vos, J G , *Langmuir*, **2000**, *16*, 7871

81 Cheng, J , Saghi-Szabo, G , Tossell, J A , Miller, C J , *J Am Chem Soc* , **1996**, *118*, 680

82 Curtiss, L A , Naleway, C A , Miller, *J Phys Chem* , **1993**, *97*, 4050

83 Liang, C , Newton, M D , *J Phys Chem* , **1993**, *97*, 3199

84 Sek, S , Bilewicz, R , *J Electroanal Chem* , **2001**, *509*, 11

85 Sumner, J J , Creager, S E , *J Am Chem Soc* , **2000**, *122*, 11914

86 Gray, H B , Winkler, J R , *Ann Rev Biochem* , **1996**, *65*, 537

87 Yu, H Z , Xia, N , Zhang, J , Liu, Z F , *J Electroanal Chem* , **1998**, 448, 119

88 Alvarez, J , Yuhua, N , Ren, T , Kaifer, A E , *J Supra Chem* , **2001**, 1, 7

89 Forster, R J , O'Kelly, J P , *J Phys Chem* , **1996**, 100, 3695

CHAPTER 2

MICROELECTRODE CONSTRUCTION, SYNTHESIS AND CHARACTERISATION OF OSMIUM POLYPYRIDYL COMPLEXES

2 1 INTRODUCTION

In this study, the major goal is to develop an understanding of how the structure of molecular bridges affects the rate of heterogeneous electron transfer In addition, some of the factors that control electron transfer rates through solids are examined Monolayers of alkanethiol compounds adsorbed at gold electrode surfaces have been extensively used to study the effects of parameters such as temperature,[1 2] electrolyte,[3] solvent[4] and free energy[5] on the rate of heterogeneous electron transfer across the electrode/monolayer interface However, over the past decade, the use of alternative adsorbates to study these effects has increased steadily Osmium polypyridyl complexes have gained significant interest as suitable adsorbate species for the study of electron transfer reactions This is due to a number of factors, including the ease of adsorption onto metals such as gold and platinum as monolayers, the facile electrochemical behaviour, the synthetic flexibility of the complexes and their stability in a number of redox states, including accessible ligand based processes [6 7 8 9 10 11 12]

Solid deposits of osmium polypyridyl complexes have been shown to exhibit unusually ideal electrochemical responses when mechanically attached to electrode surfaces [13 14 15] This approach is a relatively novel method for studying the redox properties of solid materials and permits the study of electrochemically driven processes such as mass and charge transfer in the solid state Processes such as crystallisation can also accompany redox switching of solid materials and these materials provide a convenient means of studying these phenomena [13 14]

In this study, osmium polypyridyl complexes are used to investigate the effects of bridge structure on electron transfer reactions Monolayers of surface active, monomeric osmium bipyridyl species are used to probe the effects of bridge protonation and deprotonation on the rate of electron transfer between the osmium metal centre and an electrode surface Solid deposits of a dimeric osmium

bipyridyl complex are also used to investigate electron transfer reactions within solid materials

The majority of the work carried out on these materials at electrode surfaces is performed using microelectrodes Microelectrodes are defined as electrodes whose critical dimension is in the micron range By decreasing the dimensions of electrode surfaces, adverse effects such as ohmic drop can be significantly reduced and rapid electrode response times can be achieved [16 17] The development of microelectrode technology has significantly broadened the amount of information that can be obtained from electrochemical experiments [18] Detailed examinations of the kinetics of electrode reactions can now be performed at short timescales, revolutionising our understanding of electrode reactions [19 20]

In this chapter, the construction and characterisation of gold and platinum microelectrodes are described The electrodes constructed in this study had radii in the range 2 5 – 25 μm and the short response times associated with such small electrodes are discussed m this chapter The synthesis and characterisation of the osmium polypyridyl complexes used is then described Complete characterisation of these complexes was carried out using a range of analytical techniques, including HPLC, UV-Vis spectrophotometry, NMR spectroscopy and elemental analysis

2 2 MICROELECTRODES

2 2 1 INTRODUCTION

The past two decades have seen a vast increase in the amount of scientific publications devoted to the area of microelectrodes [16-18] The reduced response time of microelectrodes compared with conventional sized macroelectrodes (millimeter dimensions) enables electrochemical experiments to be carried out at extremely short timescales [21,22] This behaviour presents electrochemists with the ability to probe not only fast electrochemical events but also novel electroanalytical applications Because of their unique mass transport properties, microelectrodes can be employed at both short and long experimental timescales, greatly increasing the amount of information that can be obtained from electrochemical experiments The immunity of microelectrodes to ohmic drop allows electrochemical experiments to be performed in media such as non-polar solvents and solids,[17] experiments that are practically impossible using macroelectrodes

In this study, the heterogeneous electron transfer kinetics of some osmium polypyridyl complexes are investigated Typical k^o values for analogous complexes are large ($\geq 10^4$ s^{-1}), requiring the use of microelectrodes, if accurate data are to be obtained [23,24] In the following sections, the construction and characterisation of microelectrodes, which have nominal radii in the range 2 5-25μm are described

2 2 2 MICROELECTRODE CONSTRUCTION

Microelectrodes were constructed using a method similar to that previously reported [25]

2 2 2 1 PLATINUM MICROELECTRODE CONSTRUCTION

Platinum microelectrodes were constructed by sealing a fine wire of platinum (Goodfellow Metals, Cambridge, UK) in soft glass The radii of the microwires used were in the range 2 5-25 μm Soft glass tubing (o d 5 mm , i d 3 mm) was cut into pieces of about 8 cm in length One end of the tube was then heated in a butane flame until the tubing partially collapsed (leaving an aperture of inner diameter approximately 1 mm) The tapered tubes were then soaked in dilute nitric acid for several hours to remove any contamination After cleaning, the tubes were rinsed with Milli-Q de-ionised water and then soaked in acetone for 2 hours Finally, the pieces of tubing were rinsed with Milli-Q water and allowed to dry

An aluminium transition wire (approximately 4 cm in length) was soldered to a piece of copper hook-up wire The transition wire was stripped of its outer plastic protective covering and bent into a zig-zig shape This configuration is used to ensure stability of the wire within the glass tubing Approximately 3 cm of the microwire was then soldered to the transition wire The microscopic wire was then cleaned in dilute nitric acid for one hour, rinsed with Milli-Q water and then soaked in acetone for another hour Finally, the wire was allowed to dry in air

The wire assembly was then passed through the glass tubing, allowing approximately 0 5 cm of the microwire to be exposed through the tapered end of the tubing The tapered end of the glass tubing was then heated in a butane flame until the glass completely collapsed around the microwire, forming a seal between the glass and the microwire A plastic cap was then glued to the top of the electrode assembly using an epoxy adhesive, both stabilising the hook-up wire and preventing contamination of the electrode interior

2 2 2 2 GOLD MICROELECTRODE CONSTRUCTION

Gold microelectrodes were constructed by sealing a fine wire of gold (Goodfellow Metals, Cambridge, UK) in soft glass The radii of the microwires used were in the range 5-25 μm Soft glass tubing (o d 5 mm , i d 3 mm) was cut into pieces of about 16 cm in length The tubes were then soaked in dilute nitric acid for several hours to remove any contamination After cleaning, the tubes were rinsed with Milli-Q de-ionised water and then soaked in acetone for 2 hours Finally, the pieces of tubing were rinsed with Milli-Q water and allowed to dry The dried glass tubes were heated in the centre and a tapered centre was formed that was approximately 4 cm long Once cool, the glass was snapped at the centre of the taper

An aluminium transition wire (approximately 4 cm in length) was soldered to a piece of copper hook-up wire The transition wire was stripped of its outer plastic protective covering and bent into a zig-zig shape This configuration is used to ensure stability of the wire within the glass tubing Approximately 3 cm of the microwire was then soldered to the transition wire The microscopic wire was then cleaned in dilute nitric acid for one hour, rinsed with Milli-Q water and then soaked in acetone for another hour Finally, the wire was allowed to dry in air

The wire assembly was then passed into the glass tubing and the closed, tapered end was sealed around the gold wire by heating in a butane flame This was done until the glass seal was approximately 4 mm from the end of the gold microwire A plastic cap was then glued to the top of the electrode assembly using an epoxy adhesive, both stabilising the hook-up wire and preventing contamination of the electrode interior The glass covering the end of the gold microwire was then removed using fine sand paper, exposing the metal

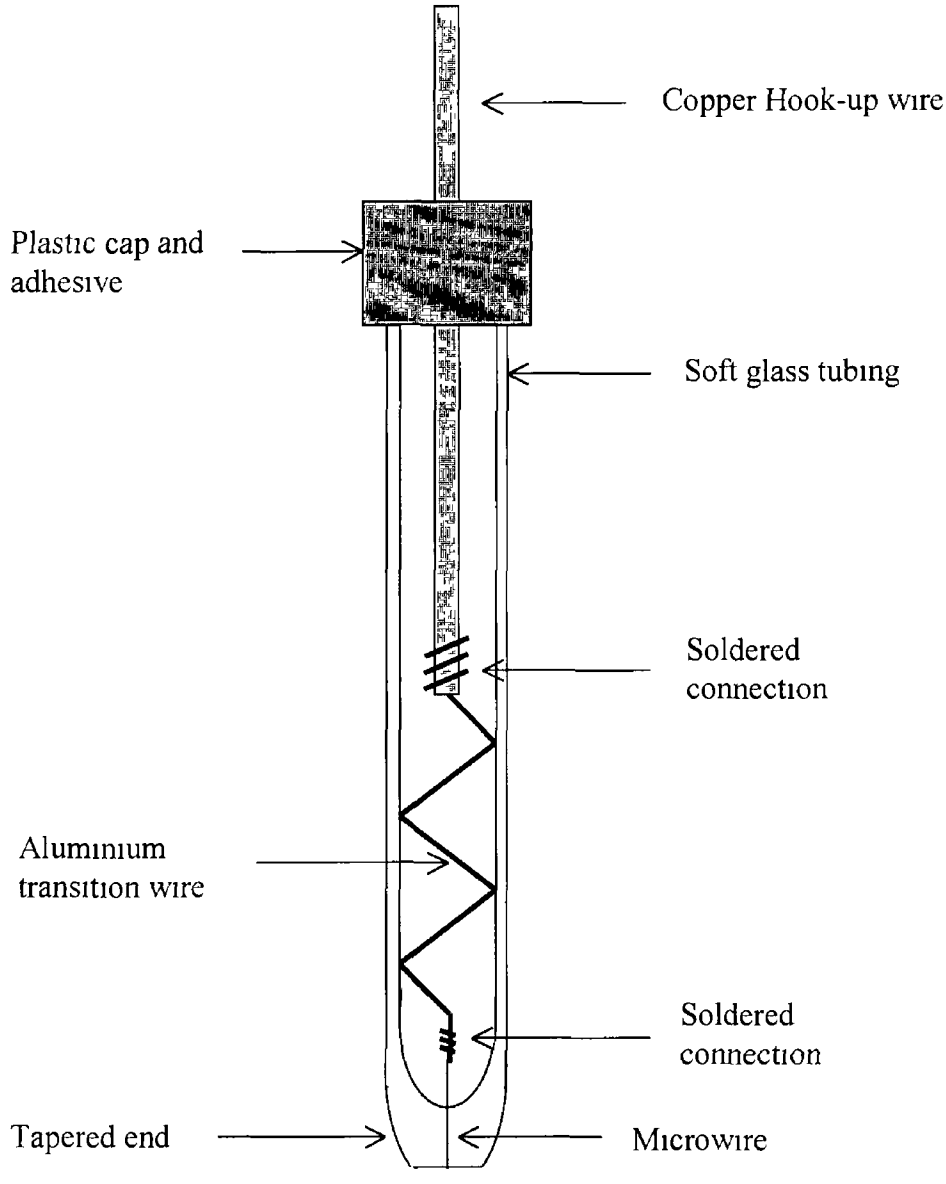

Figure 2 1 Design of the microelectrodes constructed for this study

The ends of the electrodes constructed using both techniques were then polished using fine sand paper until the end of the electrode appeared flat Electrical connection between the exposed microdisc and the hook-up wire was then verified by performing a cyclic voltammetry experiment in either 1 0 M $LiClO_4$ electrolyte or 0 1 M H_2SO_4 Once electrical connection was confirmed the electrode was allowed to stand in Milli-Q water overnight to check for any leaks into the electrode body The presence of leakage into the electrode interior was indicated by a substantial increase in the background current If any leaks were found, the electrode was discarded Approximately 90% of the electrodes constructed using this approach were successfully made and were used routinely in electrochemical experiments The design of the microelectrodes used in this study is shown in Figure 2 1

2 2 3 ELECTRODE POLISHING

Electrodes that had been successfully sealed were then polished using aqueous slurries of alumina applied to a felt polishing pad Polishing was carried out by holding the electrode surface against the polishing pad and gently performing "figure of eight" movements with the electrode Polishing was performed using successively finer grades of alumina and the alumina grades used were 12 5, 5, 1, 0 3 and 0 05 μm Between each grade of alumina the electrodes were rinsed thoroughly using Milli-Q water and then sonicated in Milli-Q water for 5 minutes

The progression of the polishing was monitored by cyclic voltammetry in 0 1 M H_2SO_4 The quantities of interest in a cyclic voltammogram of both a gold and a platinum electrode in acid solution are shown in Figures 2 2 and 2 3 In these experiments, the potential is cycled between potential limits chosen to initially oxidise and then reduce the surface The background currents and the total area under the surface oxide reduction peak were used to monitor the effect of polishing on the surface roughness In the case of platinum, the area under the

hydrogen adsorption and desorption peaks can also be used [28] Both of these quantities will decrease with decreasing electroactive surface area

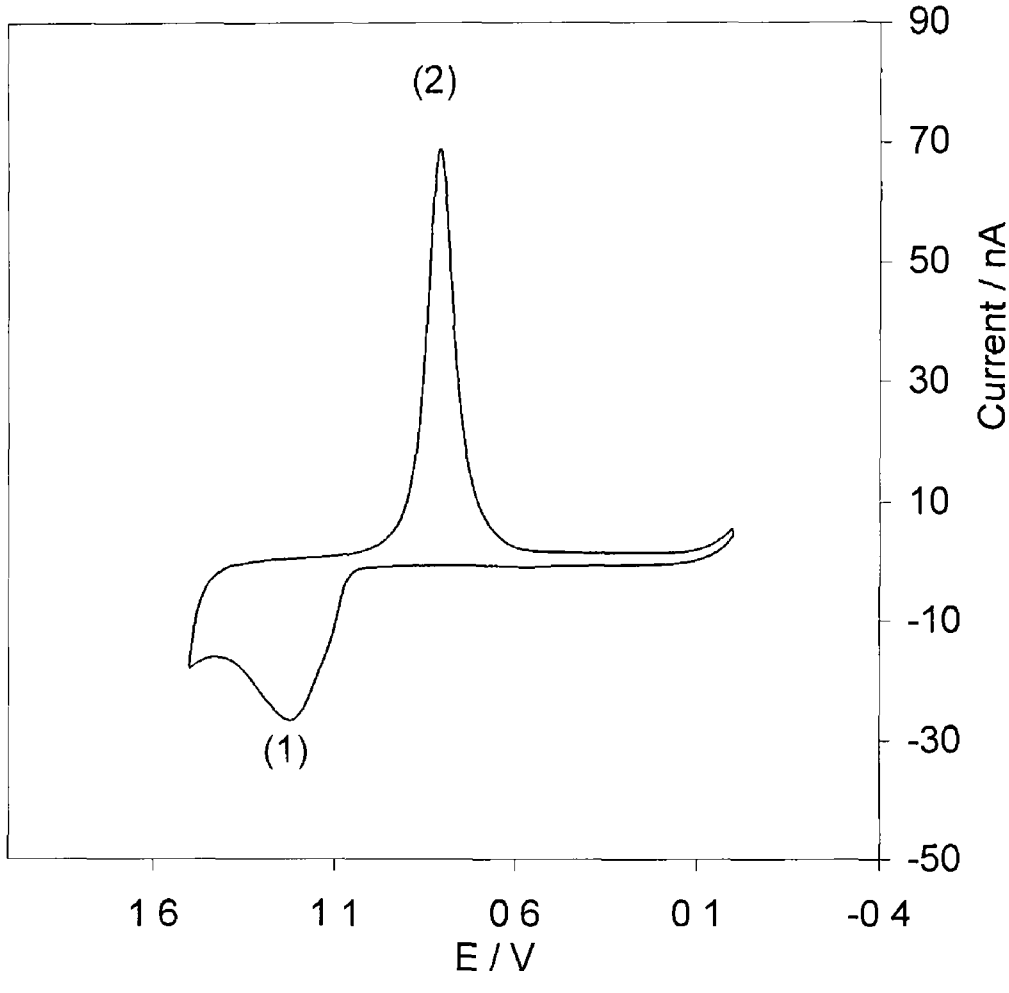

Figure 2 2 Cyclic voltammogram of a 25 μm gold microelectrode in 0 1 M H_2SO_4 The scan rate is 0 5 V s^{-1} The features of interest in the CV are (1) formation of surface oxide layer and (2) reduction of surface oxide layer

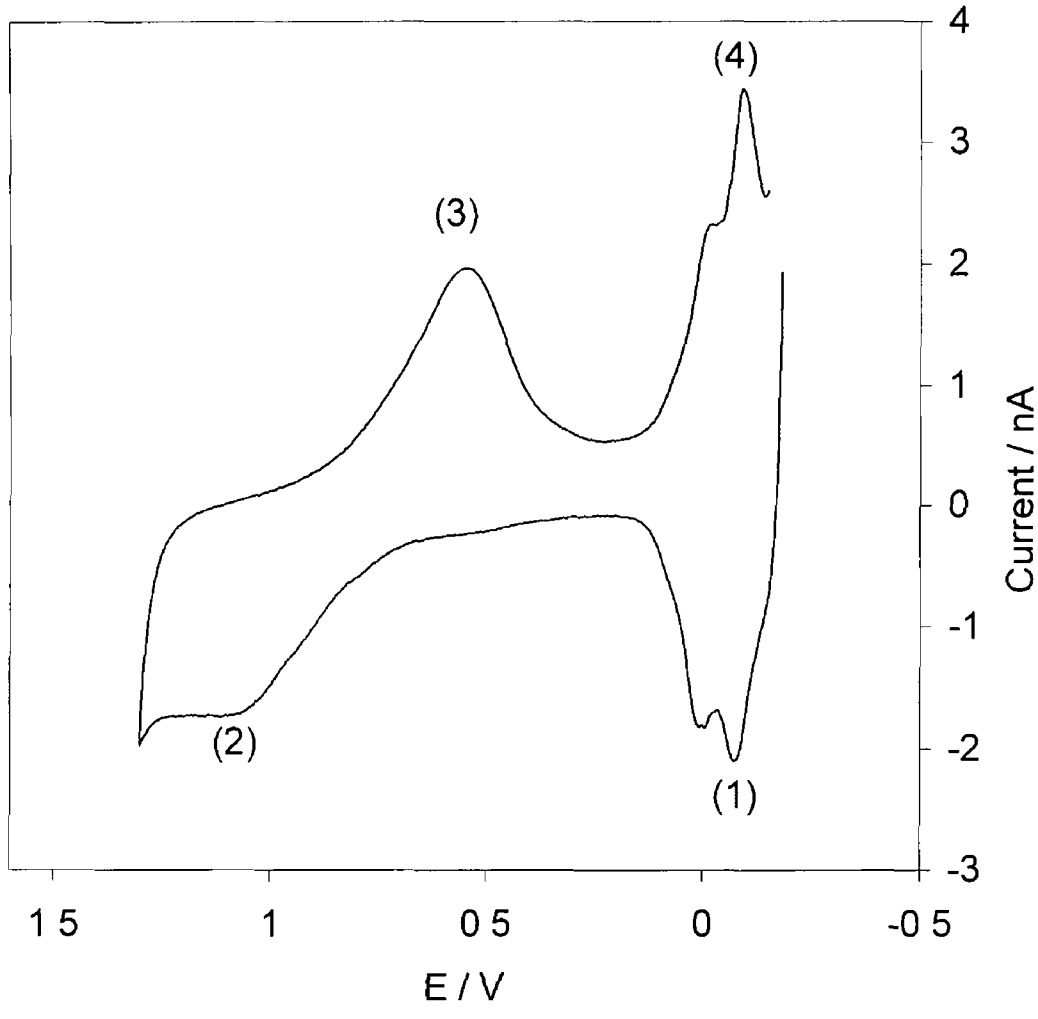

Figure 2 3 Cyclic voltammogram of a 5 μm gold microelectrode in 0 1 M H_2SO_4 cycled between –0 175 V and +1 3 V vs Ag/AgCl The scan rate is 1 V s^{-1} The features of interest in the CV are (1) oxidation of adsorbed hydrogen, (2) formation of platinum oxide layer, (3) reduction of the surface oxide layer and (4) formation of adsorbed hydrogen layer

2 2 4 DETERMINATION OF ELECTRODE AREA

Due to the well characterised formation of oxide monolayers on polycrystalline gold and platinum, the charge passed in removal of these adsorbed layers is routinely used to determine the real or microscopic surface area of these electrodes [28] Other methods for estimation of the surface area of microelectrodes include iodine adsorption at gold,[26] and the use of the geometric or projected surface area, without consideration of the microscopic roughness of the surface [27] In the case of platinum, hydrogen adsorption from solution may also be used to determine the microscopic area This is impossible at gold electrodes as adsorbed monolayers of hydrogen are not formed at gold surfaces

The method of oxide reduction for the determination of the real surface areas of both platinum and gold microelectrodes assumes that oxygen is adsorbed at the surface in a monomolecular layer and also that one oxygen atom is attached to one metal atom [28] Once the contribution from double layer charging has been subtracted, the charge passed during the reduction of the metal oxide layer can then be used to determine the real surface area of the electrodes according to Equation 2 1

$$A = \frac{Q_r}{Q_s} \qquad (2\ 1)$$

where A is the microscopic area of the electrode, Q_r is the charge under the surface oxide reduction peak and Q_s is the standard value for the surface oxide charge per unit area for each metal The reference value[28] for polycrystalline platinum is 420 $\mu C\ cm^{-2}$ and for polycrystalline gold is 390 $\mu C\ cm^{-2}$ However, some uncertainty does arise in this approach due to the difficulty in subtracting contributions from double layer charging and other Faradaic processes Also, the charge passed during reduction of the oxide monolayer depends on the crystal face of the metal [28] The surface roughness of the microelectrodes was calculated

by dividing the microscopic surface area by the geometric or projected area Typical surface roughness values for the microelectrodes were between 1 3 and 1 8

Once the microscopic areas of the electrodes were determined, the electrodes were electrochemically cycled in deoxygenated aqueous 0 1 M $LiClO_4$ electrolyte solution until a steady background response was observed This is important to ensure complete reduction of any surface oxide and also to ensure full desorption of any surface hydrogen, in the case of platinum After this final step, the electrodes were ready for use

2 2 5 DOUBLE LAYER CAPACITANCE AND CELL RESISTANCE

For any electrode in an electrolyte at a potential E_1, there is an associated charge at the surface that is counterbalanced by a layer of oppositely charged ions in solution This electrochemical double layer can, in most respects, be considered to behave like an electrolytic capacitor Upon changing the potential of the electrode to E_2, electrons must move into or away from the surface, depending on the direction of the potential change Therefore, a current must flow to achieve the desired potential at the electrode surface This is known as the charging current and must be distinguished from the Faradaic currents which flow due to electrochemical processes at the electrode surface In any electrochemical experiment, it is highly desirable to increase the ratio of Faradaic to charging current to ensure that meaningful information can be obtained from the electrochemical experiment

Upon changing an electrode potential by a value ΔE, a charging current, i_c, will flow as a function of time, t, according to Equation 2 2

$$i_C = \frac{\Delta E}{R} \exp\left(\frac{-t}{RC}\right) \qquad (2\ 2)$$

where R is the cell resistance and C is the capacitance of the microelectrode The capacitance[28] is typically of the order of 20 μF cm^{-2} Unlike real capacitors, however, the capacitance of the electrode typically depends on the applied potential The product RC is known as the cell time constant At short experimental timescales, the Faradaic and charging currents are convolved and only at timescales that are 5 to 10 times longer than the RC cell time constant can meaningful electrochemical measurements be made At these timescales, the contribution of the charging current to the observed current is negligible

The resistance, R, of an electrochemical cell is given by Equation 2 3 for a disc shaped electrode

$$R = \frac{1}{4\pi\kappa r} \qquad (2\ 3)$$

where κ is the specific conductance of the electrolytic medium and r is the electrode radius Therefore, the resistance of an electrochemical cell increases with decreasing electrode radius The capacitance is proportional to the electrode area (or r^2) and so the RC constant is proportional to r as given by Equation 2 4

$$RC \propto \frac{1}{r} \times r^2 \quad \text{or } r \qquad (2\ 4)$$

By decreasing the radius of a microelectrode, the response time of the electrode becomes smaller allowing electrochemical measurements to be performed at shorter times

When Faradaic and charging currents are flowing through an electrolytic solution, they generate a potential that acts to weaken the applied potential by an amount iR, where i is the total current and R is the cell resistance iR drop can result in distorted current responses and shifted peak potentials in cyclic voltammetry These ohmic effects can be significantly reduced with the use of microelectrodes

because the currents at microelectrodes are significantly smaller than those observed at macroelectrodes

RC cell time constants were measured for all microelectrodes by high-speed chronoamperometry using a custom-built function generator-potentiostat [6] The rise time of the instrument is less than 10 ns and allows potential steps of varying pulse width and amplitude to be applied to a two-electrode cell A platinum flag and an Ag/AgCl reference electrode were combined to form a counter electrode The flag lowered the resistance and provided a high frequency path Typical current-time transients obtained for a 12 5 μm radius platinum microelectrode are shown in Figure 2 4 Transients were recorded in aqueous $LiClO_4$ electrolytes of increasing concentration between 0 2 and 1 0 M The potential step width was 0 05 V and the potential was stepped from 0 0 V to + 0 05 V vs Ag/AgCl

From Equation 2 2, it is clear that semi-log plots of these current-time transients should be linear and from these plots the resistance and the capacitance can be elucidated Semi-log plots of the current-time transients are illustrated in Figure 2 5 The equation of the best-fit lines fitted to the data in the semi-log plot correspond to RC time constants of 400±50 ns, 700±90 ns and 1 60±0 20 μs for 1 0, 0 5 and 0 2 M $LiClO_4$ respectively These observations clearly indicate, as predicted by theory, that the RC time constant of the electrochemical cell decreases with increasing electrolyte concentration The shorter RC time constant arises because of a lower resistance in high ionic strength media Resistance and capacitance data for 12 5 μm microelectrodes are given in Table 2 1

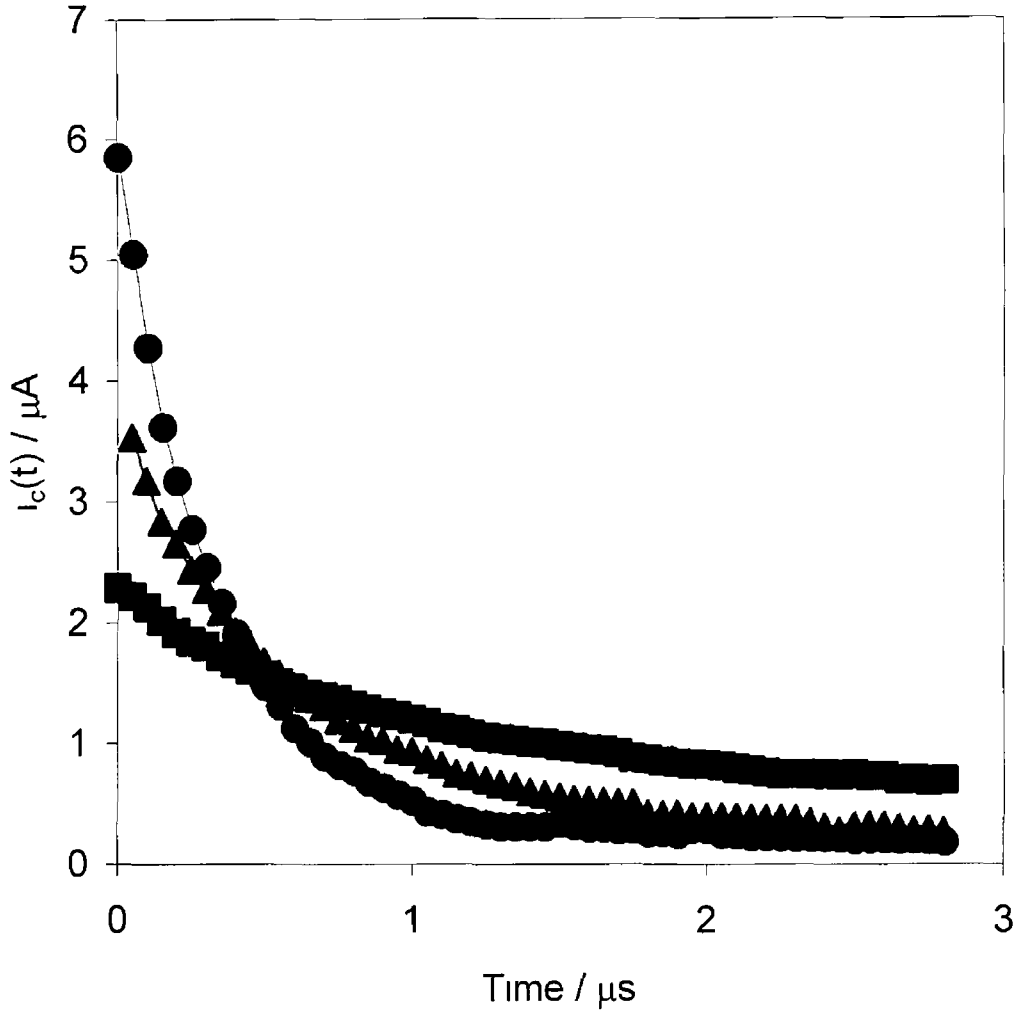

Figure 2 4 Current-time transients for a 12 5 μm platinum microelectrode in $LiClO_4$ electrolytes The electrolytes concentrations are 1 0 M (circles), 0 5 M (triangles) and 0 2 M $LiClO_4$ (squares) The potential step applied to the working electrode was from 0 0 V to 0 05 V vs Ag/AgCl

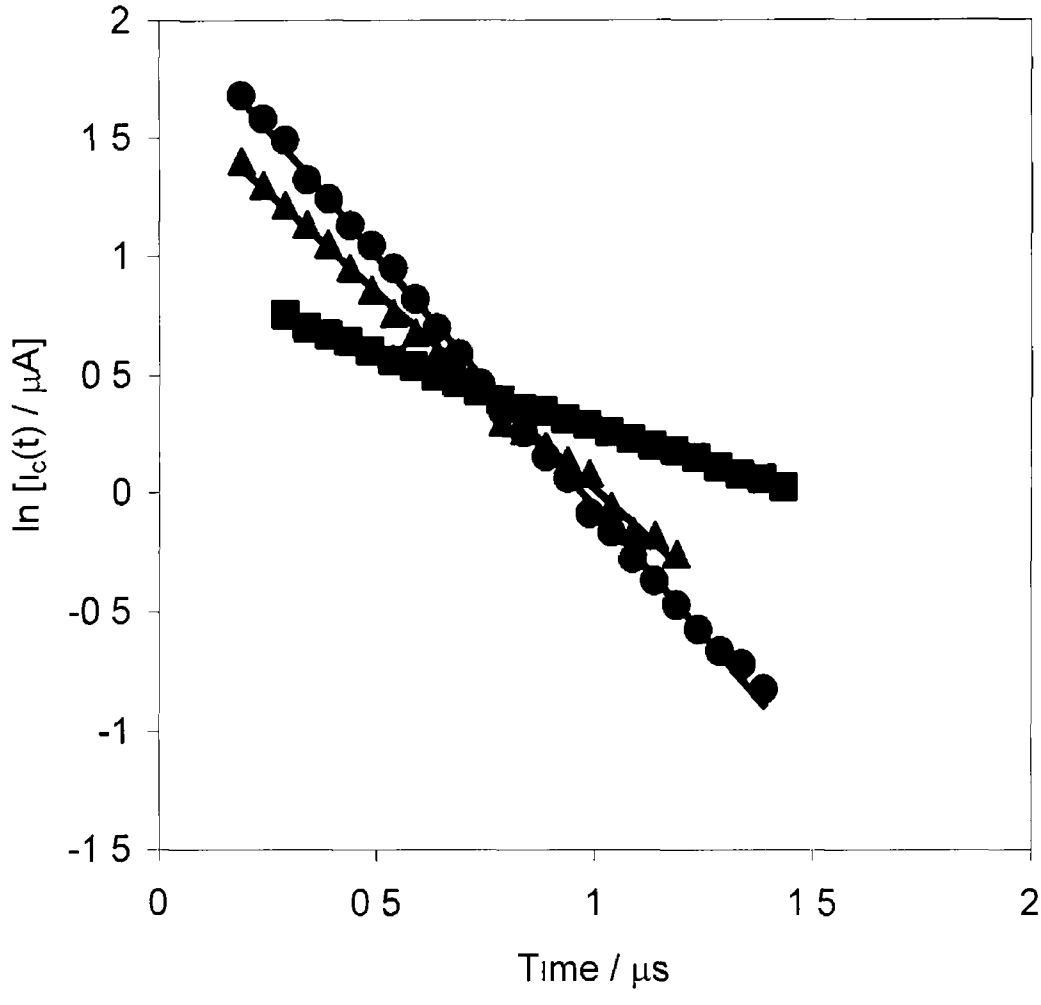

Figure 2 5 Semi-log plots of ln i versus t for a 12 5 μm platinum microelectrode in aqueous $LiClO_4$ electrolytes The electrolytes concentrations are 1 0 M (circles), 0 5 M (triangles) and 0 2 M $LiClO_4$ (squares) The potential step applied to the working electrode was from 0 0 V to 0 05 V vs Ag/AgCl

Table 2 1 Resistance, R, Double layer capacitance, C_{dl}, and electrode response times 12 5 μm radius platinum microelectrodes as the concentration of $LiClO_4$ is systematically varied

[$LiClO_4$]	R / Ω	10^{11} C_{dl} / F	RC / ns
0 2 M	22955(1500)	6 97(0 52)	1600(230)
0 5 M	10724(850)	6 42(0 45)	700(95)
1 0 M	7595(540)	5 24(0 48)	400(65)

2 3 OSMIUM POLYPYRIDYL COMPLEXES

2 3 1 INTRODUCTION

Osmium polypyridyl complexes have many properties that make them attractive model species for the study of heterogeneous and homogenous charge transfer processes Many of these complexes are stable in a number of redox states and exhibit facile electron transfer kinetics Metal complexes of this type have been shown to form unusually stable monolayers on metal surfaces under a range of electrolyte and solvent conditions [6 8 9]

As discussed in Section 2 1, abrasive deposition of films of osmium polypyridyl complexes at metal surfaces can result in highly stable films The electrochemical responses of these films can be probed under a variety of conditions, providing important insights into the mechanisms of mass and charge transfer through solids

In the following sections, the synthesis and characterisation of a series of osmium polypyridyl complexes are described These complexes have been carefully chosen to contain a moiety within the bridging ligand that is capable of undergoing a protonation/deprotonation reaction Complete characterisation of these complexes is described and an investigation into the pK_a of each complex is carried out These solution phase experiments are important references for investigations of protonation reactions either within monolayers or solid deposits

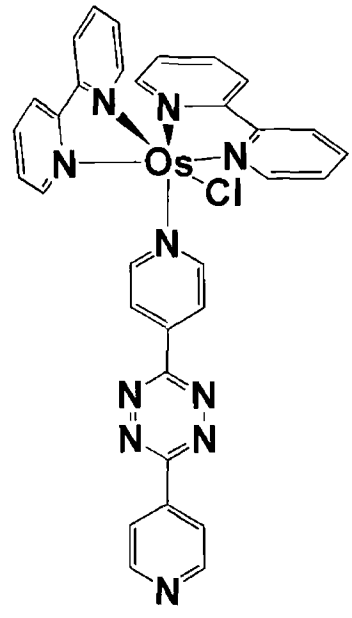

$[Os(bpy)_2\ 4\text{-tet Cl}](ClO_4)$

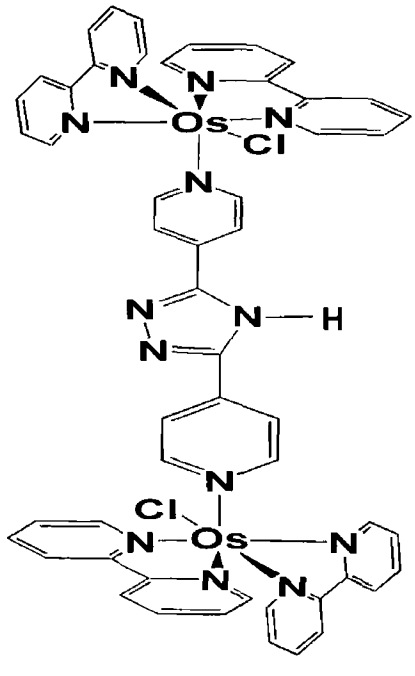

$[Os(bpy)_2Cl\text{-}4\text{-}bpt\text{-}Os(bpy)_2Cl](PF_6)_2$

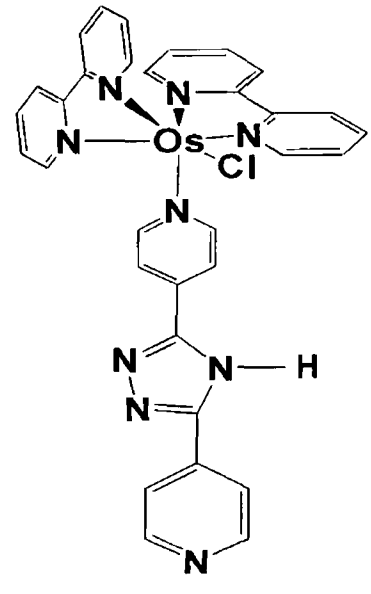

$[Os(bpy)_2\text{-}4bptCl](PF_6)$

Figure 2 6 Structure of the synthesised osmium polypyridyl complexes

2 3 2 APPARATUS

2 3 2 1 HIGH PERFORMANCE LIQUID CHROMATOGRAPHY

High performance liquid chromatography (HPLC) was performed using a Waters 510 HPLC pump and a Waters 990 photodiode array detector connected to a NEC PAC III computer, with a 20 µl injector loop and a partisil SCX radial PAK cartridge The detection wavelength used was 280 nm The mobile phase was acetonitrile water 80 20 (v/v) containing 0 08 M lithium perchlorate The flow rate used was 2 cm^3 min^{-1}, unless otherwise stated

2 3 2 2 UV-VISIBLE SPECTROPHOTOMETRY

UV-Vis spectrophotometry was performed using a Hewlett–Packard 342A diode array spectrophotometer or a Shimadzu UV-240 spectrophotometer Samples were dissolved in HPLC grade acetomtrile to a concentration of 10µM and quartz cells with a path length of 1 cm were used for all measurements The minimum slit width was 2 nm pK_a determinations were carried out in Britton-Robinson buffer, 0 04 M H_3BO_3, 0 04 M H_3PO_4, 0 04 M CH_3COOH Samples of the complexes were dissolved in the minimum amount of methanol and then added to Britton-Robinson buffer The pH was adjusted using concentrated solutions of NaOH and HCl

2 3 2 3 NMR SPECTROSCOPY

NMR spectroscopy was performed using a Bruker 400 NMR spectrometer All samples were analysed in CD_3CN or $(CD_3)_2SO$

2 3 2 4 ELECTROCHEMISTRY

Cyclic voltammetry was performed using a CH Instruments Model 660 Electrochemical Workstation and a conventional three electrode cell The gold and platinum electrodes had nominal radii ranging from 2 5 μm to 1 mm The counter electrode was a 1 cm^2 platinum flag All solutions were deoxygenated thoroughly using nitrogen, and a blanket of nitrogen was maintained over the solution during all experiments Potentials are quoted with respect to a BAS Ag/AgCl gel-filled reference electrode All experiments were performed at room temperature (22±3 °C) Solution phase cyclic voltammetry was performed in HPLC grade acetonitrile

2 3 2 5 ELEMENTAL ANALYSIS

Elemental analysis on carbon, hydrogen and nitrogen was carried out at the Microanalytical laboratory of the University College Dublin, Ireland

2 3 3 MATERIALS AND METHODS

2 3 3 1 SYNTHESIS OF [Os(bpy)$_2$-4-tet-Cl]ClO$_4$

[Os(bpy)$_2$-4-tet-Cl](ClO$_4$) was prepared using a procedure described previously [13] 3,6-Bis(4-pyridyl)-1,2,4,5-tetrazine (4-tet) was synthesised by combining 4-cyanopyridine (52 g, 0 5 mol) and hydrazine monohydrate (25 g, 0 5 mol) and heating to 100°C for 5 hours The resulting yellow solid was collected after cooling and recrystallised from hot ethanol/water, 2 1 v/v This solid was then dissolved in ethanol with a slight excess of 2,3-dichloro-5,6-dicyano-1,4-benzoquinone and stirred at room temperature for 2 hours The resulting bright pink solid was then collected by filtration and recrystallised from hot ethanol/water, 2 1 v/v The yield was 10 g (8 %)

4-tet (0 12 g, 0 51 mmol) was dissolved in 20 cm^3 of ethylene glycol and heated to reflux *cis*-Os(bpy)$_2$Cl$_2$ (0 257 g, 0 45 mmol) was also dissolved in the minimum amount of ethylene glycol and added to the refluxing solution over a period of 20 minutes The mixture was allowed to reflux for a further 4 hours After cooling, the product was precipitated by addition of a solution of concentrated NaClO$_4$ The solid product was collected by filtration and recrystallised from acetone/water, 1 1 v/v The yield was 0 322 g (82 %)

HPLC	Single peak, retention time 2 918 minutes
^{1}H NMR	Bipyridyl - H^3, 8 47-8 52 (d), H^4, 7 84-7 86 (t), H^6, 7 62-7 64 (d), H^5, 7 28-7 32 (t) 4-tet – H^2, 7 70 (d), H^3, 7 60 (dd), H^5, 7 60 (dd), H^6, 7 70 (d), H$^{2''}$, 7 98 (dd), H$^{3''}$, 8 75 (d), H$^{5''}$, 8 75 (d), H$^{6''}$, 7 98 (d)
CHN	Calculated for OsC$_{32}$H$_{24}$N$_{10}$Cl$_2$O$_4$, C 43 98%, H 2 74%, N 16 03 %, Found C 43 21%, H 2 84%, N 14 21 %

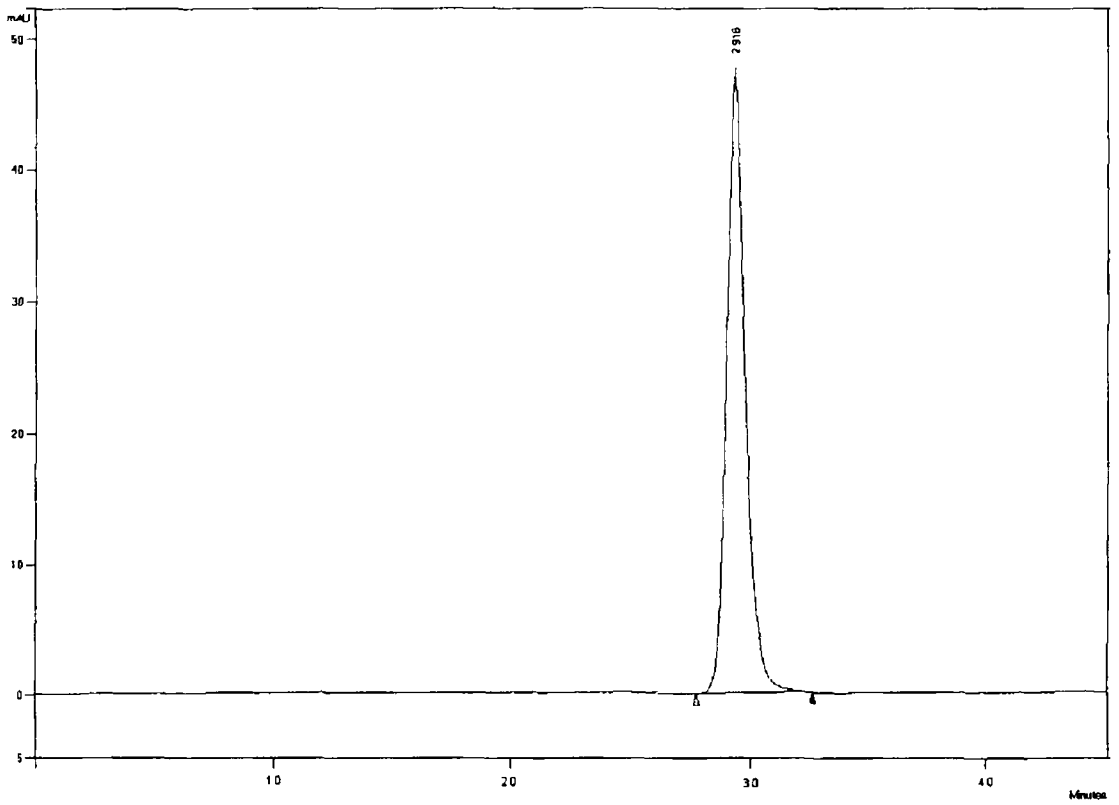

Figure 2 7 Cation-exchange HPLC chromatogram for a solution of $[Os(bpy)_2\text{-}4\text{-}tet\text{-}Cl](ClO_4)$ The mobile phase is acetonitrile water 80 20 (v/v) containing 0 08 M lithium perchlorate and the detector wavelength is 280 nm The flow rate used is 2 cm^3 min^{-1}

2 3 3 2 SYNTHESIS OF $[Os(bpy)_2\text{-}4\text{-}bpt\text{-}Cl](PF_6)$

$[Os(bpy)_2\text{-}4\text{-}bpt\text{-}Cl](PF_6)$ was prepared using a method described previously [23] 3,5-Bis(pyridin-4-yl)-1,2,4-triazole (4-bpt) was synthesised by combining 4-cyanopyridine (52 g, 0 5 mol) and hydrazine monohydrate (25 g, 0 5 mol) and heating for 5 hours at 100°C The resulting yellow solid was collected after cooling and refluxed in 2 M HCl for 20 minutes This solution was neutralised with ammonia and the resulting tan coloured solid was recrystallised from ethanol This product was then refluxed in 500 cm^3 of 5 M HNO_3 for 3 minutes After cooling to 0°C, 90 g of sodium nitrite were added slowly The solution was stirred at room temperature for 30 minutes and then heated at boiling for 5 minutes Addition of ammonia precipitated the 4-bpt product which was then recrystallised from ethanol The yield was 20 g (18 %)

4-bpt (0 15 g, 0 43 mmol) was dissolved in ethylene glycol (40 cm^3) and heated to reflux *cis*-$Os(bpy)_2Cl_2$ (0 22 g, 3 5 × 10^{-4} mol) was also dissolved in ethylene glycol (10 cm^3) and added to the solution over a period of 1 hour and this mixture was refluxed for a further 2 hours The reaction mixture was then cooled and added drop wise to a concentrated solution of NH_4PF_6 The resulting brown precipitate was collected by filtration The solid was purified by dissolving in acetone water, followed by slow evaporation of the organic solvent The yield was 0 235 g (74 %)

HPLC Single peak, retention time 2 793 minutes

^{1}H NMR Bipyridyl - H^3, 8 47-8 52 (d), H^4, 7 84-7 86 (t), H^6, 7 62-7 64 (d), H^5, 7 28-7 32 (t)
4-bpt – H^2, 8 73 (d), H^3, 7 96-7 92 (dd), H^5, 7 96-7 92 (dd), H^6, 8 73 (d), $H^{2''}$, 7 54-7 57 (dd), $H^{3''}$, 8 23 (d), $H^{5''}$, 8 23 (d), $H^{6''}$, 7 54-7 57 (dd)

CHN Calculated for $OsC_{32}H_{25}N_9ClNH_4PF_6$, C 39 26, H 3 58, N 14 3 %, Found C 38 70, H 3 62, N 14 21 %

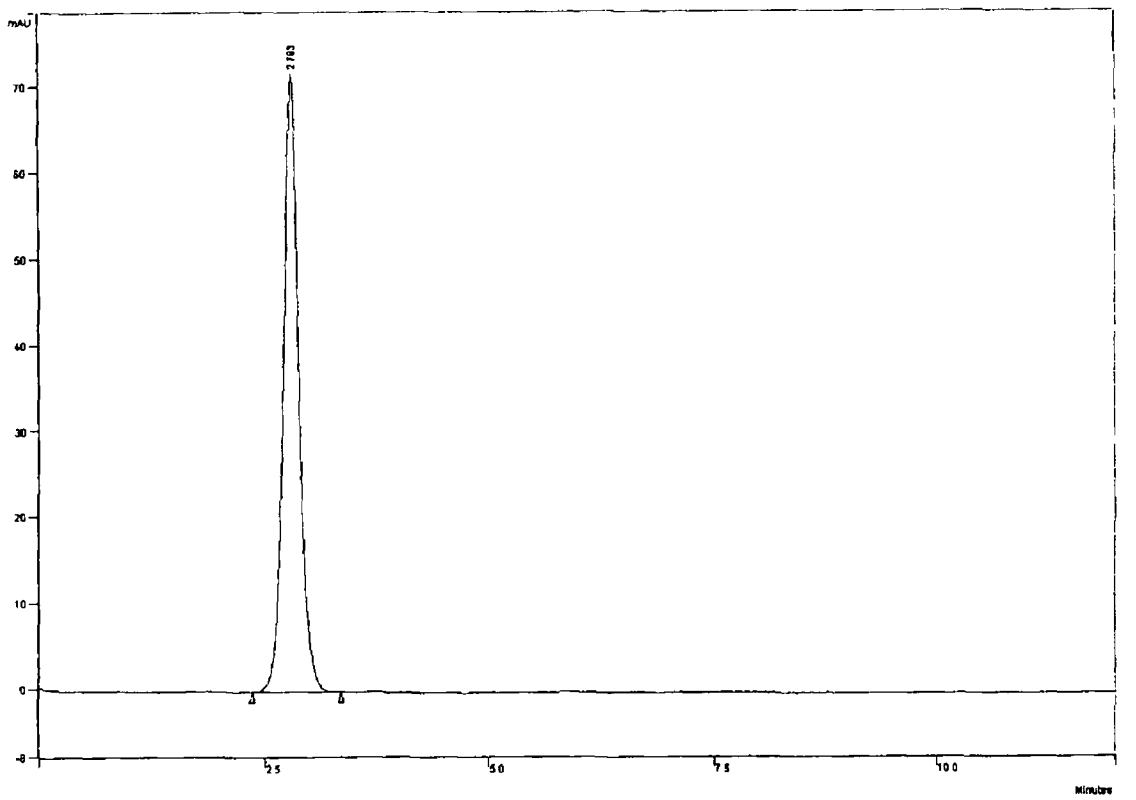

Figure 2 8 Cation-exchange HPLC chromatogram for a solution of $[Os(bpy)_2\text{-}4bpt\text{-}Cl](PF_6)$ The mobile phase is acetonitrile water 80 20 (v/v) containing 0 08 M lithium perchlorate and the detector wavelength is 280 nm The flow rate used is 2 cm^3 min^{-1}

2 3 3 3 SYNTHESIS OF [Os(bpy)$_2$ Cl 4-bpt Os(bpy)$_2$ Cl] (PF_6)$_2$

[Os(bpy)$_2$ 4-bpt Os (bpy)$_2$ Cl_2](PF_6)$_2$ was synthesized by dissolving [Os(bpy)$_2$ 4-bpt Cl]PF_6 (0 503g, 0 56 mmol) in 50 cm^3 of ethanol and bringing to reflux A molar equivalent of [Os(bpy)$_2$ Cl_2] (0 314 g, 0 55 mmol) was dissolved in 30 cm^3 of ethanol and added in three lots to the refluxing solution The solution was then refluxed for a further 36 hours After cooling, a concentrated solution of aqueous NH_4PF_6 was added to precipitate the dark purple-brown complex The product was recrystallised by dissolving the complex in 50 50 acetone water in the presence of a small amount of acid to ensure complete protonation of the 4-bpt bridge, followed by slow evaporation of the organic solvent The yield was 0 724g (83 %)

HPLC	Single peak, retention time 5 671 minutes
^{1}H NMR	Bipyridyl - H^3, 8 47-8 52 (d), H^4 , 7 84 – 7 89 (t), H^6, 7 62 – 7 64 (d), H^5, 7 28 – 7 32 (t) 4bpt - H^2, 9 43 (d), H^3, 8 50 (dd), H^5 7 96-7 92 (dd), H^6, 9 93, H^2 , 7 54 (dd), H^3 , 8 17 (d), H^5 , 8 23 (d), H^6 , 7 78
CHN	Calculated for $Os_2C_{52}H_{40}N_{13}P_2F_{12}Cl_2$, C 39 3%, H 2 5%, N 11 4 0% Found C 39 2%, H 2 7%, N 11 3%)

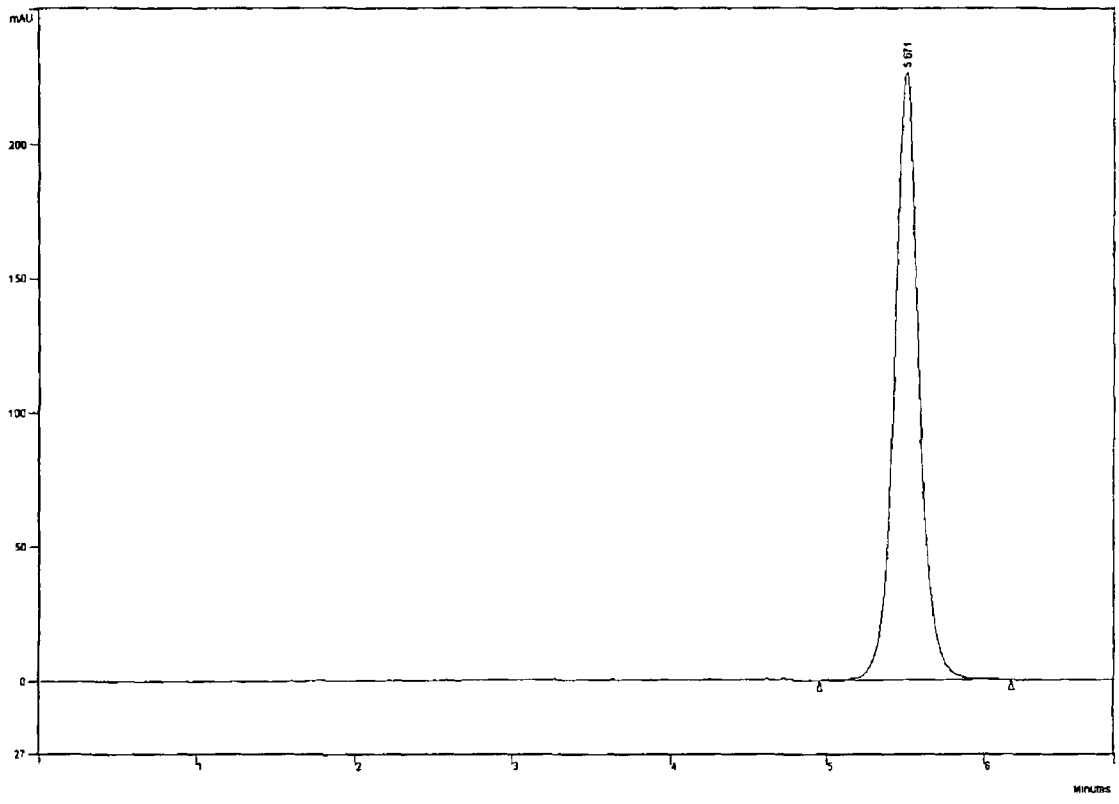

Figure 2 9 Cation-exchange HPLC chromatogram for a solution of $[Os(bpy)_2 Cl\ 4\text{-}bpt\ Os(bpy)_2 Cl](PF_6)_2$ The mobile phase is acetonitrile water 80 20 (v/v) containing 0 08 M lithium perchlorate and the detector wavelength is 280 nm The flow rate used is 2 cm^3 min^{-1}

2 3 4 RESULTS AND DISCUSSION

2 3 4 1 UV-VISIBLE SPECTROPHOTOMETRY

The various electronic transitions that a typical octahedral osmium polypyridyl complex can undergo are shown in Figure 2 10 In this diagram, the various molecular orbitals are labelled either as metal (M) or ligand (L) centred depending on their predominant localisation In the ground state, the σ_L and π_L orbitals are completely filled The π_M (t_{2g}) orbitals can be filled or partially filled and the higher orbitals are usually empty Other, less frequently observed, transitions that can be observed in the absorption spectra of octahedral complexes include ligand to metal charge transfer (LMCT), charge transfer to solvent (CTTS) and ligand to ligand charge transfer (LLCT) These processes are not shown in Figure 2 10

Metal to ligand transitions result in transfer of electronic charge from metal-localised orbitals to ligand-localised orbitals These MLCT bands appear in the spectra of the complexes in the visible region in a large band between 400 and 700 nm (Figures 2 11, 2 12 and 2 13)[29] A sharp absorption band at approximately 290 nm is observed in the spectrum This is associated with a ligand-based π-π^* transition[29] The shoulders observed at approximately 370 nm are probably due to metal centred transitions[30] The remaining bands that appear in the UV portion of the spectrum are due to ligand based π-π^* transitions, except for the bands that appear at approximately 240 nm, which are due to MLCT transitions[30] Table 2 2 contains the extinction coefficients determined for each complex at the wavelength of maximum absorbance for each transition These values have been determined from plots of absorbance versus concentration for each of the complexes

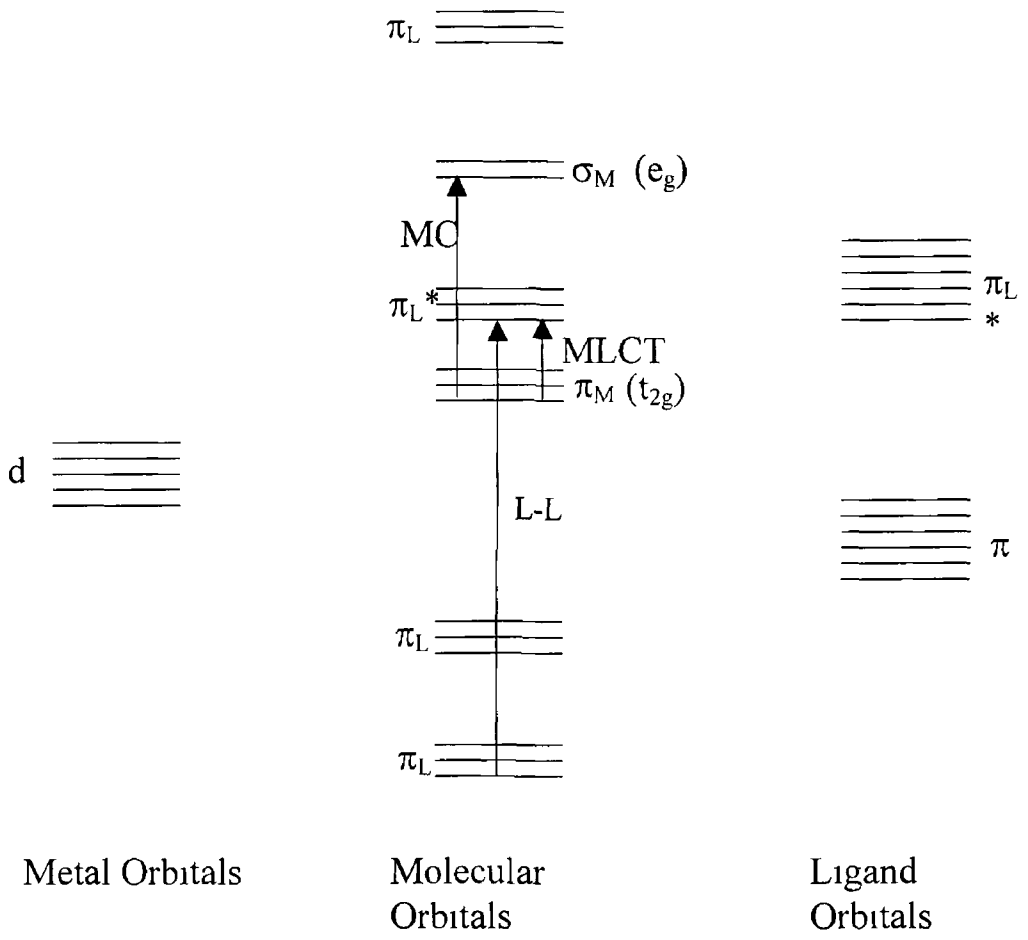

Figure 2 10 Electronic transitions that can be observed in the absorption spectra of octahedral transition metal complexes MC, MLCT and L-L transitions are metal-centred, metal to ligand charge transfer and ligand-centred transitions, respectively

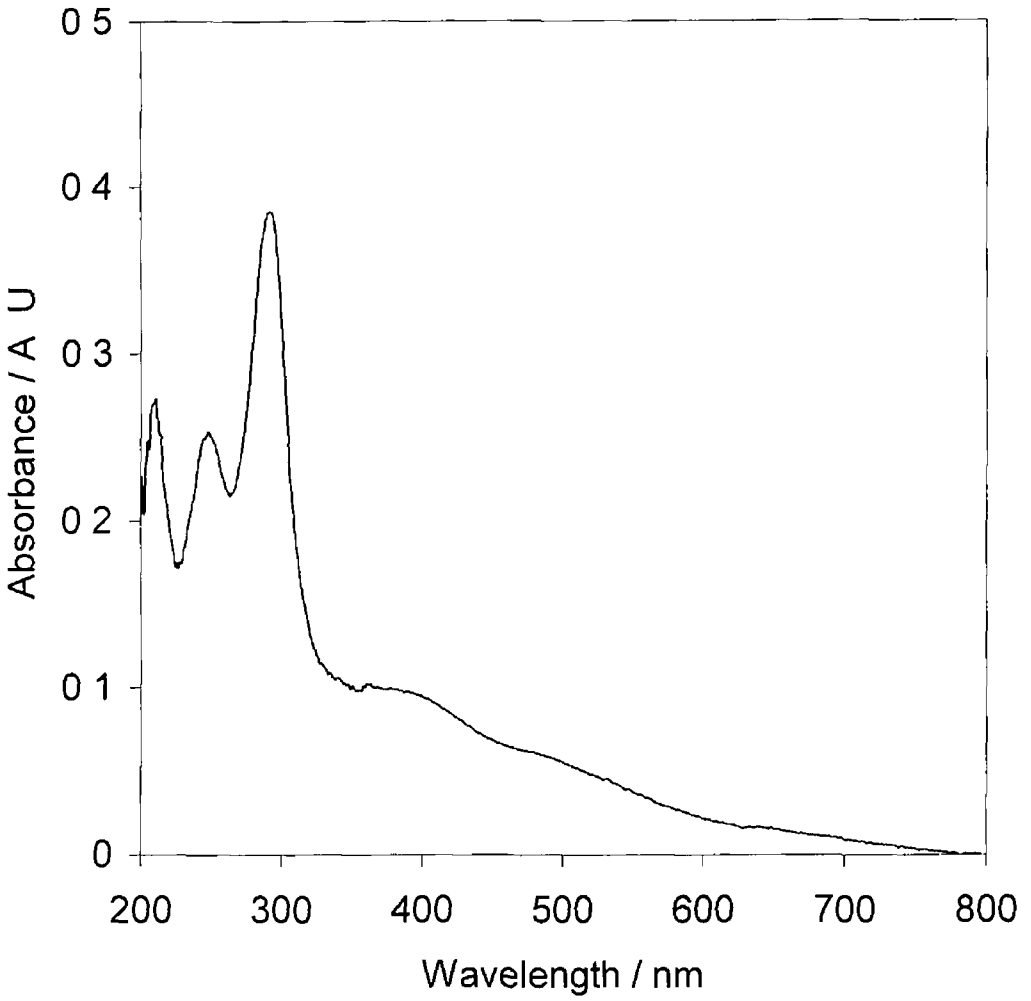

Figure 2 11 Absorption spectrum of $[Os(bpy)_2$ 4-tet $Cl](ClO_4)$ The concentration is 10 μM and the solvent is acetonitrile

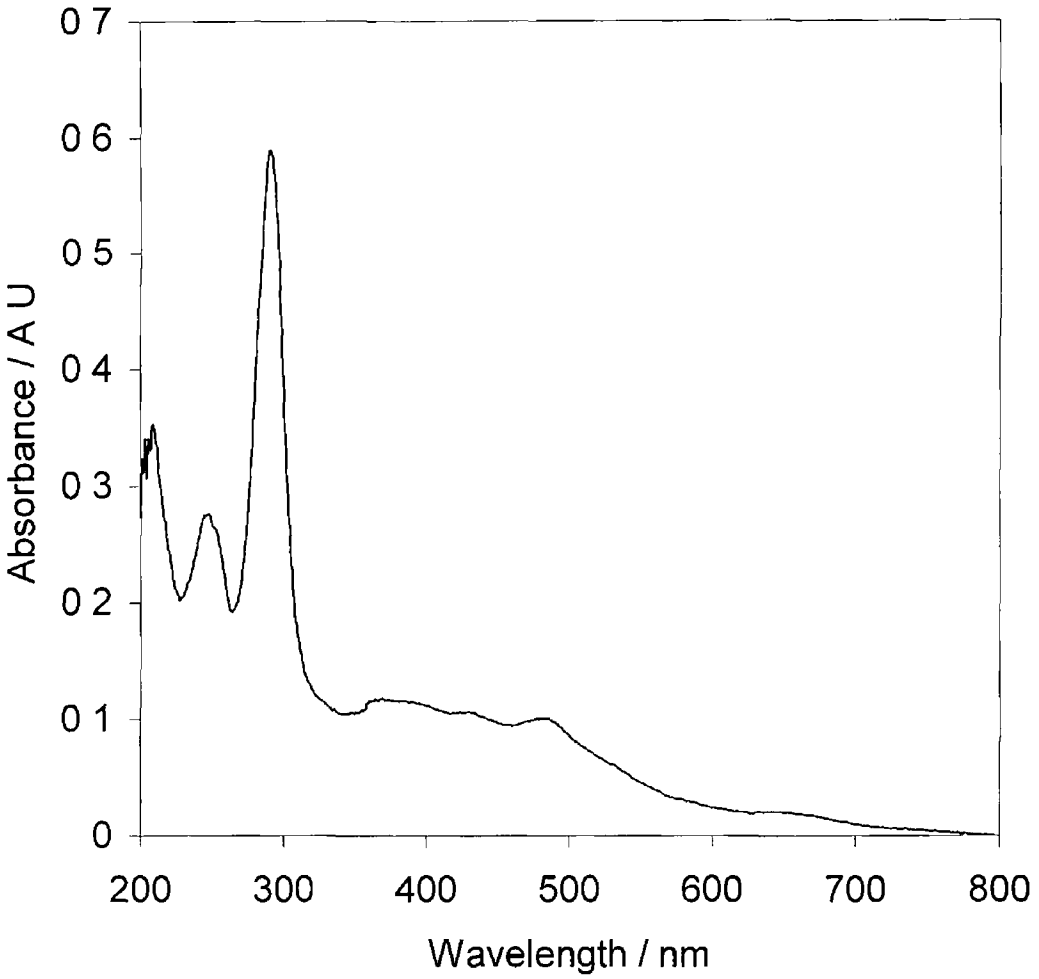

Figure 2 12 Absorption spectrum of $[Os(bpy)_2$ 4-bpt $Cl](PF_6)$ The concentration is 10 μM and the solvent is acetonitrile

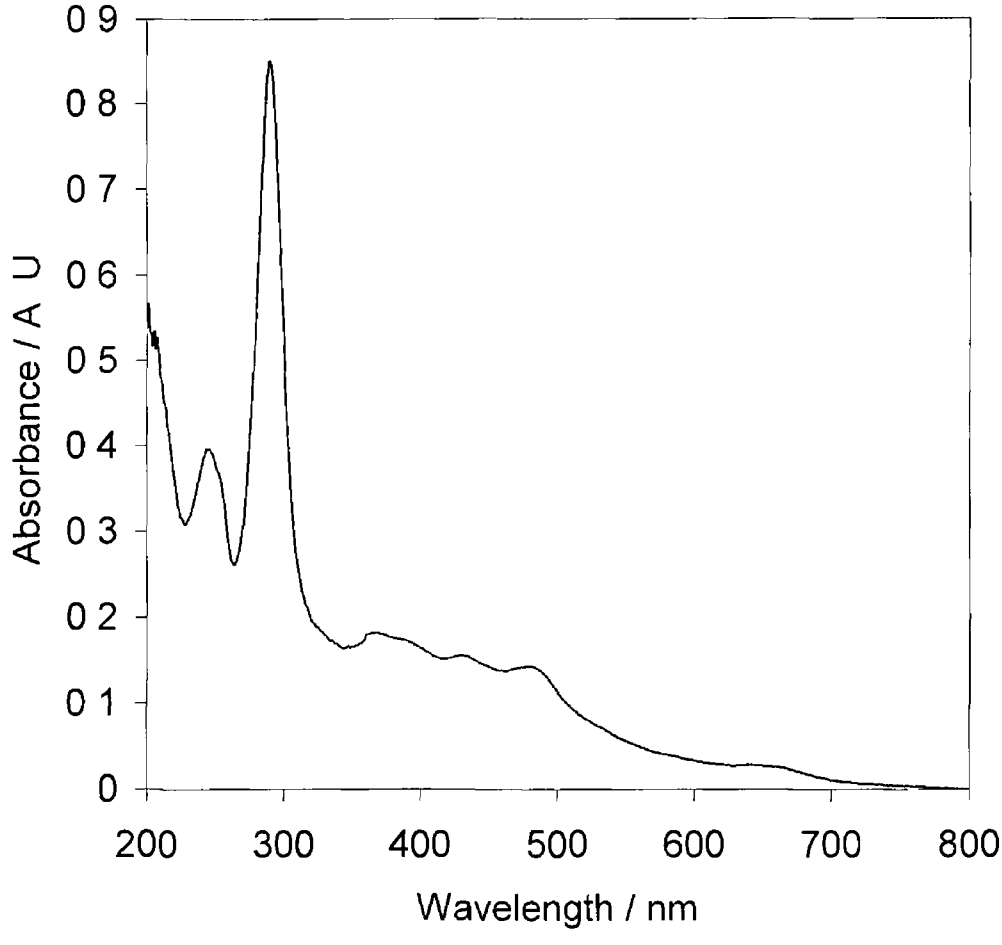

Figure 2 13 Absorption spectrum of $[Os(bpy)_2Cl$ 4-bpt $Os(bpy)_2Cl](PF_6)_2$ The concentration is 10 μM and the solvent is acetonitrile

Table 2 2 Extinction coefficients for $[Os(bpy)_2$ 4-tet Cl$]ClO_4$, $[Os(bpy)_2$ 4-bpt Cl$]PF_6$ and $[Os(bpy)_2$ Cl 4-bpt $Os(bpy)_2$ 4-bpt Cl$](PF_6)_2$ The solvent in each case is acetonitrile

Complex	Transition	Wavelength / nm	Extinction Coefficient / $M^{-1} cm^{-1}$
$[Os(bpy)_2$4-tet Cl$]ClO_4$	LC π-π*	290	38300
	MC	370	9970
	MLCT	240	24400
	MLCT	460	6390
$[Os(bpy)_2$4-bptCl$]PF_6$	LC π-π*	290	63200
	MC	370	11684
	MLCT	240	27170
	MLCT	460	9784
$[Os(bpy)_2Cl$4-bpt$Os(bpy)_2Cl](PF_6)_2$	LC π-π*	290	86000
	MC	370	19000
	MLCT	240	40000
	MLCT	470	16000

2 3 4 1 1 pK_a DETERMINATION

The pK_a of each of the complexes has been investigated using UV-Vis spectrophotometry This information is important as the effects of protonation of the 4-tet and 4-bpt ligands on the rate of electron transfer across the bridging ligand is one of the major goals of this study Changes in the absorption spectra of these complexes can provide an insight into the extent of electronic communication between the metal centre and the ligands Importantly, these studies can provide an estimate of the pK_a of the complex, a parameter that is crucially important when undertaking a study into the effects of protonation

However, the pK_a of each complex in bulk solution may be different from that found when the species are incorporated as monolayers or within solid deposits For example, the dielectric constant within a solid film or a monolayer may be distinctly different from that found in bulk solution Secondly, immobilisation of the complexes within a monolayer may alter the electron density of the ligand These effects could cause different apparent pK_a values to be observed These effects are investigated further in later chapters

The effect of changing the bulk solution pH on the absorption spectra of $[Os(bpy)_2$ 4-tet Cl$](ClO_4)$ is shown in Figure 2 14 Titrations were performed in Britton-Robinson buffer, 0 04 M H_3BO_3, 0 04 M H_3PO_4, 0 04 M CH_3COOH The pH was adjusted using concentrated NaOH and HCl solutions In this Figure, the wavelength range shown is 280-800 nm The changes in the MLCT bands that occur upon protonation of the 4-tet ligand are clearly visible As the pH of the solution decreases a decrease in the MLCT band is observed This is consistent with a reduction of the electron density on the 4-tet ligand, that occurs upon protonation of the ligand Changes in the spectra were confirmed to be reversible by first increasing and then decreasing the pH of the solution Absorbance values were reproducible to approximately 0 0025 A U upon changing the solution pH

The changes in the absorbance at 480 nm that occur upon decreasing the solution pH are illustrated in Figure 2 15 This data has been fitted to the Henderson-Hasselbach relationship

$$pH = pK_a + Log\left[\frac{A^-}{HA}\right] \qquad (2\ 5)$$

where A and HA are the deprotonated and protonated forms of the complex The solid line in Figure 2 15 is the theoretical curve using a pK_a value of 2 6 This illustrates that the model provides an adequate description of the experimental data and that the pK_a is 2 6±0 2

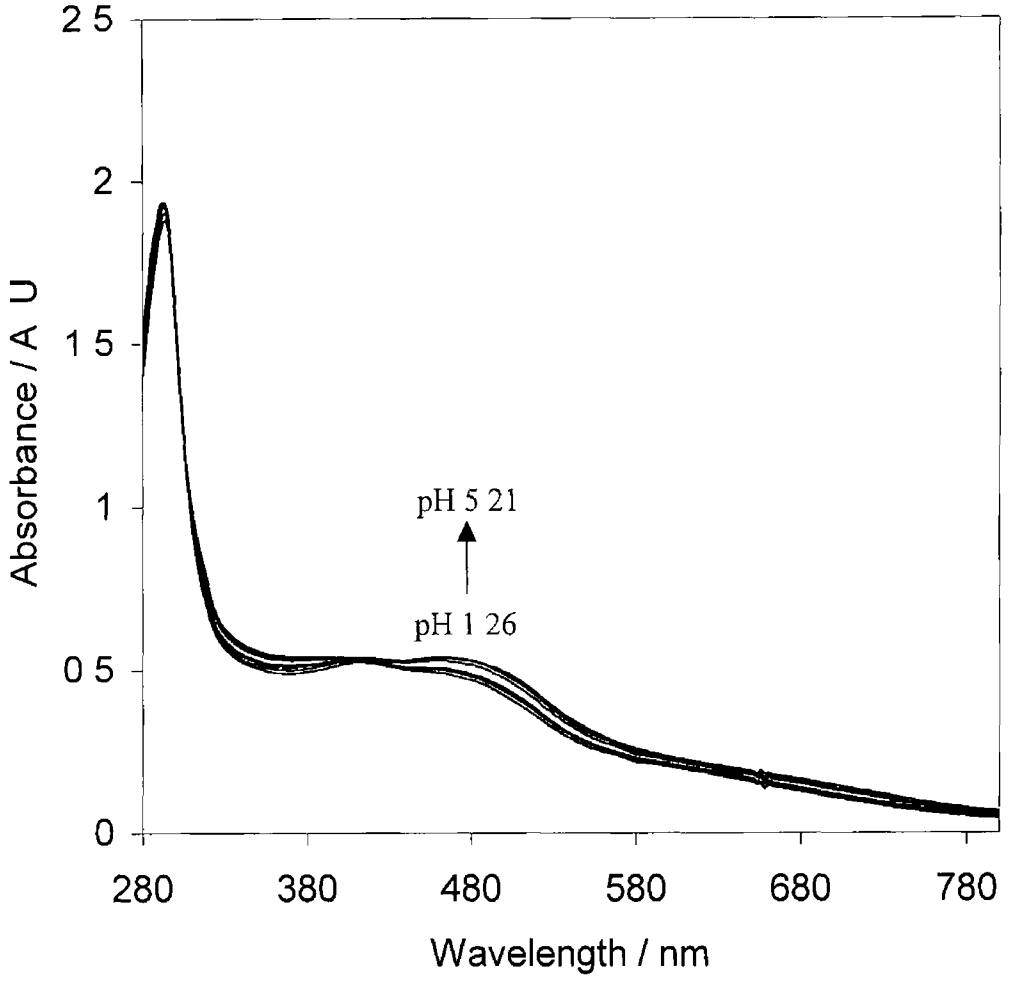

Figure 2 14 Effect of decreasing solution pH on the UV-Vis spectrum of $[Os(bpy)_2$ 4-tet Cl$]ClO_4$ The solution pH values are 1 26, 1 52, 1 89, 2 49, 3 42, 4 19, 4 64 and 5 21

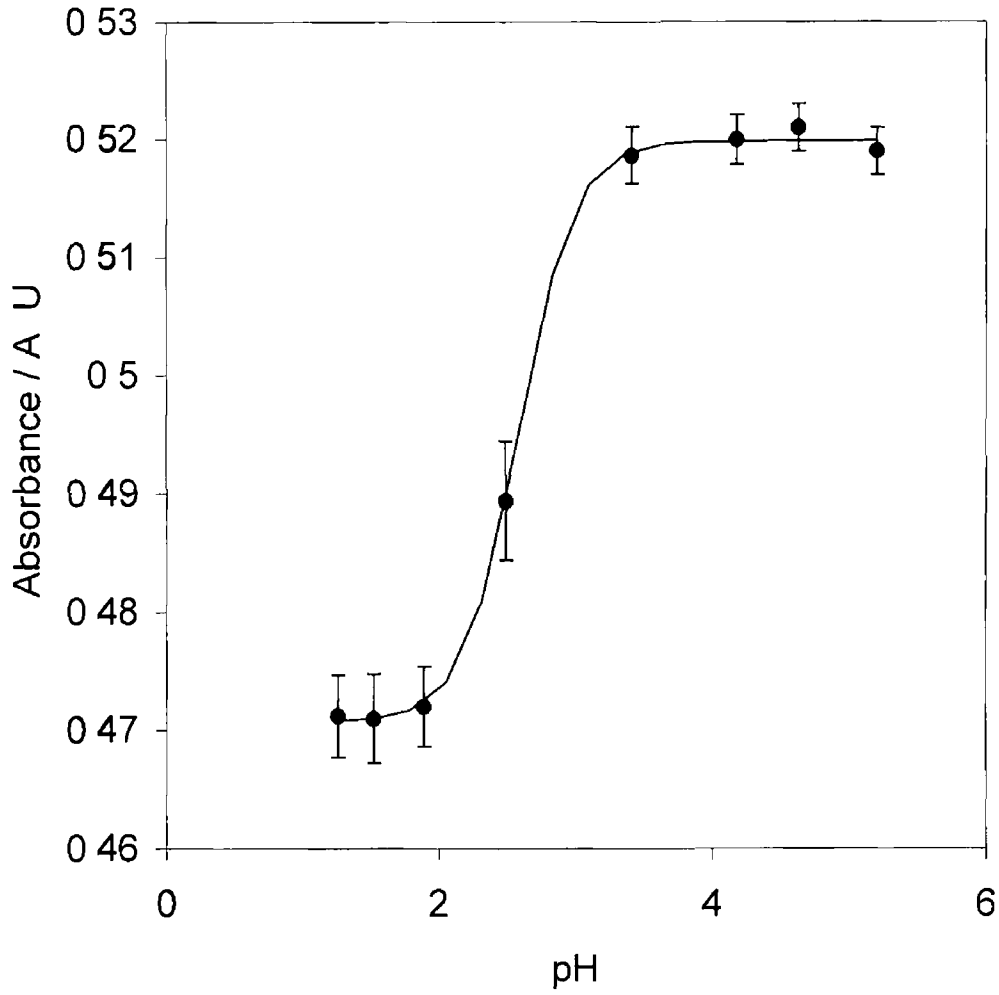

Figure 2 15 Changes in the absorbance of a solution of $[Os(bpy)_2$ 4-tet Cl$]ClO_4$ observed at 480 nm upon changing the solution pH The solvent is Britton-Robinson buffer The solid line is the calculated curve based on a pK_a value of 2 6

The changes observed in the spectrum of $[Os(bpy)_2$ 4-bpt $Cl]PF_6$ upon changing the pH of the solution are illustrated in Figure 2 16 pH titrations were performed in Britton-Robinson buffer and all changes in the spectra were confirmed to be reversible by first decreasing and then increasing the solution pH (± approximately 0 0025 A U) Changes in the MLCT band (at 480 nm) observed upon protonation of the 4-bpt ligand are illustrated in Figure 2 17 By fitting these data to the Henderson-Hasselbach equation using non-linear optimisation techniques, an estimate of the pK_a of the 4-bpt ligand was obtained The solid line in Figure 2 17 shows the theoretical curve predicted using a value of 9 60 for the pK_a of the 4-bpt ligand The error on the pK_a value is 0 2 pH units

The changes observed in the spectrum of $[Os(bpy)_2$ Cl 4-bpt $Os(bpy)_2$ $Cl]PF_6$ are illustrated in Figure 2 18 All spectra were recorded in Britton-Robinson buffer and all spectra were confirmed to be reversible by first increasing and then decreasing the pH of the solution (± approximately 0 003 A U) The changes observed in the MLCT band at 480 nm are illustrated in Figure 2 19 These data were fitted to the Henderson-Hasselbach equation using non-linear optimisation methods and the solid line in Figure 2 19 shows the curve obtained using a pK_a value of 11 1 for the 4-bpt ligand in the dimeric complex $[Os(bpy)_2$ Cl 4-bpt $Os(bpy)_2$ $Cl]PF_6$ The error on the pK_a value is 0 2 pH units

That changes in the absorption spectra of all three complexes were observed upon changing the pH of the solution suggests that the extent of electronic communication between the osmium metal centres and the attached 4-bpt and 4-tet ligands is significant These observations indicate that a simple change in the pH of the solution, causing protonation/deprotonation of the 4-tet and 4-bpt ligands, alters the electronic density on the bridge and hence, the osmium metal centre While the spectra for $[Os(bpy)_2$ 4-bpt $Cl]PF_6$ and $[Os(bpy)_2$ Cl 4-bpt $Os(bpy)_2$ $Cl]PF_6$ do not show evidence of an isosbestic point, that would indicate the presence of a single pK_a value, the pK_a values determined are comparable to that determined for free 3,5-Bis(pyridin-2-yl)-1,2,4-triazole

(pK_a = 8 4±0 1) [31] The pK_a values determined for each complex are given in Table 2 3

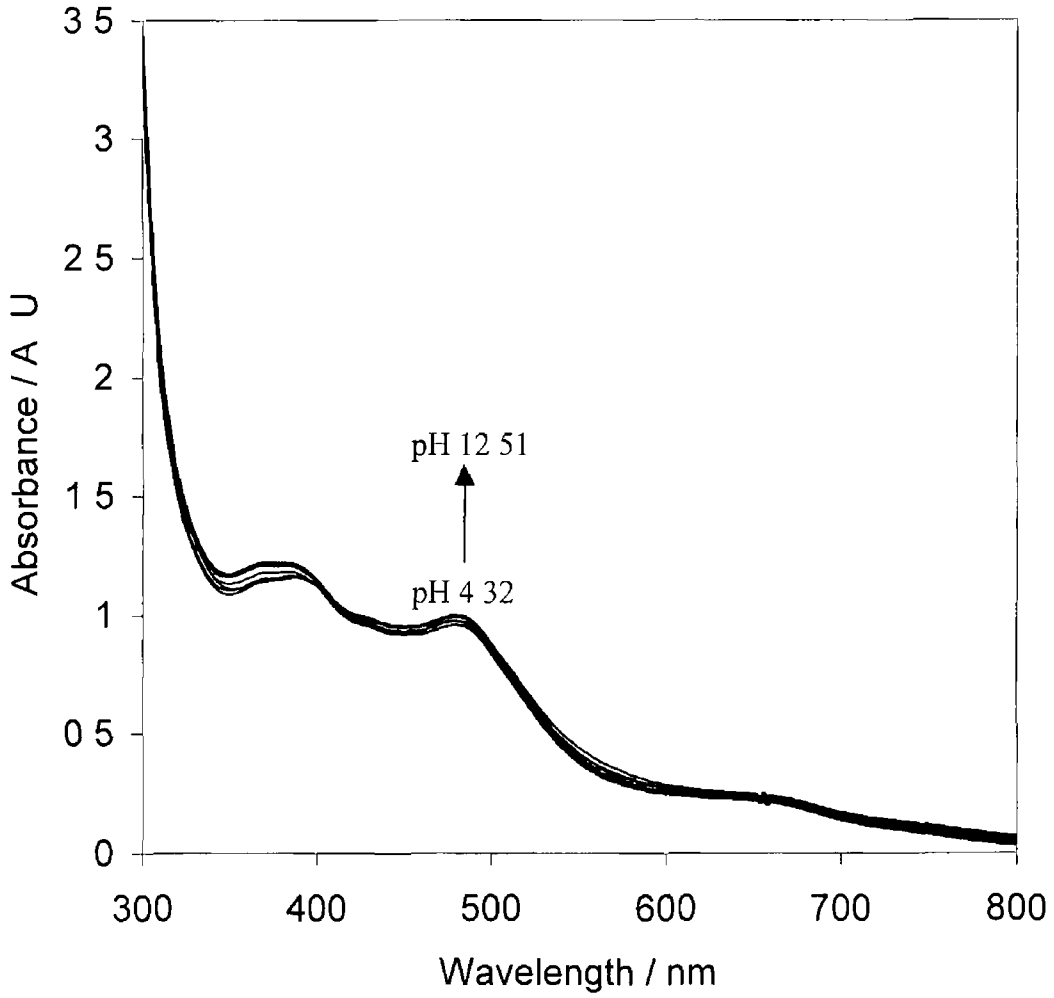

Figure 2 16 Changes in the UV-Vis spectrum of $[Os(bpy)_2$ 4-bpt Cl$]PF_6$ observed upon changing the pH of the solution The solution pH values are 4 32, 5 75, 6 25, 7 1, 9 32, 9 77, 10 4, 11 25, 11 76 and 12 51 The solvent is Britton-Robinson buffer

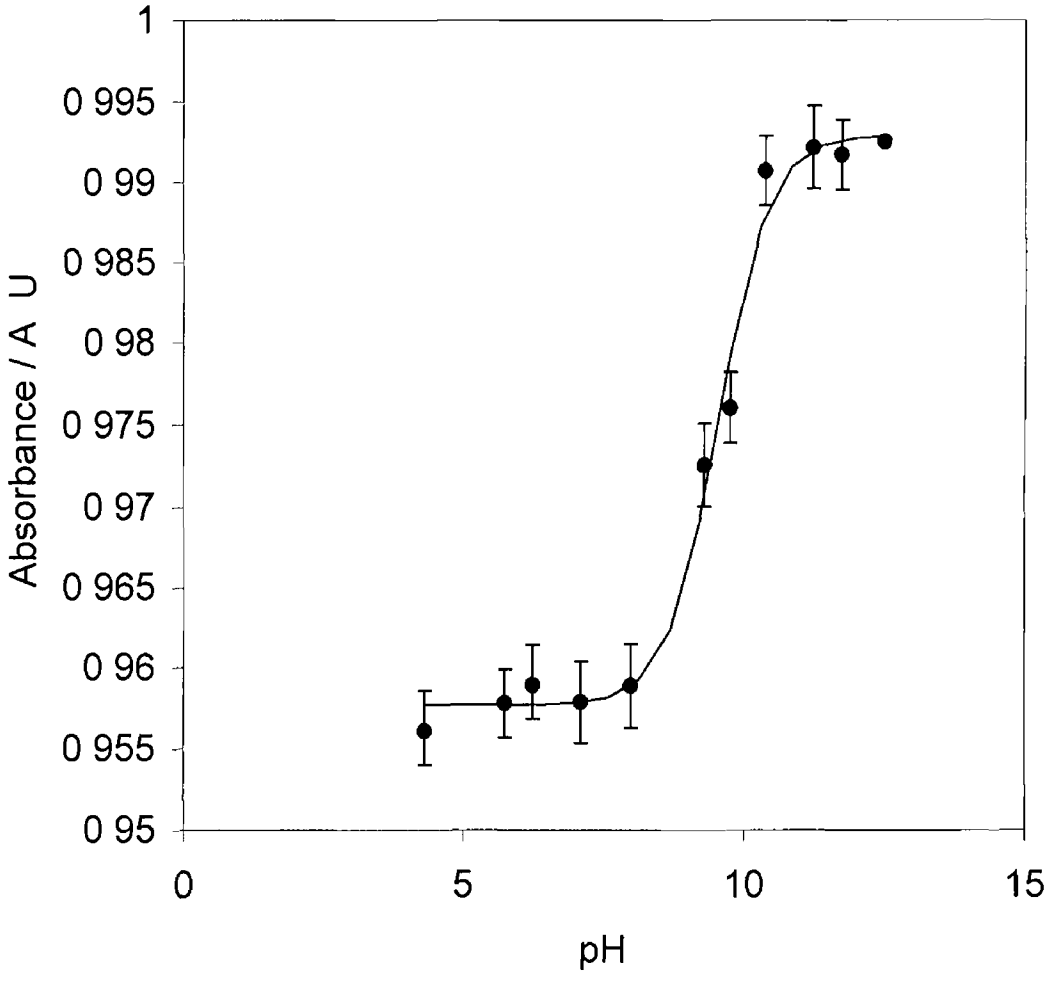

Figure 2 17 Changes in the absorbance of a solution of $[Os(bpy)_2$ 4-bpt Cl$]PF_6$ observed at 480 nm upon changing the solution pH The solvent is Britton-Robinson buffer

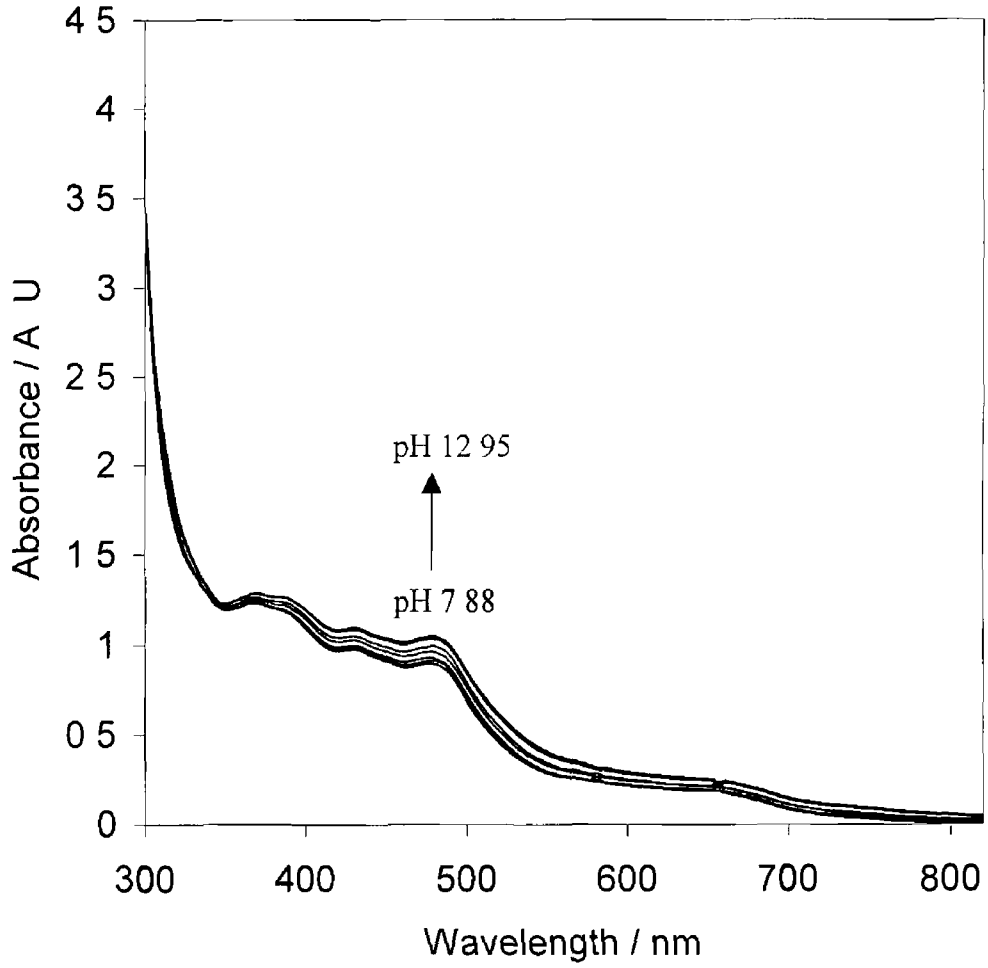

Figure 2 18 Changes in the UV-Vis spectrum of [Os(bpy)$_2$Cl 4-bpt Os(bpy)$_2$Cl]PF_6 observed upon changing the pH of the solution The solution pH values are 7 88, 8 73, 10 06, 10 72, 11 46, 12 04, 12 49 and 12 95 The solvent is Britton-Robinson buffer

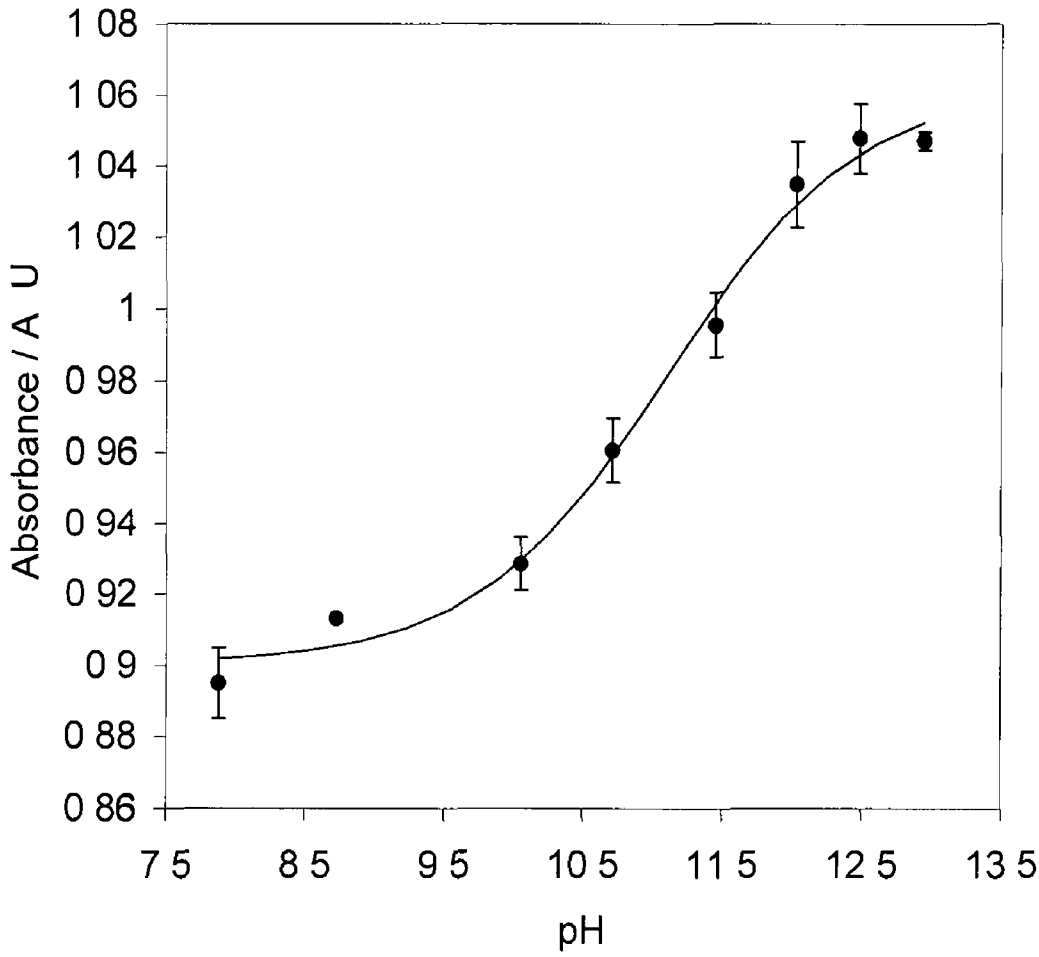

Figure 2 19 Changes in the absorbance of a solution of $[Os(bpy)_2Cl$ 4-bpt $Os(bpy)_2Cl]PF_6$ observed at 480 nm upon changing the solution pH The solvent is Britton-Robinson buffer

Table 2 3 pK_a values determined for $[Os(bpy)_2\ 4\text{-}tetCl]ClO_4$, $[Os(bpy)_2\ 4\text{-}bptCl]PF_6$ and $[Os(bpy)_2Cl\ 4\text{-}bpt\ Os(bpy)_2Cl](PF_6)_2$ [a]

Complex	pK_a
$[Os(bpy)_2\ 4\text{-}tetCl]ClO_4$	2 6
$[Os(bpy)_2\ 4\text{-}bptCl]PF_6$	9 6
$[Os(bpy)_2Cl\ 4\text{-}bpt\ Os(bpy)_2Cl](PF_6)_2$	11 1

[a] The error on pK_a values is approximately 0 2 pH units

2 3 4 2 ELECTROCHEMISTRY

By probing the electrochemical response of the osmium polypyridyl complexes, it is possible to gain an insight into the electrochemical reversibility of the $Os^{2+/3+}$ redox reaction Determination of the formal potential of the redox reaction can also provide an insight into the ease of oxidation of the metal centre The cyclic voltammetric responses of $[Os(bpy)_2$ 4-tet Cl$](ClO_4)$, $[Os(bpy)_2$ 4-bpt Cl$](PF_6)$ and $[Os(bpy)_2$ Cl 4-bpt Os$(bpy)_2$ Cl$](PF_6)$ dissolved in acetomtrile with 0 1 M $TBABF_4$ as supporting electrolyte are shown in Figures 2 20, 2 21 and 2 22, respectively In the case of the monomeric complexes, a single redox couple is observed (corresponding to the $Os^{2+/3+}$ redox reaction) and the formal potential of the couples are 0 222 V vs Ag/AgCl and 0 249 V vs Ag/AgCl for $[Os(bpy)_2$ 4-tet Cl$](ClO_4)$ and $[Os(bpy)_2$ 4-bpt Cl$](PF_6)$ respectively In each case, the peak-to-peak separation, ΔE_p, is approximately 75±5 mV and is slightly larger than the value of 57 mV expected for a redox reaction involving the transfer of a single electron [28]

Slow electron transfer kinetics would cause increased ΔE_p values at higher scan rates However, the peak to peak separation does not change for scan rates in the range $0\ 1 \leq \nu \leq 2\ 0$ V/s, indicating that slow electron transfer kinetics are not the source of this increased ΔE_p The slightly larger than expected ΔE_p values are not due to ohmic effects as the increased currents observed at higher scan rates would cause the ΔE_p values to increase with increasing scan rate The estimated iR drop in these voltammograms is less than 0 5 mV, which is insignificant compared to the ΔE_p values observed here The formal potentials (0 222 V and 0 249 V for $[Os(bpy)_2$ 4-tet Cl$](ClO_4)$ and $[Os(bpy)_2$ 4-bpt Cl$](PF_6)$ respectivelv) are typical of osmium polypyridyl complexes containing one electronegative ligand (Cl), where the overall charge on the complex is +1 [13 14]

In the case of the dimeric complex, $[Os(bpy)_2$ Cl 4-bpt Os$(bpy)_2$ Cl$](PF_6)$, two redox waves are observed with formal potentials of 0 320 V and 0 760 V The

ΔE_p values observed for the two waves are approximately 80 mV, which is slightly larger than the expected value of 57 mV expected for a one-electron redox reaction This slightly larger than expected ΔE_p value is not due to either slow heterogeneous kinetics or ohmic effects as the peak shapes and positions are independent of scan rate for $0.1 \leq \nu \leq 2.0$ Vs^{-1} There is a relatively large separation between the two formal potentials, (0.440 V) Since the dinuclear complex is highly symmetric, the extent of electronic coupling across the 4-bpt bridge is likely to be responsible for the relatively large separation between the two formal potentials [32] Based on the UV-Vis data described above, there appears to be significant electronic communication between the metal centres and the bridging ligand Therefore, the extent of electronic communication across the bridging ligand is probably the source of this large separation between the two formal potentials

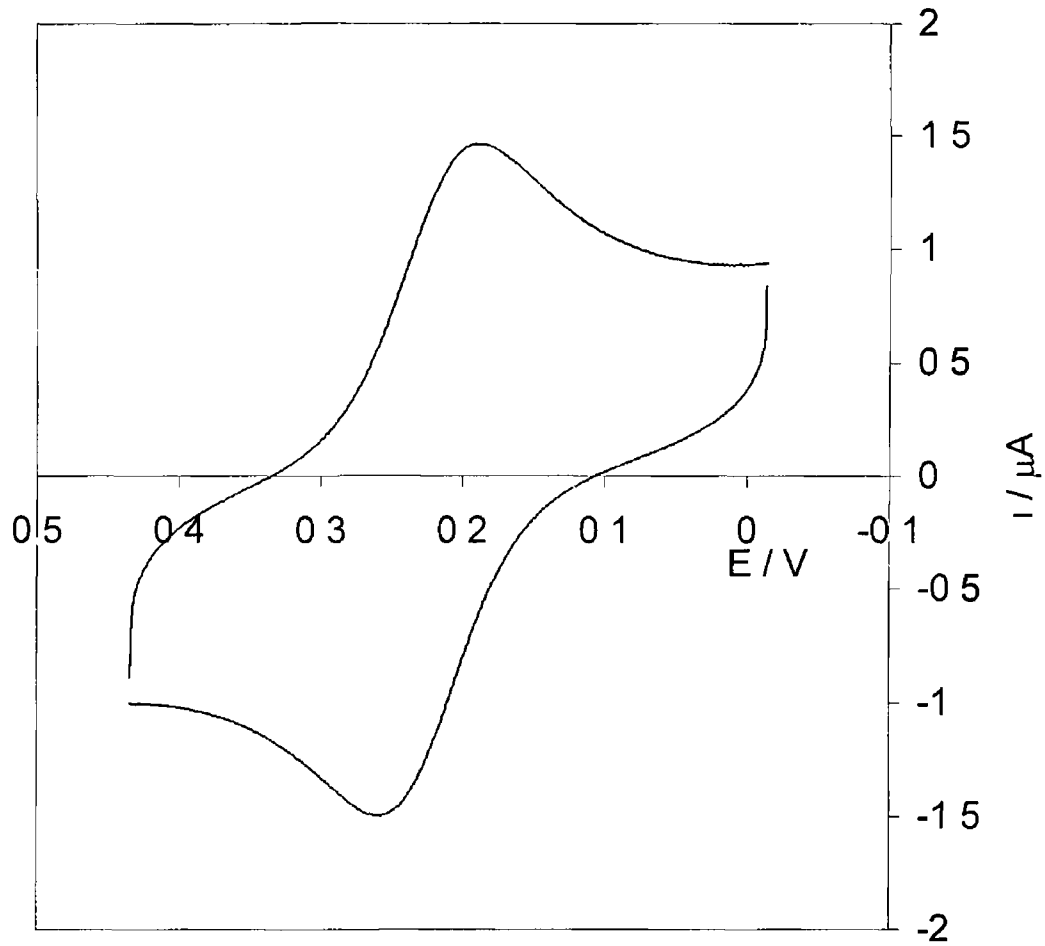

Figure 2 20 Solution phase cyclic voltammogram of $[Os(bpy)_2$ 4-tet Cl$]ClO_4$ dissolved in acetonitrile with 0 1 M $TBABF_4$ as supporting electrolyte The concentration is 100 µM The potential limits are 0 to 0 5 V vs Ag/AgCl and the scan rate is 0 1 Vs^{-1} The electrode is a 1 mm radius platinum disc electrode

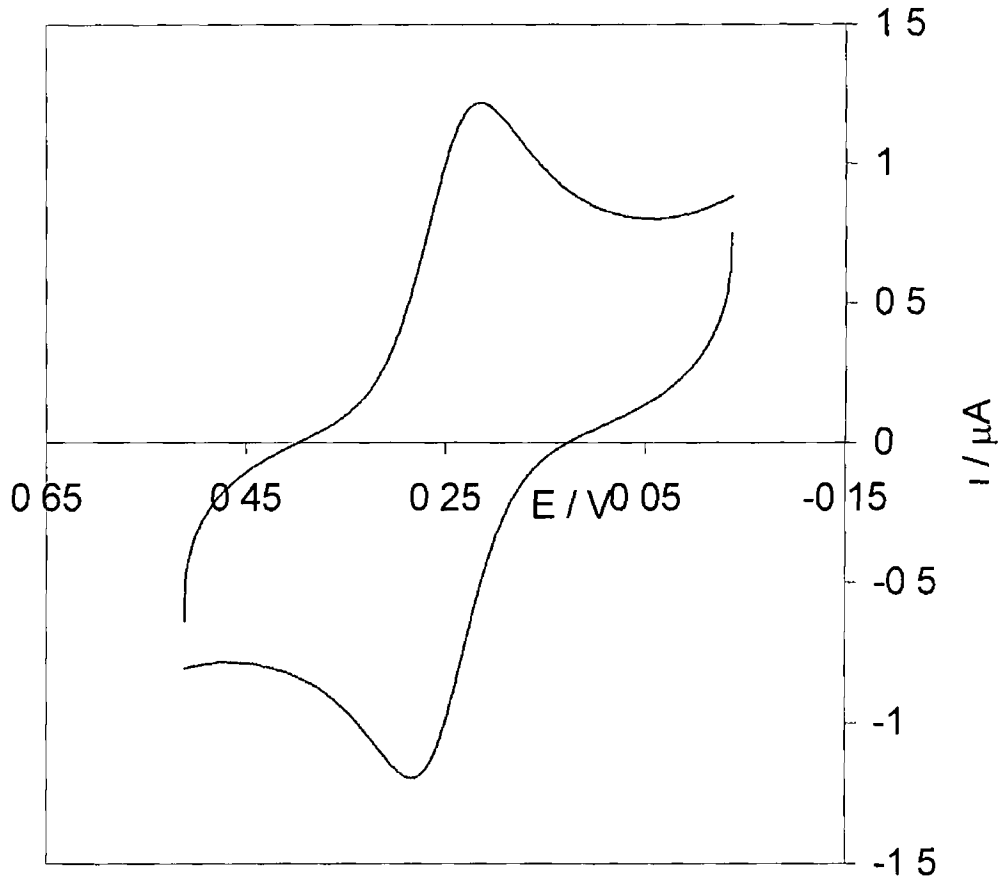

Figure 2 21 Solution phase cyclic voltammogram of $[Os(bpy)_2$ 4 bpt Cl$]PF_6$ dissolved in acetonitrile with 0 1 M $TBABF_4$ as supporting electrolyte The concentration is 100 µM The potential limits are 0 to 0 5 V vs Ag/AgCl and the scan rate is 0 1 Vs^{-1} The electrode is a 1 mm radius platinum disc electrode

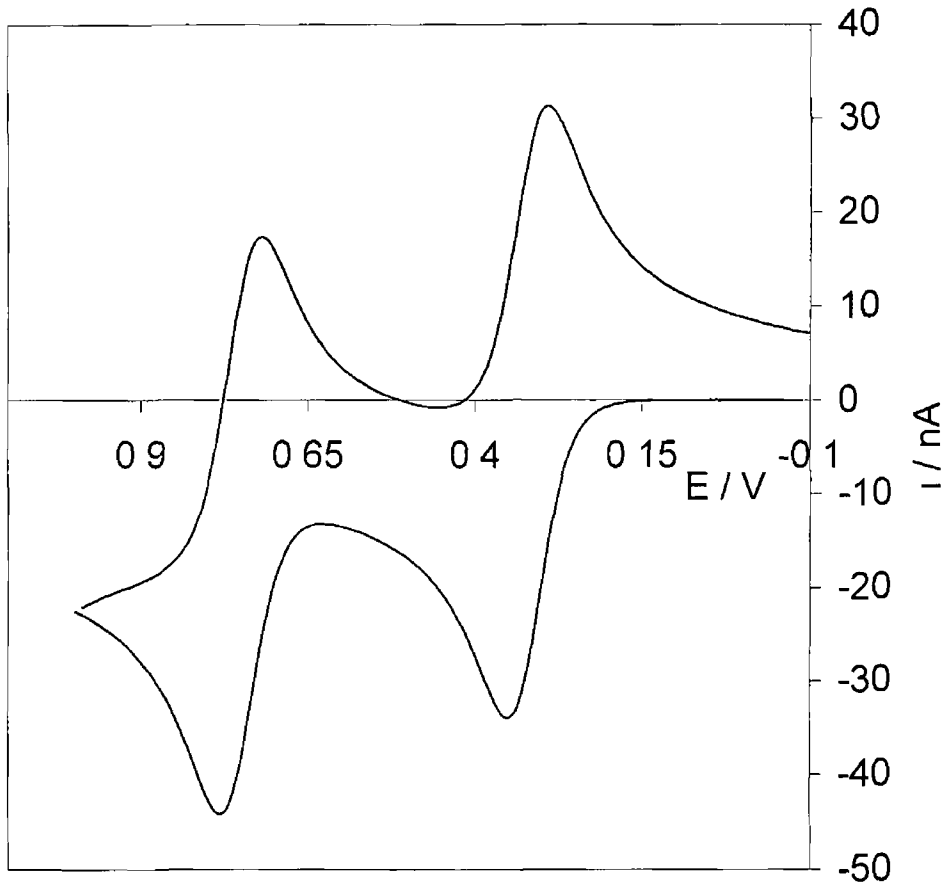

Figure 2 22 Solution phase cyclic voltammogram of $[Os(bpy)_2$ Cl 4-bpt $Os(bpy)_2$ Cl$]PF_6$ dissolved in acetonitrile with 0 1 M $TBABF_4$ as supporting electrolyte The concentration is 10 μM The potential limits are –0 1 to 1 0 V vs Ag/AgCl and the scan rate is 0 5 Vs^{-1} The initial potential is –0 1 V The electrode is a 5 μm radius platinum disc microelectrode

2 4 CONCLUSIONS

The synthesis and characterisation of a series of osmium polypyridyl complexes has been described Characterisation techniques used included NMR spectroscopy, HPLC, UV-Visible spectrophotometry, elemental analysis and cyclic voltammetry The 4-tet and 4-bpt ligands both contain moieties capable of undergoing a protonation/deprotonation reaction, the effect of which is studied in later chapters Using UV-Visible spectrophotometry, the spectral changes that occurred upon protonation of the 4-tet and 4-bpt ligands were monitored in order to determine the pK_a of the ligands in each complex

The solution phase pK_a values of these complexes are very important when undertaking a study of the effects of protonation of the ligands on the electron transfer dynamics However, as described in Section 2 3 4 1 1, the pK_a values of each complex when immobilised at electrode surfaces may be significantly different from that observed in bulk solution These effects are discussed in detail in later chapters The redox potentials of each complex are easily accessible and each complex exhibits nearly ideal electrochemical responses in solution Upon immobilisation of these complexes at electrode surfaces, comparison of the electrochemical behaviour with that observed here in solution may provide an insight into the local microenvironment of the immobilised redox species

REFERENCES

1 Finklea, H O , Ravenscroft, M S , Snider, D A , *Langmuir*, **1993**, *9*, 223

2 Richardson, J N , Peck, S R , Curtin, L S , Tender, L M , Terrill, R H , Carter, M T , Murray, R W , Rowe, G K , Creager, S E , *J Phys Chem* , **1995**, *99*, 766

3 Ju, H , Leech, D , *Phys Chem Chem Phys* , **1999**, *1*, 1549

4 Ravenscroft, M S , Finklea, H O , *J Phys Chem* , **1994**, *98*, 3843

5 Chidsey, C E D , *Science*, **1991**, *251*, 919

6 Forster, R J , Faulkner, L R , *J Am Chem Soc* , **1994**, *116*, 5444

7 Forster, R J , Faulkner, L R , *J Am Chem Soc* , **1994**, *116*, 5453

8 Hudson, J E , Abruña, H D , *J Phys Chem* , **1996**, *100*, 1036

9 Forster, R J , Figgemeier, E , Loughman, P , Lees, A , Hjelm, J , Vos, J G , *Langmuir*, **2000**, *16*, 7871

10 Acevedo, D , Abruña, H D , *J Phys Chem* , **1991**, *95*, 9590

11 Forster, R J , Keyes, T E , *J Phys Chem B* , **2001**, *105*, 8829

12 Forster, R J , O'Kelly, J P , *J Phys Chem* , **1996**, *100*, 3695

13 Forster, R J , Keyes, T E , Bond, A M , *J Phys Chem* , **2000**, *104*, 6389

14 Forster, R J , Keyes, T E , *Phys Chem Chem Phys* , **2001**, *3*, 1336

15 Keane, L , Hogan, C , Forster, R J , *Langmuir*, **2002**, *18*, 4826

16 Forster, R J , *Chem Soc Rev* , **1994**, 289

17 Pletcher, D , In *Microelectrodes Theory and Applications*, Eds Montenegro, M I , Querios, M A , Daschbach, J L , Kluwer Academic Publishers, **1991**

18 Andrieux, C P , Hapiot, P , Saveant, J -M , *Chem Rev* , **1990**, *90*, 723

19 Andrieux, C P , Hapiot, P , Saveant, J –M , *J Phys Chem* , **1988**, *92*, 5992

20 Andrieux, C P , Garreau, D , Hapiot, P , Pinson, P , Saveant, J –M , *J Electroanal Chem* , **1988**, *243*, 321

21 Wipf, D O , Wightman, R M , *Anal Chem* , **1988**, *60*, 2460

22 Wipf, D O , Kristensen, E W , Deakin, M R , Wightman, R M , *Anal Chem* , **1988**, *60*, 306

23 Forster, R J , Vos, J G , Keyes, T E , *Analyst*, **1998**, *123*, 1905

24 Forster, R J , Faulkner, L R , *Anal Chem* , **1995**, *67*, 1232

25 Xu, C , PhD Thesis, University of Illinois at Urbana-Champaign, **1992**

26 Rodriguez, J F , Mebrahtu, T , Soriaga, M P , *J Electroanal Chem* , **1987**, *233*, 283

27 Finklea, H O , Robinson, L R , Blachburn, A , Richter, B , Allara, D , Bright, T , *Langmuir*, **1986**, 2, 239

28 Bard, A J , Faulkner, L R , *Electrochemical Methods Fundamentals and Applications*, 2nd Edn , Wiley, 2001

29 Balzani, V , Juris, A , Venturi, M , *Chem Rev* , **1996**, *96*, 759

30 Juris, A , Balzani, V , Barigelletti, F , Campagna, S , Belser, P , von Zelewsky, A , *Coord Chem Rev* , **1988**, *84*, 85

31 Hage, R , Dijkhuis, A H J , Haasnoot, J G , Prins, R , Reedijk, J , Buchanan, B E , Vos, J G , *Inorg Chem* , **1988**, *27*, 2185

32 Goldsby, K A , Meyer, T J , *Inorg Chem* , **1984**, 23, 3002

CHAPTER 3

ELECTRON TRANSFER DYNAMICS ACROSS GOLD/OSMIUM BIS-BIPYRIDYL CHLORIDE MONOLAYER INTERFACES

3 1 INTRODUCTION

The ability to control the rate of electron transfer across molecular bridges impacts diverse areas ranging from the development of molecular electronics to understanding biosystems [1] To date, the only approach to modulating the rate of electron transfer across a bridge linking molecular or bulk components was to synthetically change the structure of the bridge,[2] the solvent[3] or to couple electron transfer to mass transport, e g , proton coupled electron transfer reactions [4]

A particular challenge is to develop systems in which the electronic structure of the bridge can be reversibly changed in response to the local microenvironment, e g , through a protonation reaction However, this objective can only be achieved if the role of the bridge states in the electron transfer process is understood For example, where electron transfer proceeds via a coherent superexchange mechanism[5] the rate depends algebraically on the difference between the energy levels of the bridge and donor/acceptor, $\Delta E_{Bridge\ D/A}$ Therefore, if this energy difference could be tuned, then one could control the electron transfer dynamics [6]

The influence of bridge states on electron exchange has been investigated extensively for solution phase donor-acceptor systems, e g , transition metal complexes linked by an electroactive bridge [7 8 9] In contrast, there have been relatively few investigations in which one of these molecular components is replaced by a metal surface Traditionally, self-assembled monolayers have employed alkane-thiol linkers in which the energies of both the highest occupied and lowest unoccupied molecular orbitals, the HOMO and LUMO, respectively, are energetically remote from the donor/acceptor states of the bound redox centres [10] While systems of this kind can provide dramatic new insights into the distance and potential dependence of electron transfer,[11] the large $\Delta E_{Bridge\ D/A}$ makes them unattractive for modeling biological systems For example, in DNA donor/acceptor and bridge elements are typically separated by less than 1 eV [12]

Electroactive bridging ligands offer the possibility of significant virtual coupling, superexchange, if the HOMO or the LUMO of the bridge is close in energy to the donor and acceptor moieties If the $\Delta E_{D/A\ LUMO}$ energy difference is smaller than the $\Delta E_{D/A\ HOMO}$ separation, superexchange can occur via an electron superexchange If the $\Delta E_{D/A\ HOMO}$ energy difference is smaller, superexchange will occur via a hole superexchange mechanism

In this chapter, an approach to chemically modulating the rate of heterogeneous electron transfer across metal/monolayer interfaces is described The bridge between the $[Os(bpy)_2\ Cl]^+$ moiety and the electrode surface is 3,6-bis(4-pyridyl)-1,2,4,5-tetrazine where bpy is 2,2′-bipyridyl Significantly, not only is the bridging ligand redox active, it is also capable of undergoing protonation/deprotonation reactions depending on the pH of the contacting electrolyte solution The effect of protonatmg the bridge on the dynamics of heterogeneous electron transfer has been studied using high scan rate cyclic voltammetry These responses are well-behaved over a wide range of scan rates, electrolyte concentration and pH values allowing molecular bridge effects, in particular the role of superexchange on distant charge tunneling to be investigated The complete voltammograms have been modeled to decouple the effects of protonation on the electronic coupling and the free energy of activation

3 2 MATERIALS AND REAGENTS

[$Os(bpy)_2$ 4-tet Cl] ClO_4 was prepared as described in Chapter 2 All other reagents used were of analytical grade

3 3 APPARATUS AND PROCEDURES

Gold microelectrodes were constructed and characterised as described in Chapter 2

Cyclic voltammetry was performed using a CH Instruments Model 660 Electrochemical Workstation and a conventional three electrode cell All solutions were deoxygenated thoroughly using nitrogen, and a blanket of nitrogen was maintained over the solution during all experiments Potentials are quoted with respect to a BAS Ag/AgCl gel-filled reference electrode, except where indicated otherwise All experiments were performed at room temperature (22±3 °C)

Spontaneously adsorbed monolayers were formed by immersing the microelectrodes in micromolar solutions of the metal complex in acetone/water (50/50, v/v) for periods up to 12 hours The pH of the deposition solution was controlled by addition of 1 0 M aqueous perchloric acid The complex is stable towards aerial oxidation and no precautions were taken to exclude atmospheric oxygen during monolayer formation Before electrochemical measurements were made, the electrodes were rinsed with Milli-Q water and the electrolyte solution to remove any unbound material Subsequent measurements were performed in blank electrolyte The degree of monolayer protonation was systematically altered by varying the pH of the contacting electrolyte solution over the pH range 0 50 to 8 00 by adding concentrated solutions of $HClO_4$ or NaOH to 1 0 M $LiClO_4$

Raman spectroscopy was conducted on a Dilor Jobiny-von Spex Labram The exciting 20 mW helium-neon laser (632 8 nm) was focused through a purpose made electrochemical cell onto a monolayer deposited on a gold macroelectrode (1 5 mm radius) using a 10× objective lens The beam diameter when focused is approximately 1 μm producing approximately 10^6 Wcm ^{2} at the surface Focusing was confirmed by using a CCD camera in imaging mode A spectral resolution of 1 5 cm ^{1} per pixel was achieved using a grating of 1800 lines/mm The applied potential was controlled with respect to an Ag/AgCl reference electrode using a CH instruments model 600A potentiostat

3 4 RESULTS AND DISCUSSION

3 4 1 GENERAL ELECTROCHEMICAL PROPERTIES

Figure 3 1 shows representative cyclic voltammograms for a spontaneously adsorbed monolayer of $[Os(bpy)_2$ 4-tet $Cl]^+$ at a gold electrode in aqueous 0 1 M $LiCLO_4$ electrolyte adjusted to pH 1 0 ± 0 2 by addition of concentrated $HClO_4$ The solution does not contain any dissolved complex The formal potential of the redox couple, E°', is observed at 0 245 V vs Ag/AgCl The E°' value observed for the complex dissolved in acetomtrile solution was within 25 mV of the surface-confined E°' value, suggesting that these layers are solvated [26]

The voltammograms exhibit features characteristic of those expected for an electrochemically reversible reaction involving a surface confined redox species [13] The peak shape is independent of scan rate, υ, for $0\ 05 \leq \upsilon \leq 50$ Vs^{-1} (Figure 3 2) and the peak height increases linearly with increasing scan rate (Figure 3 3) Therefore, it appears that $[Os(bpy)_2$ 4-tet $Cl]^+$ adsorbs to the surface of the gold microelectrode to give an electroactive film Repetitive cycling of these monolayers in 0 1 M $LiClO_4$ electrolyte at both neutral and low pH was carried out over a 16 hour period This did not produce any change in the shape of the voltammograms, indicating that these monolayers are extremely stable to electrochemical cycling across a wide pH range

Where there are no lateral interactions between adsorbates and a rapid redox equilibrium is established with the applied potential, a zero peak to peak splitting, ΔE_p, and a full width at half maximum, fwhm, of 90 6 mV are expected for a one electron transfer

$$\text{fwhm} = 3\ 53 \frac{RT}{nF} = \frac{90\ 6}{n}\ \text{mV}(25^\circ\text{C}) \qquad (3\ 1)$$

Monolayers of this complex exhibit non-zero ΔE_p values even at low scan rates, e g , ΔE_p is 60±10 mV at a scan rate of 0 5 Vs^{-1} This behavior has been reported previously for structurally related systems,[14] e g , for $[Os(bpy)_2$ 3,5-bis(pyridin-4-yl)-1,2,4-triazole $Cl]^+$ monolayers,[15] ΔE_P is 15±5 mV at a scan rate of 0 5 Vs^{-1} Feldberg has interpreted non-ideal responses in terms of unusual quasi-reversibility (UQR),[16] arising due to rate processes that are slow compared to the experimental timescale However, it is important to note that ΔE_p does not increase with increasing scan rate for $0\ 5 \leq \upsilon \leq 50$ V s^{-1}, suggesting that the non-ideal behavior is not caused by slow heterogeneous electron transfer Also, the observation that ΔE_P does not increase with increasing scan rate for $0\ 5 \leq \upsilon \leq 50$ V s^{-1} indicates that ohmic drop does not significantly influence the response For the voltammograms illustrated in Figure 3 2, the estimated iR drop is less than 2 mV, which is insignificant compared to the ΔE_p values observed here These monolayers exhibit fwhm values of 250±30 mV, suggesting that there may be repulsive lateral interactions between adjacent redox centers These repulsive interactions are most likely electrostatic in nature due to the net positive charge on each redox centre

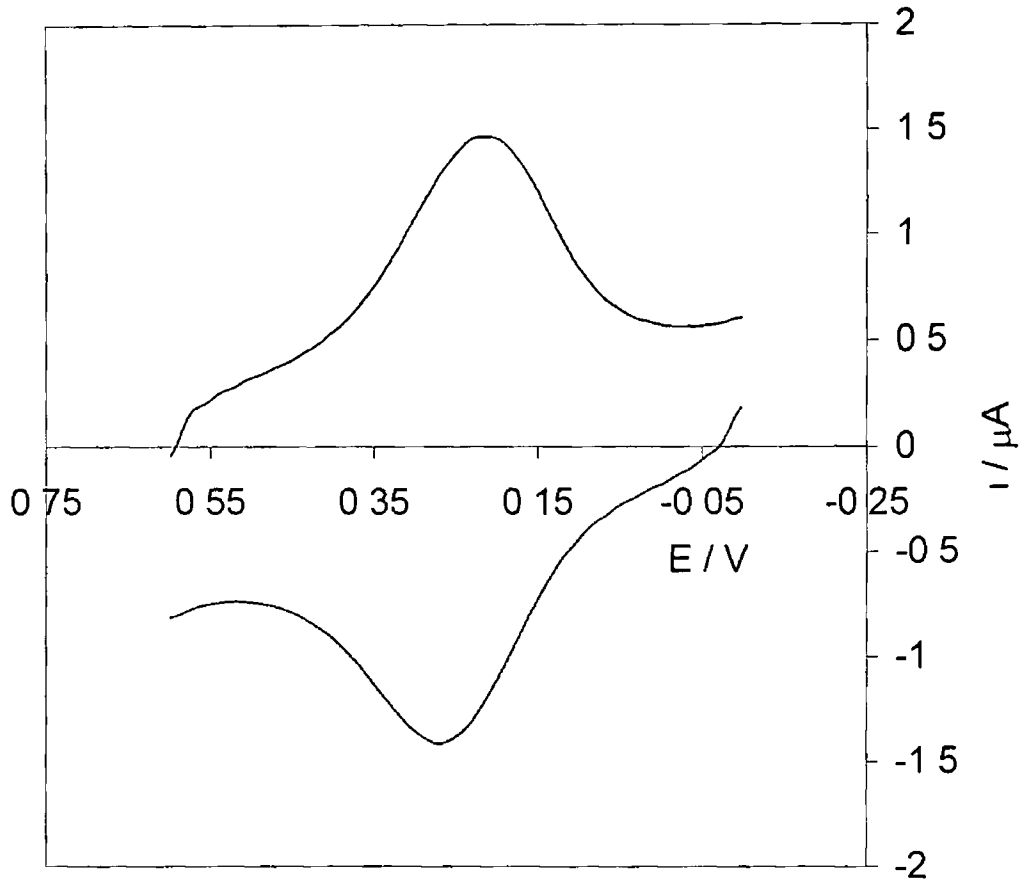

Figure 3 1 Representative cyclic voltammogram for a spontaneously adsorbed monolayer of $[Os(bpy)_2$ 4-tet $Cl]^+$ at a 1 mm radius gold electrode The scan rate is 0 2 V s^{-1} The electrolyte is aqueous 0 1 M $LiClO_4$ adjusted to pH 1 with concentrated $HClO_4$

The area under the oxidative and reductive waves of the cyclic voltammogram can be used to determine the surface coverage, Γ, of the complex on the gold surface using Equation 3 2

$$\Gamma = \frac{Q}{nFA} \qquad (3\ 2)$$

where Q is the charge under the wave, n is the number of electrons transferred in the reaction, is Faraday's constant and A is the area of the electrode The voltammetrically determined surface coverage is $8\ 1\pm0\ 25\times10^{-11}$ mol cm^{-2}, corresponding to an area occupied per molecule of 205±6 $Å^2$ This area of occupation is somewhat larger than the expected, given a radius of approximately 6 7 Å for the $[Os(bpy)_2\ Cl]^+$ moiety,[20 21] but is consistent with a surface coverage that is dictated by the $[Os(bpy)_2\ Cl]^+$ head group, rather than by the bridging ligand In the following section, the dependence of Γ on the concentration of $[Os(bpy)_2$ 4-tet $Cl]^+$ in the deposition solution is probed This may provide an insight into the nature of lateral interactions between adjacent adsorbates

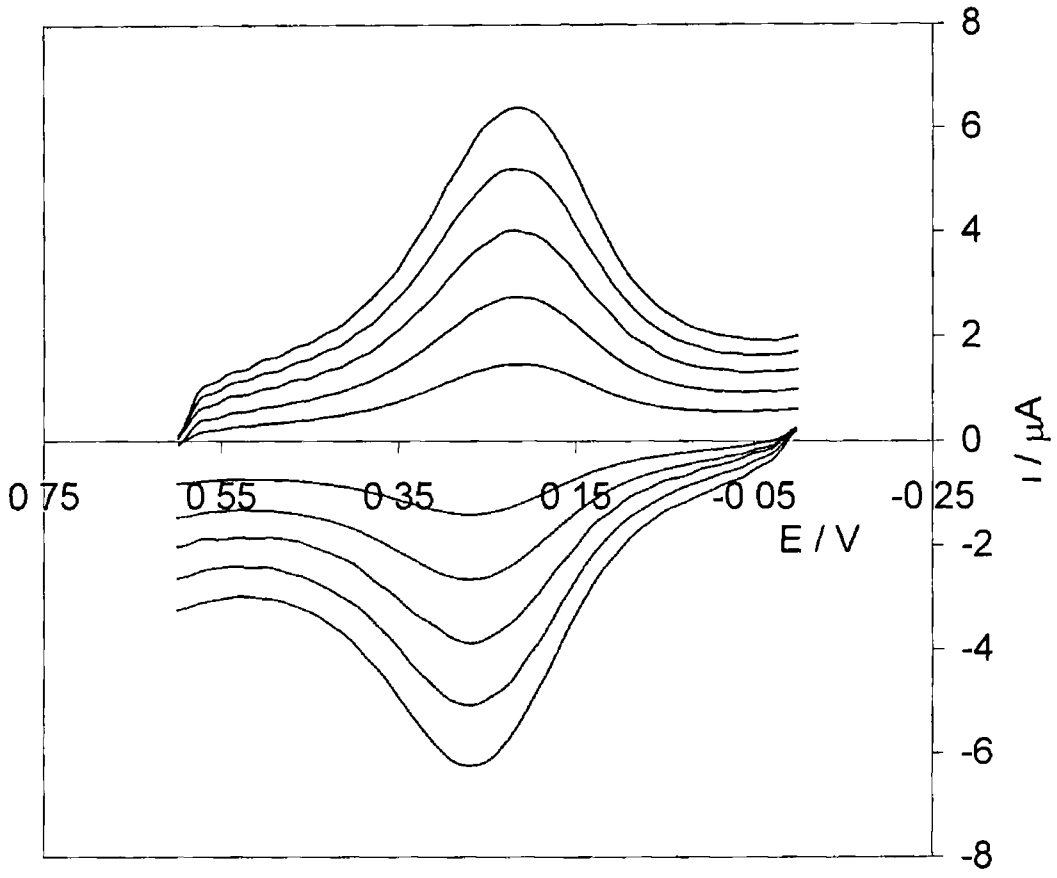

Figure 3 2 Effect of increasing scan rate on the voltammetric response of a spontaneously adsorbed monolayer of $[Os(bpy)_2$ 4-tet $Cl]^+$ at a gold disc electrode The electrolyte is aqueous 0 1 M $LiClO_4$ adjusted to pH 1 with concentrated $HClO_4$ The radius of the electrode is 1 mm Scan rates are (from top to bottom) 1 0, 0 8, 0 6, 0 4, and 0 2 V/s Cathodic currents are up and anodic currents are down

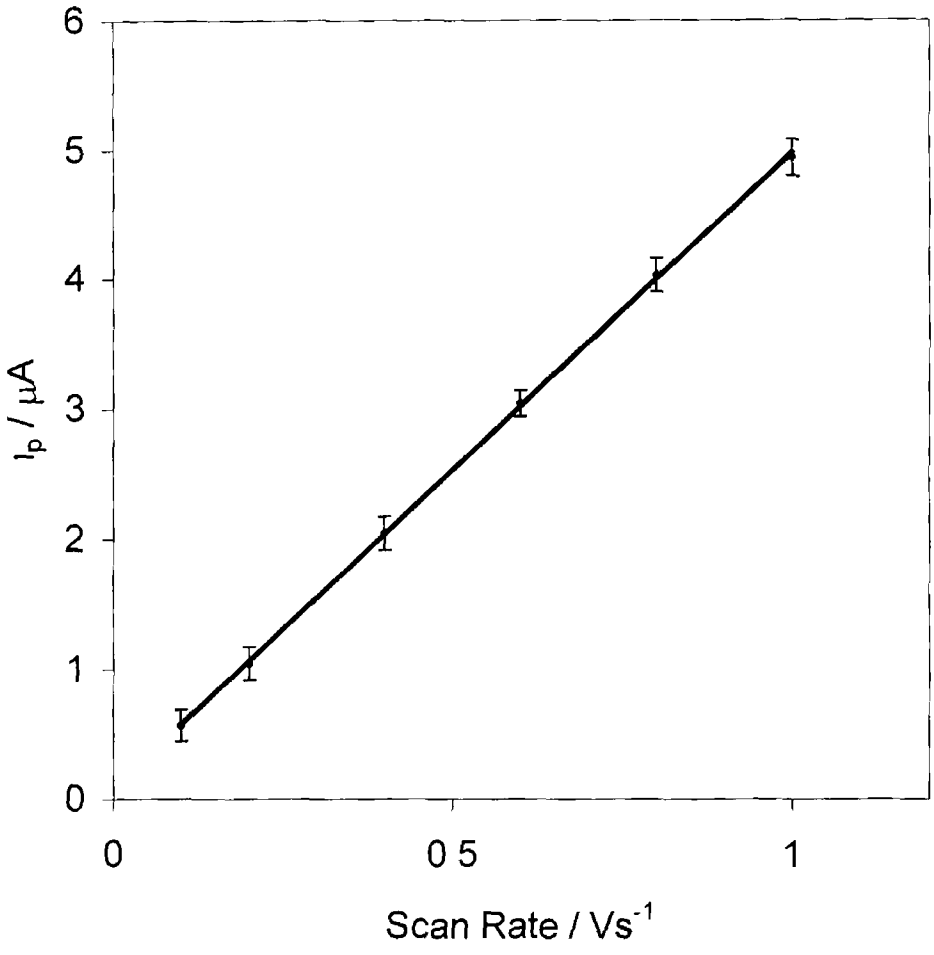

Figure 3 3 Scan rate dependence of the voltammetric peak current for a monolayer of $[Os(bpy)_2$ 4-tet Cl$]ClO_4$ at a gold microelectrode The electrolyte is aqueous 0 1 M $LiClO_4$ adjusted to pH 1 with concentrated $HClO_4$ The radius of the electrode is 1 mm The surface coverage is $8\ 1\times10^{-11}$ mol cm^{-2}

3 4 2 ADSORPTION ISOTHERMS

To examine the existence of lateral interactions between adjacent adsorbates, the effect of the bulk solution concentration of complex on the surface coverage was examined To obtain the adsorption isotherm,[17] the surface coverages at equilibrium were determined by integrating the background corrected cyclic voltammograms as the bulk concentration in the deposition solution was systematically varied Beyond the issue of lateral interactions, the pH dependence of adsorption in this system is interesting because the complex contains two possible protonation sites, i e , the pyridine and tetrazine nitrogens If protonation occurs at the pyridine nitrogen then its lone pair would not be capable of interacting with the surface thus blocking adsorption

Figure 3 4 shows the dependence of the surface coverage of $[Os(bpy)_2$ 4-tet $Cl]^+$ as the concentration of the complex in the deposition solution is systematically varied At both low and high pH the surface coverage reaches a plateau at concentrations of approximately 1 μM Adsorption clearly takes places at low pH suggesting that the tetrazine, rather than the unbound pyridine moiety, becomes protonated at low pH

The Frumkin adsorption isotherm can provide a useful insight into the lateral interactions that may exist within these monolayers since it models the free energy of adsorption as an exponential function of the surface coverage [17]

$$\beta C_i = \frac{\theta_i}{1-\theta_i} \exp(g\theta_i) \qquad (3\ 3)$$

where $\theta_i = \Gamma_i / \Gamma_{sat}$, Γ_i is the coverage of $[Os(bpy)_2$ 4-tet $Cl]^+$ in mol cm ^{2} at a bulk concentration C_i, Γ_{sat} is the saturation coverage obtained at high bulk concentrations and β is the adsorption coefficient g is the interaction parameter

and attractive interactions are indicated by $g<0$ and repulsive interactions by $g>0$, while for $g=0$ the Langmuir isotherm is obtained

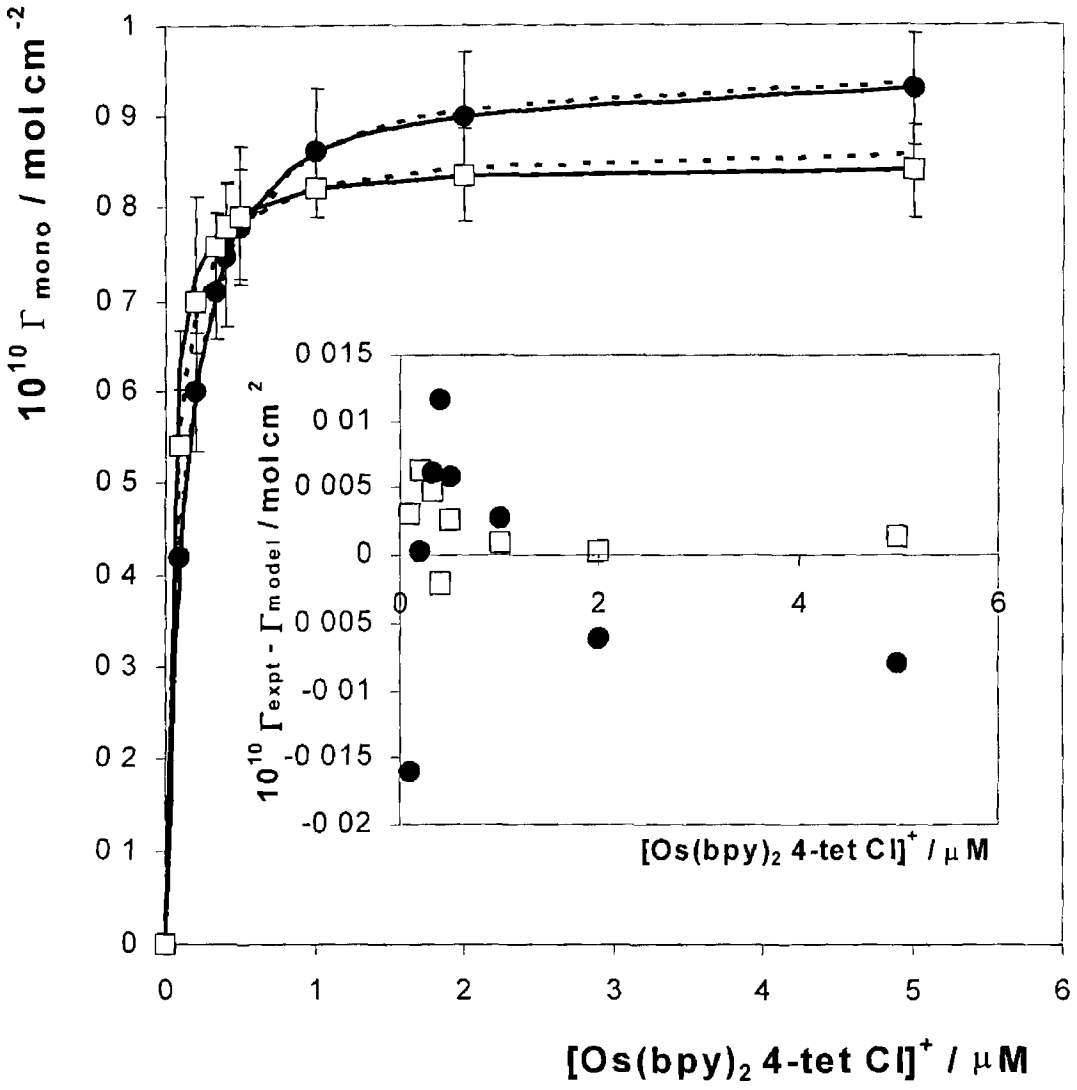

Figure 3 4 Dependence of the surface coverage on the bulk concentration of the $[Os(bpy)_2$ 4-tet Cl$]ClO_4$, • and □ denote monolayers deposited at pH values of 6 6 and 1 8, respectively The supporting electrolyte is 1 0 M $LiClO_4$ The dashed and solid lines represent the best fits to the Langmuir and Frumkin adsorption isotherms, respectively

Figure 3 4 shows that the optimised Frumkin and Langmuir isotherms provide a satisfactory fit to the experimental surface coverages for monolayers assembled from deposition solutions in which the pH is 6 6 or 1 8 However, as illustrated in the inset of Figure 3 4, the residuals associated with the best-fit Frumkin isotherm are generally smaller and less structured than those found for the best-fit Langmuir isotherm Table 3 1 contains the best-fit parameters and reveals that the interaction parameters are +0 10 ± 0 05 and +1 50 ± 0 2 for monolayers deposited at pH 6 6 and 1 8, respectively These positive interaction parameters indicate that destabilizing lateral interactions exist in both cases, but that the destabilizing interactions are stronger for monolayers that contain a protonated tetrazine bridging ligand This result suggests that electrostatic repulsion between the positively charged headgroups exists at all pH values but that protonating the bridge intensifies these destabilizing lateral interactions

The free energy of adsorption, $\Delta G°_{ads}$, can be determined from the adsorption coefficient in conjunction with Equation 3 4 [13]

$$\beta = \exp(-\Delta G°_{ads}/RT) \qquad (3\ 4)$$

The free energies of adsorption are experimentally indistinguishable for the two pHs at a value of –39 9 ± 1 1 kJ mol^{-1} indicating that protonating the tetrazine ligand does not significantly affect the molecule's propensity for adsorption This value is similar to that found for structurally related monolayers,[18 19] e g , for $[Os(bpy)_2$ Cl p3p$]^+$, $\Delta G°_{ads}$ is 37 9 ± 2 2 kJ mol^{-1} The saturation surface coverages observed at pH 6 6 and 1 8 are 0 96 ± 0 1 and 0 84 ± 0 2x10^{-10} mol cm^{-2} corresponding to areas occupied per molecule of approximately 174 ± 16 and 198 ± 38 Å^2, respectively These areas of occupation are somewhat larger than those expected given a radius of approximately 6 7 Å for the $[Os(bpy)_2Cl]^+$ moiety,[20 21] but are consistent with a surface coverage that is dictated by the redox active headgroup rather than by the bridging ligand

Table 3 1 Saturation coverages, Adsorption Coefficients and Frumkin Interaction Parameters for $[Os(bpy)_2$ 4-tet $Cl]^+$ Monolayers Assembled from deposition solutions at pH 6 6 and 1 8

	pH 6 6	**pH 1 8**
$10^{-10}\ \Gamma_{sat}$ / **mol cm**$^{-2}$	0 96 ± 0 1	0 84 ± 0 2
β / M^{-1}	9 9 ± 0 3 x 10^6	9 8 ± 0 4 x 10^6
$\Delta G°_{ads}$ / **kJ mol** ^{1}	-39 9 ± 0 8	-39 9 ± 1 1
g	+0 10 ± 0 05	+1 5 ± 0 2

3 4 3 EFFECT OF ELECTROLYTE CONCENTRATION ON THE REDOX FORMAL POTENTIAL

Given the interest in understanding protonation reactions and electron transfer dynamics within these monolayers, it is important to probe the nature of the microenvironment within the film The formal potential depends on both the solvation shell and the extent of ion-pairing [22,23 24] Upon oxidation of a monolayer of this complex, the net charge on the complex switches from +1 to +2 When this occurs, anions must move from the electrolyte solution into the layer in order to maintain electroneutrality The extent of ion pairing in these monolayers has been examined by probing the effect of electrolyte concentration on the formal potential of the $Os^{2+/3+}$ redox reaction for $0\ 1 \leq [LiClO_4] \leq 1\ 0$ M In these measurements, scan rates less than 1 Vs^{-1} were employed so as to avoid any influence from the interfacial electron transfer kinetics

When a polycationic film is placed in a dilute solution of a strong electrolyte, the concentration of counterions (ClO_4^- in this case) within the deposit is typically considerably larger than that found in the contacting solution Thus, under the influence of the concentration gradient, counterions may diffuse from the deposit into the solution until the concentrations become equal in the two phases However, if diffusion of charged counterions occurs, then electroneutrality within the deposit would be violated, and an electrical potential would develop at the interface [13] Therefore, to avoid any complications due to the ionic strength of the electrolyte, the extent of ion-pairing in these monolayers was examined in electrolytes that contained a high concentration of Na_2SO_4 as swamping electrolyte

The formal potential of the $Os^{2+/3+}$ redox reaction shifts by less than 15 mV over the electrolyte concentration range $0\ 1 \leq [Na_2SO_4] \leq 1\ 0$ M indicating that SO_4^{2-} has little tendency to ion-pair with the osmium centers Therefore, Na_2SO_4 is a suitable swamping electrolyte It is interesting to note that in the presence of

Na_2SO_4 electrolyte alone, even at low concentrations, the monolayer becomes unstable and desorbs from the electrode surface over a period of minutes However, when both Na_2SO_4 and $LiClO_4$ are present in the electrolyte solution, the perchlorate appears to stabilise the monolayer and it remains stable for periods of hours This may be due to a specific ion association between the osmium metal centre and the perchlorate ion

For $0.1 \leq [LiClO_4] \leq 1.0$ M, the peak shapes and heights are insensitive to changes in the electrolyte concentration However, as illustrated in Figures 3.5 and 3.6, $E^{\circ\prime}$ shifts in a negative potential direction as the $LiClO_4$ concentration increases indicating that it becomes increasingly easier to oxidize the osmium redox centre at higher electrolyte concentrations This behavior is consistent with ion-pairing between the perchlorate and the redox center [14] The theoretical slope of this semi-log plot is (59/p) mV/decade, where p is the difference in the number of anions pairing with the oxidized and reduced forms of the redox centre This is described in the following Nernstian relationship

$$[Os(bpy)_2 4-tetCl]^{+}\left(ClO_4^{-}\right)_{\zeta} - e^{-} + p\left(ClO_4^{-}\right) \longrightarrow [Os(bpy)_2 4-tetCl]^{2+}\left(ClO_4^{-}\right)_{\zeta+P} \qquad (3.5)$$

In this relationship, both redox forms are considered to take part in the ion-pairing equilibrium The slope determined for $[Os(bpy)_2$ 4-tet $Cl]^{+}$ monolayers was 51 ± 6 mV indicating that a single additional anion becomes bound to the redox center in the oxidized state [14]

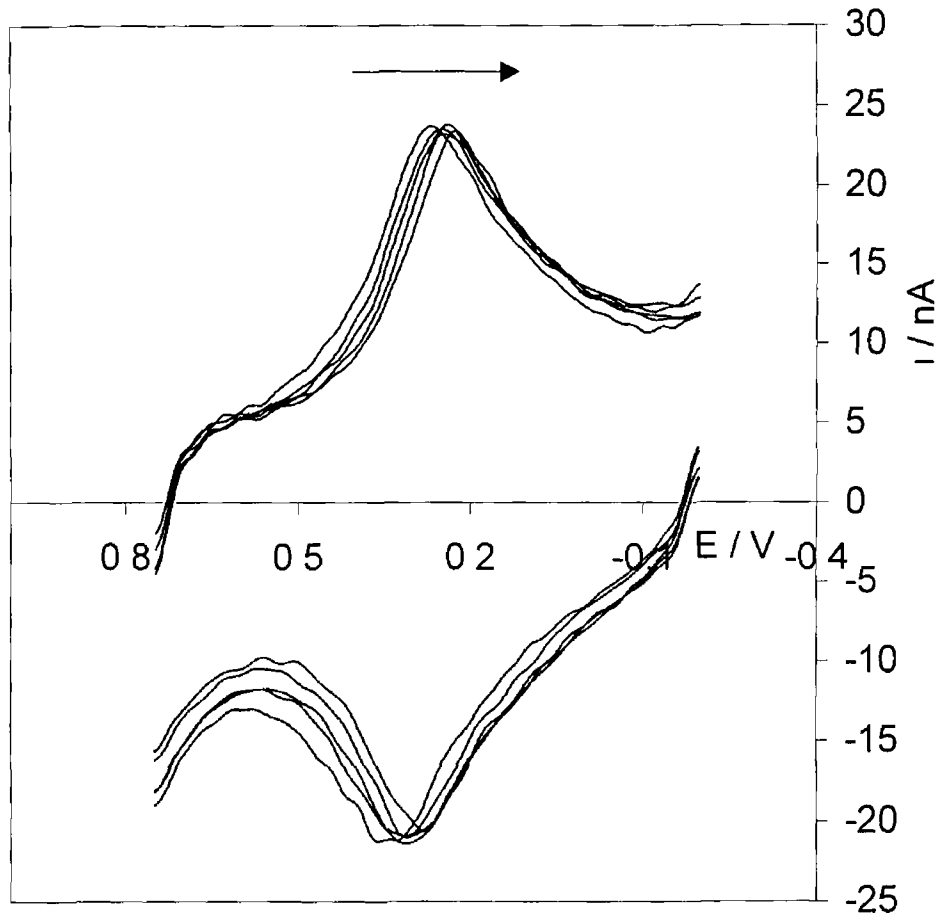

Figure 3 5 Dependence of the voltammetric response of a tetrazine monolayer adsorbed on a 12 5 μm gold microelectrode on the electrolyte concentration Lithium perchlorate concentrations are (from left to right) 0 1, 0 2, 0 4, 0 6 and 1 0 M $LiClO_4$ The concentration of Na_2SO_4 in each solution is 1 0 M

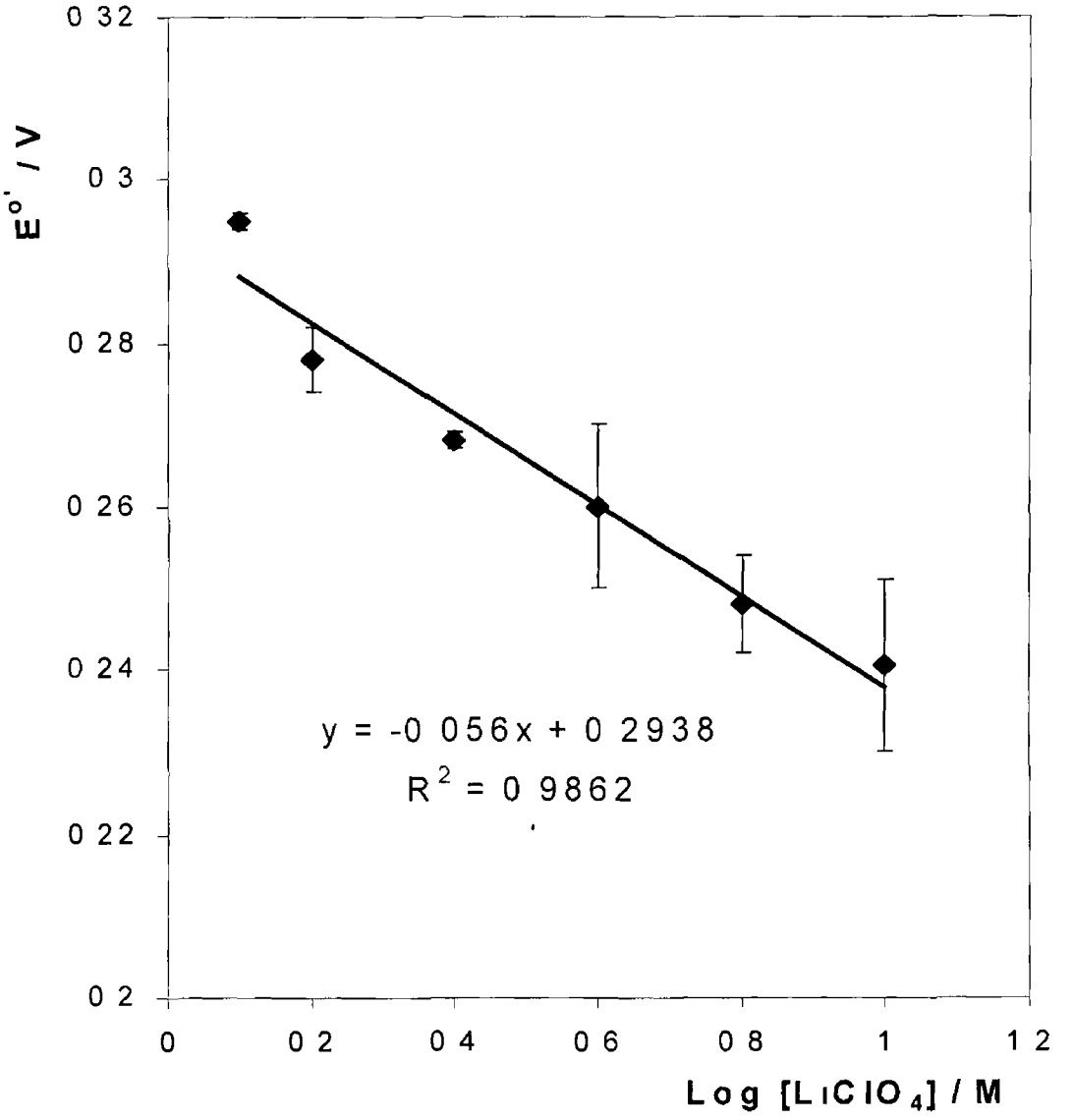

Figure 3 6 Dependence of the formal potential of the $Os^{2+/3+}$ redox reaction within an adsorbed monolayer of $[Os(bpy)_2$ 4-tet $Cl]^+$ on the concentration of perchlorate electrolyte All measurements were performed in a constant background electrolyte of 1 0 M Na_2SO_4

3 4 4 EFFECT OF pH ON THE REDOX FORMAL POTENTIAL

In this study, one of the major goals is to probe the effects of protonation on heterogeneous electron transfer dynamics across electrode/monolayer interfaces The pK_a of $[Os(bpy)_2$ 4-tet $Cl]^+$ in solution has been determined (Section 2 3 4 1 1) as 2 6±0 2 By examining the effect of protonation of the tetrazine ligand, when incorporated as a monolayer at an electrode surface, it is possible to gain an insight into the site of protonation, as well as the effects of ligand protonation on the thermodynamic facility of the redox process

Figure 3 7 shows the effect of decreasing the contacting electrolyte pH on the voltammetric response of $[Os(bpy)_2$ 4-tet $Cl]^+$ monolayers The formal potential of the $Os^{2+/3+}$ redox reaction shifts from 0 136 to 0 284 V as the pH is systematically decreased from 5 47 to 0 59 A similar behavior is observed for both the complex in solution and for mechanically attached solid state deposits,[25] where E°′ shifts in a positive potential direction by approximately 150 mV upon protonation of the tetrazine ligand This pH sensitive E°′ contrasts with $[Os(bpy)_2$ 4,4′-trimethylenedipyridine $Cl]^+$ monolayers,[26] and is consistent with protonation occurring at the tetrazine rather than the pyridine site

The shift in E°′ to more positive potentials at low pH indicates that it is more difficult to create the Os^{3+} species when the tetrazine is protonated Both a reduced electron donating ability of the protonated ligand and a higher overall positive charge on the monolayer are likely to contribute to this effect The shift of the formal potential with pH may also provide an insight into the pK_a of the ligand, when incorporated as a monolayer The inset of Figure 3 7 illustrates the effect of pH on the formal potential An inflection in the data is observed at the solution phase pK_a (2 6), suggesting that the surface-confined pK_a may be similar to that when in bulk solution Capacitance data can provide further insights into this and is described in the following sections

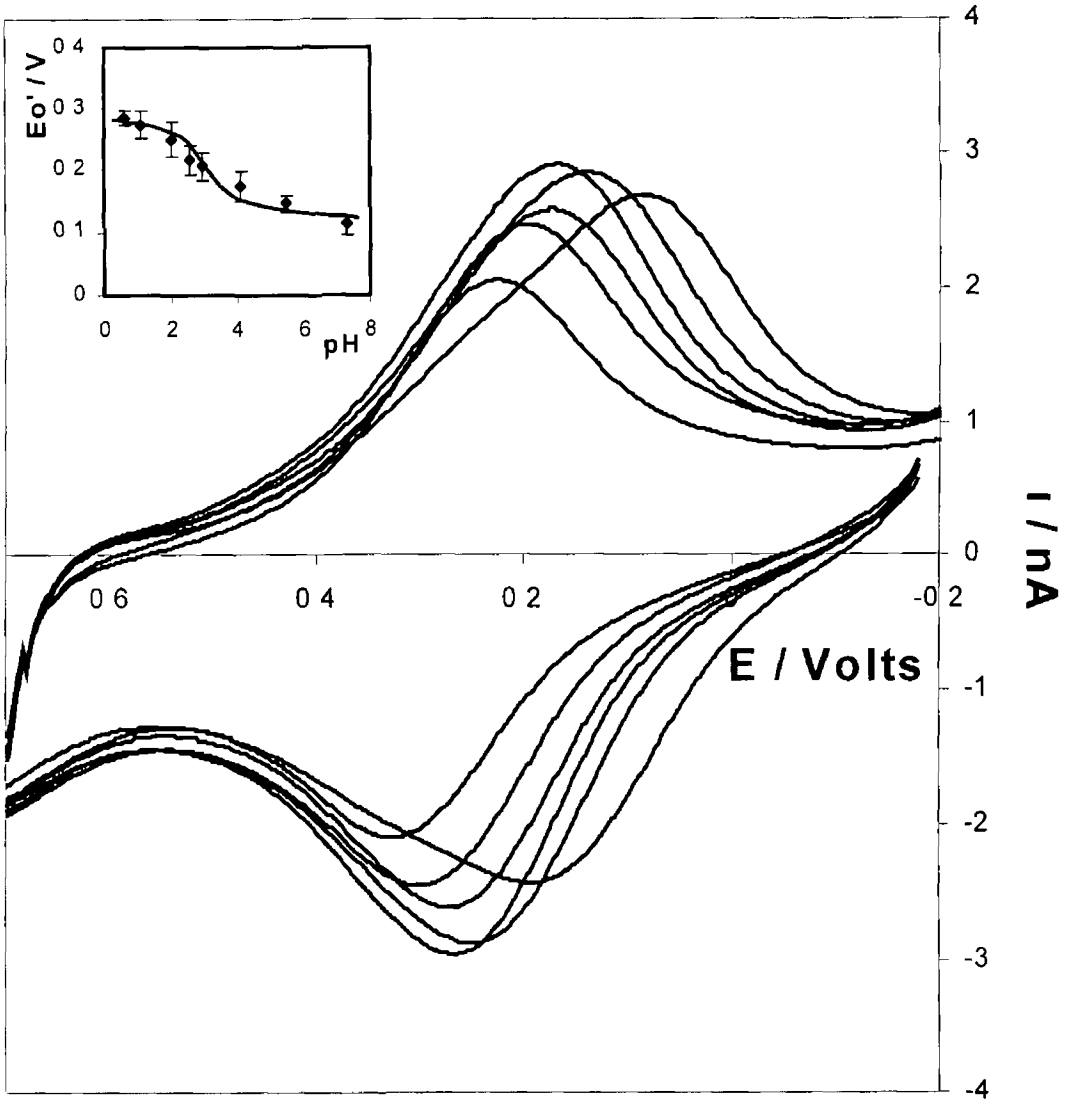

Figure 3 7 Effect of the electrolyte pH on the voltammetric response of an [Os (bpy)$_2$ 4-tet Cl]ClO_4 monolayer adsorbed on a 12 5 μm radius gold microelectrode The scan rate is 1 V s^{-1} and the supporting electrolyte is 1 0 M $LiClO_4$ The electrolyte pH was adjusted by adding concentrated $HClO_4$ or NaOH The pH values are (from left to right) 0 60, 2 00, 2 59, 2 95, 4 10, and 5 47 Cathodic currents are up and anodic currents are down

3 4 5 INTERFACIAL CAPACITANCE MEASUREMENTS

Immobilisation of this complex within organised monolayers may affect both the local dielectric constant and the electron density of the ligand Both of these effects may affect the pK_a of the tetrazine ligand Capacitance measurements may provide an insight into these issues, as well as providing an alternative to the formal potential data described above for estimation of the pK_a of the ligand, when incorporated within a monolayer There are two limiting cases for the potential profile across an adsorbed monolayer In the first, the modified electrode can behave similarly to an unmodified electrode so that all of the applied potential is dropped close to the electrode surface This is illustrated in Figure 3 8A In this case, the immobilised redox centre does not experience a large electric field

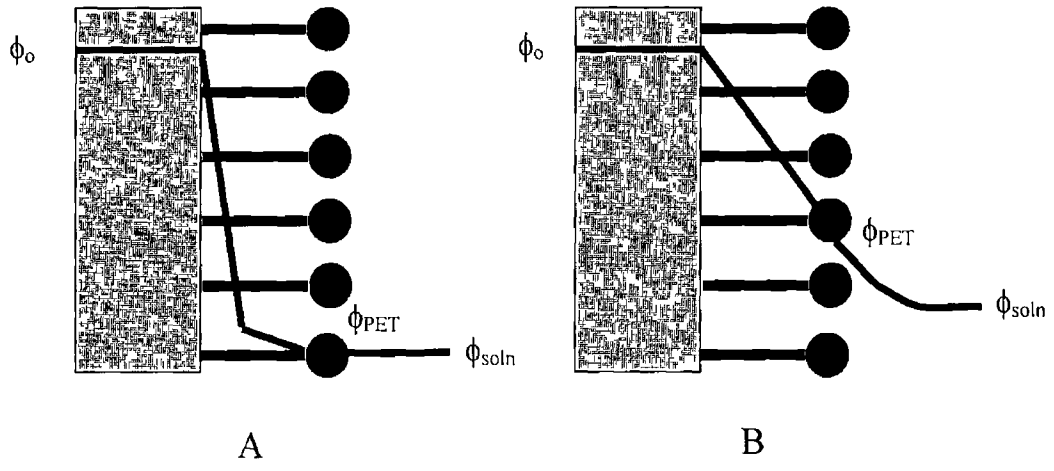

Figure 3 8 The two limiting cases for the potential profile across an adsorbed monolayer

In the second situation, as discussed by Smith and White,[27] if an impermeable monolayer that has a low dielectric constant is adsorbed at the surface, the potential may decay linearly across the monolayer and then exponentially in the solution This is illustrated in Figure 3 8B In this case, the immobilised redox

centres would experience a large electric field By probing the interfacial capacitance, an insight into the applicability of either model can be obtained

For the model illustrated in Figure 3 8B, the capacitance of both the monolayer, C_{mono}, and the diffuse layer, C_{dif}, contribute to the total differential capacitance, C_T, as given by Equation 3 6

$$C_T^{-1} = C_{mono}^{-1} + C_{dif}^{-1} \quad (3\ 6)$$

The film capacitance is given by

$$C_{mono} = \varepsilon_0 \varepsilon_{film}/d \quad (3\ 7)$$

where ε_0 is the permittivity of free space, ε_{film} is the dielectric constant of the film, and d is the thickness of the monolayer

The differential capacitance as determined using cyclic voltammetry at a potential of –0 150 V is independent of the perchlorate concentration $0\ 2 \leq [LiClO_4] \leq 1\ 0$ M This result suggests that for high electrolyte concentrations the diffuse layer capacitance becomes sufficiently large so that it no longer contributes significantly to C_T Under these circumstances $C_T \approx C_{mono}$ and the limiting interfacial capacitance, 39 5±3 6 μF cm^{-2}, can be used in conjunction with Equation 3 7 to estimate the dielectric constant of the film Energy minimized molecular modeling indicates that a fully extended monolayer is approximately 17 Å thick yielding a monolayer dielectric constant of 75 9±6 9 This value is indistinguishable from that of bulk water, 78 5, and is consistent with a well solvated monolayer that is permeable to electrolyte ions

Alternatively, the double layer may set up within the monolayer (Figure 3 8A), in which case the interfacial capacitance corresponds to the capacitance of the charges held at the outer Helmholtz plane As the distance of closest approach is

likely to be of the order of 3Å, the dielectric constant within the double layer would have to decrease from the value of 78 5 for bulk water to approximately 13 4 before a limiting interfacial capacitance of 39 5 μF cm^{-2} would be observed (Equation 3 7) This would indicate the presence of an impermeable monolayer at the electrode surface Therefore, these data do not conclusively allow an insight into which of the models (Figure 3 8 A or B) best describes the potential profile across the monolayers It is concluded that the interior of the monolayer is at least partially solvated at high concentrations of electrolyte This is consistent with the observation that the formal potential of the redox reaction is similar for the osmium centres when in solution and when incorporated as monolayers

Smith and White have further developed this model to describe the effects of monolayer protonation on the interfacial capacitance [28] This approach has been successfully used by Bryant and Crooks to determine the surface pK_a for pyridine derivatives adsorbed on gold electrodes [29] In this model, the total interfacial capacitance depends on the monolayer capacitance, the diffuse layer capacitance, and the degree of protonation of the monolayer, C(f), according to Equation 3 8

$$C_T^{-1} = C_{mono}^{-1} + [C_{dif} + C(f)]^{-1} \qquad (3\ 8)$$

Assuming that C_{mono} remains constant, the term $[C_{dif} + C(f)]^{-1}$ varies with potential and with the solution pH As the pH of the contacting solution is altered, C(f) reaches a local maximum near the pK_a, and a maximum is observed in the total interfacial capacitance Figure 3 9 shows the effect of systematically varying the pH of the contacting solution on the differential capacitance for $1\ 10 \leq pH \leq 7\ 50$ All changes in the capacitance were confirmed to be reversible by first decreasing and then increasing the pH of the supporting electrolyte The shape of the curve agrees with that predicted by theory[28] and yields a surface pK_a of 2 7±0 6 Consistent with a highly solvated monolayer, this value agrees closely with that determined using pH induced changes in the metal-to-ligand-charge-

transfer (MLCT) band observed for the complex dissolved in essentially aqueous media (2 7±0 2) [25]

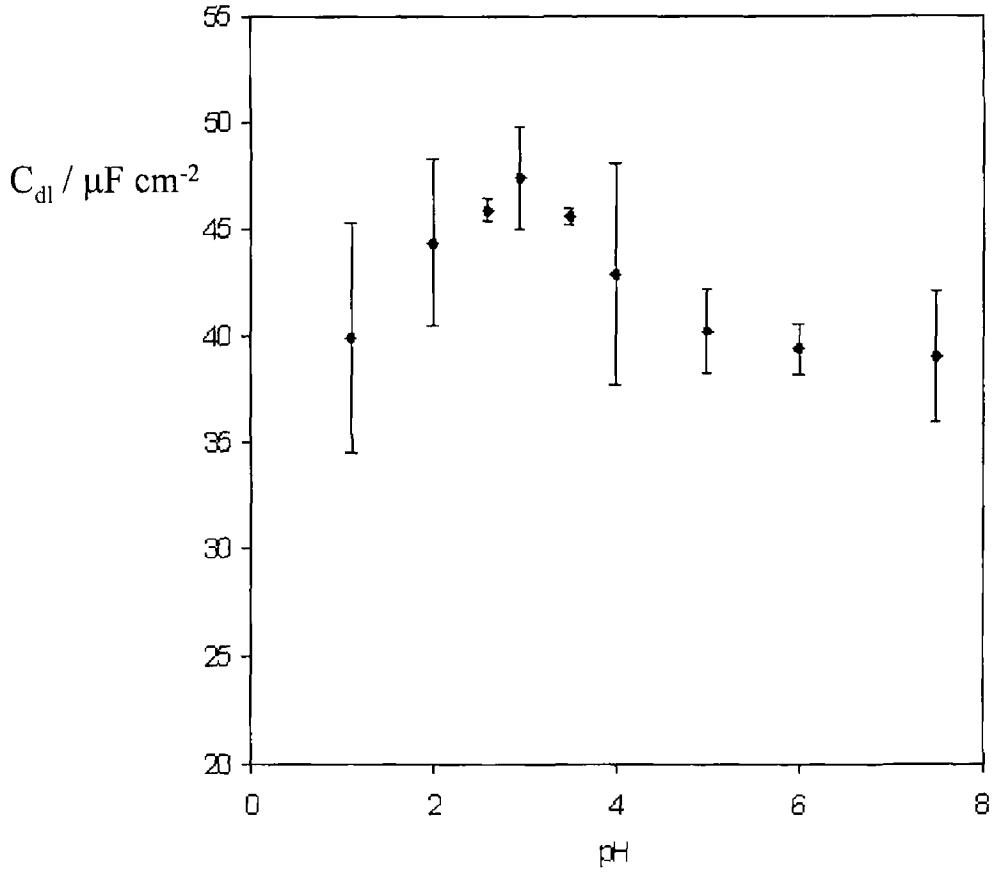

Figure 3 9 Dependence of the differential capacitance for a monolayer of [Os(bpy)$_2$ 4-tet Cl]ClO_4 at a 25 μm gold microelectrode on the pH of the contacting electrolyte solution (1 M $LiClO_4$)

3 4 6 POTENTIAL DEPENDENT RAMAN SPECTROSCOPY

Potential dependent Raman spectroscopy was carried out in order to identify any structural changes that accompany redox switching of $[Os(bpy)_2$ 4-tet Cl$]ClO_4$ monolayers Surface enhanced Raman spectroscopy, SERS is particularly useful as the enhanced sensitivity of this method allows a powerful insight into the monolayer structure, e g , packing density and adsorbate orientation, to be obtained [30] In this application, surface enhanced raman spectroscopy has been used to characterise the effects of oxidation of the Os^{2+} metal centres on the bonding between the osmium metal centre and the various ligands

The microscope Raman technique employed here allows the laser to be focused onto the modified surface eliminating any contribution from the supporting electrolyte or the electrode shroud Figures 3 9 A and B show the Raman spectra for $[Os(bpy)_2$ 4-tet Cl$]ClO_4$ monolayers immobilized on a roughened gold macroelectrode at -0 200 and 0 500 V vs Ag/AgCl, respectively, where the supporting electrolyte is 0 1 M $LiClO_4$ The UV-visible spectrum of this complex indicates that the exciting HeNe laser (632 8 nm) is preresonant with the MLCT (Os(II)-bpy*) transition (Section 2 3 4 1)

The resonance effect is confirmed through enhancement of features at 1605, 1553, 1482, 1320, 1268, 1170, 1015 and 669 cm^{-1} all of which are associated with the bipyridyl moieties [25 31] The features observed at 1206, 1042 and 848 cm^{-1} and a shoulder at 1607 cm^{-1}are associated with the 4-tet ligand [25] A weaker feature at 380 cm^{-1} is associated with the Os-N stretch [25] Oxidation results in quantitative loss of Os-N modes and 4-tet modes However, while oxidation significantly changes the relative intensities of the bipyridyl modes they persist after the monolayer is oxidized

Figures 3 10 A and B illustrate the Raman spectra of a dense monolayer at -0 200 and 0 500 V, respectively, where the supporting electrolyte is 0 1 M $HClO_4$

Vibrational features associated with the $Os(bpy)_2$ remain relatively unperturbed by the presence of acid However, consistent with protonation, the 4-tet feature at 848 cm^{-1} disappears in low pH electrolyte and the band overlapping the bpy mode at 1606 cm^{-1} is resolved

Oxidizing the monolayer has a similar impact on the Raman spectra in both neutral and low pH electrolytes Specifically, the low frequency Os(II)-N vibration collapses indicating efficient oxidation of all the metal centers and changes are observed in the relative intensities of all bpy modes Upon oxidation of the osmium metal centres, the MLCT modes are lost This is consistent with a reduced electron donating ability of the oxidised osmium metal centres Therefore, the exciting laser is no longer pre-resonant with the MLCT transition However, the fact that the bpy bands continue to be observed after oxidation of the metal centres indicates that the laser has become pre-resonant with another transition After oxidation, the laser becomes pre-resonant with a bpy*-Os ligand to metal charge transfer, LMCT, transition,[25] resulting in the appearance of the bpy based features after oxidation of the film

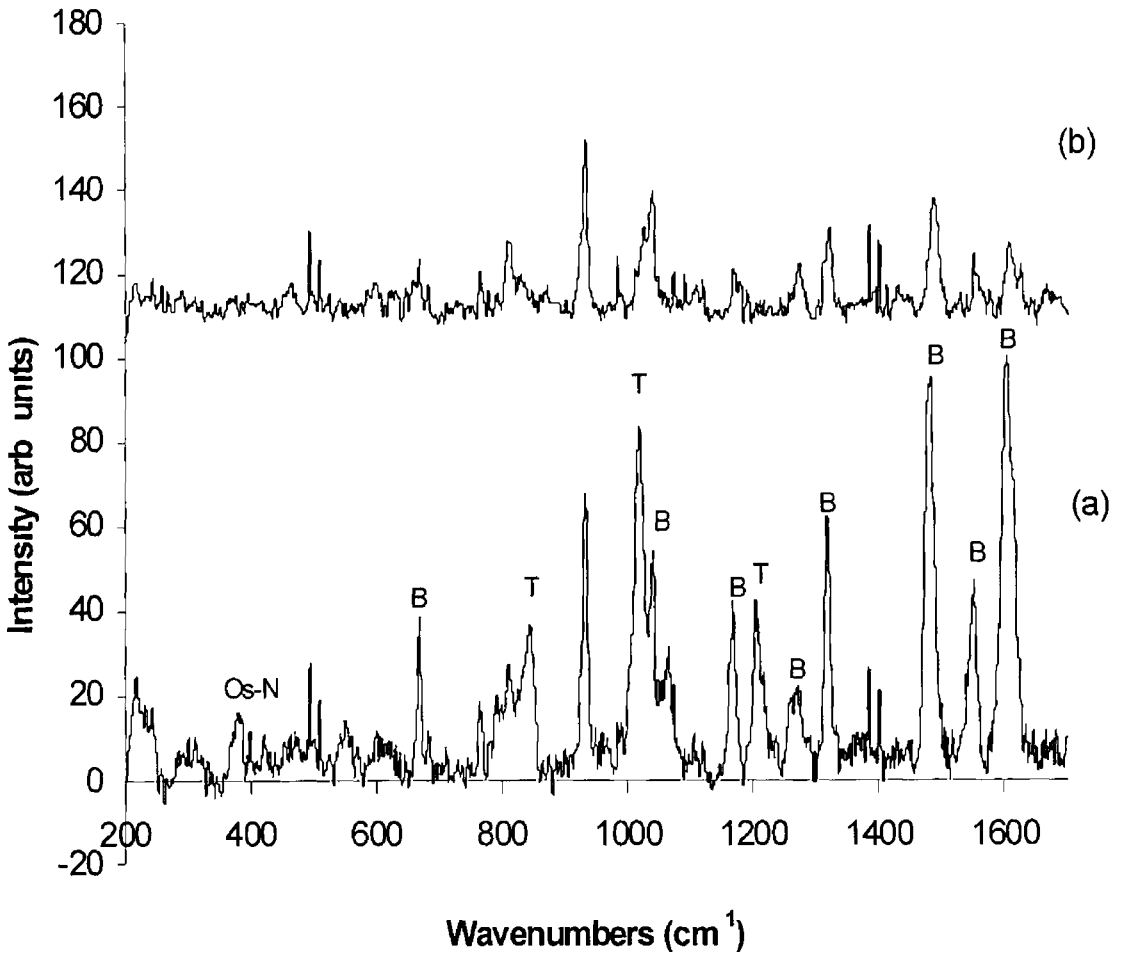

Figure 3 9 Potential controlled Raman spectra of $[Os(bpy)_2\ 4tet\ Cl]ClO_4$ monolayers on a gold macrodisc electrode where the supporting electrolyte is 0 1 M $NaClO_4$ (pH 6) (a) 0 200V (b) 0 500 V The wavelength of the exciting He-Ne laser is 632 8 nm B indicates features associated with bipyridyl moieties and T indicates features associated with the tetrazine moiety

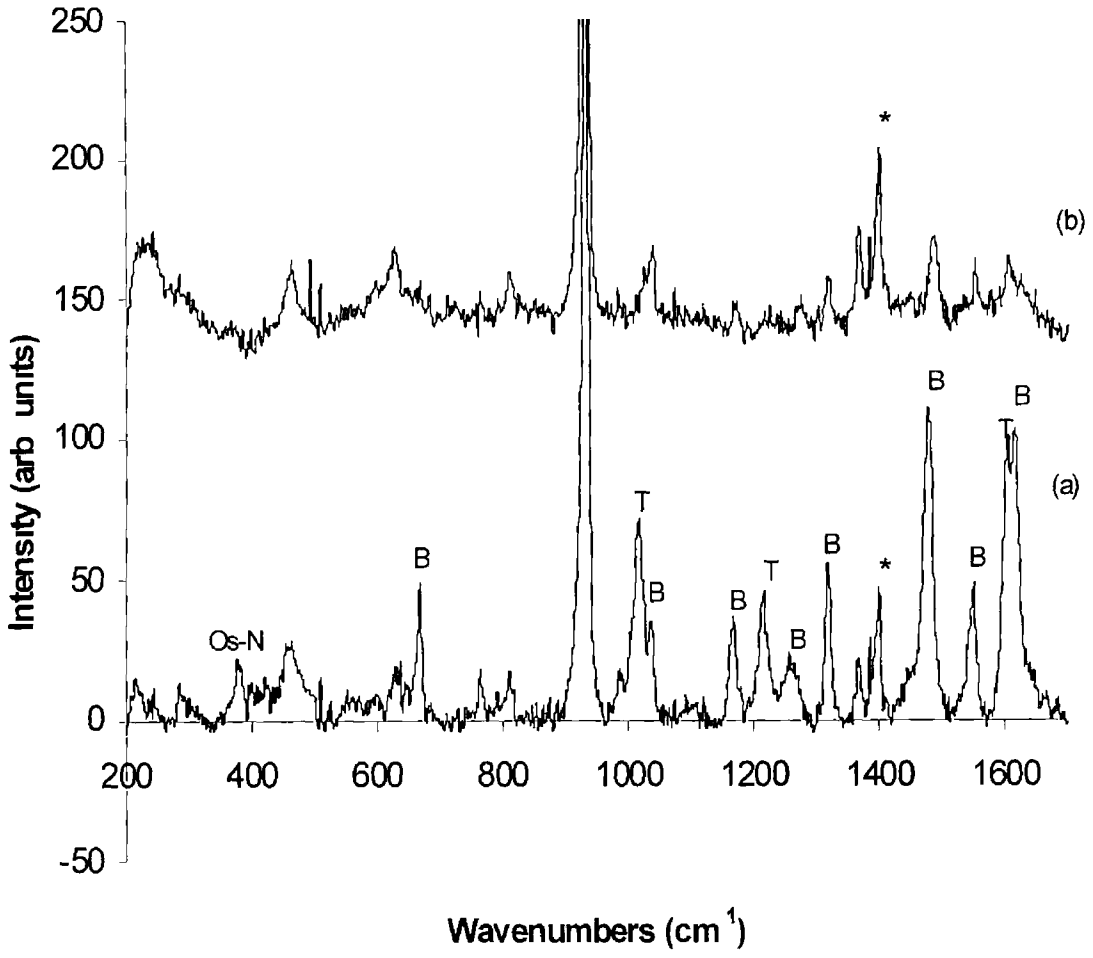

Figure 3 10 Potential controlled Raman spectra of $[Os(bpy)_2\ 4tet\ Cl]ClO_4$ monolayers on a gold macrodisc electrode where the supporting electrolyte is 0 1 M $HClO_4$ (pH 1) (a) 0 200V (b) 0 500 V The wavelength of the exciting He-Ne laser is 632 8 nm B indicates features associated with bipyridyl moieties and T indicates features associated with the tetrazine moiety

3 4 7 HETEROGENOUS ELECTRON TRANSFER DYNAMICS

Redox active bridging ligands are important in that they offer the possibility of significant virtual coupling (superexchange) depending on the difference between the redox potentials of the bridge and remote redox centres Electron transfer via superexchange may be the dominant mechanism if the LUMO of the bridge is similar in energy to the acceptor states of the remote redox centre This pathway predominates because the closeness of the bridge and redox centre energies acts to reduce the activation barrier to electron tunnelling In contrast, if the $Os_{d\pi}$-HOMO separation is relatively smaller, then HOMO mediated hole transfer will contribute significantly to the redox switching mechanism

The present system is particularly attractive for investigating this issue for two reasons First, the tetrazine ligand undergoes a reduction reaction within an electrochemically accessible potential window Second, the HOMO and LUMO levels of the bridging ligand can be altered by adjusting the pH of the supporting electrolyte, i e , protonation will decrease the electron density on the bridge simultaneously making it more difficult to oxidize but easier to reduce Therefore, unlike traditional alkane-thiol monolayers in which bridge states can be modulated only by synthetically changing the structure, e g , by introducing a heteroatom,[32] this tetrazine offers the possibility of altering the proximity of bridge and metal states by a simple change in the chemical composition of the solution

For a non-adiabatic reaction, the standard heterogeneous electron transfer rate constant, k°, depends on both a frequency factor and a Franck-Condon barrier (Section 1 2 3) [33 34 35]

$$k^{o} = \upsilon_{el} \exp(-\Delta G^{\neq}/RT) \qquad (3\ 9)$$

where υ_{el} is the electron hopping frequency and $\Delta G^{\neq}$ is the electrochemical free energy of activation [36]

It is important to decouple the free energy and pre-exponential terms since the effect of changing bridge states will be reflected in υ_{el} rather than $\Delta G^{\neq}$ One approach to decoupling these two contributions is to use classical temperature-resolved measurements of k° to measure the free energy of activation, $\Delta G^{\neq}$, allowing υ_{el} to be determined In this way, information about the strength of electronic coupling can be obtained [26] A second method involves measuring electron-transfer rate constants at a single temperature over a broad range of reaction driving forces For example, Finklea,[37] Chidsey,[10] Creager[38] and Murray,[39] have assembled non-adiabatic electron tunneling models that provide a good description of electron tunneling in monolayers of this kind [40 41] In this model, the cathodic rate constant is given by integral over energy (ε) of three functions (a) the Fermi function for the metal n(ε), (b) a Gaussian distribution of energy levels for acceptor states in the monolayer $D_{Ox}(\varepsilon)$, and (c) a probability factor for electron tunneling, P

$$k_{Ox}(\eta) = A \int_{-\infty}^{\infty} D_{Ox}(\varepsilon)\ n(\varepsilon)\, P\ d\varepsilon \qquad (3\ 10)$$

The zero point of energy is defined as the Fermi level of the metal at the particular overpotential of interest The Fermi function describes the distribution of occupied states within the metal and is defined by

$$n(\varepsilon) = \left(\frac{1}{1 + \exp[(\varepsilon - \varepsilon_F)/kT]} \right) \qquad (3\ 11)$$

where k_B is the Boltzmann constant The density of acceptor states is derived from the Marcus theory,[42] and is represented by Equation 3 12

$$D_{Ox}(\varepsilon) = \exp\left[-\frac{(\varepsilon+\eta-\lambda)^2}{4k\lambda T}\right] \qquad (3\ 12)$$

where λ is the reorganization energy The distance dependent probability of electron tunnelling is given by Equation 3 13

$$P = \exp(-\beta d) \qquad (3\ 13)$$

where d is the electron transfer distance The distance dependent tunnelling parameter,[14] β, is taken as 1 6 Å $^{-1}$

The current for the reaction of an immobilized redox center following first order kinetics is [39]

$$i_F = nFA(k_{Ox}(\eta)\,\Gamma_{Red\ \eta} - k_{Red}(\eta)\,\Gamma_{Ox\ \eta}) \qquad (3\ 14)$$

where $\Gamma_{Red\ \eta}$ and $\Gamma_{Ox\ \eta}$ are the instantaneous surface coverages of the oxidized and reduced species and $k_{Ox}(\eta)$ and $k_{Red}(\eta)$ are the reaction rate constants are given by Equation 3 10 or its compliment in which $n(\varepsilon)$ is replaced with $(1- n(\varepsilon))$ and $-\lambda$ is replaced by $+\lambda$ in Equation 3 12 Energy minimized molecular modeling indicates that that the through-bond electron transfer distance is approximately 12 6 Å Therefore, in using Equation 3 14 to model the voltammetric response, there are only two freely adjustable parameters, k° and $\Delta G^{\neq}$ $(=\lambda / 4)$ To model the experimental cyclic voltammograms, the Nelder and Mead Simplex[43] algorithm has been used to find the values of k° and $\Delta G^{\neq}$ that minimize the sum square residuals between the theoretical and experimental currents observed in anodic branches of the linear sweep voltammograms

As the sweep rate in cyclic voltammetry increases to sufficiently high values, the voltammetric response of the monolayers becomes influenced by the rate of heterogeneous electron transfer across the monolayer/electrode interface Under the influence of heterogenous kinetics, the observed ΔE_p values increase as the scan rate is increased This behaviour contrasts with that observed at low scan rates, where ΔE_p is independent of v and $\Delta E_p = 60$ mV Figure 3 11 illustrates the typical voltammetric response of these monolayers at high scan rates At a scan rate of 800 Vs^{-1}, the observed ΔE_p is 130 mV As discussed previously (Section 2 2 4), by carefully selecting the electrode radius and by using concentrated electrolytes, it is possible to keep the iR drop to less than a couple of millivolts even at high scan rates [6] The estimated iR drop at the fastest scan rate shown in Figure 3 11 is 30 mV Therefore, the observed behaviour is due to the influence of heterogenous electron transfer across the monolayer/electrode interface Figure 3 12 shows the effect of changing the electrolyte pH from 6 0 to 0 9 on the experimental background corrected cyclic voltammograms for dense $[Os(bpy)_2$ 4-tet $Cl]^+$ monolayer deposited on a 5 μm radius gold microelectrode where the scan rate is 1333 V s^{-1}

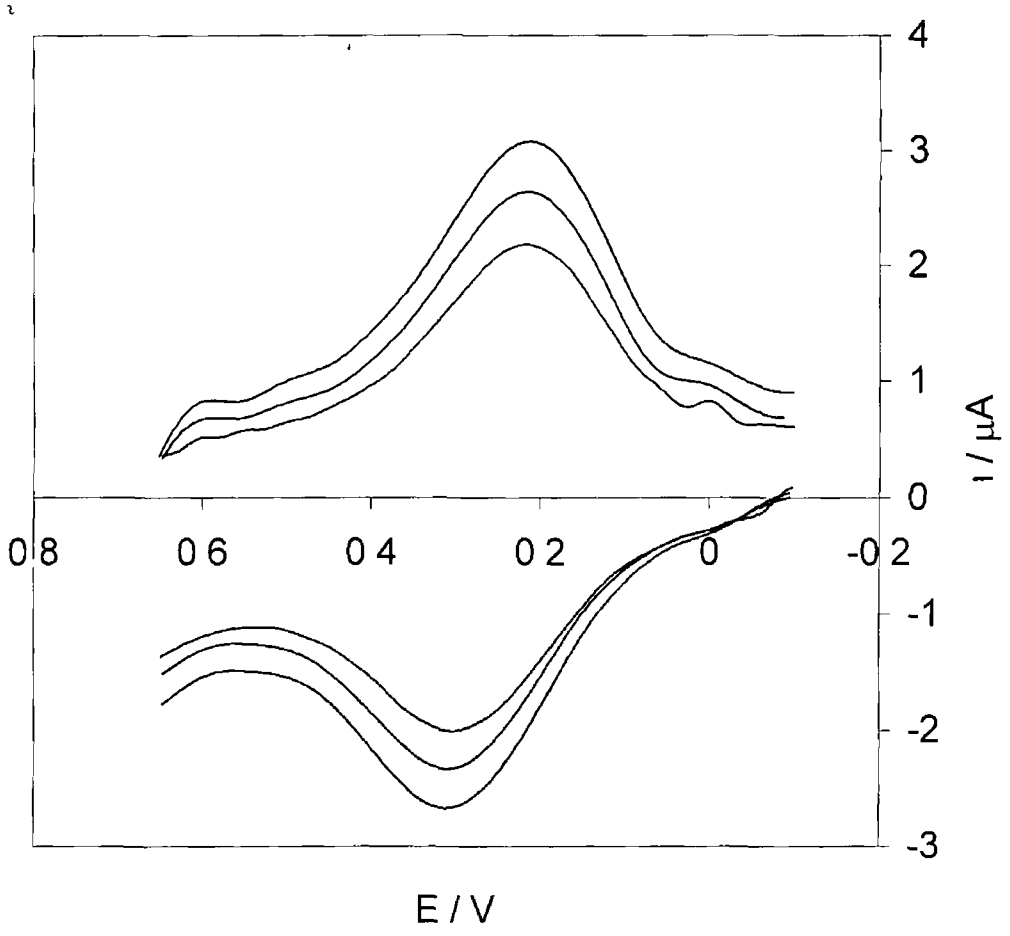

Figure 3 11 Effect of increasing scan rate on a spontaneously adsorbed monolayer of $[Os(bpy)_2$ 4-tet $Cl]^+$ at a 25 μm gold microelectrode The background electrolyte is 1 0 M $LiClO_4$ The scan rates are (from top to bottom) 800, 667 and 571 Vs^{-1}

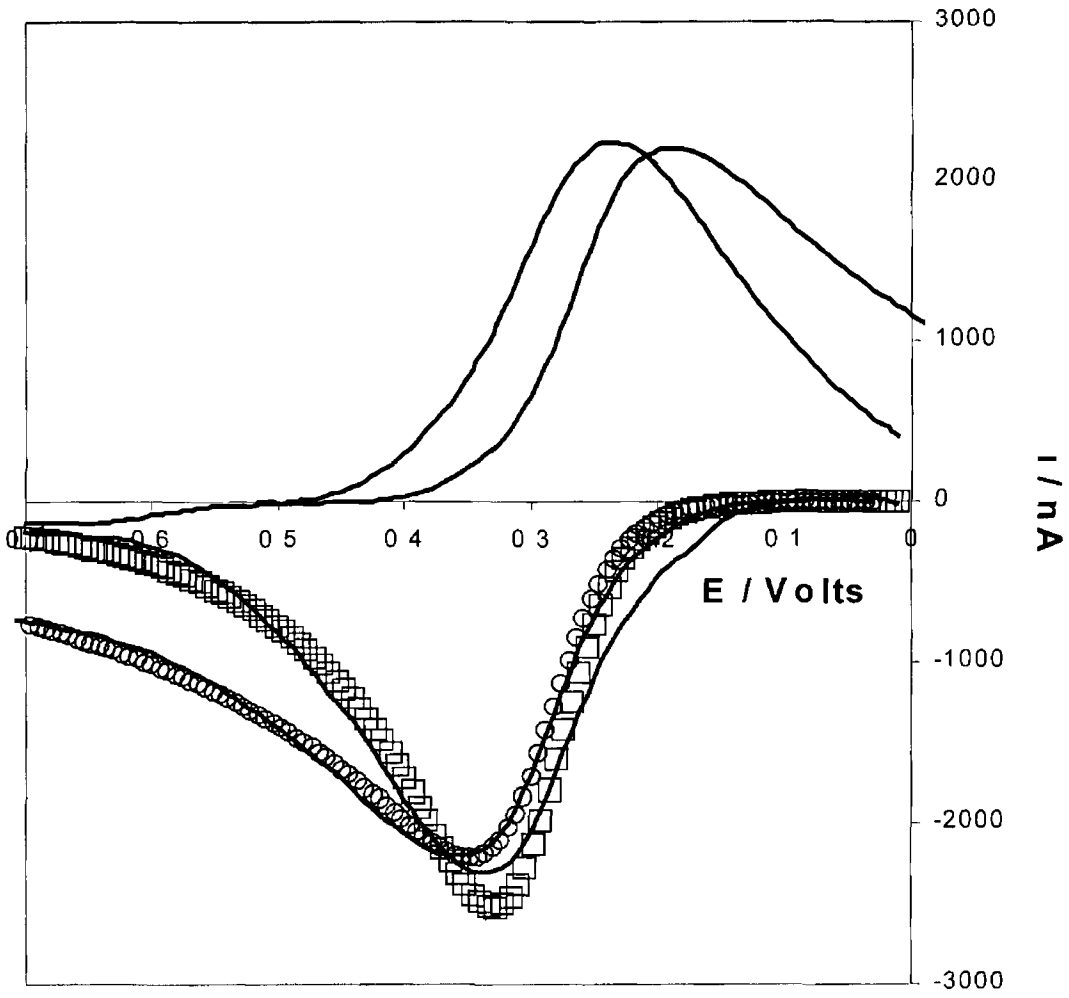

Figure 3 12 Cyclic voltammograms for a spontaneously adsorbed $[Os(bpy)_2$ 4-tet $Cl]^+$ monolayer on a 5 μm radius gold microdisc electrode where the scan rate is 1333 V s^{-1} Theoretical fits to the data using a non-adiabatic electron tunneling model at electrolyte pH values of 0 9 and 6 0 are denoted by ○ and □, respectively In both cases λ is 27 kJ mol^{-1} while k° is 1 1x10^3 and 1 1x10^4 s^{-1} at pH values of 0 9 and 6 0, respectively

Table 3 2 Standard Heterogeneous Electron Transfer Rate Constants, k°, Free Energies of Activation, $\Delta G^{\neq}$ and Pre-exponential Factors for the Metal Based Redox Reaction Within $[Os(bpy)_2$ 4-tet $Cl]^{1+/2+}$ Monolayers at Different Values of Electrolyte pH [a]

pH	$10^4 k^0$ / s^{-1}	$\Delta G^{\neq}$ / kJ mol^{-1}	$10^5 \upsilon_{el}$ / s^{-1}, [b]	H_{AB} / kJ mol^{-1}
0 87	1 15±0 25	9 2±0 4	4 7±0 8	0 41±0 04
6 01	0 12±0 02	11 4+0 3	1 2±0 1	0 21±0 01

[a] Standard deviations are for at least three individual monolayers The supporting electrolyte is aqueous 1 0 M $LiClO_4$

[b] Pre-exponential factor extracted from the standard heterogeneous electron transfer rate constant using $\Delta G^{\neq}$

Figure 3 12 shows that satisfactory agreement is observed between the experimental and theoretical anodic peak potentials and peak currents Significantly, for both pH values the optimum $\Delta G^{\neq}$ was 10 3±1 1 kJ mol^{-1} indicating that the local microenvironment around the $[Os(bpy)_2Cl]^{+}$ moiety remains largely unchanged by protonating the tetrazine ligand However, the quality of the fit shown in Figure 3 12 is not particularly sensitive to $\Delta G^{\neq}$, e g , increasing $\Delta G^{\neq}$ by 25 % increases the residual sum of squares between the predicted and experimental peak currents by less than 10% Therefore, while fitting of the cyclic voltammograms can provide a convenient approach for determining k°, for this system it appears to provide only an approximate value for $\Delta G^{\neq}$ In contrast, the quality of the fit is very sensitive to k° which directly influences both the peak shape and half-wave potential

An important test of the reliability of the standard heterogeneous electron transfer rate constants obtained is to investigate the scan rate dependence In this way, an insight into the dispersion in the kinetics can be obtained The best fits for voltammograms recorded at scan rates between 800 and 4000 Vs^{-1} range from 0 9 to 1 4x10^{4} s^{-1} and 1 0 to 1 4x10^{3} s^{-1} where the electrolyte pH is 6 01 and 0 87, respectively These results indicate that the monolayers are acceptably kinetically monodisperse The dispersion that is observed may be due to the concentration dependent destabilising interactions found in the isotherm and the rather broad peaks observed in the slow scan rate cyclic voltammograms

Perhaps the most significant conclusion of Figure 3 12 is that heterogeneous electron transfer is slower for the protonated than for the deprotonated system The optimum value of k° decreases by an order of magnitude from 1 1x10^{4} s^{-1} to 1 2x10^{3} s^{-1} when the tetrazine ligand is protonated In bridge mediated redox reactions of this type, the electronic pathway is determined by the relative gaps between the metal dπ orbital involved in the redox step and the HOMO and LUMO of the bridge Protonation decreases the electron density on the tetrazme shifting both the bridge oxidation and reduction potentials in a positive potential

direction, i e , simultaneously making it more difficult to oxidize but easier to reduce the bridge The fact that a significant *decrease* in k° is observed indicates that it is the bridge HOMO that mediates the redox process, i e , the larger dπ-HOMO separation in the protonated tetrazine causes k° to decrease This HOMO mediated hole transfer mechanism is consistent with studies on related mixed valence complexes, which suggest that electron rich π-donating linkers of this type support hole superexchange reactions [44] As illustrated in Figure 3 13, the hole is directed through the HOMO orbital of the bridge, creating a "virtual" high energy state Therefore, the energy difference between the metal and bridge will directly impact the rate of electron transfer across the bridge In the following section, the energy difference between the metal and the bridge are probed and this may provide an insight into the expected change in k^0 upon protonation of the 4-tet ligand

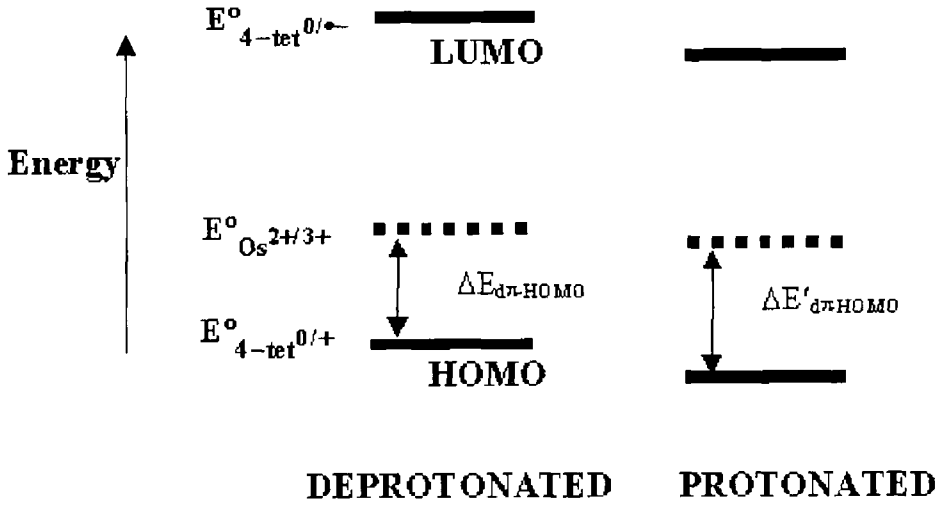

Figure 3 13 Proposed direction the hole through the HOMO of the bridge

3 4 7 1 DRIVING FORCE FOR SUPEREXCHANGE

The relative energy gaps between the metal dπ orbital and the HOMO and LUMO of the bridge determine not only the mode of superexchange (hole or electron superexchange) but also the rate of superexchange The energy gaps between the metal dπ orbitals and the HOMO and LUMO of the bridge have been probed using cyclic voltammetry The voltammetric response of the 4-tet ligand in acetonitrile solution over the potential range –2 to +2 V is illustrated in Figure 3 14 The voltammetric response over the range –1 6 V to –0 4 V is illustrated in Figure 3 15 The reduction of the ligand ($4\text{-tet}^{0/\bullet-}$) is observed at a formal potential of approximately –0 966 V vs Ag/Ag^{+} The formal potential of the ferrocene/ferrocinium couple at this reference electrode was 0 111 V Therefore, the formal potential of the $4\text{-tet}^{0/\bullet}$ couple, when corrected to the Ag/AgCl reference electrode is approximately –1 260 V [45] The electrochemically accessible potential window, when adjusted for the Ag/AgCl reference electrode is approximately –2 290 V to +1 710 V Within this electrochemically accessible window, the oxidation of the ligand ($4\text{-tet}^{0/+}$) was not observed

Therefore, the metal dπ orbitals ($E^{o'}$ = 0 245 V vs Ag/AgCl) and the LUMO of the bridge are separated by approximately 1 5 Volts, while the metal dπ orbitals and the bridge HOMO are separated by at least approximately 1 465 V This result indicates that it is not possible to accurately determine the energy gap between the metal dπ orbitals and the HOMO Therefore, it is not possible to directly assign a superexchange mechanism, or predict the change expected in k^{o} upon protonation of the bridging ligand, based on the relative energy gaps between the electronic energies of the metal orbitals and the bridge states However, based on the effects of protonation on k^{o} described above, it appears that the redox process does occur via the HOMO of the bridge

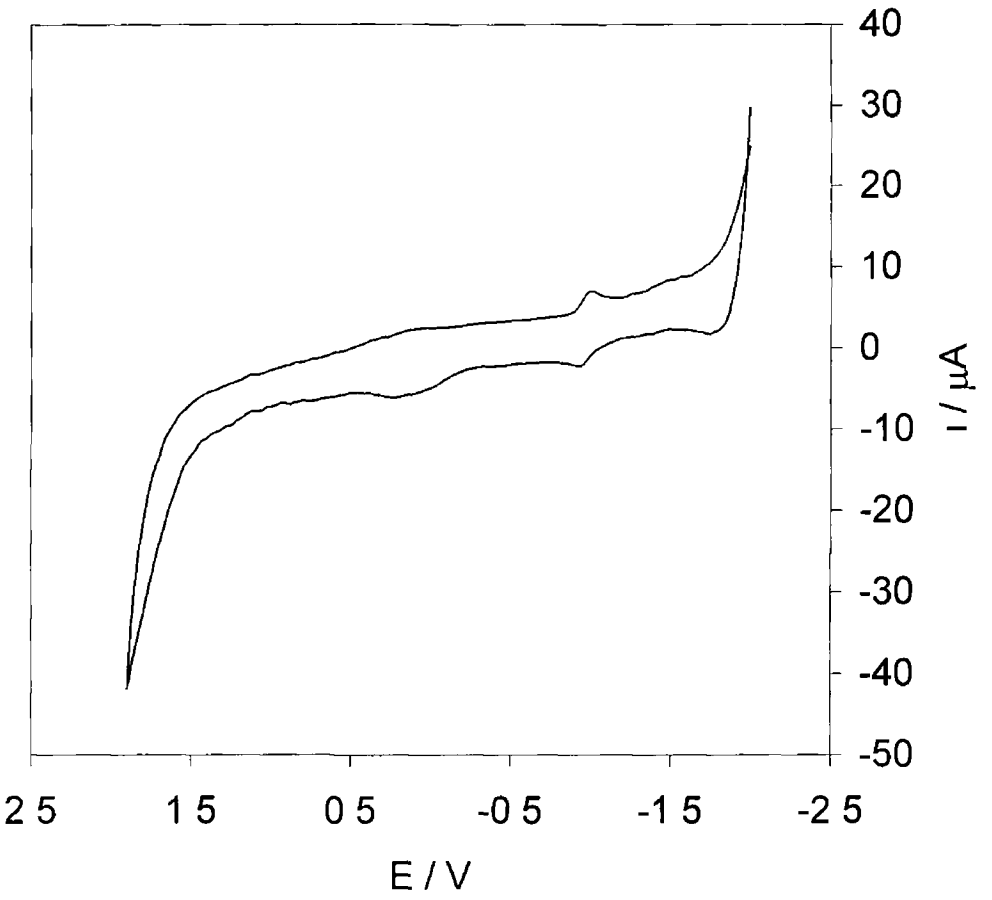

Figure 3 14 The solution phase voltammetric response of a 2 mM solution of the 4-tet ligand The supporting electrolyte is 0 1 M tetrabutyl ammonium tetrafluroborate in acetonitrile The platinum electrode radius is 1 mm and the scan rate is 0 5 Vs^{-1} The potential limits are –2 0 V to +2 0 V

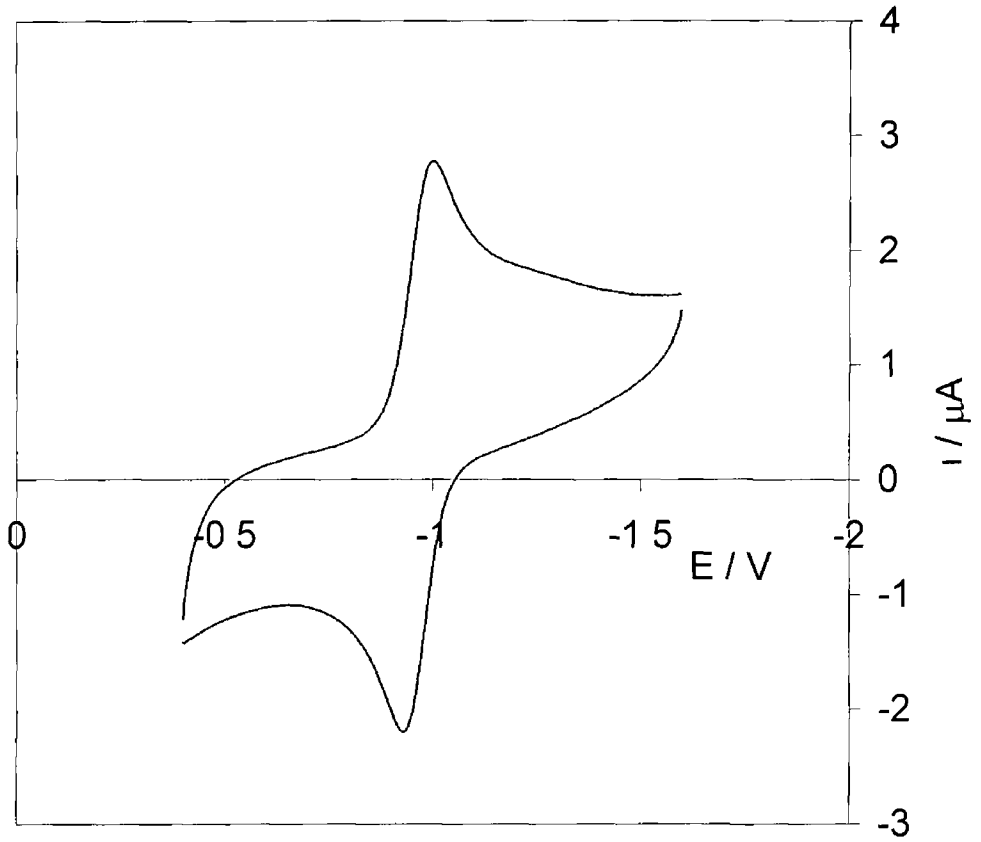

Figure 3 15 The solution phase voltammetric response of a 2 mM solution of the 4-tet ligand The supporting electrolyte is 0 1 M tetrabutyl ammonium tetrafluroborate in acetonitrile The platinum electrode radius is 1 mm and the scan rate is 0 5 Vs^{-1} The potential limits are –1 6 V to –0 4 V

3 4 7 2 GROUND VERSUS EXCITED STATE ELECTRON TRANSFER

In the preceding section, it has been shown that the energy levels of the 4-tet bridging ligand can be altered by a simple change in pH of the contacting electrolyte solution By using bridging ligands that contain metal centres it may also be possible to exert control over the rate of electron transfer by a simple change in the oxidation state of the bridge This has recently been explored by Forster and Keyes [46] The electron transfer dynamics within monolayers of a dimeric complex, the structure of which is illustrated in Figure 3 16, were described This dimeric complex was interesting in that it contains the same tetrazine bridge as the monomeric complex described in this chapter Therefore, photochemical studies of this complex offer the opportunity of directly comparing ground state and excited state electron transfer rates

It was found that the rate of photoinduced electron transfer across the tetrazine bridge was $1\ 6 \times 10^{7}\ s^{-1}$ The driving force of this photochemically driven reaction was determined using the excited state redox potentials, calculated using Equations 3 15 and 3 16

$$E^{o*}_{ox} = E^{o}_{ox} + E^{oo} \qquad (3\ 15)$$

$$E^{o*}_{red} = E^{o}_{red} + E^{oo} \qquad (3\ 16)$$

where E^{o}_{ox} and E^{o}_{red} are the formal potentials associated with the first oxidation ($Os^{2+/3+}$) and reduction (bpy/bpy) of the luminescent moiety in the ground state and E^{oo} is the energy difference between the lowest vibrational levels of the ground and excited states Using electrochemically determined values of + 0 280 and – 1 320 V for E^{o}_{ox} and E^{o}_{red} and a spectrometrically determined value of 1 67 eV for E^{oo}, values of – 1 39 and + 0 35 V were determined for E^{o*}_{ox} and E^{o*}_{red} respectively, using equations 3 15 and 3 16

The driving forces for the reductive and oxidative reactions were determined using Equations 3 17 and 3 18

$$\Delta G^{o}_{ox} = E^{o*}_{ox} - E^{o}_{red} \quad (3\ 17)$$

$$\Delta G^{o}_{red} = E^{o}_{ox} - E^{o*}_{red} \quad (3\ 18)$$

The driving forces for the oxidation and reduction reactions were identical (70 mV), preventing the authors from elucidating the mechanism of quenching of the excited state

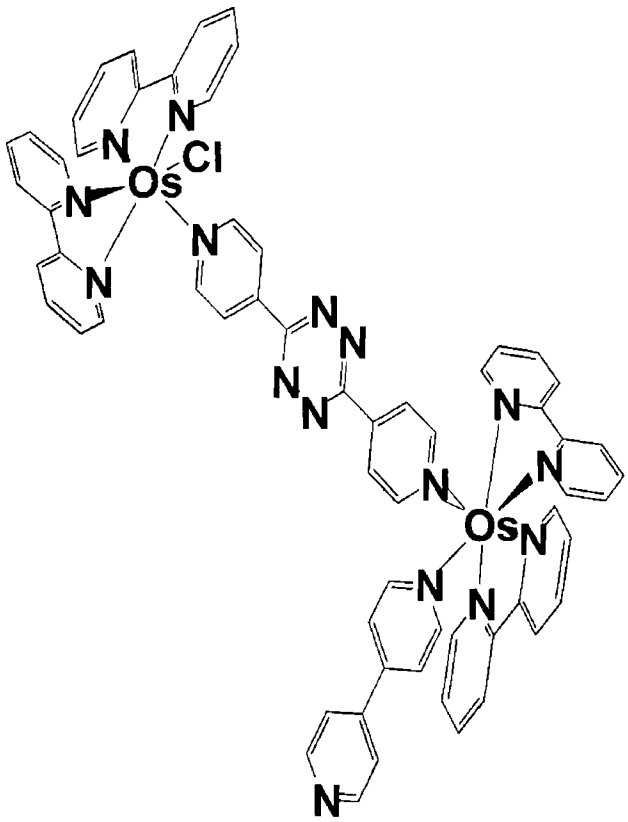

Figure 3 16 Structure of the dimeric complex used to form monolayers for the study of excited state electron transfer dynamics, reported by Forster [46]

For the monolayers described in this chapter, at a driving force of 70 mV, the rate of hole transfer across the tetrazine bridge is 4.0×10^4 s^{-1}. Therefore, the electron transfer rate for the ground state reaction is approximately 400 times smaller than that found for the photoinduced electron transfer reaction. It may be possible that the [4-tet Os(bpy)$_2$ Cl]$^+$ moiety within the dimer creates a favourable vibronic deactivation pathway in the photoinduced electron transfer reactions, causing an overestimation of k^o.

The authors also proposed that the difference in the rates of reaction between the ground and excited states was due to the relative energy gaps between the metal dπ orbitals and the bridge levels. It was found voltammetrically that the tetrazine bridge (in the dimeric complex) was reduced at potentials close to – 2.0 V. Therefore, in the ground state the formal potentials of the metal based redox reaction and the tetrazine bridge (4-tet$^{0/\bullet}$) were separated by approximately 2.3 V. In the excited state, oxidation of the excited state (bpy*) may cause quenching. In this case, the donor/acceptor and bridge are all within 0.5 V of each other. This enhanced proximity of the metal dπ orbitals and the LUMO of the bridge may have enhanced the rate of electron transfer observed in the photoinduced reaction.

However, this analysis does not consider the relative energy gap between the metal dπ orbitals and the HOMO of the bridge in the ground state. As described above, electron rich π-donating bridges of this type have been shown to support hole superexchange. This has been supported by the data presented in this chapter concerning the effects of protonation on k^o across the tetrazine bridge. The authors assumed that the superexchange mechanism was an electron superexchange. The separation between the metal dπ orbitals and the bridge levels may not be 2.3 V, but a lower value depending on the energy of the bridge HOMO. This was not investigated by the authors.

3 4 7 3 ELECTRONIC COUPLING ACROSS THE 4-TET BRIDGING LIGAND

A challenging issue in this area is to determine the extent to which orbitals on the gold electrode and on the osmium redox centre interact and how this interaction compares with molecular components interacting across similar bridges Electronic interaction of the redox orbitals and the metallic states causes splitting between the product and reactant hypersurfaces which is quantified by H_{AB}, the matrix coupling element The Landau-Zener treatment[36] of a non-adiabatic reaction yields Equation 3 19

$$\upsilon_{el} = (2H_{AB}^2 / h) (\pi^3 / \lambda RT)^{1/2} \quad (3\ 19)$$

where h is Planck's constant The matrix coupling element has been determined for each of the electrode materials and the results have been presented in Table 3 2 (Section 3 4 6) The fact that H_{AB} is less than 1 kJ mol^{-1} confirms that the system is always charge localized and non-adiabatic irrespective of the extent of protonation of the bridge [36] However, the observation that H_{AB} is approximately twice as large for the deprotonated than for the protonated ligand suggests that the extent of electronic coupling across the bridge is greater in the deprotonated state

3 5 CONCLUSIONS

Stable close-packed monolayers of $[Os(bpy)_2$ 4-tet Cl$]ClO_4$, where bpy is 2,2'-bipyridyl have been formed on gold microelectrodes, bpy is 2,2'bipyridyl and 4-tet is 3,6-bis(4-pyridyl)-1,2,4,5-tetrazine The adsorbed monolayers exhibit well defined voltammetric responses for 0 5<pH<8 0 Probing the pH dependence of the interfacial capacitance reveals that the tetrazine bridging ligand is capable of undergoing a protonation/deprotonation reaction with a pK_a of 2 7±0 6 This value is indistinguishable from that found for the complex in solution

Cyclic voltammetry at scan rates up to 4000 V s^{-1} has been used to probe the rate of heterogeneous electron transfer across the monolayer/microelectrode interface Modeling the cyclic voltammogram suggests that redox switching proceeds via a non-adiabatic through-bond tunneling mechanism Significantly, protonating the tetrazine ligand decreases the standard heterogeneous electron transfer rate constant by a order of magnitude from 1 15±0 25 to 0 12±0 02x10^4 s^{-1} This observation is consistent with mediating electronic states within the bridging ligand (superexchange) playing an important role in the redox switching process Specifically, the results suggest that hole transfer is mediated through the highest occupied molecular orbital (HOMO) of the tetrazine ligand Protonating the bridge reduces its electron density thus raising the energy of the bridge HOMO relative to the hole acceptor states of the osmium and decreasing the standard rate constant

The matrix coupling element has been determined for this system and indicates that the system is non-adiabatic, regardless of the degree of protonation of the bridge The matrix coupling element is approximately twice as large for the deprotonated state than for the protonated state, suggesting that the extent of electronic coupling across the bridge decreases upon protonation of the bridge

The rate of electron transfer across this tetrazine bridge has been compared with the photochemically driven rate of electron transfer across the same bridge Significantly, for the same driving force, the rate for the excited state process (1 6 $\times 10^7$ s^{-1}) was approximately 400 times that observed for the ground state process studied here (4 0 $\times 10^4$ s^{-1}) This observation suggests that the proximity of the donor/acceptor and bridge states in the photoimduced electron transfer reaction enhances the rate of electron transfer However, due to the lack of data regarding the oxidation potential of the bridge, the actual proximity between the metal $d\pi$ orbitals and the mediating bridge levels has not been calculated

3 6 REFERENCES

1 Bixon, M , Jortner, J , Michel-Beyerle, M E *Biochim Biophys Acta,* **1991**, *1056*, 301

2 Sek, S , Bilewicz, R , *J Electroanal Chem* , **2001**, *509*, 11

3 Weaver, M J *Chem Rev* **1992**, *92*, 463

4 Forster, R J *J Electrochem Soc* , **1997**, *144*, 1165

5 McConnell, H M *J Chem Phys* **1961**, *35*, 508

6 Forster, R J *Inorg Chem* **1996**, *35*, 3394

7 Fanni, S , Keyes, T E , Campagna, S , Vos, J G , *Inorg Chem* , **1998**, *37*, 5933

8 Barrigelletti, F , De Cola, L , Balzani, V , Hage, R , Haasnoot, J G , Reedijk, J , Vos, J G , *Inorg Chem* , **1991**, *30*, 641

9 Keyes, T E , Forster, R J , Jayaweera, P M , Coates, C G , McGarvey, J J , Vos, J G *Inorg Chem* , **1998**, *37*, 5925

10 Chidsey, C E D *Science*, **1991**, *251*, 919

11 Miller, C , Gratzel, M *J Phys Chem* **1991**, *95*, 5225

12 Bixon, M , Jortner, J , *J Phys Chem B*, **2000**, *104*, 3906

13 Bard, A J and Faulkner, L R , "Electrochemical Methods Fundamentals and Applications", Wiley, New York, 1980

14 Forster, R J , Faulkner, L R *J Am Chem Soc* **1994**, *116*, 5444

15 Forster, R J , Keyes, T E , Vos, J G , *Analyst*, **1998**, *123*, 1905

16 Feldberg, S W , Rubinstein, I , *J Electroanal Chem* , **1988**, *240*, 1

17 Trassati, S *J Electroanal Chem* , **1974**, *53*, 335

18 Forster, R J , Keyes, T E *J Phys Chem B*, **1998**, *102*, 10004

19 Forster, R J , O'Kelly, J P *J Electrochem Soc* m press

20 Goodwin, H A , Kepert, D L , Patrick, J M , Skelton, B W , White, A H Aust J Chem **1984**, *37*, 1817

21 Ferguson, J E , Love, J L , Robinson, W T *Inorg Chem* **1972**, *11*, 1662

22 Creager, S E , Rowe, G K , *Anal Chim Acta* , **1991**, *246*, 233

23 Rowe, G K , Creager, S E , *Langmuir*, **1991**, *7*, 2307

24 Nagamura, T , Sakai, K , *J Chem Soc , Faraday Trans* , **1988**, *84*, 3529

25 Forster, R J , Keyes, T E , Bond, A M , *J Phys Chem B*, **2000**, *104*, 6389

26 Forster, R J , O'Kelly, J P , *J Phys Chem* , **1996**, *100*, 3695

27 Smith, C P , White, H S , *Anal Chem* , **1992**, *64*, 2398

28 Smith, C P , White, H S , *Langmuir*, **1993**, *9*, 1

29 Bryant, M A , Crooks, R M , *Langmuir*, **1993**, *9*, 385

30 Brolo, A G , Irish, D E , Szymanski, G , Lipkowski, J , *Langmuir*, **1998**, 14, 517

31 Nakamoto, K , *Infrared and Raman Spectra of Inorganic and Coordination Compounds*, 4th Edn , Wiley, **1986**

32 Cheng, J , Saghi-Szabo, G , Tossell, J A , Miller, C J , *J Am Chem Soc* , **1996**, *118*, 680

33 Bagchi, G , *Ann Rev Chem* , **1989**, *40*, 115

34 Sutin, N , *Acc Chem Res* , **1982**, *15*, 275

35 Barr, S W , Guyer, K L , Li, T T -T , Liu, H Y , Weaver, M J , *J Electrochem Soc* , **1984**, *131*, 1626

36 Brunschwig, B S , Sutin, N , *Coord Chem Rev* , **1999**, *187*, 233

37 Finklea, H O , Hanshaw, D D , *J Am Chem Soc* , **1992**, *114*, 3173

38 Weber, K , Creager, S E , *Anal Chem* , **1994**, *66*, 3164

39 Tender, L , Carter, M T , Murray, R W , *Anal Chem* , **1994**, *66*, 3173

40 Forster, R J , Loughman, P J , Figgemeier, E , Lees, A C , Hjelm, J , Vos, J G , *Langmuir*, **2000**, *16*, 7871

41 Forster, R J , Loughman, P J , Keyes, T E , *J Am Chem Soc* , in press

42 Marcus, R A , *J Phys Chem* , **1963**, *67*, 853

43 Ebert, K , Ederer, H , Isenhour, T L , *Computer Applications in Chemistry An Introduction for PC Users*, VCH Publishers, New York, **1989**

44 Barigelletti, F , De Cola, L , Balzani, V , Hage, R , Haasnoot, J G , Reedijk, J , Vos, J , G , *Inorg Chem* , **1989**, *28*, 4344

45 Pavlıshchuk, V V , Addıson, A W , *Inorg Chım Acta* , **2000**, 298, 97

46 Forster, R J , Keyes, T E , *J Phys Chem B*, **2001**, *105*, 8829

CHAPTER 4

SOLID STATE REDOX PROPERTIES OF TRIAZOLE BRIDGED OSMIUM BIS-BIPYRIDYL DIMERS

4 1 INTRODUCTION

The dynamics of electron transfer and mass transport processes within solids have only been investigated relatively recently [1 2] This situation is striking given the pivotal roles that solid-state redox active materials play in devices including optical detectors, energy storage, molecular electronics, catalysts and sensors [3 4 5 6 7 8,9 10] However, these applications demand that the redox composition of the solid can be rapidly switched in response to an applied potential, i e , diffusion of charge compensating counterions through the solid must be rapid compared to electron self-exchange between adjacent centres Osmium complexes ought to be particularly useful in this regard because of their stability in numerous oxidation states and very large self-exchange rate constants [11 12]

It was recently demonstrated that the rate determining step for charge transport through solid-deposits of [Os(bpy)$_2$ 4-bpt Cl] is limited by counterion diffusion rather than electron self-exchange [13] However, using complexes with bulkier side groups appears to increase the free volume within the solid deposit facilitating rapid redox switching rates and electron self-exchange as the rate determining step [14]

In this chapter, solid-state deposits of the dimeric complex [Os(bpy)$_2$ Cl 4-bpt Os(bpy)$_2$ Cl](PF$_6$)$_2$ (Figure 4 1) that are mechanically attached to a platinum microelectrode are described This complex is insoluble in water, allowing the solid state redox properties to be examined when the deposits are in contact with an aqueous electrolyte These deposits exhibit unusually ideal voltammetric responses for the $Os^{2+/3+}$ redox reaction The remarkable ideality of the voltammetric response of these materials allows us to obtain an insight into charge transfer within the solid deposit as the concentration of the supporting electrolyte is systematically varied at both high and low pH values Moreover, at high

voltammetric scan rates, the rate of electron transfer across the deposit/electrode interface influences the observed response allowing the standard heterogeneous electron transfer rate constant, k°, to be determined Importantly, the bridge between the two osmium polypyridyl groups (4-bpt) is identical to that used previously to determine heterogeneous electron transfer rates across an electrode/monolayer interface [15] It is possible, therefore to compare the rate of heterogenous electron transfer across the electrode/solid film interface with that observed in monolayers containing the same bridging ligand These studies provide an insight into how the method of attachment of molecular materials onto metal substrates affects the rate of interfacial electron transfer

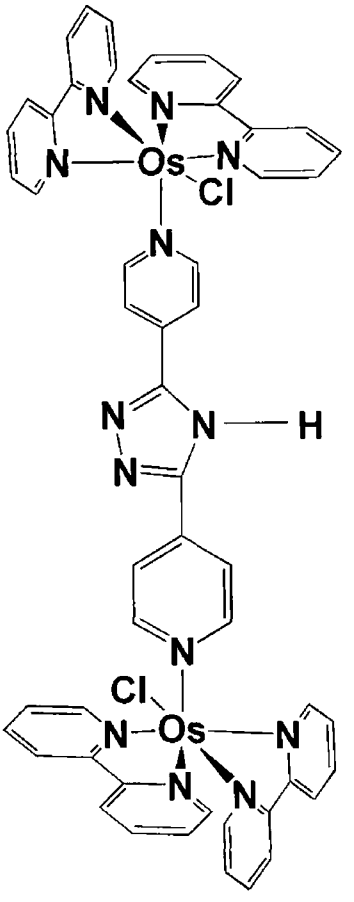

Figure 4 1 Structure of $[Os(bpy)_2Cl$ 4-bpt $Os(bpy)_2Cl](PF_6)_2$

4 2 MATERIALS AND REAGENTS

[Os(bpy)$_2$ Cl 4-bpt Os(bpy)$_2$ Cl] (PF_6)$_2$ was synthesised as described in Chapter 2

4 3 APPARATUS AND REAGENTS

Microelectrodes were constructed and characterised as described in Chapter 2

Cyclic voltammetry was performed using a CH Instruments Model 660 Electrochemical Workstation and a conventional three electrode cell All solutions were deoxygenated thoroughly using nitrogen, and a blanket of nitrogen was maintained over the solution during all experiments Potentials are quoted with respect to a BAS Ag/AgCl gel-filled reference electrode All experiments were performed at room temperature (22±3 °C)

Two approaches were used to transfer the solid onto the surface of the working electrode In the first method, the solid was transferred from a filter paper onto the surface of the electrode by mechanical abrasion This process caused some of the complex to adhere to the surface as a random array of microparticles In the second approach that was used to achieve high surface coverages, a drop of Milli-Q water was first added to the complex before applying the material to the electrode surface as a paste Prior to electrochemical measurements the paste was allowed to dry Deposits prepared by both methods give indistinguishable electrochemical responses The stability of the solid deposits prepared by the two methods is comparable After use, the electrode surface was renewed by polishing using an aqueous slurry of 0 05 μm alumina

Scanning electron microscopy (SEM) was performed using a Hitachi S-3000N system For SEM investigations, deposits were formed on 3 mm radius graphite disks that were mounted directly in the microscope In electrochemical

investigations, the modified disks were electrochemically cycled and then the layers were allowed to soak in electrolyte free Milli-Q water for at least 30 min before being washed copiously and then dried in a vacuum dessicator for several hours

UV-Visible spectra for the solid state deposits were recorded using a Nikon Eclipse ME600 microscope equipped with both a 100W halogen lamp and a 100 W mercury arc source The films were deposited on conducting glass slides (ITO) and were positioned against a water-immersion objective (10 x magnification) and observed through the microscope An Ag/AgCl reference electrode and a large area platinum wire completed the three electrode electrochemical cell Spectra were recorded using an Andor Technology gated intensified CCD coupled to an Oriel model MS125 spectrograph fitted with a 600 lines/inch grating Typically the gate width was 2 ms and for surface coverages less than $1x10^{-7}$ mol cm^{-2} signal averaging was necessary The potential of the working ITO electrode was controlled using a CH Instruments Model 660 Electrochemical Workstation A Dell Dimension Pentium PC was used for data acquisition and analysis

4 4 RESULTS AND DISCUSSION

4 4 1 "BREAK IN" PHENOMENA

Figure 4 2 illustrates the initial voltammetric response obtained when a solid deposit of $[Os(bpy)_2$ Cl 4-bpt $Os(bpy)_2$ Cl$](PF_6)_2$ is first voltammetrically cycled in 80 20 H_2O acetonitrile where the supporting electrolyte is 0 1 M $LiClO_4$ During these initial scans, the peak shape changes and the anodic peak current, i_{pa}, decreases by approximately 40% while the cathodic peak current, i_{pc}, decreases by approximately 15% After approximately 50 scans, the response no longer changes when the deposit is repeatedly cycled and remains stable for more than 24 hours

As the film becomes oxidised, the overall charge on the complex increases and counteranions must be incorporated into the film from solution to maintain electroneutrality Therefore, as the greatest increase in the peak currents during initial cycling is observed in the anodic branch, this may be due to the gradual ingress into the film of charge balancing perchlorate ions from the electrolyte It is also possible that the oxidised and reduced forms of the complex have different solubilities in the electrolyte and this response may be indicative of some dissolution of the oxidised form of the complex

Films of this type have been shown to undergo structural changes upon redox switching Repeated electrochemical cycling of solid films of similar complexes has, for example, been shown to induce crystallisation of the microparticles within the solid films [14] The changes in the voltammetric response of these films upon initial electrochemical cycling, therefore, may be linked to some structural changes in the film In order to probe whether these voltammetric changes are caused by structural changes within the film, physical characterisation of the

surface before and after electrochemical cycling is required Scanning electron microscopy provides a convenient means to characterise solid layers of this type [16]

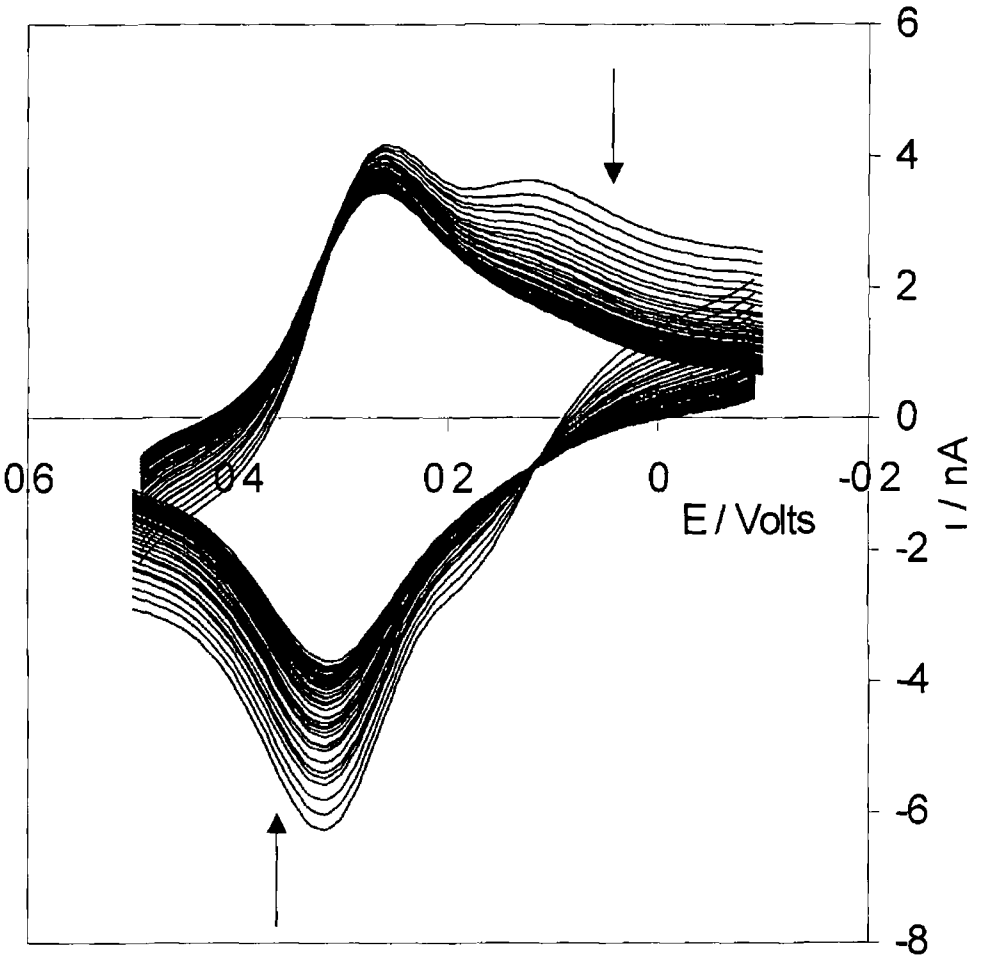

Figure 4 2 First 50 sweeps of a voltammetric cycle for a solid state $[Os(bpy)_2\ 4bpt\ Os(bpy)_2\ Cl_2]\ (PF_6)_2$ deposit attached to a 25 μm radius platinum microelectrode The supporting electrolyte is 0 1 M $LiClO_4$ dissolved in 80 20 water acetonitrile v/v The scan rate is 0 2 Vs^{-1}

4 4 2 SCANNING ELECTRON MICROSCOPY

Scanning electron microscopy has been used to probe whether cycling the redox composition of the solid deposits changes their morphology SEM images have been obtained after solid deposits have been repeatedly cycled for up to 2000 scans at 0 1 V s^{-1} As described in the previous section, the voltammetric response of the films changes over the first approximately 50 cycles and then remains constant for a period of hours Figure 4 3A shows that prior to voltammetric cycling, the deposits are unstructured and show no evidence of being significantly crystalline Figures 4 3B and 4 3C reveal that after cycling the layers in both neutral (1 0 M $LiClO_4$) and low pH electrolytes (1 0 M $HClO_4$) the deposits remain in a non-crystalline, largely amorphous state This behaviour contrasts sharply with that found for the corresponding monomer, $[Os(bpy)_2$ 4-bpt Cl$](PF_6)$, that electrocrystallised when cycled in 1 0 M $HClO_4$ [13]

It is perhaps significant that the overall charge is higher for the oxidised dimer, i e , +3 at the pH values used here The corresponding charges for the monomer is +1 Therefore, greater electrostatic repulsion as well as the greater difficulty of achieving efficient close packing in the dimers may inhibit electrocrystallisation However, the most significant result of Figure 4 3 is that the changes observed in the voltammetry when the deposits are first cycled, do not correspond to a significant change in the morphology of the deposits

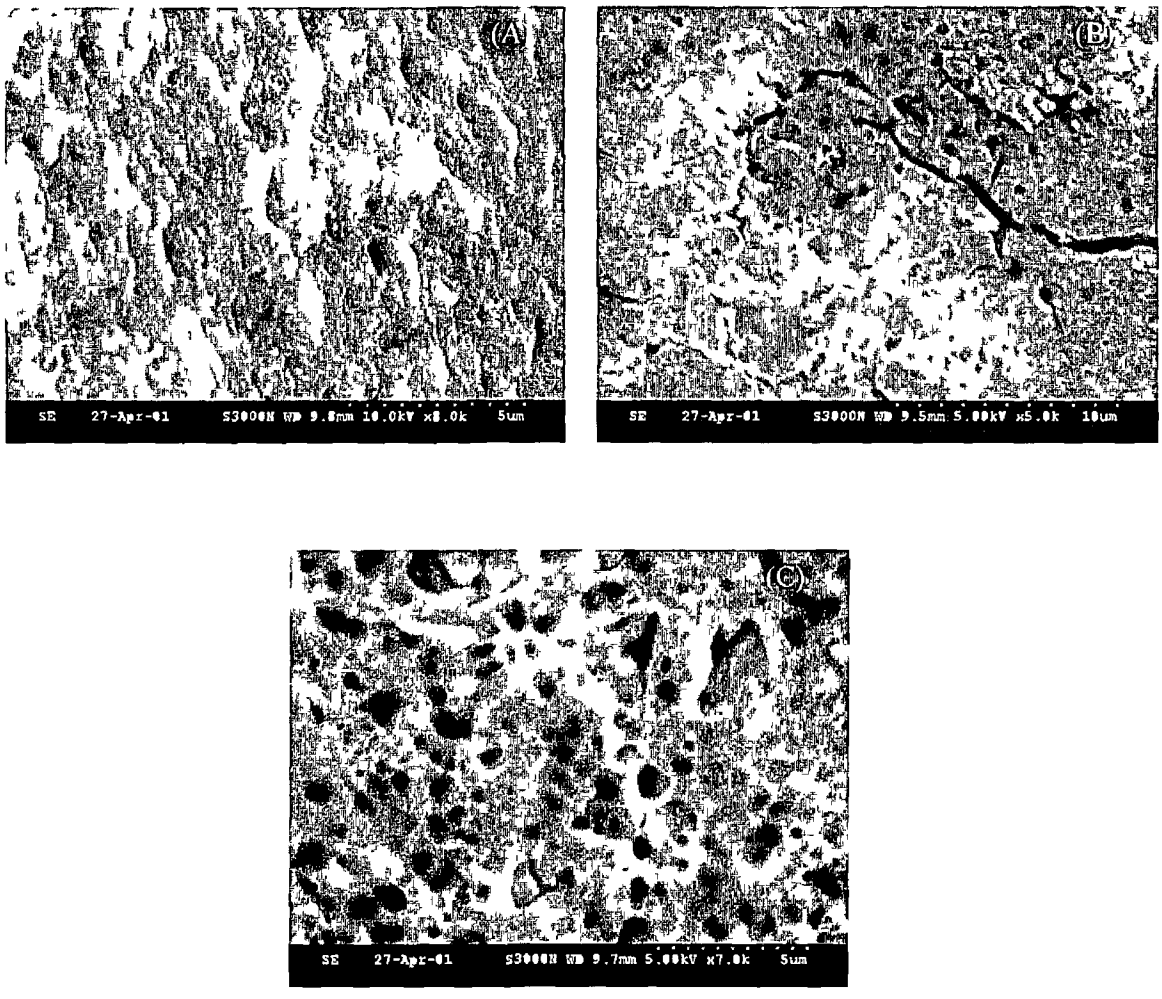

Figure 4 3 Scanning electron microscopy images of a 3 mm radius graphite disk modified with a mechanically attached layer of $[Os(bpy)_2\ 4bpt\ Os(bpy)_2\ Cl_2]\ (PF_6)_2$ (A) is the film prior to voltammetric cycling, (B) is after 2000 scans in 1 0 M $LiClO_4$ and (C) is after 2000 scans in 1 0 M $HClO_4$ Electrochemical scans were performed at 100 mVs^{-1} between –100 mV and +800 mV vs Ag/AgCl

4 4 3 GENERAL ELECTROCHEMICAL PROPERTIES

Figure 4 4 illustrates the voltammetric response obtained for a 2 mM solution of $[Os(bpy)_2\ Cl\ 4\text{-bpt}\ Os\ (bpy)_2\ Cl]^{2+}$ dissolved in acetonitrile where the supporting electrolyte is 0 1 M $LiClO_4$ For the dimer dissolved in solution, two, electrochemically reversible, waves are observed with formal potentials of 0 320 and 0 760 V These redox waves correspond to metal based $Os^{2+/3+}$ redox reaction The fact that two redox waves are observed for the complex in solution indicates that oxidation of the metal centres occurs in two distinct steps rather than as an apparently 2 electron process Since the dinuclear complex is highly symmetrical, the extent of electronic coupling across the 4-bpt bridge is likely to be responsible for the relatively large separation between the two formal potentials [17]

Figure 4 5 illustrates the voltammetric response observed for a solid deposit of the complex after approximately 50 repetitive scans Significantly, only a single redox process is observed even when the positive potential limit is extended to 1 200 V However, the response observed is unusually ideal for a solid deposit and is similar to that found for the complex dissolved in acetomtrile (Figure 4 4) For a reversible redox reaction under semi-infinite diffusional control (Section 1 3 2 2 1), the peak to peak separation, ΔE_p, and the difference between the peak potential, E_p, and the half peak potential, $E_{p/2}$ are given by Equations 4 1 and 4 2 respectively [20]

$$\Delta E_p = 2\ 3\frac{RT}{nF} \quad \text{or} \quad 59/n\ \text{mV at } 25°C \qquad (4\ 1)$$

$$\left|E_p - E_{p/2}\right| = 2\ 20\frac{RT}{nF} \quad \text{or} \quad 56\ 5/n\ \text{mV at } 25°C \qquad (4\ 2)$$

For a reversible electrochemical process under semi-infinite diffusion control, the peak currents also increase linearly with increasing square root of the scan rate, υ This is found to be the case for these films and is described in Section 4 4 7

From Figure 4 5, it is found that ΔE_p and E_p - $Ep_{/2}$, are both 57 ± 3 mV Significantly, these values are consistent with a reversible electrochemical reaction involving the transfer of a single electron Therefore, it appears that only one of the osmium sites within the dimer can be oxidized when the complex is immobilized within a solid deposit This behaviour could arise because of increased electrostatic interactions due to the close proximity of adjacent redox centres in the solid deposit or from a relatively high free energy barrier to anion insertion into the solid

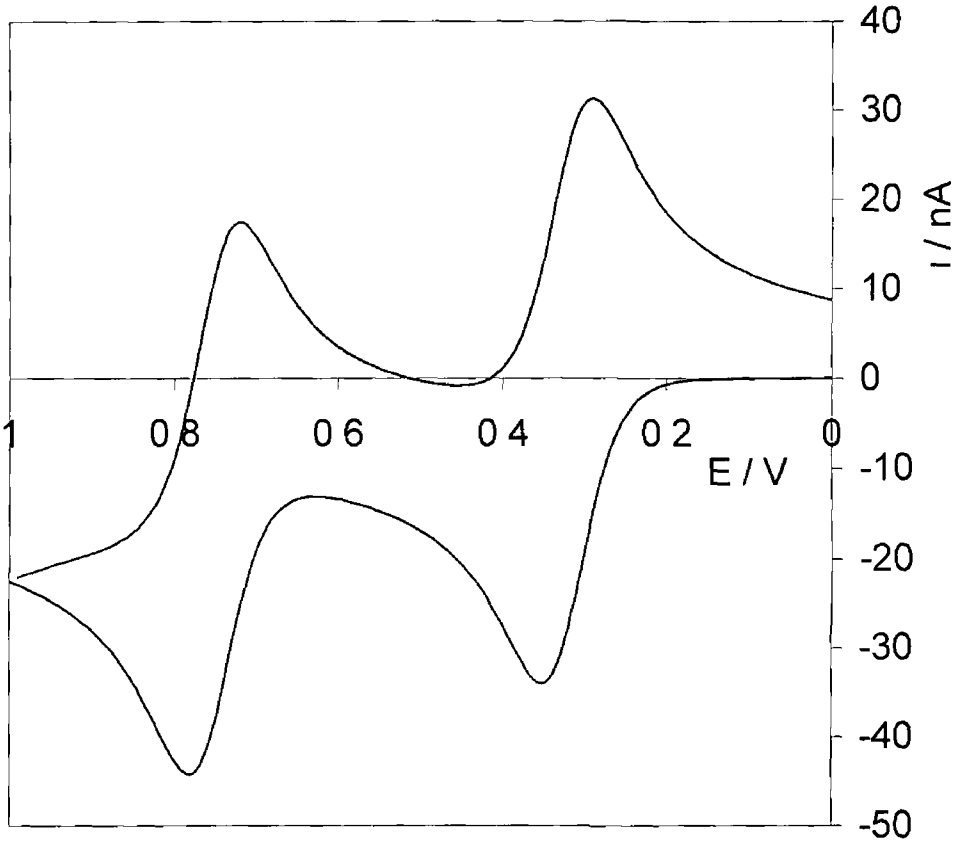

Figure 4 4 Voltammetric response for a 2 mM solution of $[Os(bpy)_2\ Cl\ 4\text{-}bpt\ Os\ (bpy)_2\ Cl]^{2+}$ dissolved in acetonitrile The supporting electrolyte is 0 1 M $LiClO_4$ The platinum microelectrode radius is 12 5 μm and the scan rate is 0 2 Vs^{-1}

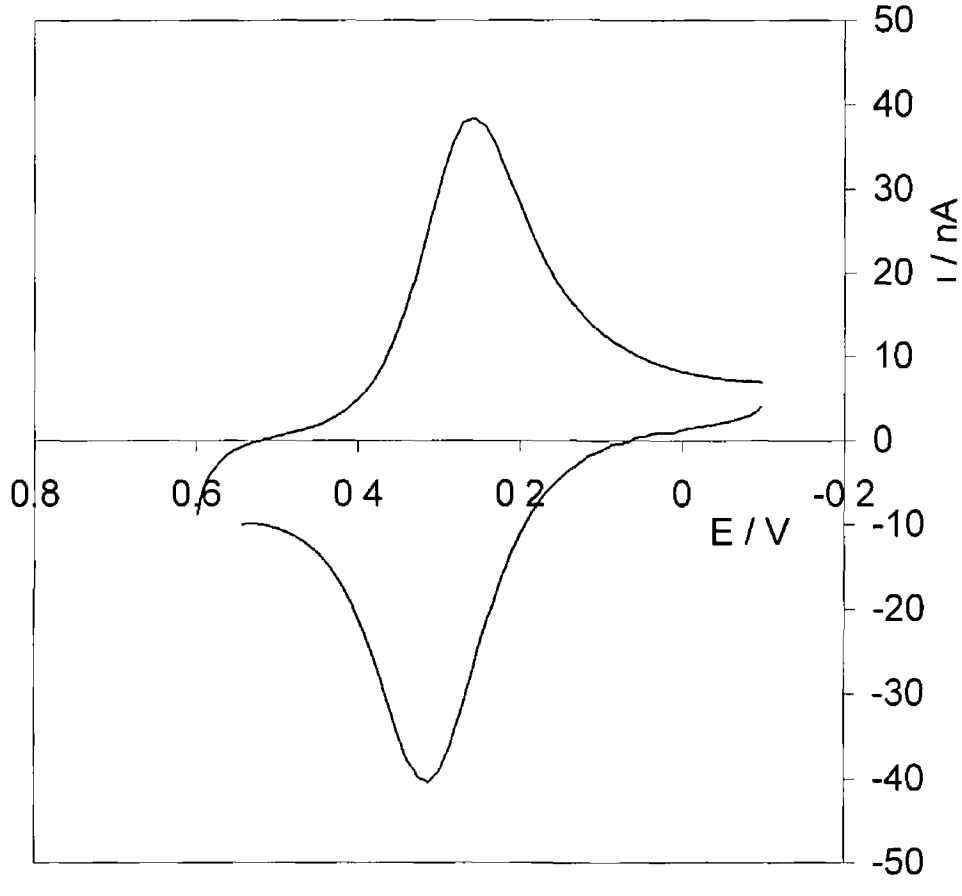

Figure 4 5 Votammetric response of a solid state layer of $[Os(bpy)_2\ 4bpt\ Os(bpy)_2\ Cl_2]^{2+}$ mechanically attached to a 25 μm radius Pt microelectrode at a scan rate of 2 Vs^{-1} The electrolyte is aqueous 0 1 M $LiClO_4$ containing 20 % acetonitrile

The formal potential of the $Os^{2+/3+}$ redox couple (0 280 V) is 40±5 mV less positive for the solid deposit compared to the dimer dissolved in acetonitrile As switching the oxidation state of these films is linked to counterion movement into and out of the film, the rate of the oxidation and reduction reactions may be different depending on the rate of ion movement both into the film and out of the film This may cause a shift in either the anodic or the cathodic peak potential, resulting in a shift in $E^{0'}$ Therefore, the designation of a formal potential in these deposits is subject to the rate of oxidation and reduction reactions being equal With this in mind, comparison of the formal potential in solution with that in the solid suggests that oxidising the metal centre is thermodynamically more facile when the dimer is immobilised within a solid deposit However, while this behaviour suggests that the free energy barrier to anion insertion is not significant, the small differences in $E^{0'}$ observed most likely reflect a higher dielectric constant within the solid deposits that that of acetomtrile This suggests that the redox centres within the deposit are at least partially solvated, which is consistent with the nearly ideal voltammetry illustrated in Figure 4 5

Figure 4 6 illustrates the electrochemical response of solid deposits of $[Os(bpy)_2$ Cl 4-bpt $Os(bpy)_2$ $Cl]^{2+}$ when they are cycled in either entirely aqueous 0 1 M $LiClO_4$ or 80 20 H_2O ACN containing 0 1 M $LiClO_4$ as supporting electrolyte Even where the electrolyte solution contains 20% v/v acetonitrile, i_{pa} and i_{pc} change by less that 10 % over an 8 hour period suggesting that significant dissolution does not occur At this scan rate, the voltammetric response observed for the deposit in contact with the solution containing the organic solvent is sharper (FWHM is 135 ± 5 mV compared to 190 ± 10 mV in the absence of acetonitrile) and the peak shape is consistent with mixed semi-infinite linear diffusion and finite diffusion control These observations suggest that the rate of charge transport through the deposit may be faster when the contacting solution contains acetonitrile

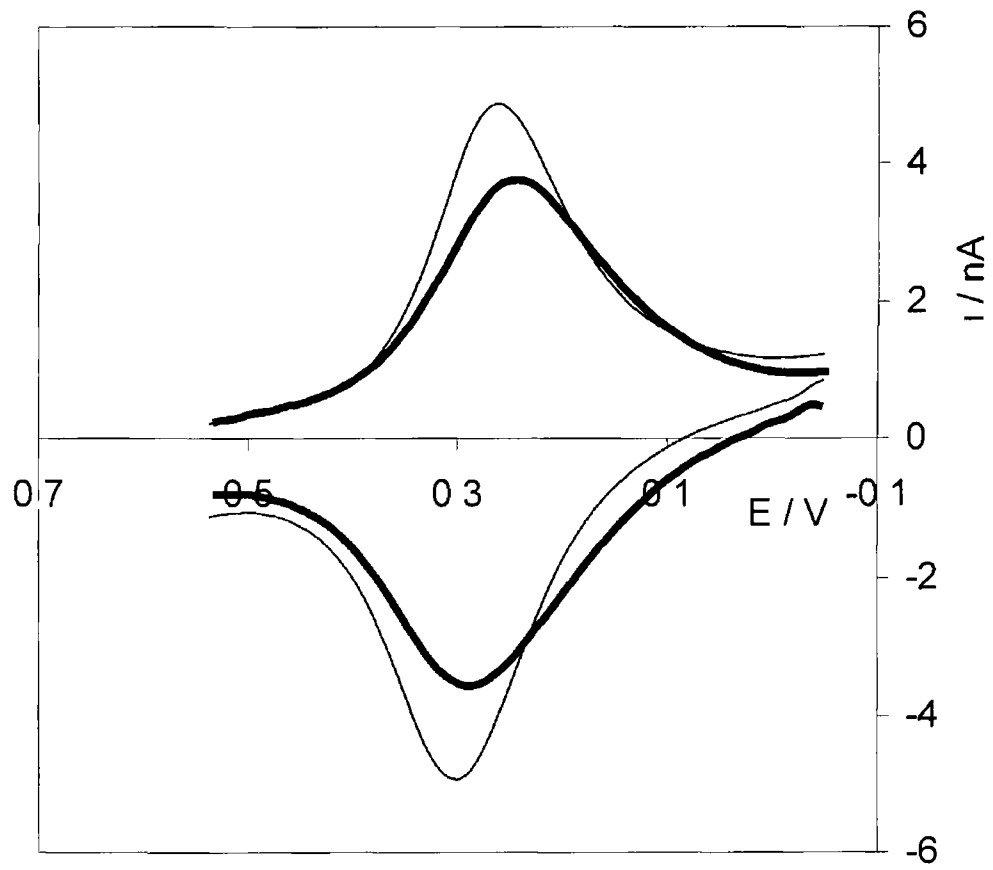

Figure 4 6 Cyclic voltammograms for an $[Os(bpy)_2\ 4bpt\ Os(bpy)_2\ Cl_2]\ (PF_6)_2$ deposit that is mechanically attached to a 25 μm radius platinum microelectrode in aqueous 0 1 M $LiClO_4$ (thick line) and in 0 1 M $LiClO_4$ containing 20% acetonitrile (thin line) The scan rate is 0 2 Vs^{-1}

4 4 4 POTENTIAL DEPENDENT UV-VIS SPECTROSCOPY

Since these deposits consist of discrete particles, not all of which may be in direct electrical contact with the electrode, it is important to determine what percentage of the deposit is electrochemically active In this way, an insight can be obtained into the extent to which individual particles are interconnected Potential dependent UV-vis spectroscopy represents a convenient approach to probing this issue Figure 4 7 illustrates the changes in the UV-vis spectrum that occur during electrolysis of a solid state deposit in aqueous 1 0 M $LiClO_4$ at +0 600 V All changes are completely reversible, i e , the peak intensities return to greater than 95% of their initial value when the deposit is oxidised and then re-reduced This behaviour persists over at least five potential cycles

The surface coverage determined from the background corrected charge passed in the 5 mVs^{1} anodic branch of the voltammogram is approximately $5x10^{8}$ mol cm^{2} Prior to oxidation, the deposit shows strong absorbances between 330 and 530 nm that are attributed to Os ($d\pi$) to bpy and bpt (π^*) MLCT transitions [18] The dashed line of Figure 4 7 shows the spectrum obtained for the complex dissolved in acetonitrile and indicates that the spectroscopic transitions and relative peak intensities of the solid deposits are generally consistent with those observed for the complex in solution However, the absorption maxima are typically shifted to lower energy by approximately 10 nm for the solid deposits Consistent with oxidation of the Os^{2+} centres, the intensity of the MLCT bands decrease systematically with increasing electrolysis time Significantly, despite the fact that this deposit is less than a micron thick, the spectrum changes continuously for periods up to 40 seconds suggesting that solid state charge transport is relatively slow in this system

Figure 4 8 shows that the absorbance (490 nm) vs time profile for the deposit and indicates that even for very long electrolysis times the absorbance at 490 nm never

decays to zero This behaviour contrasts with previously reported systems where exhaustive electrolysis caused complete collapse of the MLCT wave [13] The observation that exhaustive electrolysis decreases the absorbance to approximately 50% of its initial value is significant and supports the voltammetric data presented earlier which suggested that only one Os^{2+} site within the dimer is oxidized for the solid deposits Moreover, this observation suggests that the individual particles are highly interconnected and that close to 100 % of the immobilised particles are electrochemically active, at least on a hundreds of seconds timescale

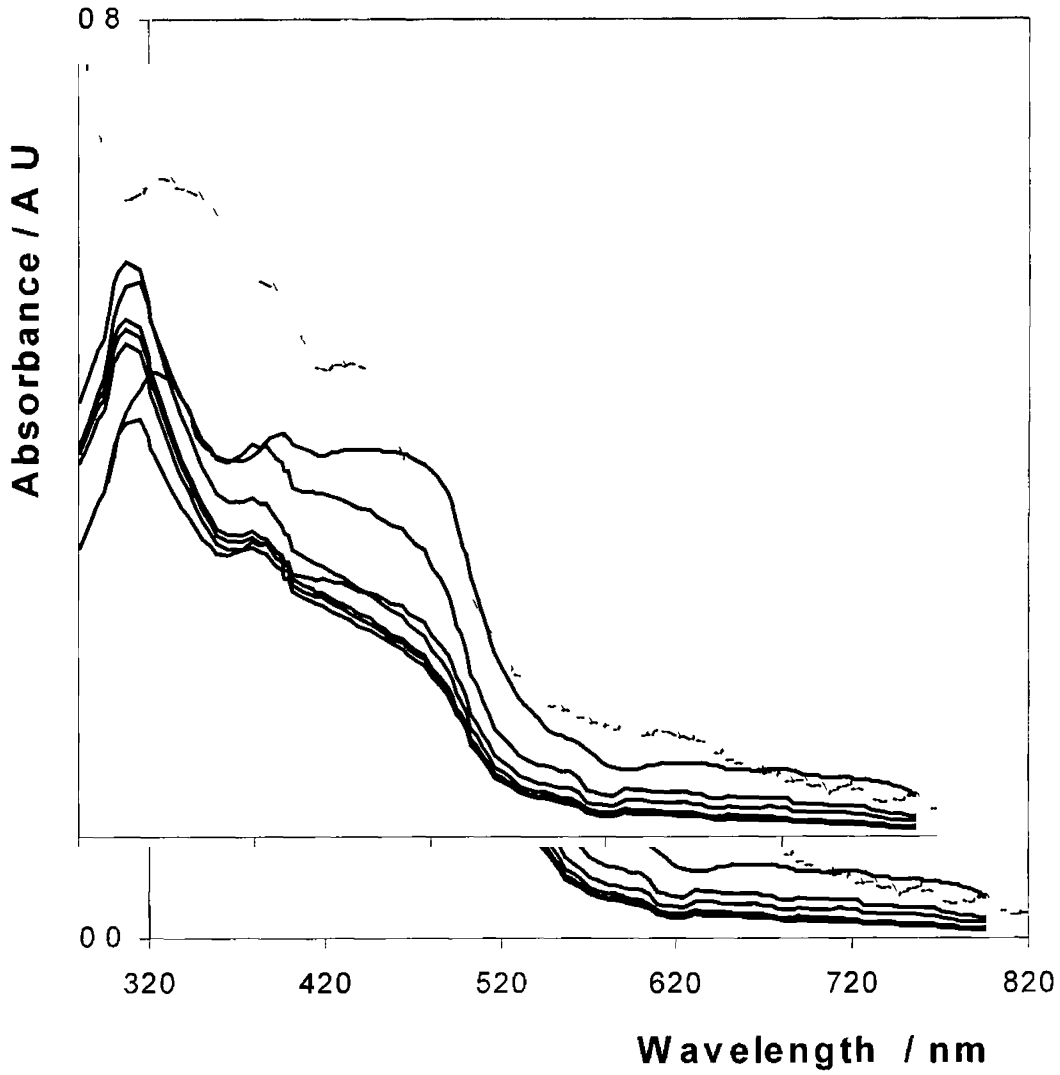

Figure 4 7 Time dependent changes in the UV-vis spectrum of a solid state $[Os(bpy)_2\ 4bpt\ Os(bpy)_2\ Cl_2]\ (PF_6)_2$ deposit attached to an ITO electrode when electrolysed at +0 600 V in aqueous 1 0 M $LiClO_4$ From top to bottom (solid lines), the spectra represent electrolysis times of 0, 10, 20, 40, 80, 120 and 140 seconds The dashed line is the spectrum obtained for the complex dissolved in acetomtrile

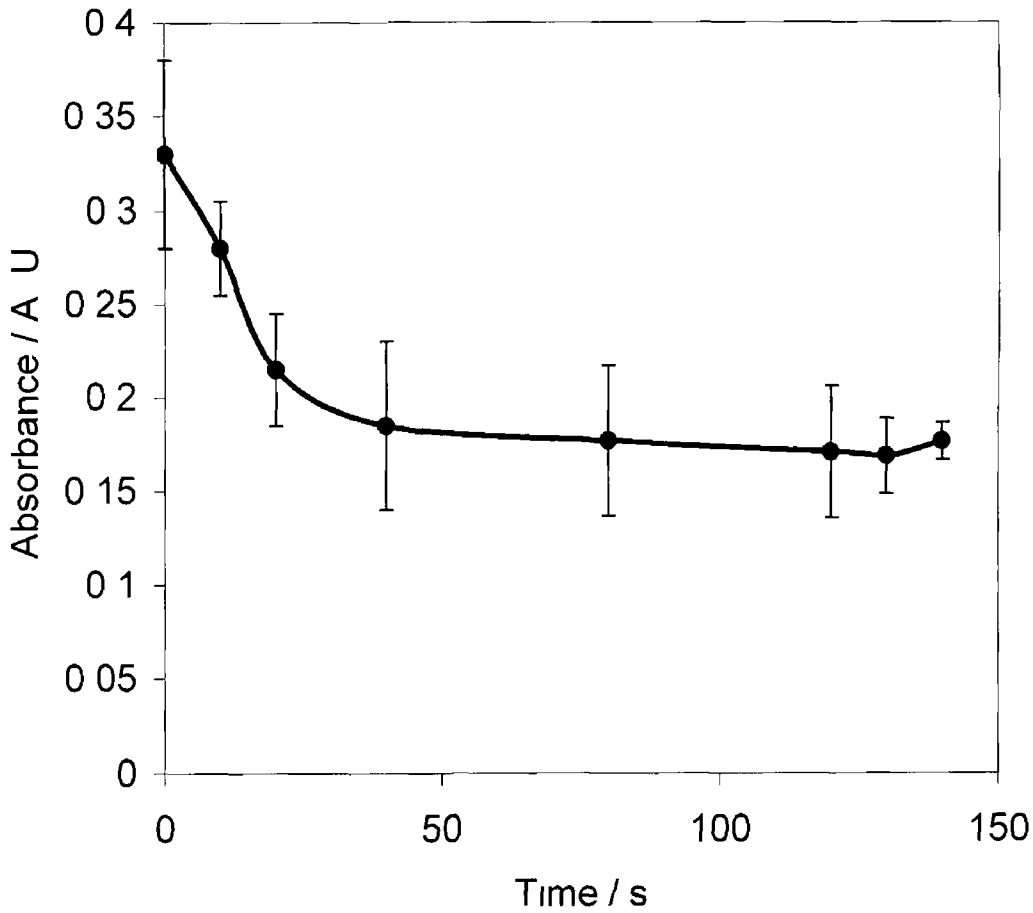

Figure 4 8 Absorbance at 490 nm of a solid state $[Os(bpy)_2\ 4bpt\ Os(bpy)_2\ Cl_2](PF_6)_2$ deposit attached to an ITO electrode when electrolysed at +0 600 V in 1 0 M $LiClO_4$

4 4 5 EFFECT OF ELECTROLYTE pH

The 4-bpt bridge is capable of undergoing a protonation/deprotonation reaction which will influence both the strength of electronic coupling between the two metal centres and the overall charge on the complex There have been surprisingly few studies on the impact of protonation reactions on the structure of solid state materials This situation is striking because careful studies on biosystems have proven that both the secondary structure and hydrogen bonding play critical roles in dictating the efficiency of long-range electron transfer [19]

Figure 4 9 illustrates the voltammetric response obtained for solid deposits of the dimers in 0 1 M $HClO_4$ and 0 1 M $LiClO_4$ adjusted to pH 12 with NaOH, where the solvent is 80 20 H_2O ACN The peak shapes observed at each pH are similar and do not change significantly upon repetitive cycling in either electrolyte However, in low pH electrolyte, the formal potential is approximately 35 mV more positive than that found in near neutral electrolyte The observation that $E^{o\prime}$ is more positive in low pH electrolyte indicates that the Os^{2+} centres are thermodynamically more difficult to oxidise when the 4-bpt ligand is protonated A reduced electron donating ability of the protonated ligand and the higher overall positive charge within the layer are likely to contribute to this effect

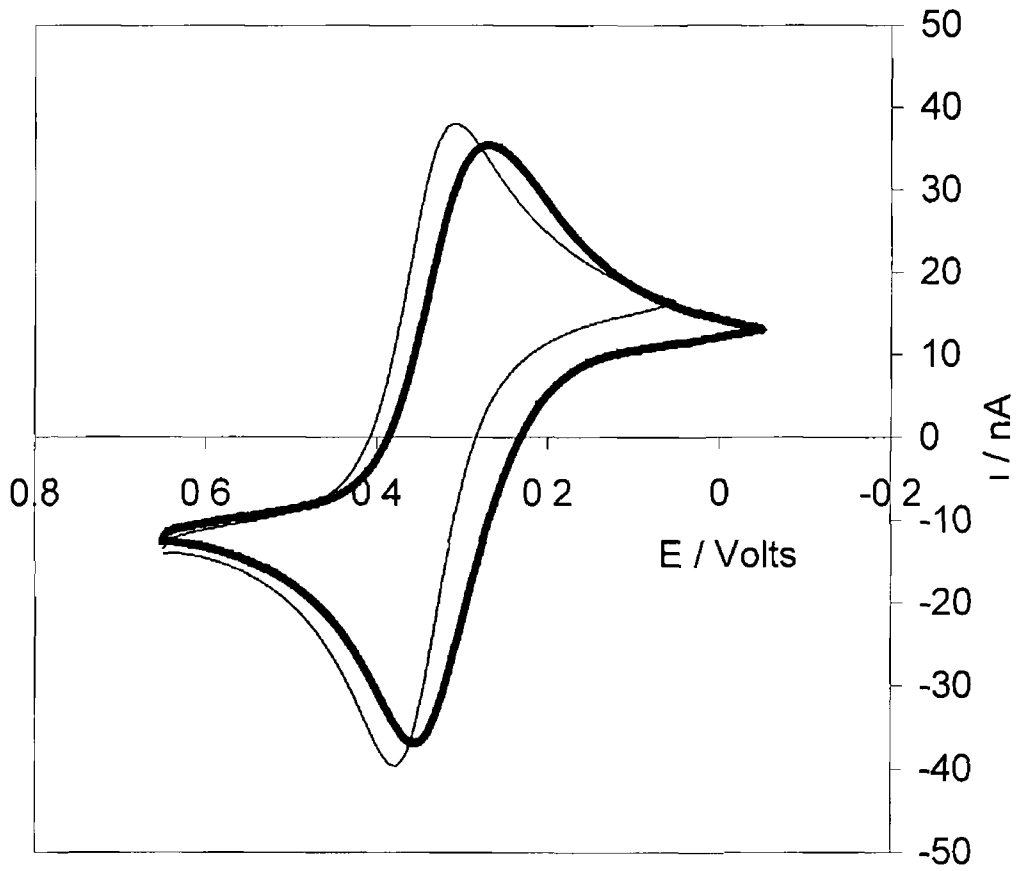

Figure 4 9 Cyclic voltammograms for an $[Os(bpy)_2\ 4bpt\ Os(bpy)_2\ Cl_2]\ (PF_6)_2$ deposit that is mechanically attached to a 12 5 μm radius platinum microelectrode in aqueous 0 1 M $LiClO_4$ containing 20% acetonitrile adjusted to pH 12 0 (thick line) and in aqueous 0 1 M $HClO_4$ containing 20% acetonitrile (thin line) The scan rate is 2 0 Vs^{-1}

4 4 6 RESISTANCE AND INTERFACIAL CAPACITANCE

When attempting to extract quantitative data from voltammetric data, e g , formal potential, charge transport diffusion coefficients or heterogeneous electron transfer rate constants, it is important to consider the effects of both the electrode response time and ohmic effects Also, by examining the resistance as a function of the supporting electrolyte concentration, it ought to be possible to obtain a limited insight into the permeability of the deposit towards electrolyte ions

When a polycationic deposit is placed in a dilute solution of a strong electrolyte, the concentration of counterions (PF_6 in this case) within the deposit is typically considerably larger than that found in the contacting solution For the deposits considered here, the anion concentration initially present in the deposit is expected to be between 1 5 and 3 M depending on the extent of protonation of the 4-bpt ligand Thus, under the influence of the concentration gradient, counterions may diffuse from the deposit into the solution until the concentrations become equal in the two phases However, if diffusion of charged counterions occurs, then electroneutrality within the deposit would be violated, and an electrical potential would develop at the interface This "Donnan potential" would then increase until an equilibrium was reached in which it completely opposes the tendency of the counterions to move down the concentration gradient Under these equilibrium conditions the net diffusion of counterions across the interface would be zero, and co-ions would be excluded from the solid deposit [20]

The existence of such a permselective response for these solid deposits was probed by determining the contribution of the deposit resistance to the total cell resistance as the supporting electrolyte concentration is systematically varied In the case of an ideally permselective response, ions would be effectively excluded from the membrane, and the deposit resistance would be independent of the supporting electrolyte concentration To determine the total cell resistance, short

timescale, small amplitude, potential step chronoamperometry has been performed, in a potential region where no Faradaic response is observed In a typical experiment, the potential was stepped from -50 to 0 mV at both bare and modified microelectrodes, and the resulting current was recorded over the following 20 μs This capacitive current vs time transient can be described by Equation 4 3 [21]

$$i_c(t) = (\Delta E / R) \exp(-t / RC_{dl}) \quad (4\ 3)$$

where ΔE is the pulse amplitude, R is the total cell resistance, and C_{dl} is the integral double layer capacitance For both modified and bare electrodes, the current decays in time according to a single exponential, which is consistent with double layer charging alone [20] Figures 4 10 and 4 11 illustrate $i_c(t)$ vs t and semi-log current vs time plots for the solid deposits as the lithium perchlorate concentration is changed from 0 1 to 0 5 to 1 0 M The absolute slope of the semi-log plots represents the reciprocal of the cell time constant RC_{dl}

Table 4 1 presents RC_{dl} values for an electrode before, and after modification with the dimer as a function of the perchlorate concentration This table shows that both the bare and the modified electrode cell time constants decrease with increasing electrolyte concentration as expected [20] However, the response time is considerably more sensitive to the supporting electrolyte concentration for the microelectrode coated with the solid deposit It is apparent from Equation 4 3 that R can be extracted from the intercepts of the semi-log plots shown in Figure 4 11 Figure 4 12 shows the total cell resistance for a bare and a coated electrode as the perchlorate concentration is changed from 0 1 to 1 0 M It is apparent that in both circumstances R is reduced at high electrolyte concentrations reflecting a reduced solution resistance Significantly, for perchlorate concentrations greater than about 0 5 M, the total cell resistance with and without the deposit are indistinguishable This result suggests that, for relatively high electrolyte

concentrations, the deposit resistance is low probably because electrolyte can permeate the individual particles that exist on the microelectrode surface

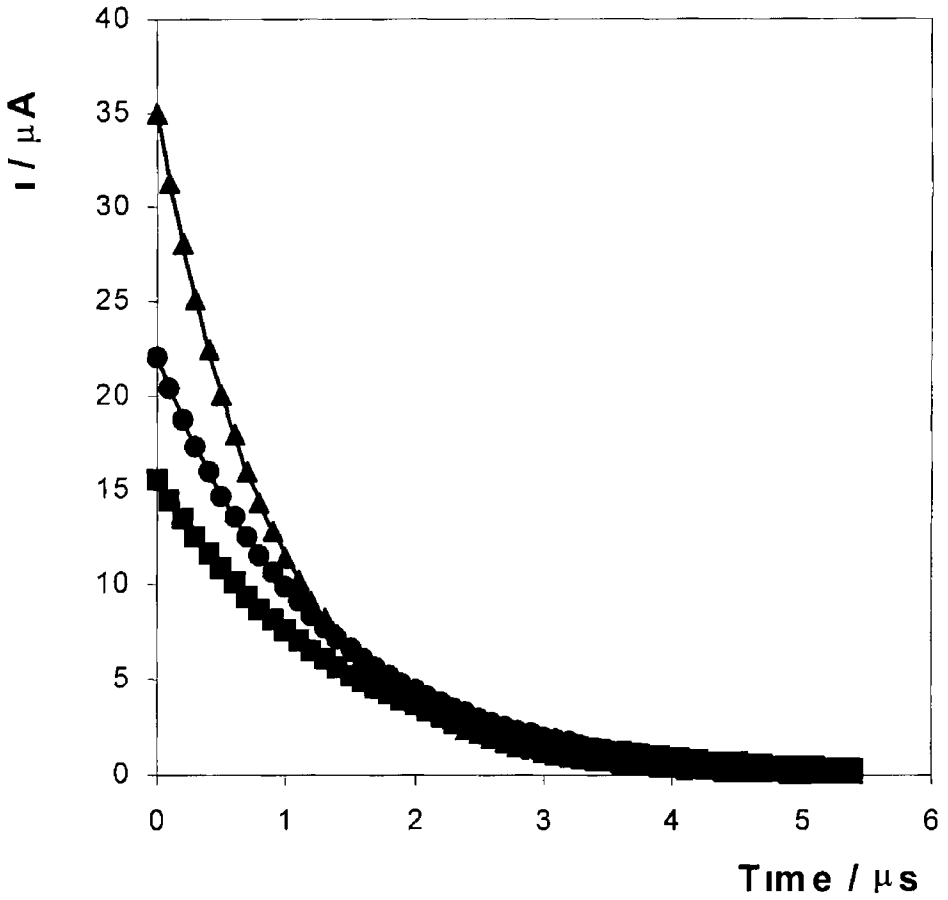

Figure 4 10 Current-time transients for a 25 μm radius platinum microelectrode modified with an $[Os(bpy)_2\ 4bpt\ Os(bpy)_2\ Cl_2]\ (PF_6)_2$ deposit following potential steps from –0 050 to 0 000 V From top to bottom, the data correspond to aqueous 0 1, 0 5 and aqueous 1 0 M $LiClO_4$ containing 20% acetonitrile as supporting electrolyte

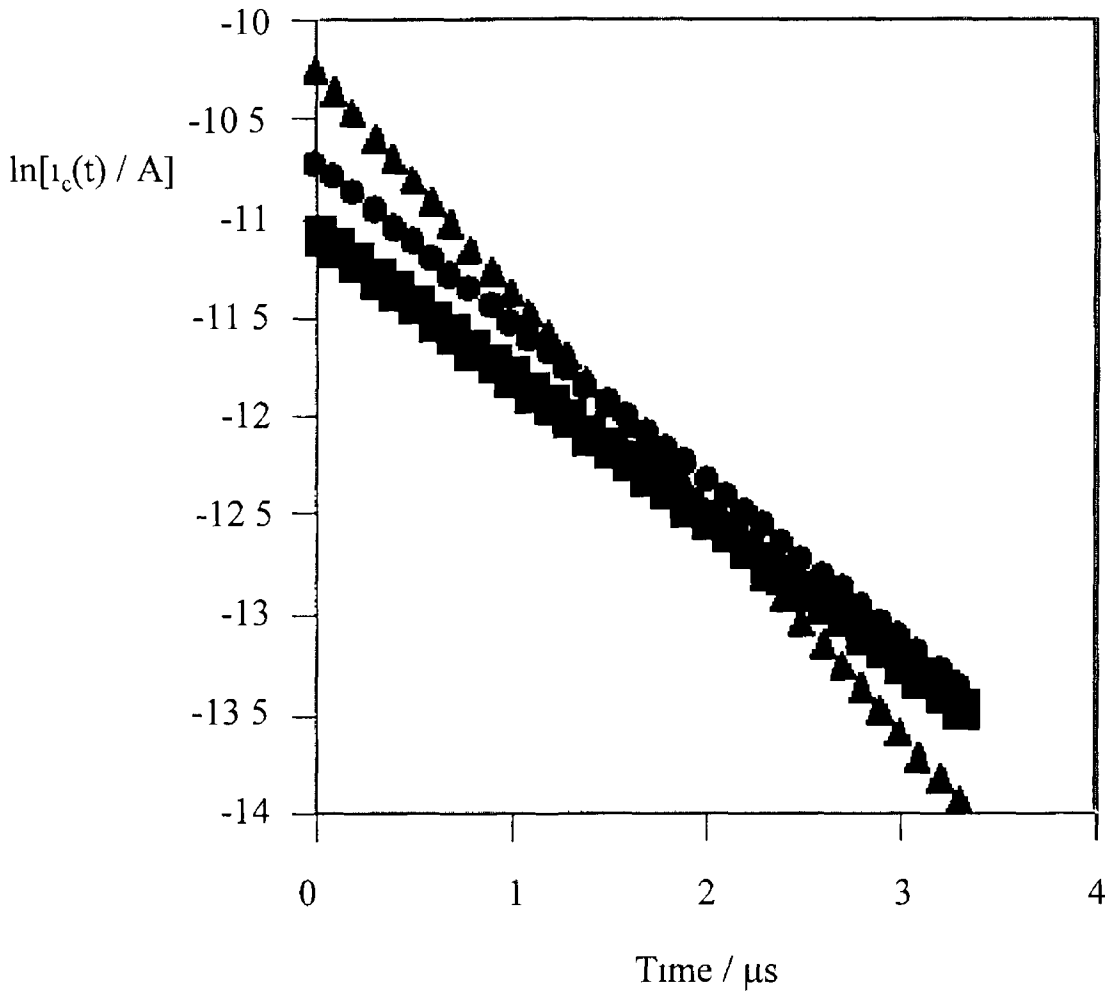

Figure 4 11 Semi-log plots for current-time transients obtained using a 25 μm radius platinum microelectrode modified with an $[Os(bpy)_2\ 4bpt\ Os(bpy)_2\ Cl_2](PF_6)_2$ deposit following potential steps from –0 050 to 0 000 V From top to bottom (left side), the data correspond to aqueous 0 1, 0 5 and 1 0 M $LiClO_4$ as supporting electrolyte

Table 4 1 Resistance, R, Double Layer Capacitance, C_{dl}, and Electrode Response Times, RC, for 25 μm Radius Platinum Microelectrodes Before and After Modification with a Solid Deposit of $[Os(bpy)_2\ 4bpt\ Os(bpy)_2\ Cl_2]\ (PF_6)_2$ as the Concentration of $LiClO_4$ is Systematically Varied *

	Bare			Modified		
$[LiClO_4]$ / M	R / Ω	$10^{10}\ C_{dl}$ / F	RC_{dl} / μs	R / Ω	$10^{10}\ C_{dl}$ / F	RC_{dl} / μs
0 0	2400(192)	5 89(0 53)	1 41(0 25)	3169(253)	4 10(0 23)	1 29(0 18)
0 1	2200(188)	6 28(0 50)	1 38(0 23)	3212(198)	4 64(0 21)	1 49(0 17)
0 2	2056(132)	6 48(0 58)	1 33(0 21)	3034(215)	5 05(0 28)	1 53(0 19)
0 4	1877(140)	7 06(0 14)	1 32(0 12)	2800(184)	5 60(0 33)	1 56(0 20)
0 6	1700(119)	7 06(0 28)	1 20(0 13)	1890(195)	5 44(0 16)	1 02(0 14)
0 8	1550(15 5)	7 46(0 74)	1 15(0 12)	1636(156)	5 89(0 14)	0 95(0 10)
1 0	1400(70)	8 24(0 49)	1 15(0 13)	1475(35)	6 41(0 31)	0 94(0 07)

* The numbers in parentheses represent errors obtained from at least 3 independent experiments

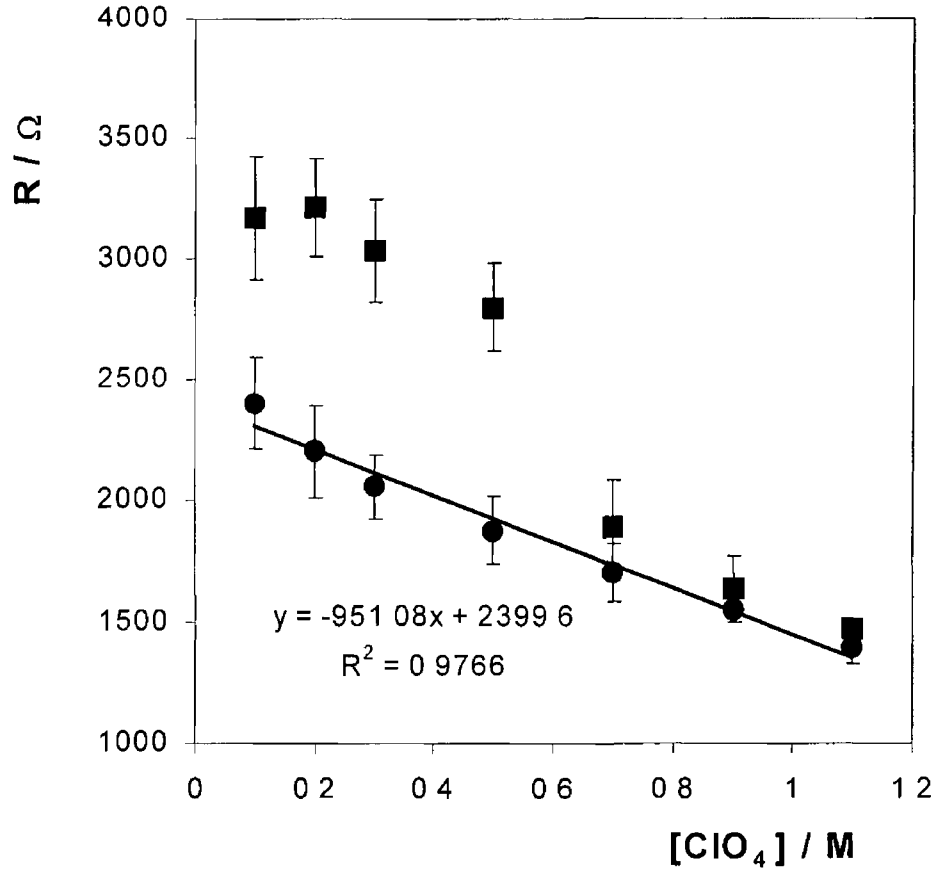

Figure 4 12 Dependence of the total cell resistance, R, on the concentration of $LiClO_4$ as supporting electrolyte Data for a bare 25 μm radius platinum microelectrode are shown on the lower curve (●) while the upper curve is for the same microelectrode modified with an $[Os(bpy)_2\ 4bpt\ Os(bpy)_2\ Cl_2]\ (PF_6)_2$ solid deposit (■)

4 4 7 HOMOGENEOUS CHARGE TRANSPORT RATES

The well-defined metal-based oxidation observed for this solid deposit makes them attractive systems for investigating the dynamics of charge transport in the solid state To achieve this objective, cyclic voltammetry has been used to determine apparent charge transport diffusion coefficients as the concentration of supporting electrolyte is systematically varied Figures 4 13 and 4 14 show how the voltammetric responses obtained for solid deposits changes as the scan rate is systematically varied from 200 to 800 mVs^{-1} in acidic and neutral electrolytes, respectively For this range of scan rates, the voltammetric peak currents increase as $\upsilon^{1/2}$ (Figures 4 15 and 4 16) This behaviour is consistent with semi-infinite linear diffusion control in which the deposit is not exhaustively electrolysed and the depletion zones remain within individual microparticles Under these circumstances, the peak current, i_p, can be described in terms of the Randles-Sevçik equation

$$i_p = 2\ 69\times10^5\ n^{3/2}\ A\ D_{CT}^{1/2} C_{eff}\ \upsilon^{1/2} \qquad (4\ 4)$$

where n is the number of electrons transferred, A is the area of the working electrode, D_{CT} is the apparent charge transport diffusion coefficient and C_{eff} is the effective fixed site concentration of the redox centres

Previous studies on structurally related systems and crystallographic data suggest that the fixed site concentration is 1 7±0 05 M [13 22] Analysing the data presented in Figures 4 14 and 4 16 using this approach, yields D_{CT} values of $2\ 0\pm0\ 6\times10^{-10}$ and $2\ 0\pm0\ 5\times10^{-10}$ cm^2s^{-1} in 0 1 M $LiClO_4$ and 0 1 M $HClO_4$ respectively While these diffusion coefficients are large for solid deposits,[16] they are still many orders of magnitude smaller than those found for the complex dissolved in solution, $5\ 6\pm1\ 1\times10^{-6}$ cm^2s^{-1} These relatively small diffusion coefficients are likely to significantly limit the technological exploitation of materials of this kind For

example, under semi-infinite linear diffusion conditions it would take approximately 15 seconds to switch a 1 μm thick film from one oxidation state to another

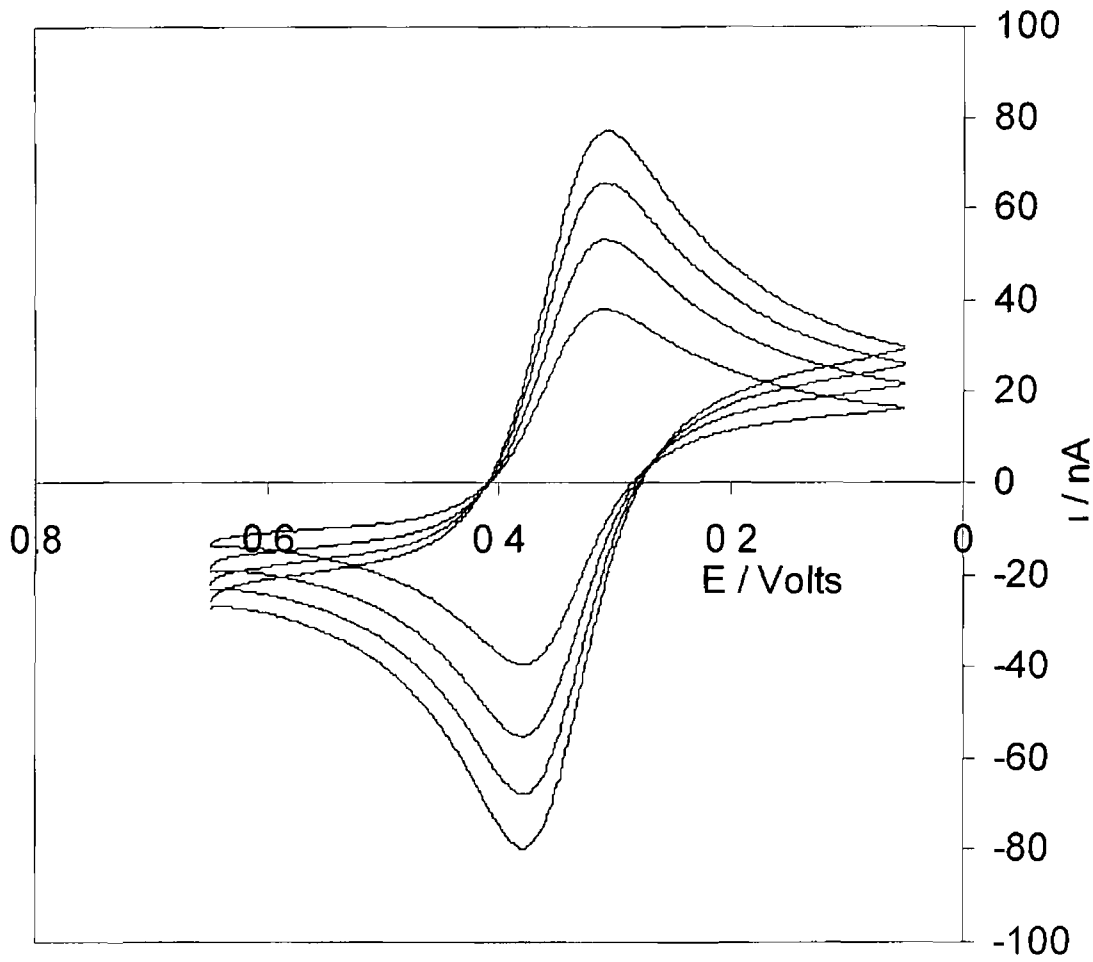

Figure 4 13 Scan rate dependence of the voltammetric response for a deposit of $[Os(bpy)_2\ 4bpt\ Os(bpy)_2\ Cl_2]\ (PF_6)_2$ formed on a 25 μm radius platinum microelectrode The supporting electrolyte is aqueous 0 1 M $HClO_4$ containing 20% acetonitrile From top to bottom the scan rates are 800, 600, 400 and 200 mVs^{-1}

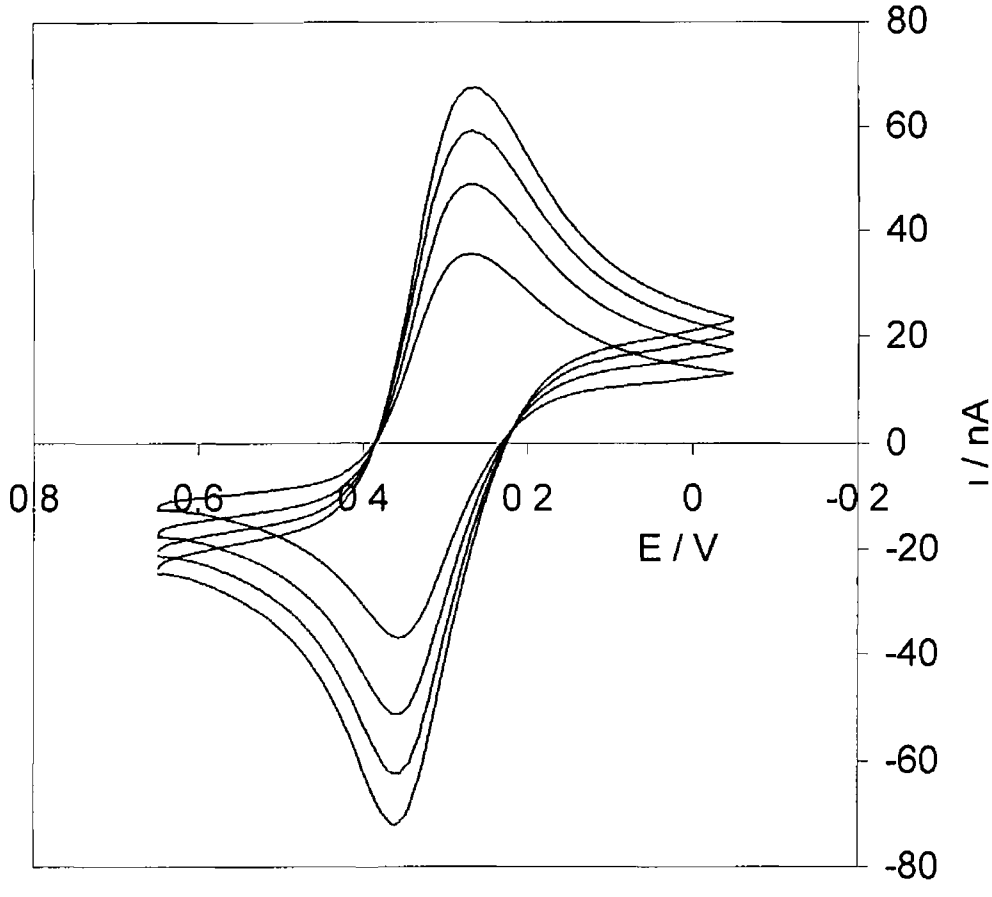

Figure 4 14 Scan rate dependence of the voltammetric response for a deposit of $[Os(bpy)_2$ 4bpt $Os(bpy)_2$ $Cl_2]$ $(PF_6)_2$ formed on a 25 μm radius platinum microelectrode The supporting electrolyte is 0 1 M $LiClO_4$ containing 20% acetonitrile From top to bottom the scan rates are 800, 600, 400 and 200 mVs^{-1}

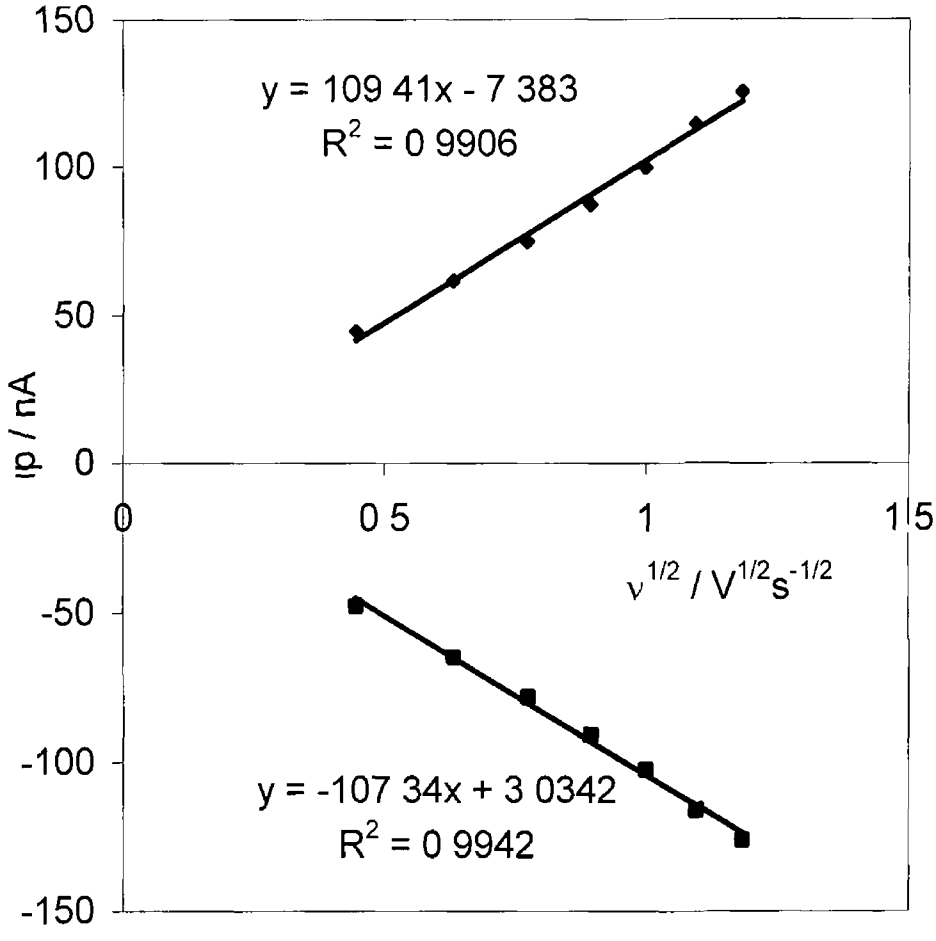

Figure 4 15 Plot of i_p versus the square root of scan rate for a mechanically attached solid layer of $[Os(bpy)_2 Cl\ 4\text{-}bpt\ Os(bpy)_2 Cl](PF_6)_2$ at 25 μm platinum microelectrode The supporting electrolyte is aqueous 0 1 M $HClO_4$ containing 20% acetonitrile Cathodic currents are positive and anodic currents are negative

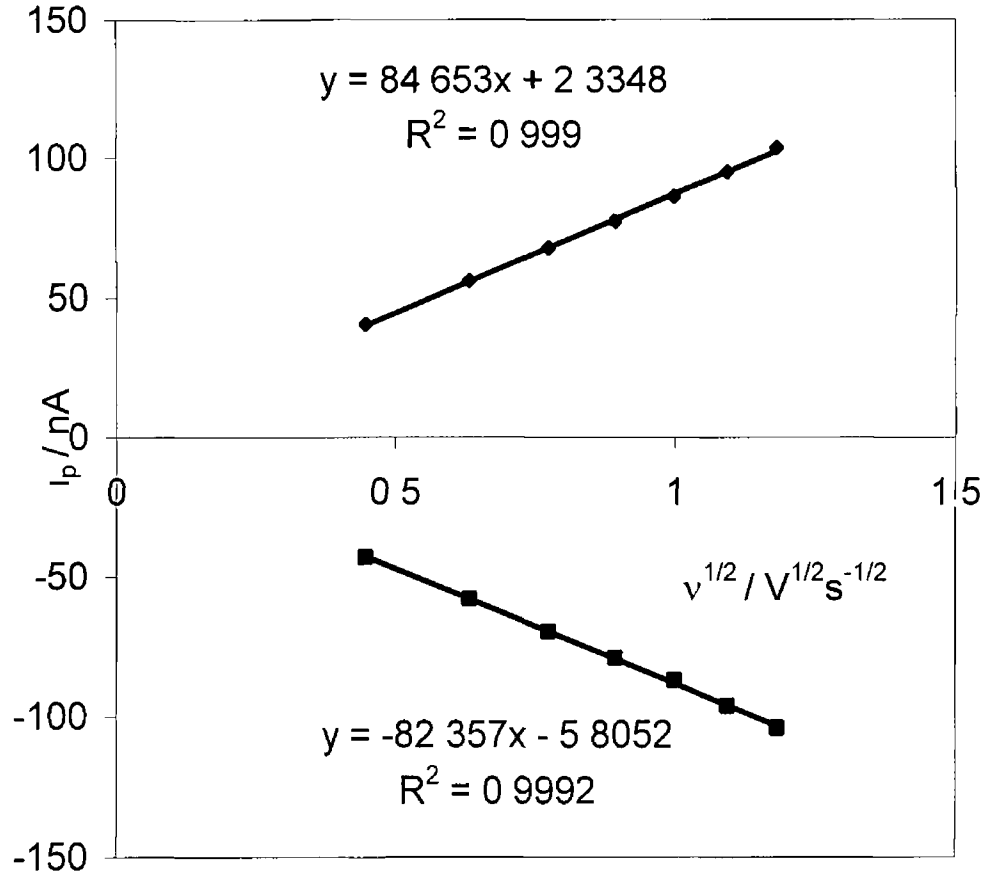

Figure 4 16 Plot of i_p versus the square root of scan rate for a mechanically attached solid layer of $[Os(bpy)_2$ Cl 4-bpt $Os(bpy)_2$ Cl$](PF_6)_2$ at a 25 μm platinum microelectrode The supporting electrolyte is aqueous 0 1 M $LiClO_4$ containing 20% acetonitrile Cathodic currents are positive and anodic currents are negative

In this system, SEM analysis (Section 4 4 2) reveals that the physical structure of the deposit does not appear to change significantly as the oxidation state is switched Under these circumstances, homogenous charge transport through the deposit is limited either by electron self-exchange between the osmium sites or counterion diffusion through the solid If electron self-exchange is the rate determining step, charge compensating counterions must be freely available within the deposit and D_{CT} is expected to at best depend only weakly on the electrolyte concentration Significantly, Table 4 2 shows that D_{CT} does not depend on the concentration of electrolyte in either $LiClO_4$ or $HClO_4$ This observation suggests that ion transport is facile and that the rate of charge transport is limited by the rate of electron self-exchange between Os^{2+} and Os^{3+} couples within the deposit

The Dahms Ruff expression allows the second order rate constant, k_{SE}, describing the dynamics of self-exchange between adjacent $Os^{2+/3+}$ moieties, to be determined

$$D_{CT} = D_{phys} + 1/6\, k_{SE}\, \delta^2\, C_{eff} \qquad (4\ 5)$$

where D_{phys} described physical diffusion in the absence of electron hopping and δ is the inter-site separation between adjacent redox centres Given that the osmium redox centres are immobilised within a solid deposit, D_{phys} is assumed to be zero The inter-site separation is estimated from the x-ray crystal structure as a through-space distance of 13 4 Å [23 24] Using these values, Equation 4 5 yields rate constants for electron self-exchange of are $1\ 8\times10^7$ and $3\ 0\times10^7$ $M^{-1}s^{-1}$ at pH 6 0 and pH 0, respectively These values are comparable with those reported for osmium polypyridyl complexes in solution[25] or within monolayers [26 27 28]

Table 4 2 Effect of the Identity and Concentration of Supporting Electrolyte on the Homogenous Charge Transport Diffusion Coefficient Through Solid-State $[Os(bpy)_2 Cl\ 4\text{-bpt}\ Os(bpy)_2 Cl](PF_6)_2$ deposits [a]

Concentration / M	$10^{10} D_{CT}$ / $cm^2 s^{-1}$ ($LiClO_4$)	$10^{10} D_{CT}$ / $cm^2 s^{-1}$ ($HClO_4$)
0 1	2 0 (0 6)	2 0 (0 5)
0 5	2 0 (0 4)	1 8 (0 3)
0 7	1 8 (0 6)	1 6 (0 3)
1 0	2 0 (0 1)	1 7 (0 4)
1 5	2 0 (0 4)	1 5 (0 1)
2 0	2 1 (0 3)	1 6 (0 3)

[a] Errors are in parentheses and represent the standard deviation on at least three independently formed deposits

4 4 8 HETEROGENOUS ELECTRON TRANSFER DYNAMICS

As discussed above, the voltammograms shown in Figures 4 13 and 4 14 are controlled by electron self-exchange between adjacent osmium centres However, at higher scan rates the rate of heterogeneous electron transfer across the electrode/deposit interface influences the voltammetric response causing an increase in ΔE_p Figure 4 17 illustrates the voltammograms obtained for solid deposits of the dimer where $500 \leq \upsilon \leq 4000$ Vs^{-1} The resistance data illustrated in Figure 4 12 confirm that the ohmic drop never exceeds 15 mV which is negligible compared to the ΔE_p observed Therefore, slow heterogeneous electron transfer is the dominant factor controlling the large peak-to-peak separation illustrated in Figure 4 17

Under these circumstances, the standard rate constant for heterogeneous electron transfer, k°, can be determined by investigating the dependence of E_p - E°′ on υ in conjunction with Equation 4 6

$$E_p = E^{o\prime} - \frac{RT}{\alpha nF}\left[0\ 780 + \ln\left(\frac{D_{app}}{k^o}\right) + \ln\left(\frac{\alpha nF\upsilon}{RT}\right)^{1/2}\right] \qquad (4\ 6)$$

Equation 4 6 predicts that a plot of (E_p-E°′) vs ln υ should be linear Figure 4 18 confirms that a linear response is observed experimentally suggesting that Equation 4 6 provides a suitable model for the determination of k° and α Figure 4 17 indicates that k° is $1\ 03 \pm 0\ 08 \times 10^{-3}$ cm s^{-1}

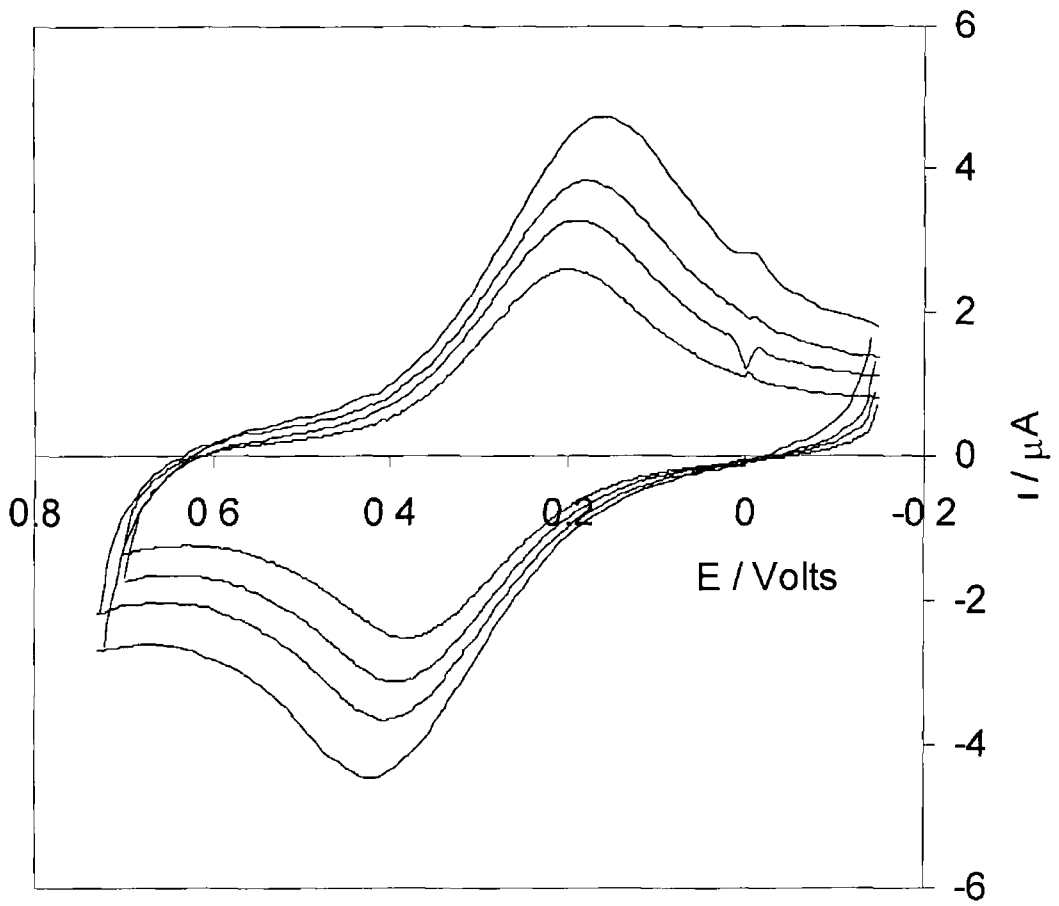

Figure 4 17 Scan rate dependence of the voltammetric response for a mechanically attached solid layer of $[Os(bpy)_2$ 4bpt $Os(bpy)_2$ $Cl_2]$ $(PF_6)_2$ formed on a 25 µm radius platinum microelectrode The supporting electrolyte is aqueous 0 1 M $LiClO_4$ containing 20% acetonitrile From top to bottom the scan rates are 1333, 1000, 800 and 571 Vs^{-1}

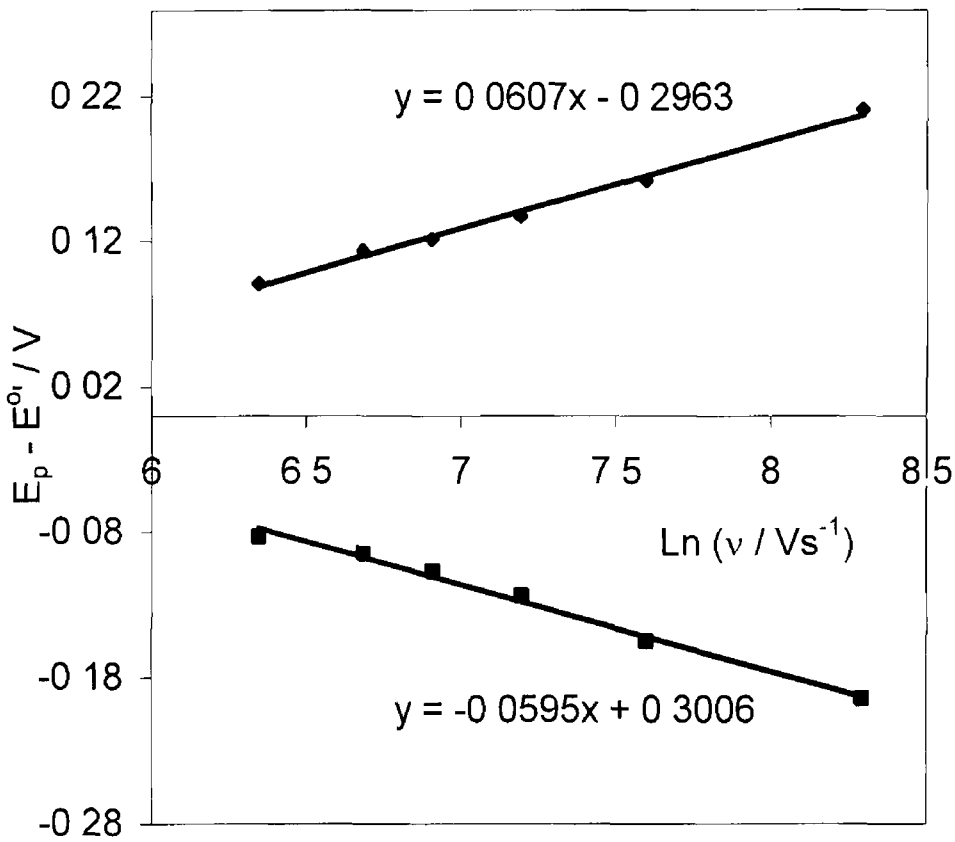

Figure 4 18 Graph of E_p - E°′ vs ln υ for deposits of $[Os(bpy)_2$ Cl 4-bpt $Os(bpy)_2$ Cl$](PF_6)_2$ formed on a 25 μm radius platinum microelectrode The supporting electrolyte is aqueous 0 1 M $LiClO_4$ containing 20% acetomtrile

Figure 4 19 and 4 20 illustrate theoretical fits to the experimental cyclic voltammograms generated according to the Butler-Volmer formalism of electrode kinetics at scan rates of 200 and 571 Vs^{-1} [29] In fitting these voltammograms, the residual sum of squares between the experimental and theoretical reduction currents were minimized and then the oxidation branch of the voltammogram was predicted The satisfactory agreement observed between theory and experiment suggests that the voltammograms for the solid deposits can be approximately described by conventional solution phase models based on semi-infinite linear diffusion Moreover, the satisfactory fits suggest that the deposits are solvated and that electrochemical double layer sets up at the electrode/layer interface This conclusion is consistent with the observation that the formal potentials of solution phase and solid deposits are similar

For $5<\upsilon<100$ Vs^{-1}, the best fit simulated voltammogram is obtained where D_{CT} is 2.0×10^{-10} cm^2s^{-1} and the standard heterogeneous electron transfer rate constant, k°, is $1.08\pm0.05\times10^{-3}$ cms^{-1} The diffusion coefficient obtained by fitting the complete voltammogram is identical to that found using the Randle-Sevçik analysis to within 5% Significantly, the standard heterogeneous electron transfer rate constant is independent of the scan rate indicating that the layers are kinetically homogeneous The observation that the rate constants for all redox centres capable of undergoing heterogeneous electron transfer are experimentally indistinguishable suggests that the local microenvironments, electron transfer distances and reorganization energies are identical for individual redox centres

A challenging issue is to probe the effect of supramolecular order on the rate of heterogeneous electron transfer The heterogeneous electron transfer dynamics of spontaneously adsorbed monolayers of $[Os(bpy)_2Cl\ 4\text{-bpt}]^{2+}$ has been examined previously [15] For these monolayers, apparent k° values of 1.6×10^{5} s^{-1} and 4.4×10^{4} s^{-1} were found for monolayer oxidation and reduction, corresponding to distance normalised heterogonous electron transfer rate constants of 1×10^{-2} cms^{-1} and

4.4×10^{-3} cms^{-1} respectively. Significantly, these values are less than an order of magnitude larger than those found for the solid state layers described here. This observation suggests that the 4-bpt bridge does not support strong electronic communication between the delocalised electronic states of an electrode and the localised redox orbitals of the $[Os(bpy)_2Cl]^+$ moiety.

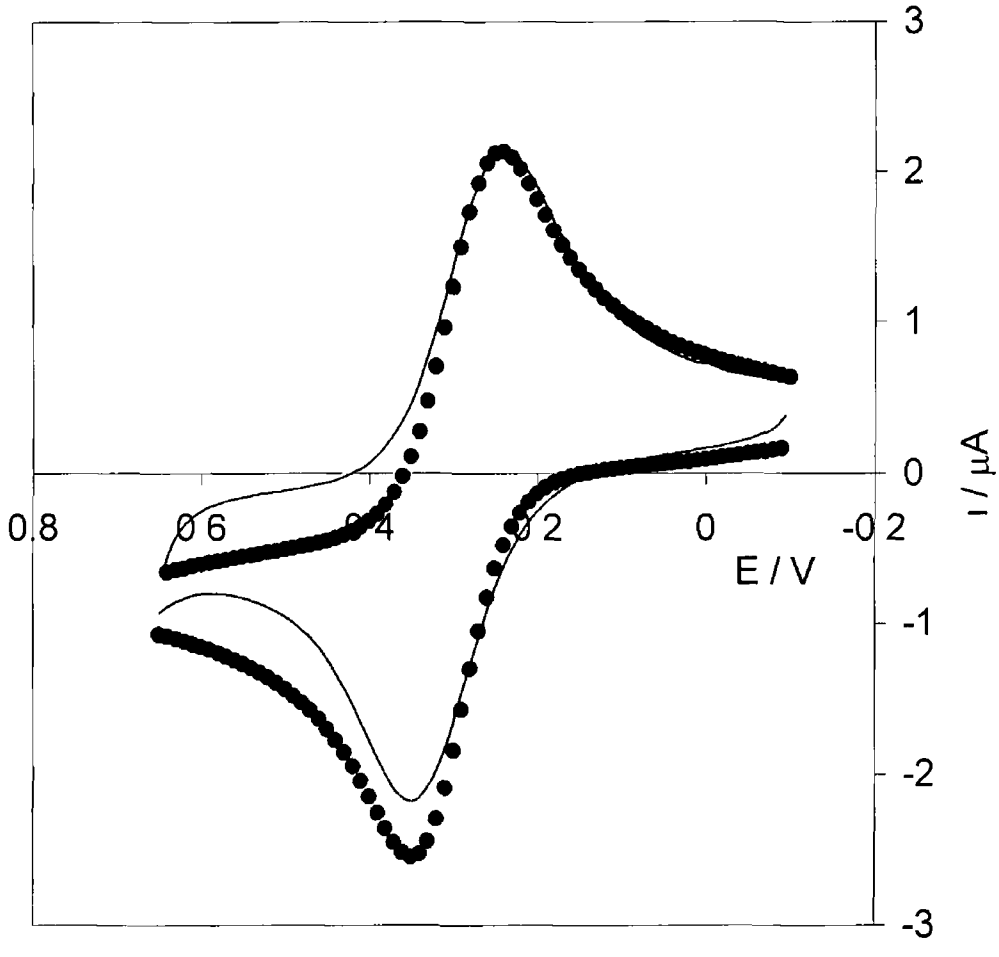

Figure 4 19 Cyclic voltammograms for a mechanically attached deposit of $[Os(bpy)_2$ 4bpt $Os(bpy)_2$ $Cl_2]$ $(PF_6)_2$ formed on a 25 µm radius platinum microelectrode The scan rate is 200 V s^{-1} Experimental voltammograms are denoted by the solid line The theoretical voltammogram obtained generated according to the Butler-Volmer formalism of electrode kinetics is denoted by •

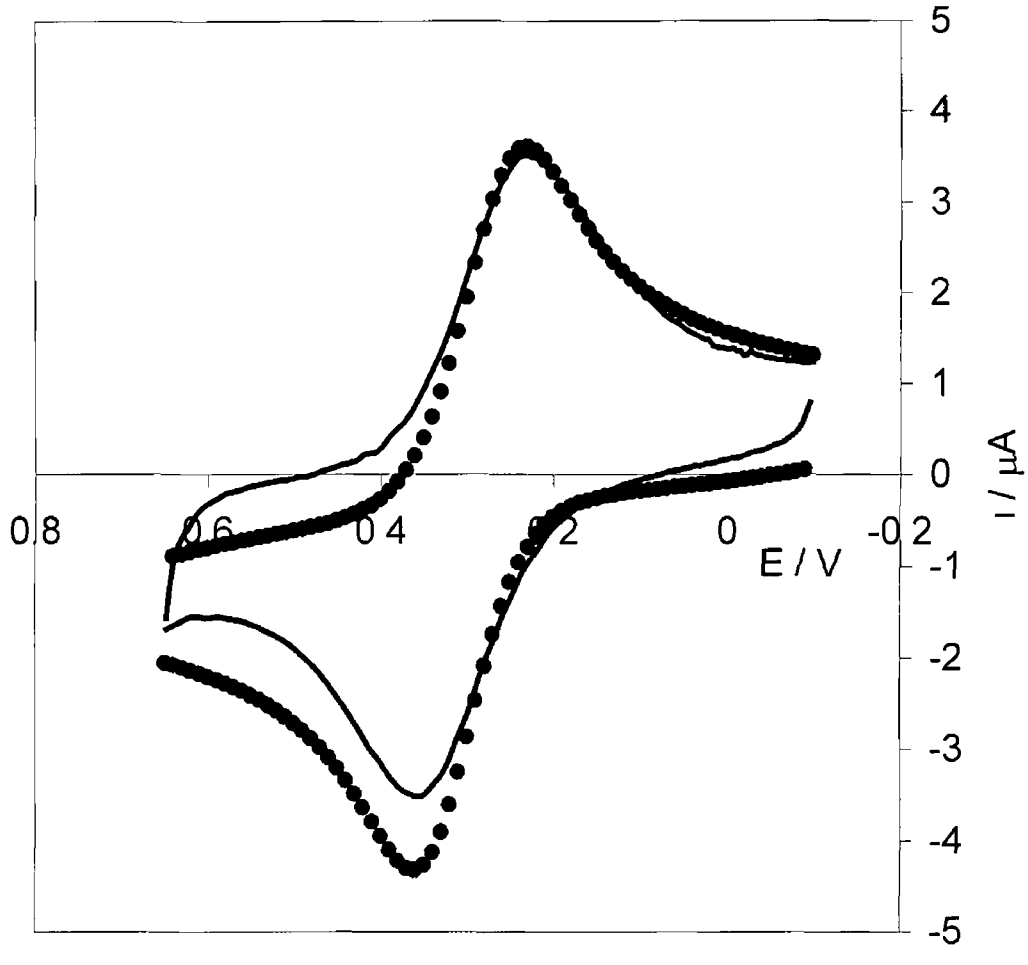

Figure 4 20 Cyclic voltammogram for a mechanically attached deposit of $[Os(bpy)_2$ 4bpt $Os(bpy)_2$ $Cl_2]$ $(PF_6)_2$ formed on a 25 μm radius platinum microelectrode The scan rate is 571 V s^{-1} Experimental voltammograms are denoted by the solid line The theoretical voltammogram obtained generated according to the Butler-Volmer formalism of electrode kinetics is denoted by •

4 5 *CONCLUSIONS*

Solid deposits of $[Os(bpy)_2$ 4-bpt $Os(bpy)_2$ $Cl_2]$ $(PF_6)_2$ have been formed on platinum microelectrodes, bpy is 2,2′-bipyridyl and bpt is 3,5-bis(pyridin-4-yl)-1,2,4,-triazole In both aqueous $LiClO_4$ and $HClO_4$ electrolytes containing 20% acetonitrile the voltammetric response arising from the $Os^{2+/3+}$ redox couple is close to ideal and is reminiscent of that associated with an electrochemically reversible solution phase redox couple Significantly, while both metal centres can be oxidised within an experimentally accessible potential window when the dimer is dissolved in acetonitrile, only a single one-electron transfer process is observed for the solid deposits This behaviour is most likely due to electrostatic interactions between adjacent Os metal centres caused by the close proximity of the metal centres within the solid film

The dependence of the apparent diffusion coefficient on the concentration of the supporting electrolyte suggests that the rate of charge transport through the solid is controlled by electron hopping rather than charge-compensating ion diffusion into the solid The rate of heterogeneous electron transfer across the electrode/deposit interface, k°, is $1\ 08\times10^{3}$ cms^{1} and is independent of the electrolyte pH This value is approximately one order of magnitude lower than that found for a similar monomeric complex in which the 4-bpt bridging ligand is attached directly to the electrode This suggests that the 4-bpt bridging ligand does not promote strong electronic communication between the localised electronic orbitals of the $[Os(bpy)_2Cl]^+$ moiety and the delocalised electronic orbitals of a metal electrode

4 6 REFERENCES

1 Scholz, F , Nitschke, L , Henrion, G , *Electroanalysis*, **1990**, *2*, 85

2 Scholz, F , Lange, B , *Trends Research Anal Chem* , **1992**, *11*, 359

3 Yang, C , He, G , Wang, R , Li, Y , *J Electroanal Chem* , **1999**, *471*, 32

4 Wrighton, M S , *Science*, **1986**, 231, 32

5 Chidsey, C E D , Murray, R W , *Science*, **1986**, 231, 25

6 Nazar, L F , Goward, G , Leroux, M , Duncan, H , Kerr, T , Gaubicher, J , *Internat J Inorg Mat* , **2001**, *3*, 191

7 MacLachlan, M J , Asefa, T , Ozin, G A , *Chem Eur J* , **2000**, 6, 2507

8 Wrighton, M S , *Science*, **1986**, *231*, 32

9 Chidsey, C E D , Murray, R W , *Science*, **1986**, *231*, 25

10 Tredicucci, A , Gmachi, C Capasso, F Sivco D L Hutchinson, A L Cho, A Y , *Nature*, **1998**, *396*, 350

11 Quaranta, F , Rella, R , Siciliano, P , Capone, S , Epifani, M , Vasanelli, L , Licciulli, A , Zocco, A , *Sensors and Actuators B*, **1999**, 350

12 Ni, J , Ju, H , Chen, H , Leech, D , *Anal Chim, Acta* , **1999**, *378*, 151

13 Forster, R J , Keyes, T E , *Phys Chem Chem Phys* , **2001**, *3*, 1336

14 Keane, L , Hogan, C , Forster, R J , *Langmuir*, , **2002**, *18*, 4826

15 Forster, R J , Keyes, T E , Vos, J, G , *Analyst*, **1998**, *123*, 1905

16 Forster, R J , Keyes, T E , Bond, A M , *J Phys Chem B*, **2000**, *104*, 6389

17 Goldsby, K A , Meyer, T J , *Inorg Chem* , **1984**, 23, 3002

18 Balzani, V , Juris, A , Venturi, M , *Chem Rev* , **1996**, *96*, 759

19 Gray, H B , Winkler J R *Ann Rev Biochem* **1996**, *65*, 537

20 Bard, A J , Faulkner, L R Electrochemical Methods Fundamentals and Applications, Wiley, New York, 1980

21 Wightman, R M , Wipf, D O *Electroanalytical Chemistry*, vol 15, Bard, A J Ed , Marcel Dekker, New York, 1989

22 Juris, F , Balzani, V , Barigelletti, F , Campagna, S , Belser, P, von Zelewsky, A , *Coord Chem Rev* **1988**, 82, 85

23 Ferguson, J E , Love, J L , Robinson, W T , *Inorg Chem* , **1972**, *11*, 1662

24 Rillema, D P , Jones, D S , Levy, H A , *J Chem Soc , Chem Comm* , **1979**, 849

25 Chan, M S , Wahl, A C , *J Phys Chem* , **1978**, 82, 2542

26 Charych, D H , Majda, M , *Thin Solid Films*, **1992**, 210, 348

27 Charych, D H , Anvar, D J , Madja, M , *Thin Solid Films*, **1994**, 242, 1

28 Lee, W -Y, Majda, M , Brezesinski, G , Wittek, M, Mobius, D , *J Phys Chem B* , **1999**, 103, 6950

29 Garay, F , Solis, V , Lovire, M *J Electroanal Chem* **1999**, *478*, 17

CHAPTER 5

ELECTRON TRANSFER DYNAMICS ACROSS OSMIUM BIS-BIPYRIDYL TRIAZOLE MONOLAYER/PLATINUM INTERFACES

5 1 INTRODUCTION

The study of electron donor-acceptor systems, in which electron transfer occurs across molecular bridges, has wide-ranging implications, from the development of molecular electronics to elucidating biological transfer mechanisms [1,2,3] The structure of the bridging ligand between donor and acceptor moieties can drastically affect the rate of electron transfer For example, the effects of synthetically altering the bridge structure on the rate of bridge mediated electron transfer have been investigated (Section 1 4 4) [4,5] However, an important goal is to develop systems in which the bridge structure can be reversibly altered by a change in the local environment, so as to modulate the rate of electron transfer These systems can provide an insight into the role of bridge electronic levels in mediated electron transfer reactions

In Chapter 3, a novel system whereby $[Os(bpy)_2 Cl]^+$ is tethered to an electrode surface via a redox-active ligand, that is capable of undergoing a reversible protonation reaction, was described Redox switching of the remote redox centres occurs by virtual coupling, i e , superexchange, between the metal orbitals and the localised orbitals of the redox centre By protonating the bridging ligand, it was shown that the bridge energy levels could be tuned reversibly, leading to reversible modulation of the heterogeneous electron transfer rate

In this chapter, the effects of bridge protonation on the dynamics of electron transfer are studied further An approach to chemically modulating the rate of heterogeneous electron transfer across an electrode/monolayer interface is described The bridge between the $[Os(bpy)_2 Cl]^+$ moiety and the electrode surface is 3,5-bis(pyridin-4-yl)-1,2,4-triazole (4-bpt) Monolayers of this complex are highly stable in a wide range of electrolytes and at both high and low pH The 4-bpt bridge is electroactive and is also capable of undergoing a protonation/deprotonation reaction depending on the pH of the contacting electrolyte solution The electrochemical response of these monolayer films are

unusally ideal under a wide range of conditions, providing an insight into the microenvironment of the redox centres within the monolayer The effects of protonating the bridging ligand on the dynamics of heterogeneous electron transfer between the metal electrode surface and the remote redox centre have been studied using high speed chronoamperometry The nearly ideal response of these monolayers at short experimental timescales has allowed direct examination of the apparent rates of electron transfer over a wide range of overpotentials

5 2 MATERIALS AND REAGENTS

[$Os(bpy)_2$ 4-bpt Cl] ClO_4 was prepared as described in Chapter 2 All other reagents used were of analytical grade

5 3 APPARATUS AND PROCEDURES

Microelectrodes were constructed and characterised as described in Chapter 2

Cyclic voltammetry was performed using a CH Instruments Model 660 Electrochemical Workstation and a conventional three electrode cell All solutions were degassed thoroughly using nitrogen, and a blanket of nitrogen was maintained over the solution during all experiments Potentials are quoted with respect to a BAS Ag/AgCl gel-filled reference electrode All experiments were performed at room temperature (22±3°C) Small-timescale chronoamperometry was conducted using a custom-built function generator, with a rise time of less than 10 ns Using this instrument, potential steps of varying pulse width and amplitude were applied to a two-electrode cell A square platinum flag (1 cm width) and an Ag/AgCl reference electrode were combined to form a counter electrode The purpose of the Pt flag was to lower the resistance and to provide a high frequency path

Spontaneously adsorbed monolayers were formed by immersing the microelectrodes in micromolar solutions of the metal complex in methanol/water (50/50, v/v) for periods up to 12 hours The complex is stable towards aerial oxidation and no precautions were taken to exclude atmospheric oxygen during monolayer formation Before electrochemical measurements were made, the electrodes were rinsed with acetone and electrolyte solution to remove any unbound material Subsequent measurements were performed in blank electrolyte

Raman spectroscopy was conducted on a Dilor Jobiny-von Spex Labram The exciting 20 mW helium-neon laser (632 8 nm) was focused through a purpose made electrochemical cell onto a monolayer deposited on a gold macroelectrode (1 5 mm radius) using a 10× objective lens The beam diameter when focused is approximately 1 μm producing approximately 10^6 Wcm ^{2} at the surface Focusing was confirmed by using a CCD camera in imaging mode A spectral resolution of 1 5 cm ^{1} per pixel was achieved using a grating of 1800 lines/mm The applied potential was controlled with respect to an Ag/AgCl reference electrode using a CH instruments model 660A potentiostat

5 4 RESULTS AND DISCUSSION

5 4 1 GENERAL ELECTROCHEMICAL PROPERTIES

Figure 5 1 shows a representative cyclic voltammogram for a spontaneously adsorbed monolayer of $[Os(bpy)_2\ 4bpt\ Cl]^+$ upon electrochemical cycling in aqueous 0 1 M $LiClO_4$ The solution does not contain any dissolved complex The formal potential of the $Os^{2+/3+}$ redox reaction is 0 276±0 005 V vs Ag/AgCl The formal potential of the complex, when dissolved in acetonitrile solution, is 0 249±0 004 V That the solution phase formal potential of this complex is within 30 mV of that observed for the surface confined complex suggests that these monolayers are solvated [6] Upon repetitive cycling in this electrolyte at both high (pH 14) and low (pH 0) pH over periods up to 12 hours, the peak heights change by less than 5%, indicating that these films are highly stable over a wide range of pH values

The response obtained for these films is similar to that previously reported for structurally similar complexes[7] and is consistent with that expected for an electrochemically reversible reaction involving a surface-confined species [8] The peak shape is independent of υ for $0\ 05 \leq \upsilon \leq 50\ Vs^{-1}$ and the peak height increases linearly with increasing scan rate (Figures 5 2 and 5 3), rather than the $\upsilon^{1/2}$ dependence observed for the complex dissolved in dimethyl formamide Therefore, it appears that $[Os(bpy)_2$ 4-bpt $Cl]^+$ adsorbs to the surface of the platinum electrode to give an electroactive film

Monolayers of this complex exhibit non-zero ΔE_p values even at low scan rates, e g , ΔE_p is 35 ± 5 mV at a scan rate of 0 5 Vs^{-1} This behaviour has been reported previously for monolayers of analogous osmium polypyridyl complexes [9 10] ΔE_p is independent of scan rate up to at least 50 Vs^{-1}, indicating that slow heterogenous kinetics are not responsible for the observed behaviour Ohmic effects are not responsible for this behaviour as the increased currents at higher

scan rates would cause the ΔE_p value to increase Feldberg has interpreted similar non-ideal responses in terms of unusual quasi-reversibility (UQR), arising due to rate processes which are slow compared to the experimental timescale [11]

Where there are no lateral interactions occurring between immobilised species and a rapid equilibrium is established with the metal electrode, the full width at half-maximum (fwhm) of either the anodic or cathodic wave is given by 90 6 / n mV according to the following equation, where n is the number of electrons transferred

$$\Delta E_p = 3\ 53\frac{RT}{nF} = \frac{90\ 6}{n}\text{mV} \qquad (25°C) \qquad (5\ 1)$$

Monolayers of this type exhibit fwhm values of 120 ± 10 mV, indicating that there may be repulsive interactions between adjacent adsorbates These are examined in more detail in a later section

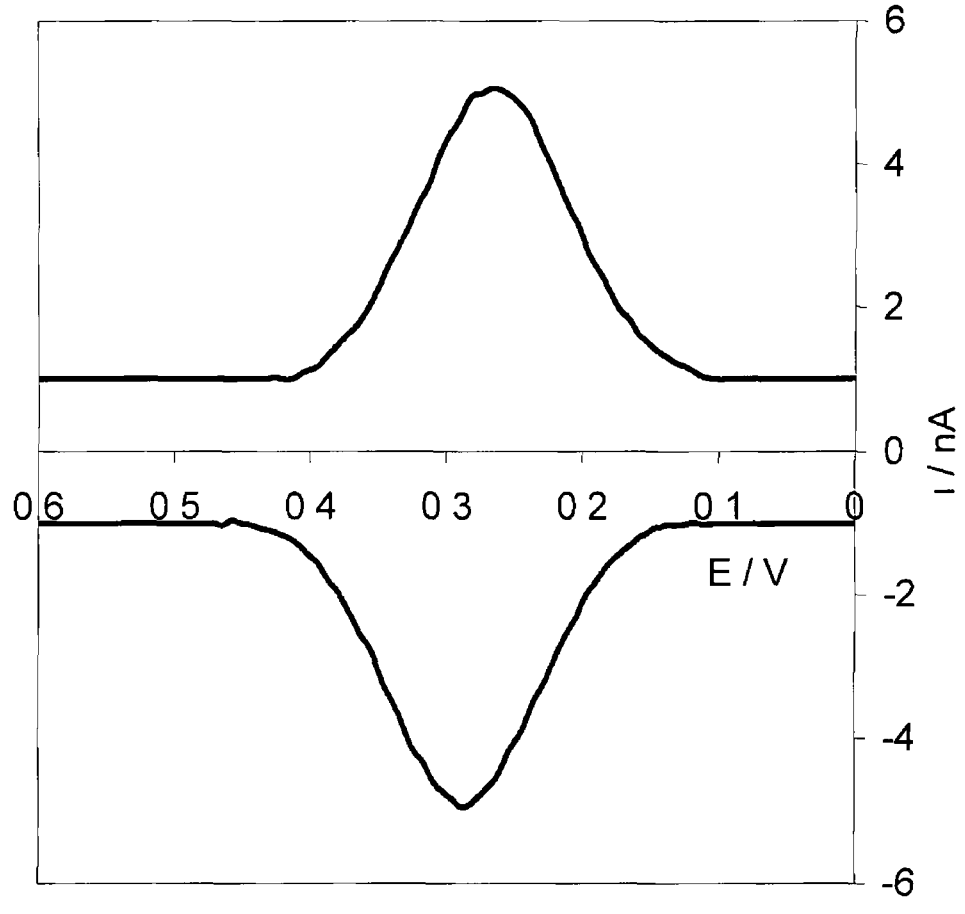

Figure 5 1 Representative cyclic voltammogram obtained for a spontaneously adsorbed monolayer of $[Os(bpy)_2$ 4-bpt $Cl]^+$ at a platinum microelectrode The radius of the microelectrode is 25 μm The scan rate is 2 0 Vs^{-1} and the supporting electrolyte is aqueous 0 1 M $LiClO_4$ Cathodic currents are up and anodic currents are down The potential limits are 0 to 0 6 V vs Ag/AgCl and the initial potential is 0 V

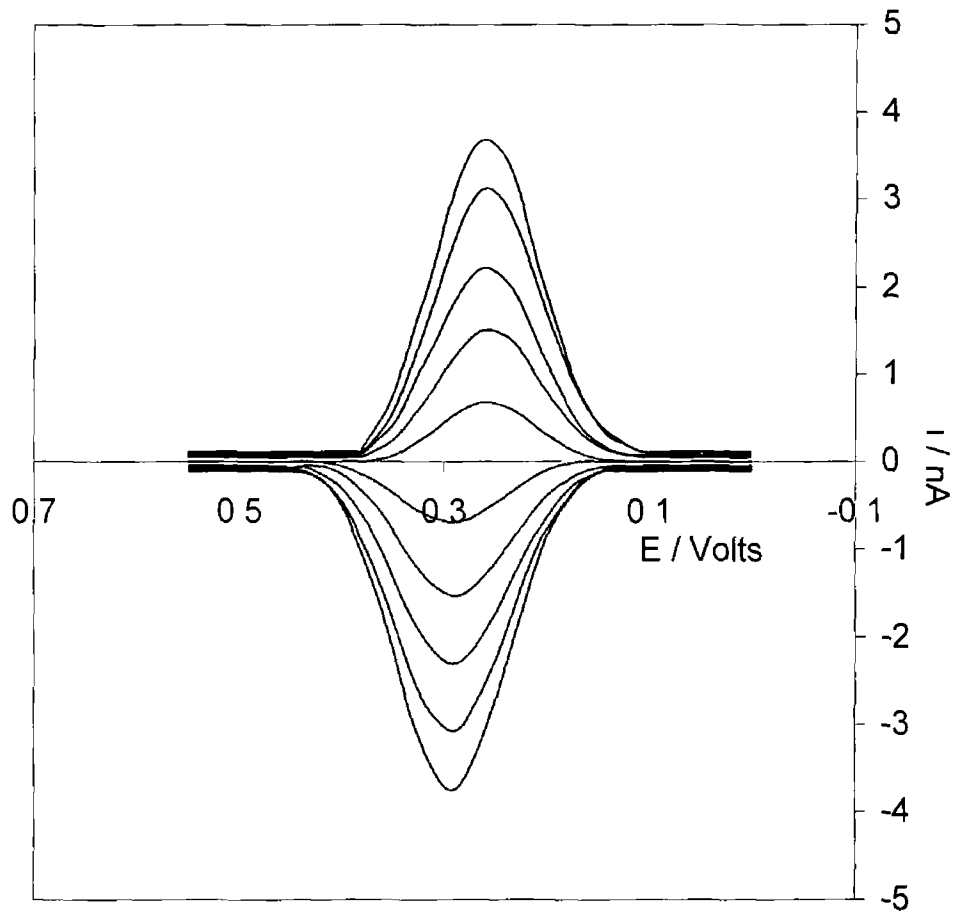

Figure 5 2 Dependence of the cyclic voltammetry of a dense, spontaneously adsorbed monolayer of $[Os(bpy)_2\ 4bpt\ Cl]^+$ on the scan rate All voltammograms are background corrected for charging current Scan rates are (from top to bottom) 2 0, 1 6, 1 2, 0 8 and 0 4 V s^{-1} The radius of the platinum microelectrode is 25 μm The supporting electrolyte is aqueous 0 1 M $LiClO_4$ Cathodic currents are up and anodic currents are down

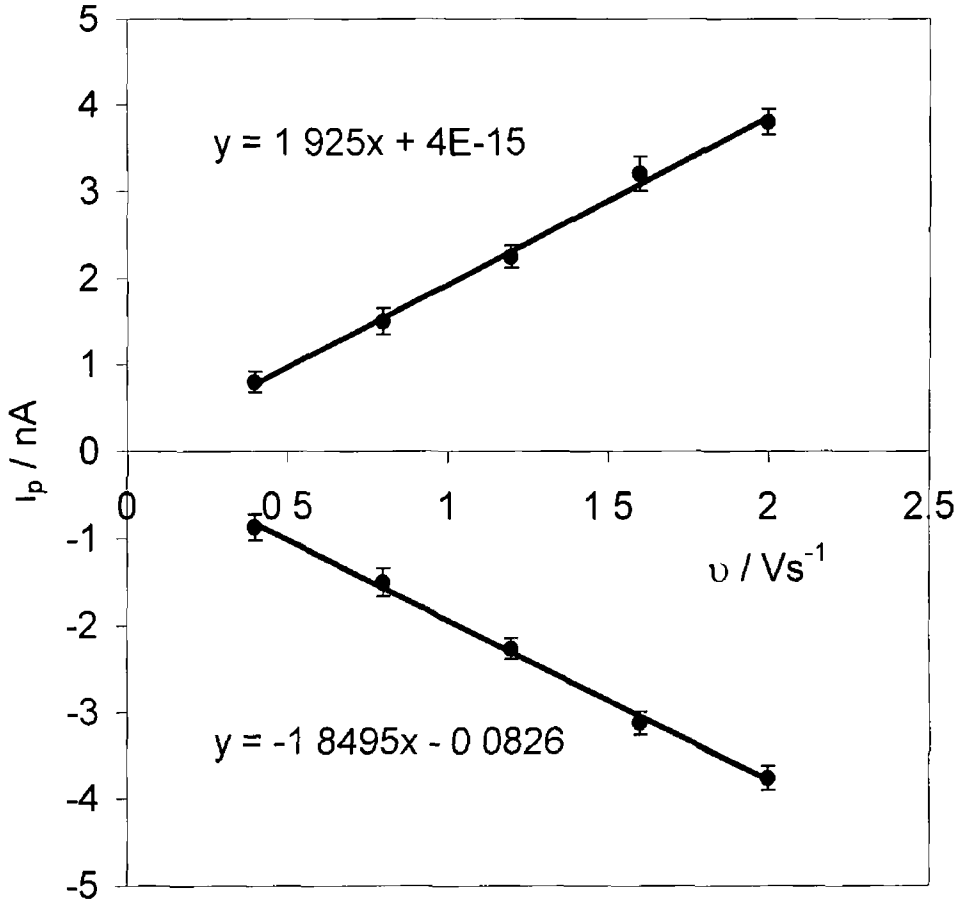

Figure 5 3 Scan rate dependence of the voltammetric peak current for monolayers of $[Os(bpy)_2$ 4-bpt Cl$]PF_6$ at a 25 μm radius platinum microelectrode The surface coverage is 1 1 × 10^{-10} mol cm^{-2} and the supporting electrolyte is aqueous 1 0 M $LiClO_4$

The total charge introduced or withdrawn to reduce or oxidise the monolayer, Q, can be found from the area under the voltammetric peak after correcting for the background charging current This charge, together with the real surface area can then be used to calculate the surface coverage, Γ, or the number of moles of $[Os(bpy)_2\ 4bpt\ Cl]^+$ per cm^2 according to Equation 5 2

$$\Gamma = \frac{Q}{nFA} \qquad (5\ 2)$$

The surface coverage provides important information about the packing density of the monolayer The surface coverage, as experimentally determined from the area under the cyclic voltammetry wave, was found to be $1\ 10\pm0\ 09 \times 10^{-10}$ mol cm^{-2}, corresponding to an area occupied per molecule of 151±11 $Å^2$ This area is in agreement with that previously reported for this complex[12] and is consistent with the surface coverage being dictated by the redox active head group rather than by the bridging ligand This area of occupation is comparable to that reported for similar complexes adsorbed within monolayers [13 14] In the following section, the dependence of Γ on the concentration of $[Os(bpy)_2$ 4-bpt $Cl]^+$ in the deposition solution is probed This may provide an insight into the nature of the lateral interactions between adjacent adsorbates evident in the voltammetric behaviour of this complex

5 4 2 ADSORPTION ISOTHERMS

The larger than ideal fwhm values determined for these monolayers (120 ± 10 mV) indicates that there may be some repulsive interactions between adjacent adsorbates within the monolayers of this complex By examining the surface coverage as a function of the concentration of the deposition solution, it is possible to obtain some insight into the extent of these interactions To obtain the adsorption isotherm, the surface coverages at equilibrium were determined by integrating the background corrected cyclic voltammograms as the bulk concentration in the deposition solution was systematically varied Figure 5 4 illustrates the dependence of the surface coverage of $[Os(bpy)_2$ 4-bpt $Cl]^+$ on the concentration of the complex in the deposition solution The surface coverage reaches a plateau at a solution concentration of approximately 2 μM

The Frumkin adsorption isotherm can provide a useful insight into the lateral interactions that may exist within these monolayers since it models the free energy of adsorption as an exponential function of the surface coverage [15]

$$\beta C_i = \frac{\theta_i}{1-\theta_i} \exp(g\theta_i) \qquad (5\ 3)$$

where $\theta_i = \Gamma_i / \Gamma_{sat}$, Γ_i is the coverage of $[Os(bpy)_2$ 4-bpt $Cl]^+$ in mol cm^{-2} at a bulk concentration C_i, Γ_{sat} is the saturation coverage obtained at high bulk concentrations and β is the adsorption coefficient Attractive interactions are indicated by $g<0$ and repulsive interactions by $g>0$, while for $g=0$ the Langmuir isotherm is obtained

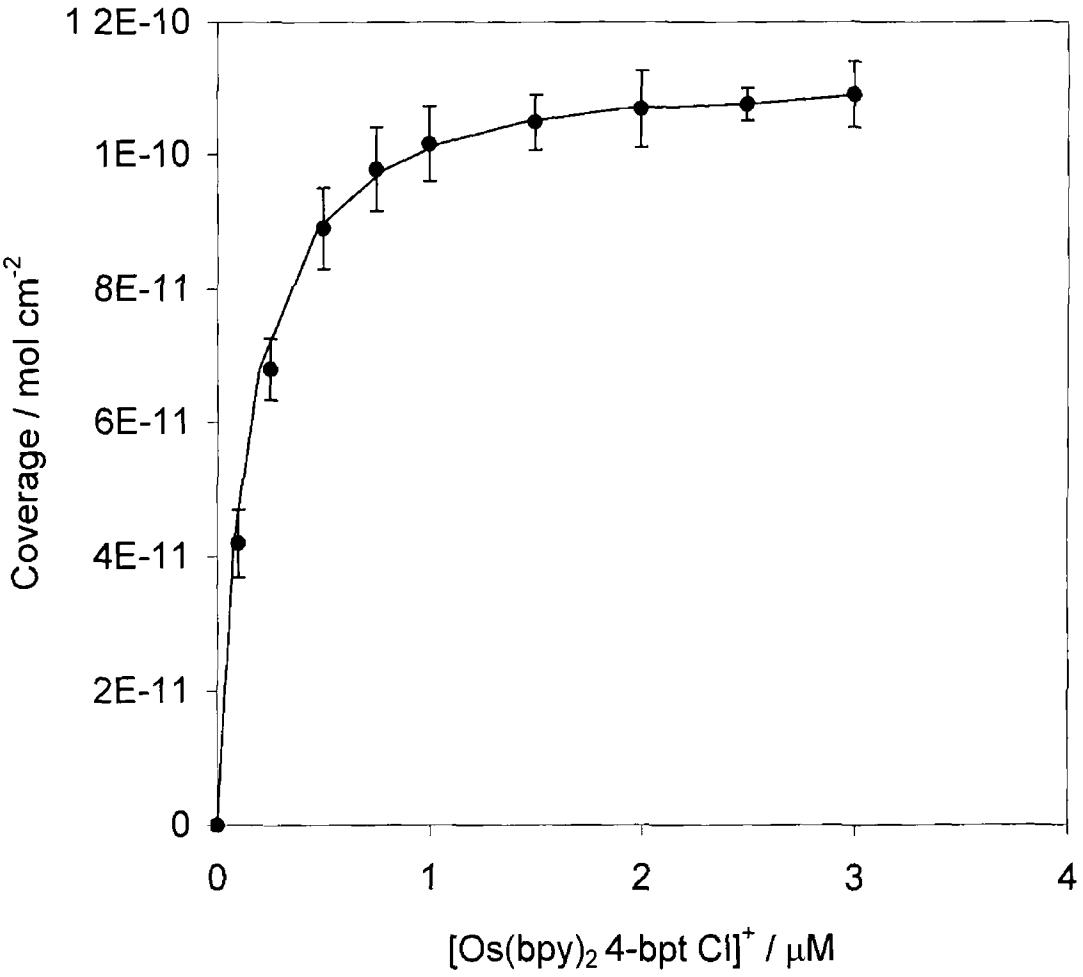

Figure 5 4 Dependence of the voltammetrically determined surface coverage of $[Os(bpy)_2\ 4\text{-bpt Cl}]^+$ as a function of deposition solution concentration The solid line represents the best fit to the Frumkin isotherm

Figure 5 4 shows that the optimized Frumkin isotherm provides a satisfactory fit to the experimental surface coverages for these monolayers The interaction parameter is +0 057 ± 0 01 This positive interaction parameters indicates that destabilizing lateral interactions do exist within these monolayers While these measurements do not provide any insight into the nature of these interactions, they are likely to be electrostatic in nature due to the presence of the charged $[Os(bpy)_2 Cl]^+$ head group

5 4 3 EFFECT OF ELECTROLYTE CONCENTRATION ON THE FORMAL REDOX POTENTIAL

The formal potential depends on both the solvation shell and the extent of ion-pairing [16 17] By examining the effect of the electrolyte concentration on the formal potential of the redox reaction, it is possible to gain an insight into the extent of ion-pairing between the immobilised redox centres and counterions from the electrolyte The effect of electrolyte concentration on the formal potential of the $Os^{2+/3+}$ redox reaction has been examined for $0\ 1 \leq [LiClO_4] \leq 1\ 0$ M At high scan rates, the rate of heterogeneous electron transfer across the monolayer/electrode interface can influence the voltammetric response Therefore, in these measurements, scan rates less than 0 5 Vs^{-1} were employed so as to avoid any influence from the interfacial electron transfer kinetics

To avoid complications due to changes in the ionic strength of the solution a fixed background of 1 0 M Na_2SO_4 was used as a swamping electrolyte The formal potential of the $Os^{2+/3+}$ redox reaction shifts by less than 10 mV over the electrolyte concentration range $0\ 1 \leq [Na_2SO_4] \leq 1\ 0$ M indicating that SO_4^{2-} has little tendency to ion-pair with the osmium centers

For $0\ 1 \leq [LiClO_4] \leq 1\ 0$ M, the peak shapes and heights are independent of the electrolyte concentration However, as illustrated in Figure 5 5, $E^{\circ\prime}$ shifts in a negative potential direction as the $LiClO_4$ concentration increases indicating that it becomes increasingly easier to oxidize the osmium redox center at higher electrolyte concentrations This behavior is consistent with ion-pairing between the perchlorate and the redox center The theoretical slope of this semi-log plot is (59/p) mV/decade, where p is the difference in the number of anions pairing with the oxidized and reduced forms of the redox center This behaviour can be described by Equation 5 5

$$[Os(bpy)_2\ 4bpt\ Cl]^{+}\left(ClO_4^{-}\right)_{\zeta} - e^{-} + p\left(ClO_4^{-}\right)$$

$$\downarrow \qquad (5\ 5)$$

$$[Os(bpy)_2\ 4bptCl]^{2+}\left(ClO_4^{-}\right)_{\zeta+P}$$

The slope determined for $[Os(bpy)_2\ 4bpt\ Cl]^{+}$ monolayers was 60±3 mV (Figure 5 6) indicating that a single additional anion becomes bound to the redox center in the oxidized state

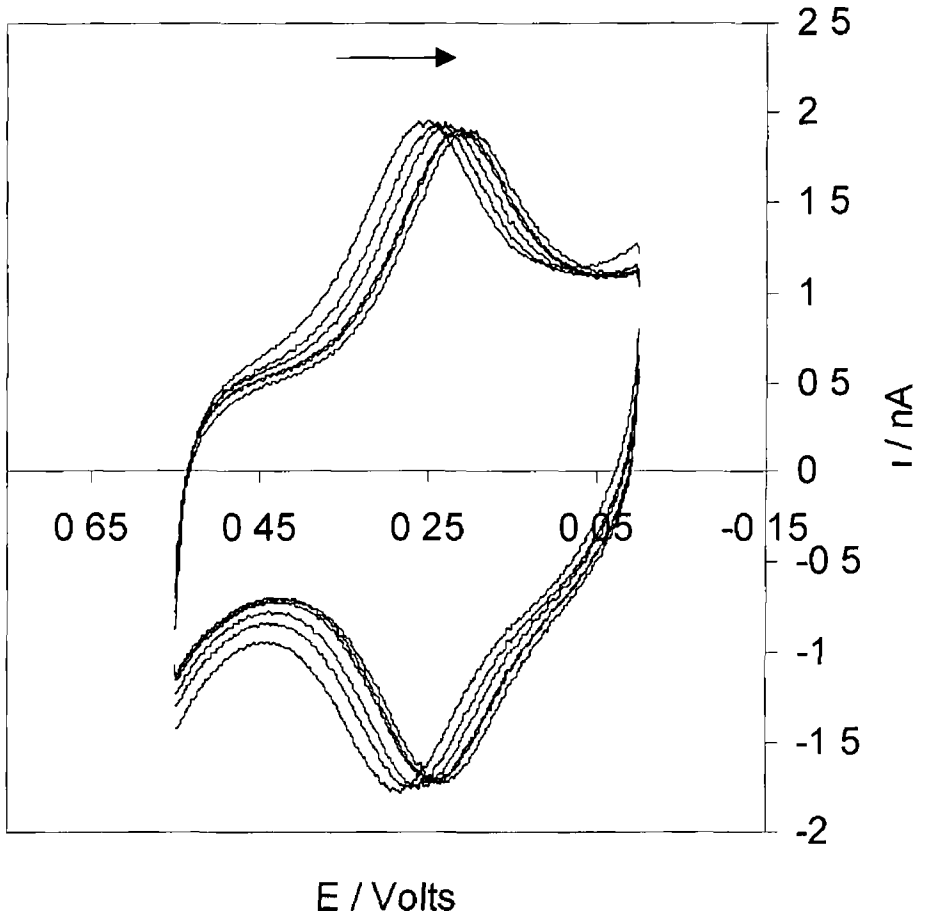

Figure 5 5 Effect of electrolyte concentration on the voltammetric response of an $[Os(bpy)_2\ 4bpt\ Cl]^+$ monolayer adsorbed on a 25 μm radius platinum microelectrode The scan rate is 0 5 V s^{-1} $LiClO_4$ concentrations are (from left to right) 0 1, 0 2, 0 4, 0 6, 0 8 and 1 0 M All measurements were performed in a constant-background electrolyte of 1 0 M Na_2SO_4

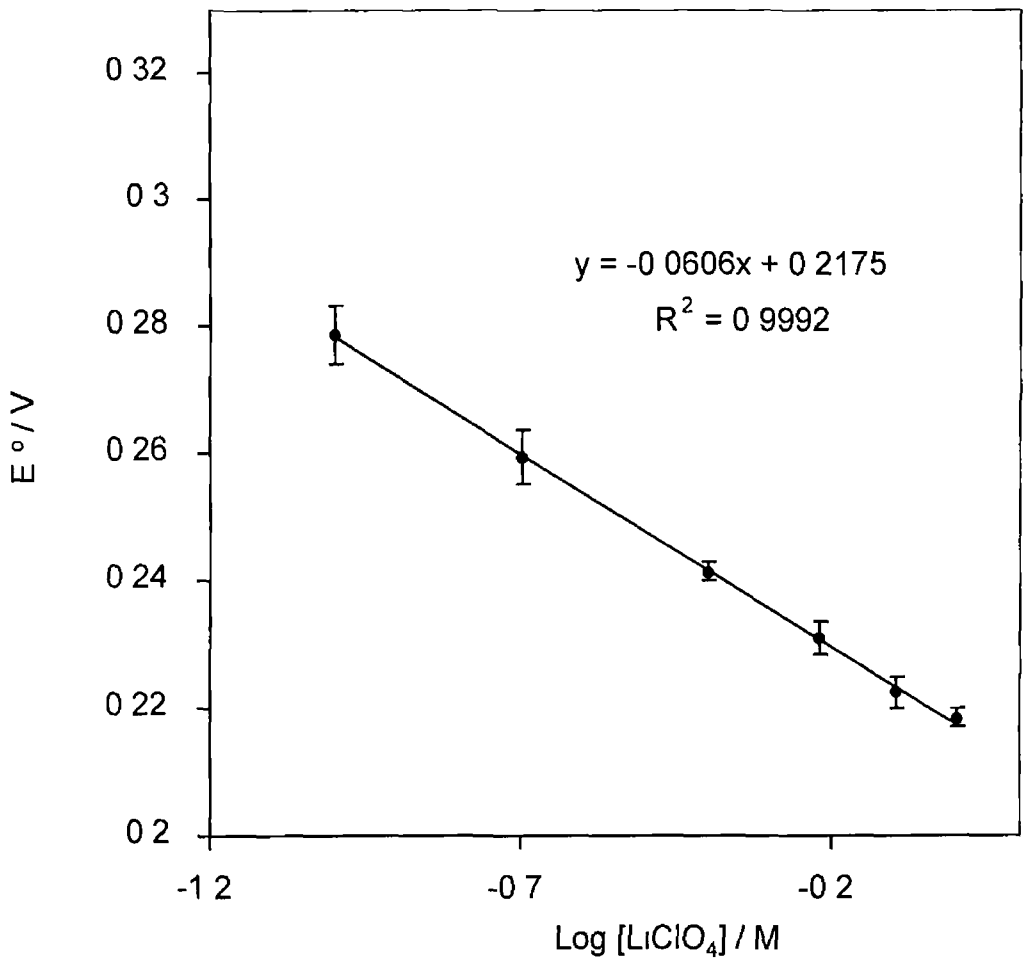

Figure 5 6 Effect of electrolyte concentration on the formal potential of the $Os^{2+/3+}$ redox reaction for monolayers of $[Os(bpy)_2\ 4\text{-bptCl}]^+$ adsorbed at a 25 μm platinum radius microelectrode All measurements were performed in a constant background electrolyte of 1 0 M Na_2SO_4

5 4 4 EFFECT OF pH ON THE REDOX FORMAL POTENTIAL

The 4-bpt bridging ligand is capable of undergoing a protonation/deprotonation reaction depending on the pH of the contacting solution The solution phase pK_a of $[Os(bpy)_2$ 4-bpt Cl$](PF_6)$ has been determined as 9 6±0 2 (Chapter 2) Protonation of the 4-bpt bridge within a monolayer may affect the extent of electronic coupling between the electrode surface and the remote $[Os(bpy)_2Cl]^+$ redox centre By probing the effect of the contacting electrolyte solution on the voltammetric response of these monolayers, an insight into the effect of protonation of the 4-bpt bridge may be obtained

The effect of altering the pH of the contacting electrolyte solution on the voltammetric response of a monolayer of $[Os(bpy)_2$ 4-bpt $Cl]^+$ is shown in Figure 5 7 The formal potential of the $Os^{2+/3+}$ redox reaction shifts by 40±3 mV in a positive direction upon changing the pH of the contacting electrolyte solution from pH 12 0 to 6 0 The change in $E^{o'}$ upon altering the pH of the electrolyte solution was confirmed to be reversible by first decreasing and then increasing the pH of the electrolyte The positive shift of $E^{o'}$ with decreasing pH indicates that oxidation of the Os^{2+} metal centre becomes thermodynamically more difficult when the 4-bpt bridge is protonated This may be due to a reduced electron donating ability of the ligand upon protonation By reducing the electron donating ability of the ligand, the electron density at the Os^{2+} metal centre is reduced, causing a positive shift in $E^{o'}$ Protonation of the 4-bpt ligand causes an increase in the overall charge on the complex This may also lead to a positive shift in $E^{o'}$ as it becomes more difficult to create the Os^{3+} species due to electrostatic effects

These data do not provide an insight into the pK_a of the 4-bpt ligand when immobilised at the electrode surface The pK_a of the ligand may be altered upon immobilisation at an electrode surface for a number of reasons First, the dielectric constant within a dense monolayer may be distinctly different from that

in bulk solution Second, immobilisation of the complex at an electrode surface may significantly alter the electron density of the ligand Both of these effects could cause significant changes in the pK_a to be observed Capacitance data can provide a useful insight into this issue

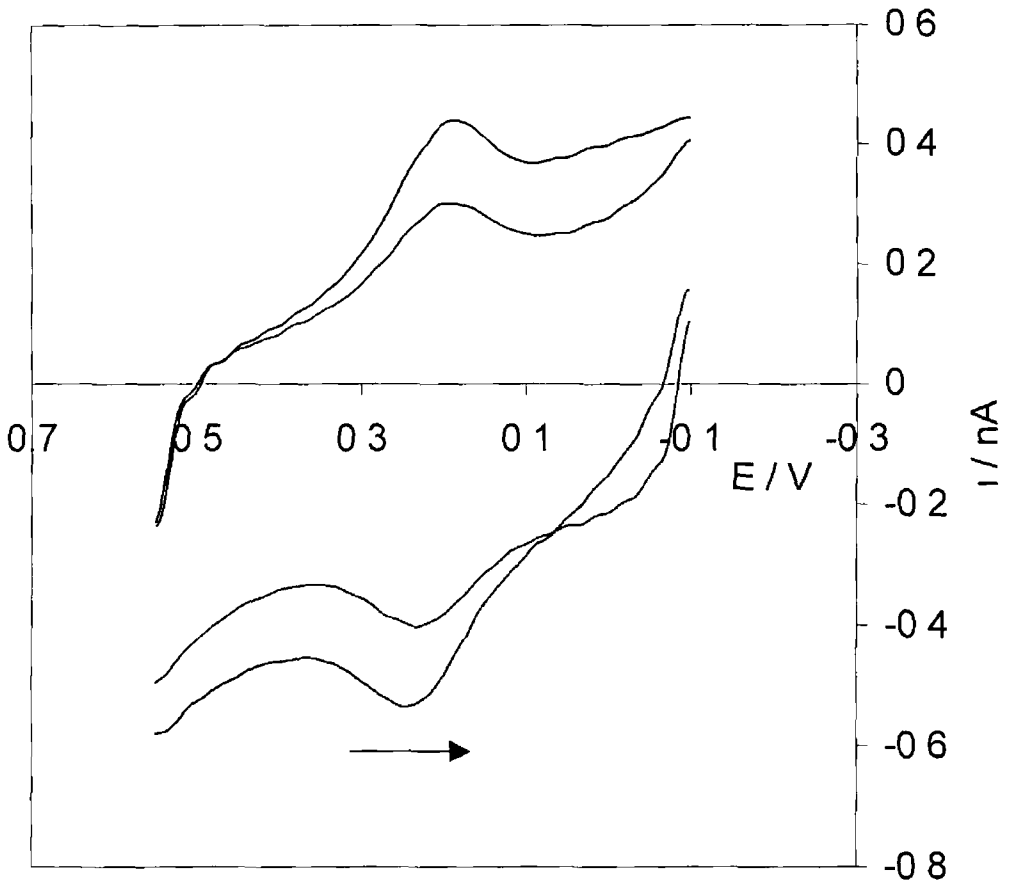

Figure 5 7 Effect of pH on the voltammetric response of a monolayer of $[Os(bpy)_2$ 4-bpt $Cl]^+$ adsorbed at a 12 5 μm radius platinum microelectrode The scan rate is 0 2 Vs^{-1} and the supporting electrolyte is aqueous 1 0 M $LiClO_4$ The pH of each solution is (from left to right) 6 6 and 12 0 The pH of the electrolyte solution was adjusted using concentrated aqueous NaOH Cathodic currents are up and anodic currents are down

5 4 5 INTERFACIAL CAPACITANCE

The two limiting cases for the potential profile across a monolayer have been described in Section 3 4 4 [18] If the monolayer is highly impermeable and has a low dielectric constant, the potential may decay linearly across the monolayer and then exponentially in the external electrolyte solution In this case, the capacitance of the diffuse layer, C_{dif}, and the monolayer capacitance, C_{mono}, contribute to the total interfacial capacitance according to Equation 5 6

$$C_T^{-1} = C_{dif}^{-1} + C_{mono}^{-1} \quad (5\ 6)$$

The capacitance of the monolyer is given by Equation 5 7

$$C_{mono} = \varepsilon_o \varepsilon_{mono}/d \quad (5\ 7)$$

where ε_o is the permittivity of free space, ε_{mono} is the monolayer dielectric constant and d is the monolayer thickness

Potential step chronoamperometry has been used to determine the interfacial capacitance as a function of the concentration of electrolyte This technique was chosen due to the ease of implementation and the ability to time resolve double layer charging and Faradaic currents As described in Section 1 3 4 2 2, after a potential step, charging current, i_c, will flow according to Equation 5 8 [19]

$$i_c(t) = \frac{\Delta E}{R} \exp\left(\frac{-t}{RC}\right) \quad (5\ 8)$$

where ΔE is the magnitude of the potential step, R is the cell resistance and C is the total interfacial capacitance A plot of ln $i_c(t)$ versus t was used to obtain R and C Figure 5 8 illustrates the interfacial capacitance values determined for a

12 5 μm radius platinum microelectrode modified with a monolayer of $[Os(bpy)_2$ 4-bpt $Cl]^+$ as a function of the concentration of electrolyte

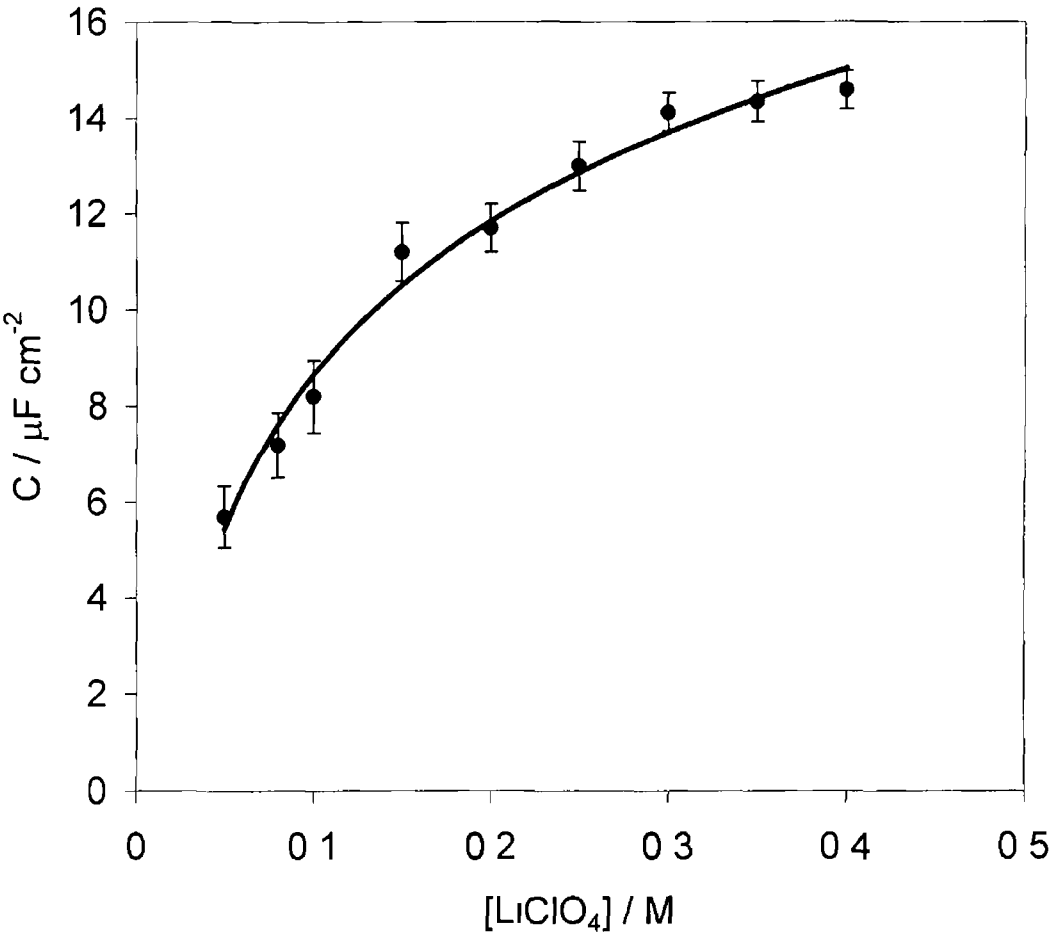

Figure 5 8 Dependence of the total interfacial capacitance on $LiClO_4$ concentration for spontaneously adsorbed monolayers of $[Os(bpy)_2$ 4-bpt $Cl]^+$ on a 12 5 μm radius platinum microelectrode The potential step size was 0 025 V and was from 0 400 to 0 425 V

Equation 5 6 indicates that the total interfacial capacitance depends on the diffuse layer capacitance and the capacitance of the monolayer Unlike the monolayer capacitance, the diffuse layer capacitance depends on the concentration of the electrolyte, as well as, the potential Figure 5 8 clearly illustrates that the total interfacial capacitance is sensitive to the electrolyte concentration, as the capacitance increases up to an electrolyte concentration of approximately 0 40 M The limiting capacitance is approximately 14 5 $\mu F\ cm^{-2}$, and at high concentrations of electrolyte is likely to be dominated by the monolayer capacitance Energy minimised molecular modelling indicates that the thickness of a fully extended monolayer is approximately 10 Å [12] Hence, the limiting capaitance can be used, in conjunction with Equation 5 7, yielding a monolayer dielectric constant of 16 This is far from the value for bulk water (78 5), suggesting the formation of a monolayer that is impermeable to solvent However, the limiting capacitance is significantly larger than that expected for a monolayer that is completely impermeable to electrolyte [20] Therefore, it appears that this monolayer is at least partially solvated at high electrolyte concentrations

The effects of monolayer protonation has been examined by Smith and White [21] In their model, the interfacial capacitance depends on the diffuse layer capacitance, the monolayer capacitance and the degree of protonation of the monolayer, C(f), according to Equation 5 9

$$C_T^{-1} = C_{mono}^{-1} + [C_{dif} + C(f)]^{-1} \qquad (5\ 9)$$

Assuming that C_{mono} remains constant, the term $[C_{dif} + C(f)]^{-1}$ varies with potential and with the solution pH As the pH of the contacting electrolyte solution is altered, C(f) reaches a local maximum near to the pK_a, and a maximum is observed in the total interfacial capacitance Figure 5 9 illustrates the effect of systematically varying the electrolyte pH on the differential capacitance between $6\ 0 \leq pH \leq 12\ 5$ All changes in the interfacial capacitance were confirmed to be reversible by first increasing and then decreasing the pH of the contacting

electrolyte solution The shape of the curve agrees with that predicted by theory and yields a surface pK_a of 7 0±0 2 Consistent with a monolayer that is only partially solvated, this value differs from that observed in bulk solution by greater than two pH units (solution phase pK_a = 9 1) Therefore, it appears that the 4-bpt bridge behaves as a stronger acid when immobilised within a monolayer film This is most likely due to the decreased dielectric constant within the monolayer than in bulk solution

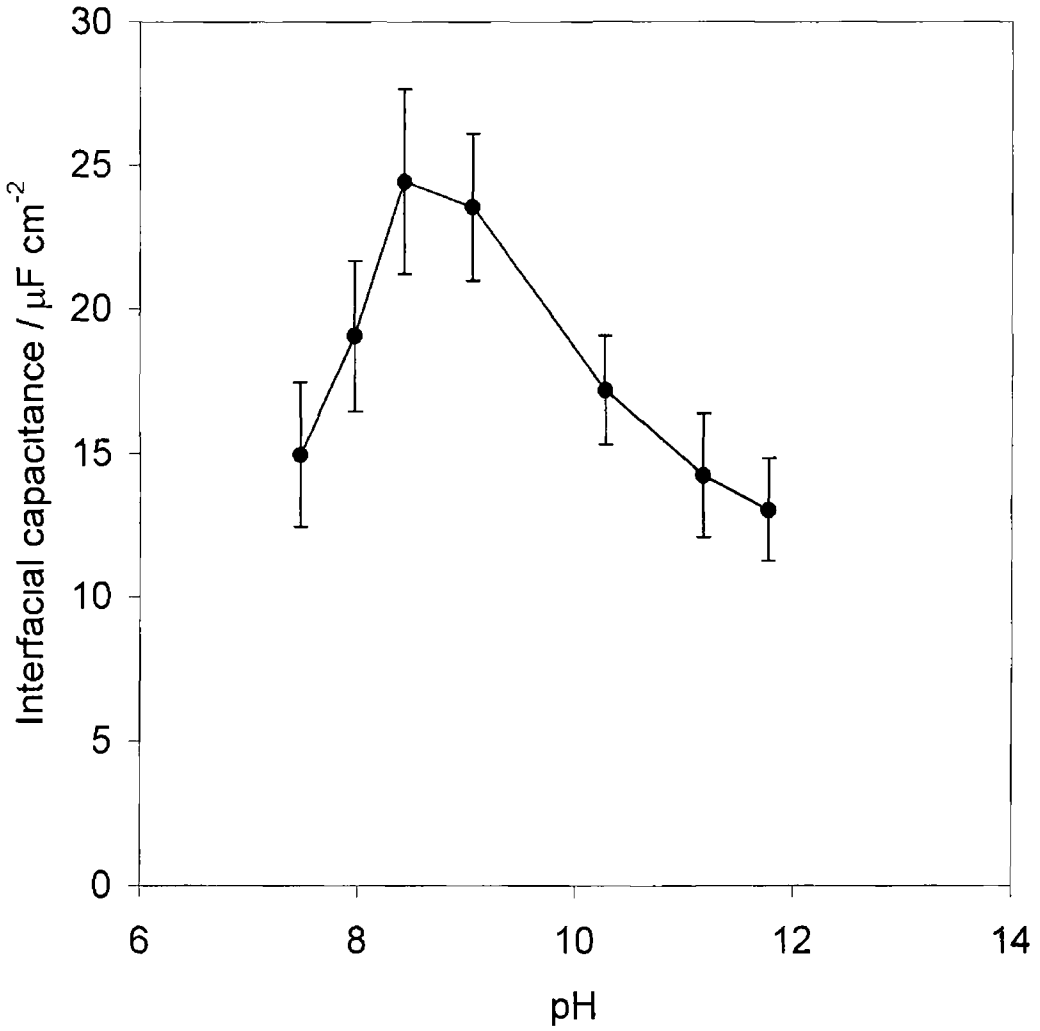

Figure 5 9 Effect of systematically varying the contacting electrolyte pH on the total differential capacitance of monolayers of $[Os(bpy)_2$ 4-bpt $Cl]^+$ at 12 5 μm platinum microelectrode The supporting electrolyte is aqueous 1 0 M $LiClO_4$ and the pH was altered using concentrated aqueous solutions of NaOH and $HClO_4$

5 4 6 POTENTIAL DEPENDENT RAMAN SPECTROSCOPY

Potential dependent raman spectroscopy can provide very useful information regarding the structural changes that may occur upon redox switching of monolayers of $[Os(bpy)_2$ 4-bpt Cl$]PF_6$ Surface enhanced raman spectroscopy (SERS) was employed to probe these monolayers, as this may provide information regarding the structure of the monolayer due to the enhanced sensitivity of the technique

Figure 5 10 illustrates the raman spectra obtained for monolayers of $[Os(bpy)_2$ 4-bpt Cl$]PF_6$ immobilised on a roughened gold electrode at 0 and 0 6 V vs Ag/AgCl, respectively In all experiments, the responses were completely reversible, i e any changes in the spectra were reversible upon redox switching of the monolayer The UV-visible spectrum of this complex indicates that the exciting HeNe laser (632 8 nm) is preresonant with the MLCT (Os(II)-bpy*) transition (Section 2 3 4 1) The resonance effect is confirmed by enhancement of features at 1607, 1565, 1491, 1320 and 1266 cm^{-1} [22] The feature at 1043 cm^{-1} is associated with the 4-bpt ligand The feature at 380 cm^{-1} is associated with the Os-N stretch [23] Oxidation of the monolayer results in a loss of the Os-N modes and the 4-bpt modes This occurs due to loss of the MLCT upon oxidation This loss is significant, however, the modes do exist after oxidation of the monolayer This is because upon oxidation, the laser becomes pre-resonant with a bpy*-Os LMCT transition and the bpy based bands continue to be observed This is similar to the behaviour observed for monolayers of $[Os(bpy)_2$ 4-tetCl$]^+$ (Section 3 4 6)

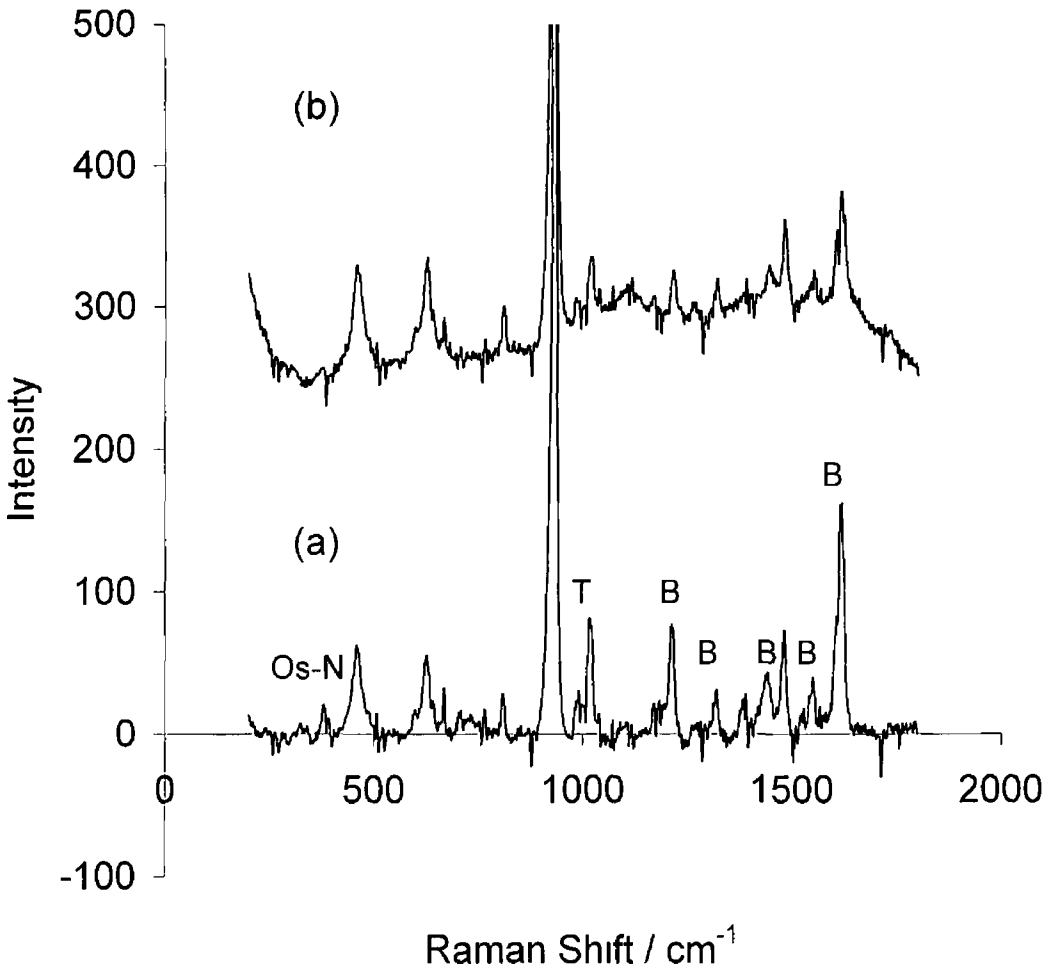

Figure 5 10 Potential controlled raman spectrum of a monolayer of $[Os(bpy)_2$ 4-bpt Cl$]PF_6$ at a roughened gold macroelectrode The supporting electrolyte is aqueous 1 0 M $LiClO_4$ (a) Potential is 0 0 V vs Ag/AgCl (b) Potential is 0 6 V vs Ag/AgCl The wavelength of the exciting He-Ne laser is 632 8 nm

5 4 7 HETEROGENEOUS ELECTRON TRANSFER DYNAMICS

Redox active bridging ligands are important in that they offer the possibility of significant virtual coupling (superexchange) depending on the difference between the redox potentials of the bridge and remote redox centers Electron transfer via resonant superexchange may be the dominant mechanism if the LUMO of the bridge is similar in energy to the acceptor states of the remote redox center This pathway predominates because the closeness of the bridge and redox center energies acts to reduce the activation barrier to electron tunneling In contrast, if the $Os_{d\pi}$-HOMO separation is relatively smaller, then HOMO mediated hole transfer will contribute significantly to the redox switching mechanism Electron rich π-donating linkers of the kind used here (4-bpt) have been shown to support hole superexchange reactions[24] and this has been supported by the data discussed in Section 3 4 6 for $[Os(bpy)_2$ 4-tet $Cl]^+$ monolayers

Significantly, the 4-bpt bridge is also capable of undergoing a protonation/deprotonation reaction, triggered by altering the pH of the contacting electrolyte solution The surface pK_a of the 4-bpt ligand has been determined by capacitance measurements and agrees relatively well with that determined for the complex dissolved in solution Therefore, the present system provides an attractive means to investigating the effect of protonation of the bridging ligand on the rate of heterogeneous electron transfer across the electrode/monolayer interface

In order to determine the rates of heterogeneous electron transfer across the electrode/monolayer using this system, high speed chronoamperometry has been employed Chronoamperometric measurements have three distinct advantages over cyclic voltammetric experiments for extracting kinetic data[25] First, the kinetics for different potentials (i e , different reaction free energies) are not convoluted by a potential scan Second, the kinetic homogeneity of the sites can

be judged by the functional form of the current transient Third, electron transfer rates can be measured far from $E^{o'}$, i e , at large reaction free energies

As described in Section 1 3 4 2 2, after a potential step, a charging current will flow at the working electrode according to [19]

$$i_C(t) = \frac{\Delta E}{R} \exp\left(\frac{-t}{RC}\right) \qquad (5\ 10)$$

where ΔE is the magnitude of the potential step, R is the cell resistance and C is the total interfacial capacitance For an ideal electrochemical reaction involving a surface confined species, the faradaic current, i_F, following a potential step that changes the redox composition of the monolayer exhibits a single exponential decay in time according to [9,26]

$$i_F(t) = kQ \exp(-kt) \qquad (5\ 10)$$

where k is the apparent rate constant for the reaction and Q is the total charge passed in the redox transformation

Figure 5 11 illustrates typical chronoamperometric responses for the oxidation of a monolayer of $[Os(bpy)_2$ 4-bpt $Cl]^+$ on a 2 5 μm radius platinum microelectrode where the electrolyte is aqueous 1 0 M $LiClO_4$, adjusted to pH 12 In these experiments, the overpotential ($E-E^{o'}$) was 0 148 and –0 181 V (solid line and broken line, respectively) This figure shows that on a nanosecond timescale, two current decays can be separated These responses, which arise from double layer charging and Faradaic current flow, are time resolved due to the much shorter time constant of double layer charging compared to that of the Faradaic reaction

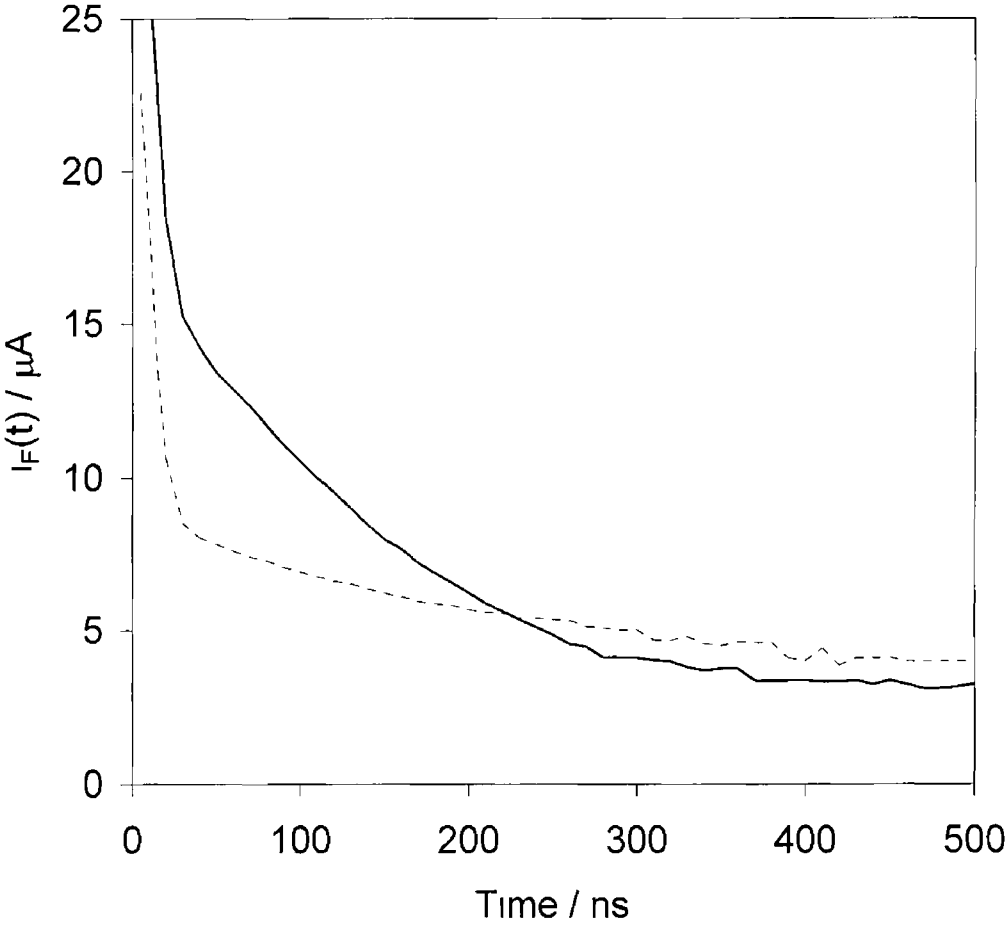

Figure 5 11 Current response for a 2 5 µm radius platinum microelectrode modified with a monolayer of $[Os(bpy)_2$ 4-bpt Cl] following a potential step where the overpotential is 0 148 V (—) and –0 181 V (----) The supporting electrolyte is aqueous 1 0 M $LiClO_4$ adjusted to pH 12 0 with NaOH

The RC time constant of the 2 5 μm microelectrode has been estimated from the semi-log plot of the current-time transient (Figure 5 12) as approximately 15 ns Semi-log plots of ln $i_F(t)$ versus t have been used in order to extract kinetic information from this system Faradaic currents were recorded only at times that were 5-10 times that of the RC constant At these times, the contribution of the charging current to the overall current is negligible The linearity of the ln $i_F(t)$ versus t plots shown in Figure 5 12 indicates that electron transfer is characterised by a single rate constant over the time required to collect greater than 95% of the total charge for the redox reaction Deviations from linearity would be expected if ohmic drop were present Uncompensated resistance would cause the potential, and hence the apparent rate, to evolve with time Therefore, iR drop would cause deviations to be observed at short experimental times All of the transients recorded displayed nearly ideal chronoamperometric responses, suggesting that ohmic losses are negligible

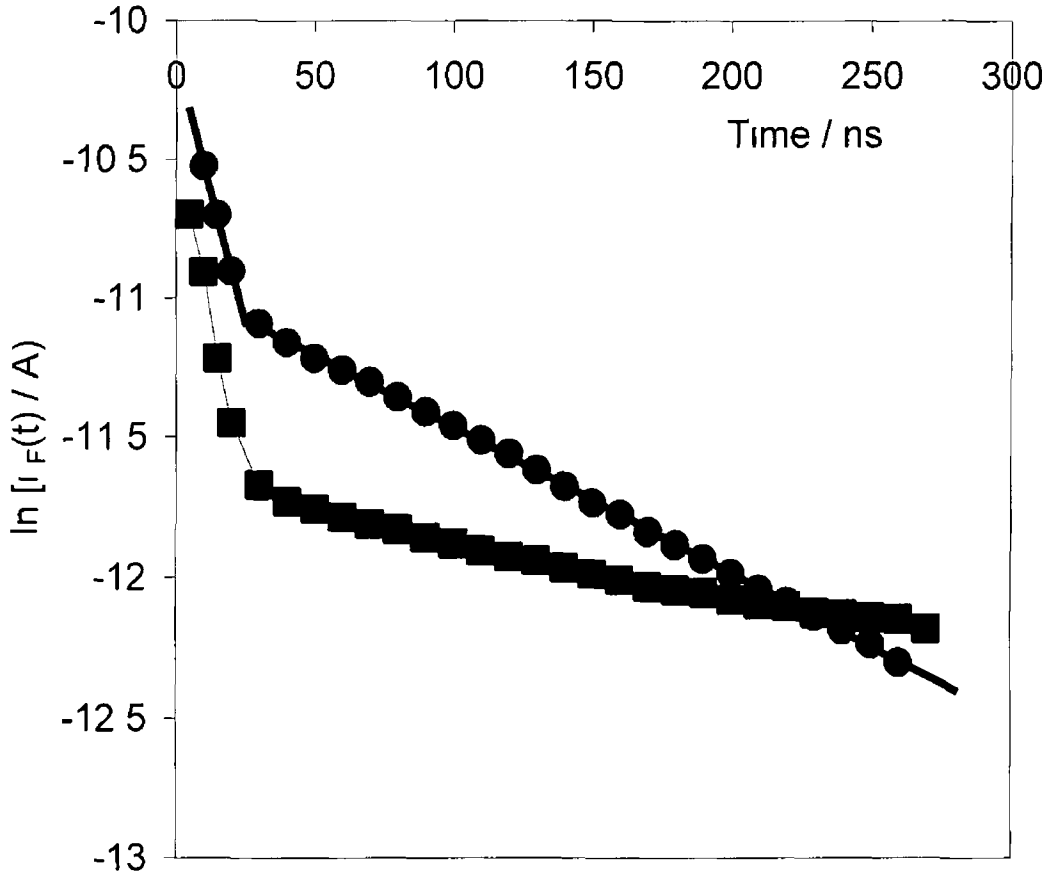

Figure 5 12 ln $i_F(t)$ versus t plots for a 2 5 μm radius platinum microelectrode modified with a monolayer of [$Os(bpy)_2$ 4-bpt Cl] The overpotential is 0 148 V (circles) and –0 181 V (squares) and the supporting electrolyte is aqueous 1 0 M $LiClO_4$ adjusted to pH 12 with NaOH

The importance of carefully selecting the size of the microelectrode in these experiments is emphasised by Figure 5 13 that illustrates the chronoamperometric response for the oxidation of a monolayer of $[Os(bpy)_2$ 4-bpt $Cl]^+$ at a 12 5 μm radius platinum microelectrode From this illustration, it is clear that two distinct current decays cannot be separated This is due to the increased time constant of double layer charging of the larger microelectrode The RC constant of this electrode has been estimated as approximately 0 4 μs Therefore, the fastest rate constants that could be measured at this electrode are of the order of 5×10^5 s^{-1} Thus, it appears that at an electrode of radius 12 5 μm the Faradaic current for the redox reaction is convoluted with the charging current over the timescale of the experiment

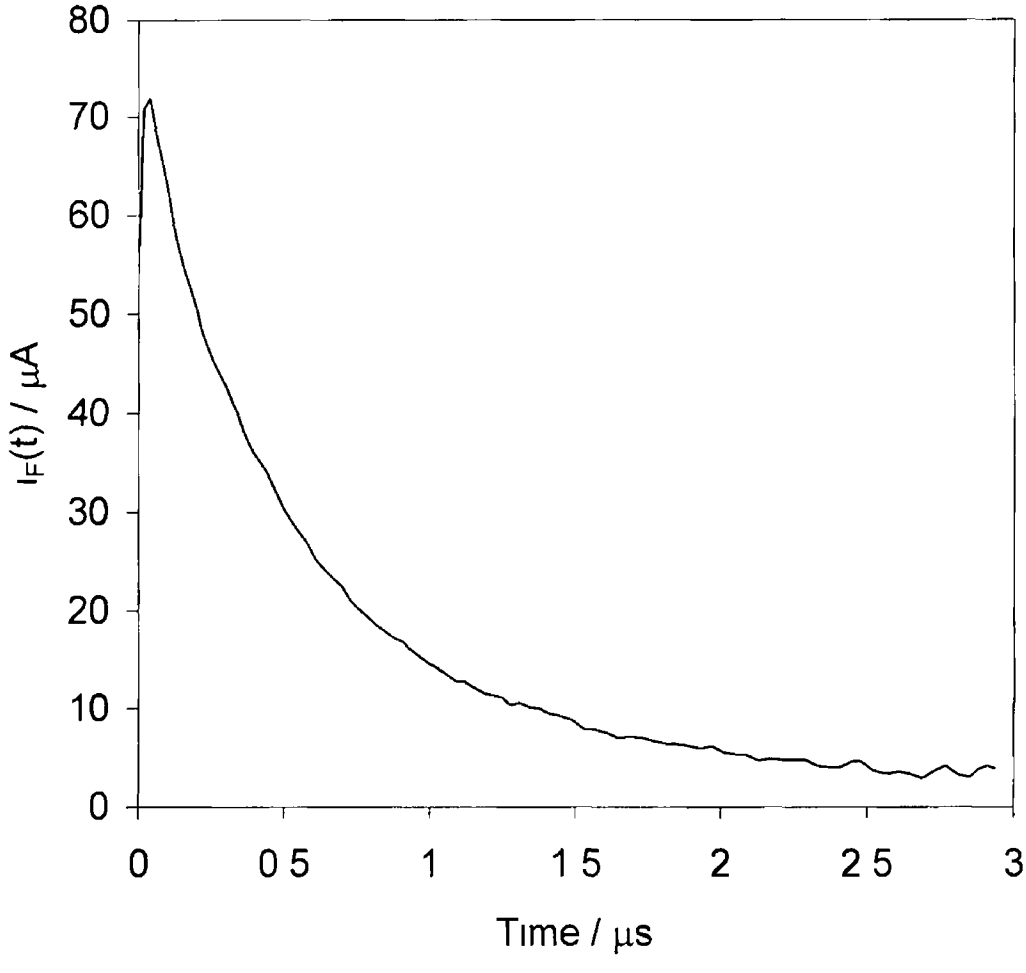

Figure 5 13 Current response for a 12 5 μm radius platinum microelectrode modified with a monolayer of $[Os(bpy)_2$ 4-bpt Cl] following a potential step where the overpotential was 0 148 V The supporting electrolyte is aqueous 1 0 M $LiClO_4$ adjusted to pH 12 0 with NaOH

The apparent rate constants for the oxidation and reduction of the Os^{2+} redox centres, obtained from the semi-log plot shown in Figure 5 12 in conjunction with Equation 5 10, are 5 3 × 10^6 and 3 4 × 10^6 s^{-1} for overpotentials of 148 and -181 mV, respectively Given that the RC time constant of the platinum microelectrode is approximately 15 ns, the maximum rate constant that can be determined is approximately 1 3 × 10^7 s^{-1} A Tafel plot of ln k versus overpotential for a monolayer of [$Os(bpy)_2$ 4-bpt Cl] in which the supporting electrolyte is 1 0 M $LiClO_4$ adjusted to pH 12 5 with NaOH is illustrated in Figure 5 14 For overpotentials less than about 250 mV, ln k depends approximately linearly on the overpotential Despite the limitations in the fastest rates that can be measured, the linear responses observed in the Tafel plots are consistent with the Butler-Volmer formulation of the potential dependence of electrochemical reaction rates Moreover, the fact that linear responses are observed for both the oxidation and reduction of the monolayers up to overpotentials up to 250 mV suggests that the Marcus reorganisation energy is at least 30 kJ mol^{-1} [12]

As illustrated in Figure 5 14, specifying the overpotential with respect to the formal potential determined using cyclic voltammetry gives rate constants that are not equal for zero overpotential Figure 5 14 illustrates that for $\eta = 0$ (at the cyclic voltammetrically determined E^{o}), 'standard' heterogeneous electron transfer rate constants of 1 60 × 10^6 and 2 67 × 10^6 s^{-1} for reduction and oxidation of the monolayer are obtained, respectively The non-equal intercepts at $\eta = 0$ in Figure 5 14 suggests that the effective formal potential in short timescale chronoamperometry (i e the potential where the forward and backward reaction rate are equal) is shifted by approximately –40 mV compared to the cyclic voltammetry value This may be due to the influence of ion-pairing The cyclic voltammetrically determined formal potential represents a fully ion-paired situation, whereas high speed chronoamperometry may not allow sufficient time for complete ion-pairing

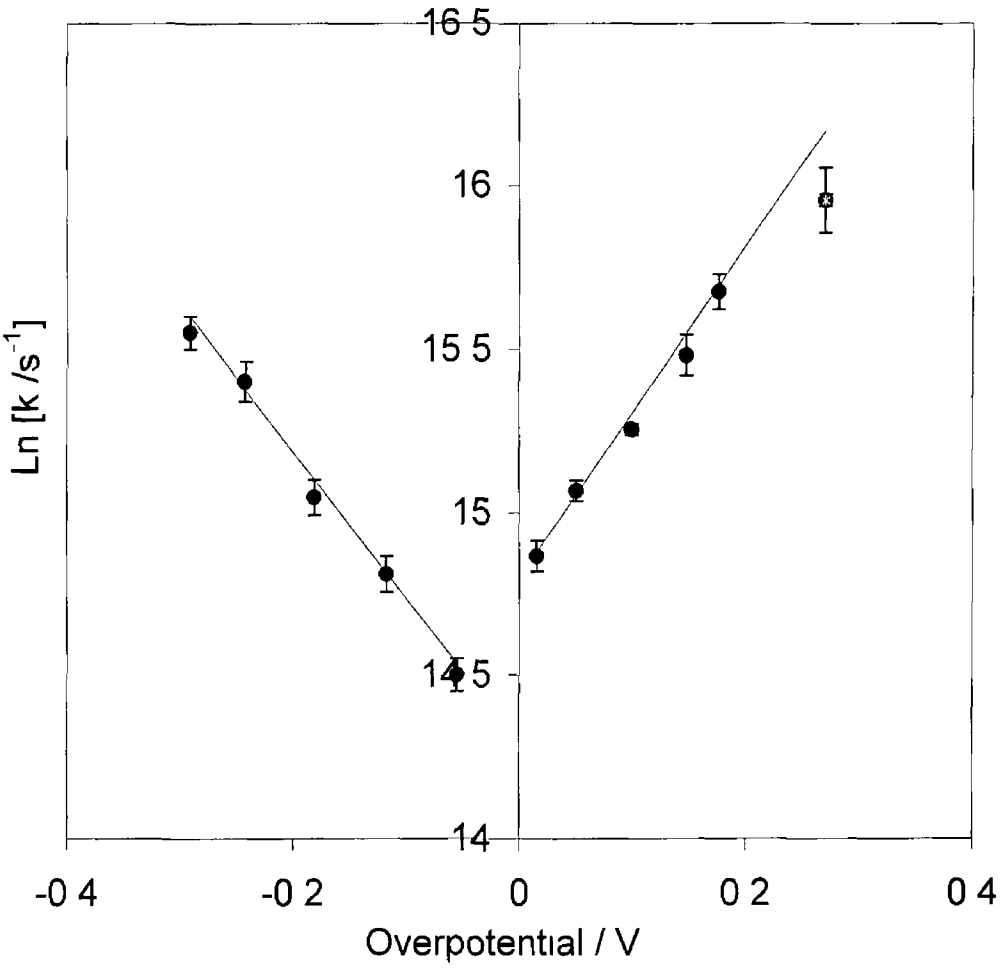

Figure 5 14 Tafel plot of ln k versus overpotential for a 2 5 μm radius platinum microelectrode modified with a monolayer of [Os(bpy)$_2$ 4-bpt Cl] The supporting electrolyte is aqueous 1 0 M $LiClO_4$ adjusted to pH 12 5 with concentrated NaOH

A Tafel plot of ln k versus overpotential for a 2 5 μm radius platinum microelectrode modified with an adsorbed monolayer of $[Os(bpy)_2$ 4-bpt Cl] where the supporting electrolyte is 1 0 M $LiClO_4$ (pH 5 5) is shown in Figure 5 15 The shape of this curve agrees with that previously reported for monolayers of this complex where the supporting electrolyte is neutral aqueous lithium perchlorate solution Figure 5 15 also shows a shift of the apparent 'chronoamperometry' formal potential compared to the cyclic voltammetry formal potential The 'standard' heterogeneous electron transfer rate constants determined at $\eta = 0$ (based on the cyclic voltammetry formal potential) agree with those previously reported for these monolayers ($1\ 9 \times 10^5$ and $4\ 5 \times 10^4\ s^{-1}$ for the reduction and oxidation processes, respectively) [12]

The most significant conclusion of these observations is that the rate of heterogeneous electron transfer for the reduction reaction decreases by approximately an order of magnitude upon protonation of the 4-bpt ligand The rate of heterogeneous electron transfer for the oxidation reaction decreases by a larger amount, almost two orders of magnitude, upon protonation of the 4-bpt bridging ligand While it is not clear why the largest decrease in k^o occurs in the oxidative branch, this modulation of the electron transfer rate based on a change in the electrolyte pH is significant

As discussed above, electron rich bridging ligands of this type have been shown to support superexchange mechanisms Electron superexchange may be the dominant mechanism if the LUMO of the bridge is close in energy to the metal dπ orbitals of the remote redox centre In contrast, if the HOMO of the bridge is closer in energy to the metal dπ orbitals, hole superexchange may be the dominant mechanism Protonation of the 4-bpt bridging ligand in this monolayer system will decrease the electron density on the ligand, making it harder to oxidise and easier to reduce the bridge This will cause the formal potential of the HOMO and the LUMO of the bridge to shift in a positive direction, thereby increasing the dπ-HOMO difference This is illustrated in Figure 5 16

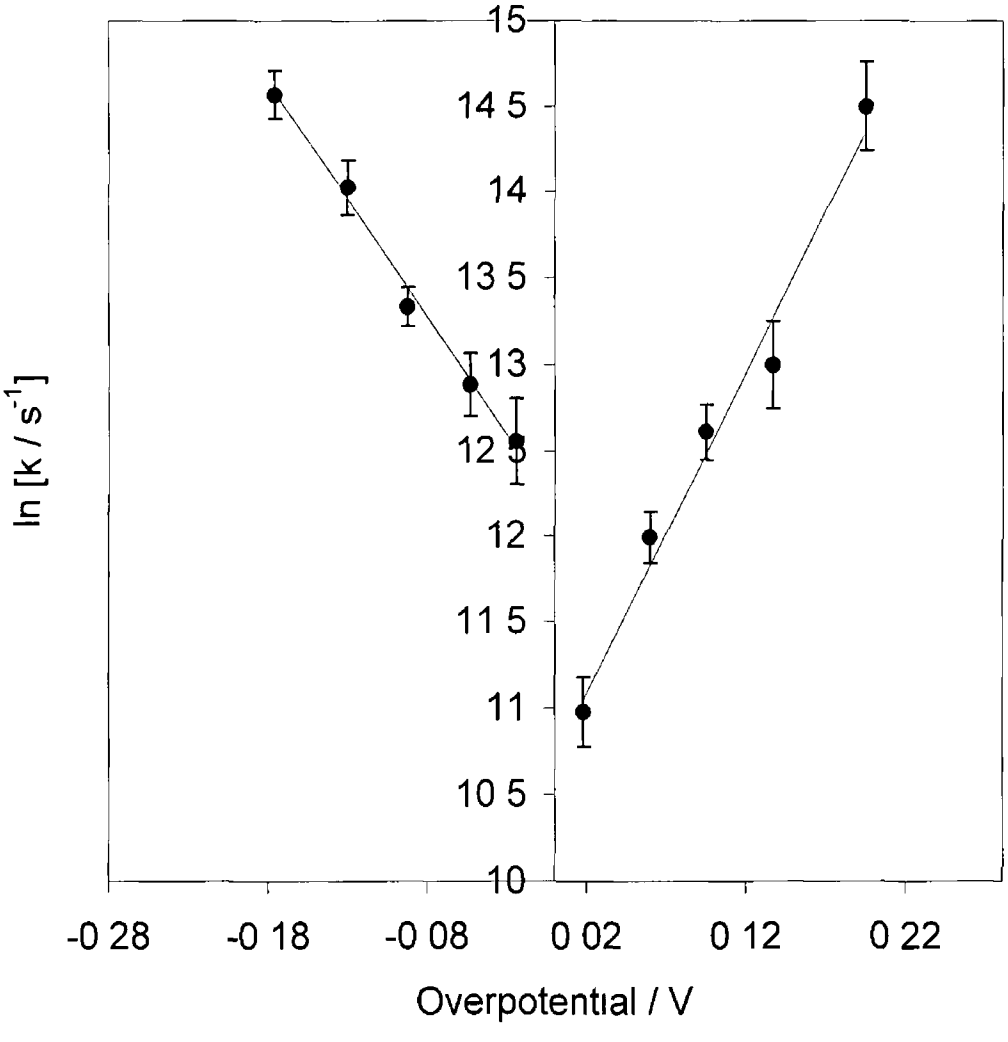

Figure 5 15 Tafel plot of ln k versus overpotential for a 2 5 μm radius platinum microelectrode modified with a monolayer of $[Os(bpy)_2$ 4-bpt Cl] The supporting electrolyte is aqueous 1 0 M $LiClO_4$ (pH 5 5) The solid lines are the theoretical responses expected on the basis of the Butler-Volmer formalism of heterogeneous electron transfer

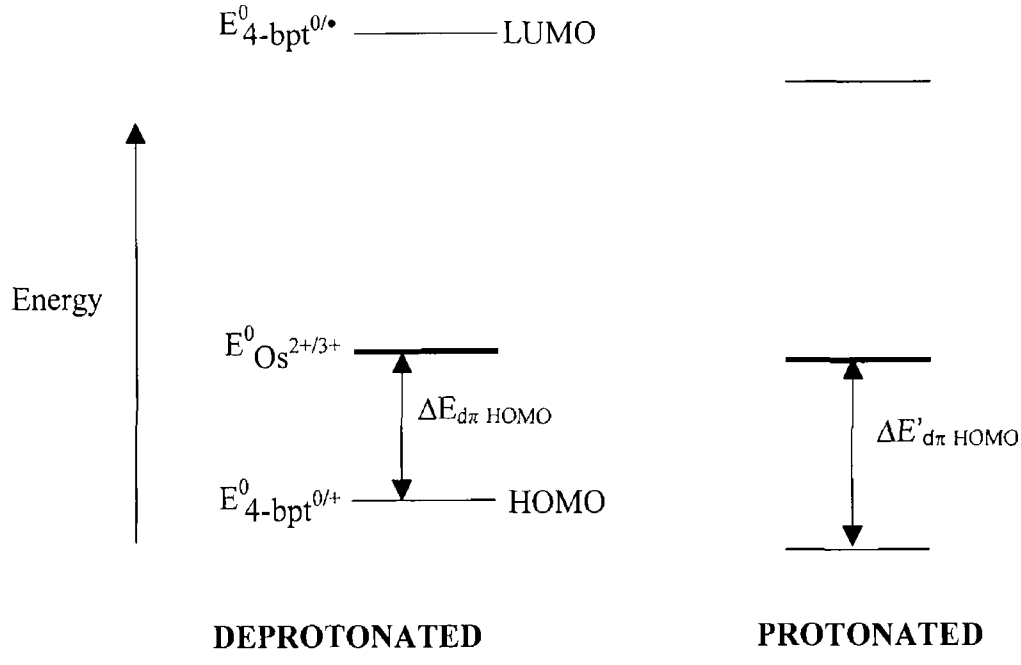

Figure 5 16 Proposed effect of protonation of the 4-bpt bridging ligand on hole superexchange

Thus, it appears that protonation of the 4-bpt bridge causes a positive shift in the bridge formal potential, i e , thereby increasing the energy difference between the metal dπ orbitals and the HOMO of the bridge This increased energy difference between the bridge orbitals and the metal orbitals in the protonated state causes a decrease in the rate of electron transfer If the dominant superexchange mechanism was electron superexchange, the decreased $Os_{d\pi}$-LUMO separation should cause an increase in the rate of electron transfer upon protonation of the bridging ligand While the shift in the formal potentials of the bridge HOMO and LUMO upon protonation have not been determined directly, the data shown suggests that electron transfer occurs via a hole superexchange mechanism

5 5 CONCLUSIONS

Stable close-packed monolayers of [Os(bpy)$_2$ 4-bpt Cl]PF_6 have been formed on gold microelectrodes, bpy is 2,2'-bipyridyl and 4-bpt is 3,5-Bis(pyridin-4-yl)-1,2,4-triazole The adsorbed monolayers exhibit well defined voltammetric responses for 1 0<pH<12 0 Probing the pH dependence of the interfacial capacitance reveals that the triazole bridging ligand is capable of undergoing a protonation/deprotonation reaction with a pK_a of 7 0±0 6 This value differs from that found for the complex in solution and this may be due to partial solvation of the adsorbates within the monolayer

High speed chronoamperometry has been used to probe the rate of heterogeneous electron transfer across the electrode/monolayer interface Significantly, upon protonation of the 4-bpt bridge, the standard heterogeneous electron transfer rate constant decreases by greater than an order of magnitude for both the oxidation and reduction reactions This observation is consistent with mediating electronic states within the bridging ligand (superexchange) playing an important role in the redox switching process Specifically, the results suggest that hole transfer is mediated through the highest occupied molecular orbital (HOMO) of the 4-bpt ligand Protonating the bridge reduces its electron density thus lowering the energy of the bridge HOMO relative to the hole acceptor states of the osmium and decreasing the standard rate constant

5 6 REFERENCES

1 Moser, C C , Keske, J M , Warnacke, K , Farıd, R S , Dutton, P L , *Nature*, **1992**, *355*, 796

2 Bıxon, M , Jortner, J , *J, Phys Chem B*, **2000**, *104*, 3906

3 Moser, C C , Keske, J M , Warnacke, K , Farıd, R S , Dutton, P L , *Nature*, **1992**, *355*, 796

4 Sek, S , Bılewıcz, R , *J Electroanal Chem* , **2001**, *509*, 11

5 Sumner, J J , Weber, K S , Hockett, L A , Creager, S E , *J Phys Chem B*, **2000**, *104*, 7449

6 Forster, R J , O'Kelly, J P , *J Phys Chem* , **1996**, *100*, 3695

7 Forster, R J , Fıggemeıer, E , Loughman, P , Lees, A , Hjelm, J , Vos, J G , *Langmuır*, **2000**, *16*, 7871

8 Bard, A J and Faulkner, L R , "Electrochemıcal Methods Fundamentals and Applıcatıons", Wıley, New York, 1980

9 Forster, R J , Faulkner, L R , *J Am Chem Soc* , **1994**, *116*, 5453

10 Forster, R J , Faulkner, L R , *Langmuır*, **1995**, *11*, 1014

11 Feldberg, S W , Rubınstein, I , *J Electroanal Chem* , **1988**, *240*, 1

12 Forster, R J , Keyes, T E , Vos, J G , *Analyst*, **1998**, *123*, 1905

13 Tırado, J D , Abruña, H D , *J Phys Chem* , **1996**, *100*, 4556

14 Hudson, J E , Abruña, H D , *J Phys Chem* , **1996**, *100*, 1036

15 Trassatı, S *J Electroanal Chem* , **1974**, *53*, 335

16 Rowe, G K , Creager, S E , *Langmuır*, **1991**, *7*, 2307

17 Creager, S E , Rowe, G K , *Anal Chım Acta* , **1991**, *246*, 233

18 Smıth, C P , Whıte, H S , *Anal Chem* , **1992**, *64*, 2398

19 Wıghtman, R M , Wıpf, D O , ın *Electroanalytıcal Chemıstry*, vol 15, Bard, A J , Ed , Marcel Dekker, New York, **1989**

20 Porter, M D , Brıght, T B , Allara, D L , Chıdsey, C E D , *J Am Chem Soc* , **1987**, *109*, 3559

21 Smıth, C P , Whıte, H S , *Langmuır*, **1993**, *9*, 1

22 Nakamoto, K , *Infrared and Raman Spectra of Inorganic and Coordination Compounds*, Wiley, **1986**

23 Forster, R J , Keyes, T E , Bond, *J Phys Chem B*, **2000**, *104*, 6389

24 Barigelletti, F , De Cola, L , Balzani, V , Hage, R , Haasnoot, J G , Reedijk, J , Vos, J G , *Inorg Chem* , **1989**, *28*, 4344

25 Chidsey, C E D , *Science*, **1991**, *251*, 919

26 Finklea, H O , Hanshaw, D D , *J Am Chem Soc* , **1992**, *114*, 3173

APPENDIX A

PUBLICATIONS

Protonation Effects on Superexchange across Gold/Osmium Bis(bipyridyl) Tetrazine Chloride Monolayer Interfaces

Darren A Walsh,[†] Tia E Keyes,[‡] Conor F Hogan,[†] and Robert J Forster*[†]

National Center for Sensor Research School of Chemical Sciences Dublin City University Dublin 9 Ireland and School of Chemistry Dublin Institute of Technology Dublin 4 Ireland

Received October 27 2000 In Final Form January 19 2001

Monolayers of $[Os(bpy)_2(4\text{-tet})Cl]^+$, where bpy is 2,2′ bipyridyl and 4 tet is 3,6-bis(4-pyridyl) 1,2,4,5-tetrazine, have been formed by spontaneous adsorption onto clean gold microelectrodes These monolayers are stable and exhibit well defined voltammetric responses for the $Os^{2+/3+}$ redox reaction across a wide range of solution pH values The shift in the formal potential with increasing perchlorate concentration indicates that the oxidized form is ion paired to a single additional perchlorate anion The tetrazine bridge between the $[Os(bpy)_2Cl]^+$ moiety and the electrode surface undergoes a reversible protonation/deprotonation reaction The pK_a of the tetrazine within the monolayer has been determined as 2 7 ± 0 3 from the pH dependence of the interfacial capacitance Significantly, this value is indistinguishable from that found for the complex dissolved in essentially aqueous solution suggesting that these monolayers are highly solvated High-speed cyclic voltammetry reveals that the redox switching mechanism is best described as a nonadiabatic, through bond tunneling process Significantly while protonating the bridging ligand does not influence the free energy of activation, 10 3 ± 1 1 kJ mol^{-1}, $k°$ decreases by 1 order of magnitude from 1 1 × 10^4 to 1 2 × 10^3 s^{-1} on going from a deprotonated to protonated bridge These observations are interpreted in terms of a through bond hole tunneling mechanism in which protonation decreases the electron density on the bridge and reduces the strength of the electronic coupling between the metal center and the electrode

Introduction

The ability to control the rate of electron transfer across molecular bridges impacts diverse areas ranging from the development of molecular electronics to understanding biosystems [1] Traditionally, the only approach to modulating the rate of electron transfer across a bridge linking molecular or bulk components was to synthetically change the structure of the bridge[2] or the solvent[3] or to couple electron transfer to mass transport, e g proton-coupled electron-transfer reactions [4] A particular challenge is to develop systems in which the electronic structure of the bridge can be reversibly changed in response to the local microenvironment e g , through a protonation reaction However, this objective can only be achieved if the role of the bridge states in the electron-transfer process is understood For example, where electron-transfer proceeds via a coherent superexchange mechanism,[5] the rate depends algebraically on the difference between the energy levels of the bridge and donor/acceptor, $\Delta E_{Bridge-D/A}$ Therefore if this energy difference could be tuned, then one could control the electron-transfer dynamics [6]

The influence of bridge states on electron exchange has been investigated extensively for solution phase donor−acceptor systems, e g transition metal complexes linked by an electroactive bridge [7] In contrast there have been relatively few investigations in which one of these molecular components is replaced by a metal surface Traditionally, self-assembled monolayers have employed alkanethiol linkers in which the energies of both the highest occupied and lowest unoccupied molecular orbitals, the HOMO and LUMO, respectively, are energetically remote from the donor/acceptor states of the bound redox centers [8] While systems of this kind can provide dramatic new insights into the distance and potential dependence of electron transfer,[9] the large $\Delta E_{Bridge-D/A}$ makes them unattractive for modeling biological systems For example, in DNA donor/acceptor and bridge elements are typically separated by less than 1 eV [10]

CHART 1

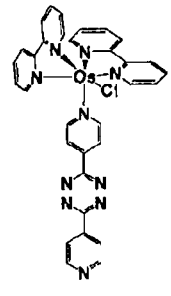

This contribution reports an approach to chemically modulating the rate of heterogeneous electron transfer across metal/monolayer interfaces The bridge between the $[Os(bpy)_2Cl]^+$ moiety and the electrode surface is 3,6-bis(4-pyridyl)-1,2,4,5-tetrazine (Chart 1) where bpy is 2,2 -bipyridyl Significantly, not only is the bridging ligand redox active, it is also capable of undergoing protonation/deprotonation reactions depending on the pH of the contacting electrolyte solution The effect of protonating the bridge on the dynamics of heterogeneous electron transfer has been studied using high scan rate cyclic voltammetry These responses are well-behaved over a wide range of scan rates electrolyte concentration, and pH values

* To whom correspondence should be addressed
† Dublin City University
‡ Dublin Institute of Technology

10 1021/jp003984n CCC $20 00
Published on Web 00/00/0000 PAGE EST 7 1

allowing molecular bridge effects in particular the role of superexchange on distant charge tunneling, to be investigated The complete voltammograms have been modeled to decouple the effects of protonation on the electronic coupling and the free energy of activation This analysis reveals that, while the free energy of activation is insensitive to the extent of bridge protonation, the standard heterogeneous electron-transfer rate constant *decreases* when the tetrazine bridge is protonated These results are interpreted in terms of the effects of bridge protonation on the energy difference between the $Os_{d\pi}$ and bridge HOMO levels

Experimental Section

The synthesis of the bridging ligand and metal complex has been described in detail previously [11]

Instrumentation Microelectrodes were prepared using gold microwires of radii between 1 and 25 μm sealed in a glass shroud that were mechanically polished as described previously [6,11] Electrochemical cleaning of the electrodes was carried out by cycling in 0 1 M H_2SO_4 between potential limits chosen to initially oxidize and then reduce the surface of the gold electrode Excessive cycling was avoided in order to minimize the extent of surface roughening The real surface areas of the electrodes were determined by calculating the charge under the gold oxide reduction peak Typically surface roughness values were between 1 6 and 2 0 Determining the real, as opposed to the geometric, area of the electrodes is important if the area of occupation of the adsorbate is to be accurately determined

Cyclic voltammetry was performed using a CH Instruments model 660 electrochemical workstation and a conventional three-electrode cell All solutions were degassed thoroughly using nitrogen, and a blanket of nitrogen was maintained over the solution during all experiments Potentials are quoted with respect to a BAS Ag/AgCl gel-filled reference electrode All experiments were performed at room temperature (22 ± 3 °C)

Spontaneously adsorbed monolayers were formed by immersing the microelectrodes in micromolar solutions of the metal complex in acetone/water (50/50, v/v) for periods up to 12 h The pH of the deposition solution was controlled by addition of 1 0 M aqueous perchloric acid The complex is stable toward aerial oxidation, and no precautions were taken to exclude atmospheric oxygen during monolayer formation Before electrochemical measurements were made, the electrodes were rinsed with Milli-Q water and the electrolyte to remove any unbound material Subsequent measurements were performed in blank electrolyte The degree of monolayer protonation was systematically altered by varying the pH of the contacting electrolyte solution over the pH range 0 50−8 00 by adding concentrated solutions of $HClO_4$ or NaOH to 1 0 M $LiClO_4$

Raman spectroscopy was conducted on a Dilor Jobiny–von Spex Labram The exciting 20 mW helium–neon laser (632 8 nm) was focused through a purpose made electrochemical cell onto monolayer deposited on a gold macroelectrode (1 5 mm radius) using a 10× objective lens The beam diameter when focused is approximately 1 μm producing approximately 10^6 W cm^{-2} at the surface Focusing was confirmed by using a CCD camera in imaging mode A spectral resolution of 1 5 cm^{-1}/pixel was achieved using a grating of 1800 lines/mm The applied potential was controlled with respect to an Ag/AgCl reference electrode using a CH instruments model 600A potentiostat

Results and Discussion

General Electrochemical Properties Figure 1 shows representative background corrected cyclic voltammograms for a

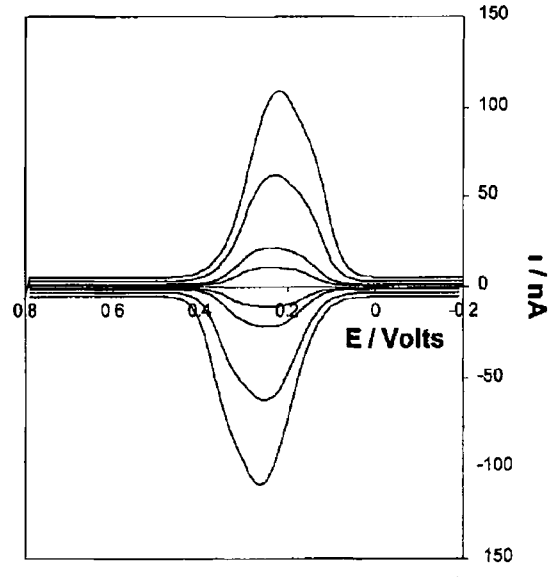

Figure 1 Cyclic voltammograms for a spontaneouslyadsorbed monolayer of $[Os(bpy)_2(4\text{-}tet)Cl]ClO_4$ in 0 1 M $LiClO_4$ at an electrolyte pH of 1 0 ± 0 2 Scan rates are (top to bottom) 50 28 6 10 and 5 V s^{-1} The radius of the gold microelectrode is 25 μm The monolayer surface coverage is 8 1 × 10^{-11} mol cm^{-2} Cathodic currents are up and anodic currents are down

spontaneously adsorbed $[Os(bpy)_2(4\text{-}tet)Cl]^+$ in aqueous 0 1 M $LiCLO_4$ electrolyte adjusted to pH 1 0 ± 0 2 by addition of $HClO_4$ The solution does not contain any dissolved complex These voltammograms are consistent with those expected for an electrochemically reversible reaction involving a surface-confined species [12,13] The peak shape is independent of scan rate, v, for 0 05 ≤ v ≤ 50 V s^{-1}, and the peak height increases linearly with increasing scan rate, rather than the $v^{1/2}$ dependence observed for the complex dissolved in acetonitrile Therefore, it appears that $[Os(bpy)_2(4\text{-}tet)Cl]^+$ adsorbs to the surface of the gold microelectrode to give an electroactive film Repetitive cycling of these monolayers in 0 1 M $LiClO_4$ electrolyte at both neutral and low pH over a 16 h period did not produce any change in the shape of the voltammograms, indicating that these monolayers are extremely stable to electrochemical cycling across a wide pH range

Where there are no lateral interactions between adsorbates and a rapid redox equilibrium is established with the applied potential, a zero peak to peak splitting (ΔE_p) and a full width at half-maximum (fwhm) of 90 6 mV are expected for a one electron transfer Monolayers of this complex exhibit nonzero ΔE_p values even at low scan rates, e g , ΔE_p is 60 ± 10 mV at a scan rate of 0 5 V s^{-1} This behavior has been reported previously for structurally related systems,[14] e g , for $[Os(bpy)_2$-(3,5-bis(pyridm-4-yl)-1 2 4-triazole)$Cl]^+$ monolayers,[15] ΔE_p is 15 ± 5 mV at a scan rate of 0 5 V s^{-1} Feldberg has interpreted similar nonideal responses in terms of unusual quasi-reversibility (UQR) [16] arising due to rate processes which are slow compared to the experimental time scale However, it is important to note that ΔE_p does not increase with increasing scan rate suggesting that the nonideal behavior is not caused by slow heterogeneous electron transfer Also, the observation that ΔE_p does not increase with increasing scan rate for 0 5 ≤ v ≤ 50 V s^{-1} indicates that ohmic drop does not significantly influence the response These monolayers exhibit fwhm values of 250 ± 30 mV suggesting that there may be repulsive lateral interactions between adjacent redox centers We have probed this issue by

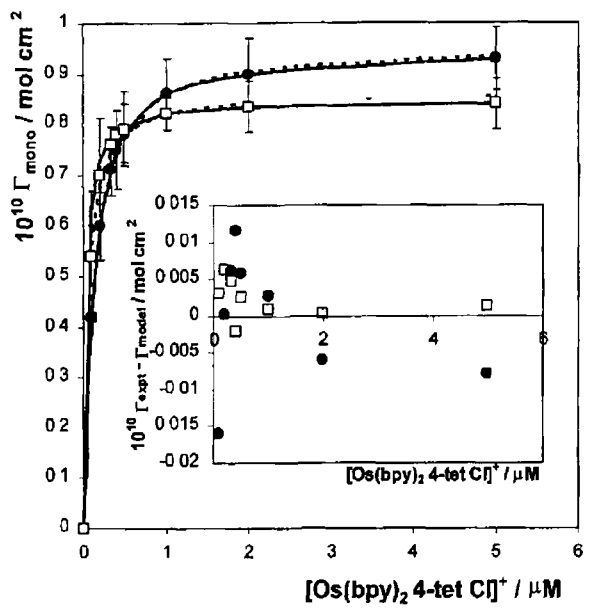

Figure 2 Dependence of the surface coverage on the bulk concentration of the $[Os(bpy)_2(4\text{-tet})Cl]ClO_4$ ● and □ denote monolayers deposited at pH values of 6 6 and 1 8 respectively The supporting electrolyte is 1 0 M $LiClO_4$ The dashed and solid lines represent the best fits to the Langmuir and Frumkin adsorption isotherms respectively

determining how the equilibrium surface coverage changes as the bulk concentration of the complex is systematically varied

Adsorption Isotherms To obtain the adsorption isotherm,[17] the surface coverages at equilibrium were determined by integrating the background-corrected cyclic voltammograms as the bulk concentration in the deposition solution was systematically varied Beyond the issue of lateral interactions, the pH dependence of adsorption in this system is interesting because the complex contains two possible protonation sites, i e , the pyridine and tetrazine nitrogens If protonation occurs at the pyridine nitrogen, then its lone pair would not be capable of interacting with the surface thus blocking adsorption Changes in the UV−visible spectrum of the complex in solution[11] indicate that a single protonation/deprotonation reaction occurs between pH 0 5 and 7 0 with an apparent pK_a of 2 7 ± 0 2 Therefore as illustrated in Figure 2 we have probed the effect of the bulk concentration of the complex on the surface coverage for deposition solutions at pH 6 6 and 1 8 Adsorption clearly takes places at low pH indicating that the tetrazine rather than the unbound pyridine moiety, becomes protonated at low pH In a later section, we use capacitance measurements to determine the pK_a of the tetrazine when it is incorporated within a dense monolayer

The Frumkin adsorption isotherm can provide a useful insight into the lateral interactions that may exist within these monolayers since it models the free energy of adsorption as an exponential function of the surface coverage [17]

$$\beta C_i = \frac{\theta_i}{1-\theta_i}\exp(g\theta_i) \qquad (1)$$

Here $\theta_i = \Gamma_i/\Gamma_{sat}$, Γ_i is the coverage of $[Os(bpy)_2(4\text{-tet})Cl]^+$ in mol cm^{-2} at a bulk concentration C_i, Γ_{sat} is the saturation coverage obtained at high bulk concentrations, and β is the adsorption coefficient Attractive interactions are indicated by $g < 0$ and repulsive interactions by $g > 0$ while for $g = 0$ the Langmuir isotherm is obtained

TABLE 1 Saturation Coverages, Adsorption Coefficients, and Frumkin Interaction Parameters for $[Os(bpy)_2(4\text{-tet})Cl]^+$ Monolayers Assembled from Deposition Solutions at pH 6 6 and 1 8

	pH 6 6	pH 1 8
$10^{-10}\Gamma$/mol cm^{-2}	0 96 ± 0 1	0 84 ± 0 2
β/M^{-1}	(9 9 ± 0 3) × 10^6	(9 8 ± 0 4) × 10^6
$\Delta G°_{ads}$/kJ mol^{-1}	−39 9 ± 0 8	−39 9 ± 1 1
g	+0 10 ± 0 05	+1 5 ± 0 2

Figure 2 shows that the optimized Frumkin and Langmuir isotherms provide a satisfactory fit to the experimental surface coverages for monolayers assembled from deposition solutions in which the pH is 6 6 or 1 8 However, as illustrated in the inset of Figure 2 the residuals associated with the best-fit Frumkin isotherm are generally smaller and less structured than those found for the best-fit Langmuir isotherm Table 1 contains the best-fit parameters and reveals that the interaction parameters are +0 10 ± 0 05 and +1 50 ± 0 2 for monolayers deposited at pH 6 6 and 1 8, respectively These positive interaction parameters indicate that destabilizing lateral interactions exist in both cases but that the destabilizing interactions are stronger for monolayers that contain a protonated tetrazine bridging ligand This result suggests that electrostatic repulsion between the positively charged headgroups exists at all pH values but that protonating the bridge intensifies these destabilizing lateral interactions

The free energy of adsorption, $\Delta G°_{ads}$, can be determined from the adsorption coefficient in conjunction with eq 2 [18]

$$\beta = \exp(-\Delta G°_{ads}/RT) \qquad (2)$$

The free energies of adsorption are experimentally indistinguishable for the two pHs at a value of −39 9 ± 1 1 kJ mol^{-1} indicating that protonating the tetrazine ligand does not significantly affect the molecule's propensity for adsorption This value is similar to that found for structurally related monolayers,[19,20] e g , for $[Os(bpy)_2Cl(p3p)]^+$ $\Delta G°_{ads}$ is 37 9 ± 2 2 kJ mol^{-1} The saturation surface coverages observed at the pH 6 6 and 1 8 are (0 96 ± 0 1) × 10^{-10} and (0 84 ± 0 2) × 10^{-10} mol cm^{-2} corresponding to areas occupied per molecule of approximately 174 ± 16 and 198 ± 38 Å^2, respectively These areas of occupation are somewhat larger than those expected given a radius of approximately 6 7 Å for the $[Os(bpy)_2Cl]^+$ moiety[21,22] but are consistent with a surface coverage that is dictated by the redox active headgroup rather than by the bridging ligand

Effect of Electrolyte Concentration on the Formal Redox Potential, $E°'$ Given our interest in understanding protonation reactions and electron-transfer dynamics within these monolayers, it is important to probe the nature of the microenvironment within the film The formal potential depends on both the solvation shell and the extent of ion-pairing [23−25] The effect of electrolyte concentration on the formal potential of the $Os^{2+/3+}$ redox reaction has been examined for $0\,1 \le [LiClO_4] \le 1\,0$ M In these measurements, scan rates less than 1 V s^{-1} were employed so as to avoid any influence from the interfacial electron-transfer kinetics To avoid complications due to changes in the ionic strength of the solution a fixed background of 1 0 M Na_2SO_4 was used as a swamping electrolyte The formal potential of the $Os^{2+/3+}$ redox reaction shifts by less than 15 mV over the electrolyte concentration range $0\,1 \le [Na_2SO_4] \le 1\,0$ M indicating that SO_4^{2-} has little tendency to ion pair with the osmium centers For $0\,1 \le [LiClO_4] \le 1\,0$ M, the peak shapes and heights are insensitive to changes in the electrolyte

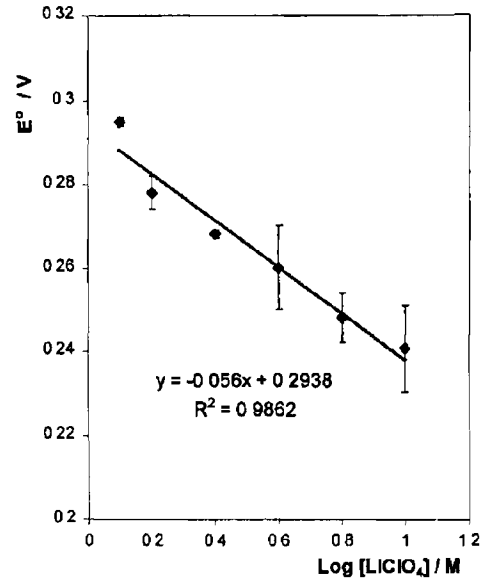

Figure 3 Dependence of the formal potential of the $Os^{2+/3+}$ redox reaction within an adsorbed monolayer of $[Os(bpy)_2(4\ tet)Cl]^+$ on the concentration of perchlorate electrolyte All measurements were performed in a constant background electrolyte of 1 0 M Na_2SO_4

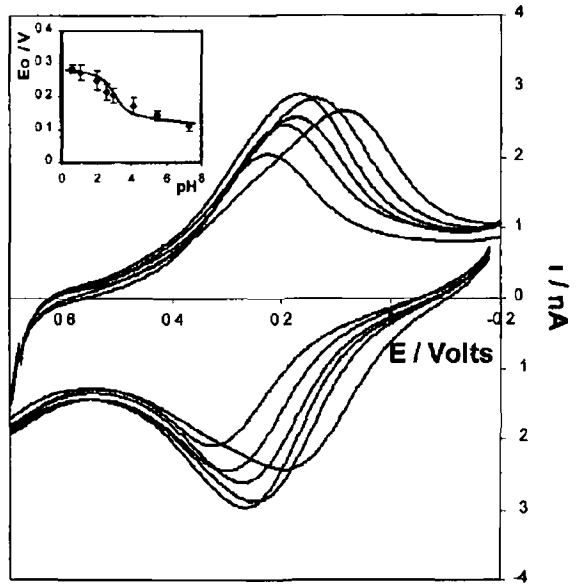

Figure 4 Effect of the electrolyte pH on the voltammetric response of an $[Os(bpy)_2(4\ tet)Cl]ClO_4$ monolayer adsorbed on a 12 5 μm radius gold microelectrode The scan rate is 1 V s^{-1} and the supporting electrolyte is 1 0 M $LiClO_4$ The electrolyte pH was adjusted by adding by concentrated $HClO_4$ or NaOH The pH values are (from left to right) 0 60, 2 00, 2 59 2 95 4 10 and 5 47 Cathodic currents are up and anodic currents are down

concentration However, as illustrated in Figure 3, $E^{\circ\prime}$ shifts in a negative potential direction as the $LiClO_4$ concentration increases indicating that it becomes increasingly easier to oxidize the osmium redox center at higher electrolyte concentrations This behavior is consistent with ion-pairing between the perchlorate and the redox center The theoretical slope of this semilog plot is (59/p) mV/decade, where p is the difference in the number of anions pairing with the oxidized and reduced forms of the redox center The slope determined for $[Os(bpy)_2(4\text{-tet})Cl]^+$ monolayers was 51 ± 6 mV indicating that a single additional anion becomes bound to the redox center in the oxidized state

Effect of pH on $E^{\circ\prime}$ Figure 4 shows the effect of decreasing the contacting electrolyte pH on the voltammetric response of $[Os(bpy)_2(4\text{-tet})Cl]^+$ monolayers The formal potential of the $Os^{2+/3+}$ redox reaction shifts from 0 136 to 0 284 V as the pH is systematically decreased from 5 47 to 0 59 A similar behavior is observed for both the complex in solution and for mechanically attached solid-state deposits,[11] where $E^{\circ\prime}$ shifts in a positive potential direction by approximately 150 mV upon protonation of the tetrazine ligand This pH-sensitive E° contrasts with $[Os(bpy)_2(4,4'\text{-trimethylenedipyridine})Cl]^+$ monolayers[26] and is consistent with protonation occurring at the tetrazine rather than the pyridine site The shift in E° to more positive potentials at low pH indicates that it is more difficult to create the Os^{3+} species when the tetrazine is protonated Both a reduced electron donating ability of the protonated ligand and a higher overall positive charge on the monolayer are likely to contribute to this effect However, these data do not allow the pK_a of the tetrazine monolayer to be determined This information is important for two distinct reasons First the dielectric constant within a dense monolayer may be distinctly different from that found in bulk solution Second immobilization may significantly alter the electron density of the ligand Both of these effects could cause significant differences in apparent pK_a values to be observed Capacitance data can provide a useful insight into these issues

Interfacial Capacitance As discussed by Smith and White,[27] the capacitance of both the monolayer, C_{mono}, and the diffuse layer C_{dif}, contribute to the total differential capacitance, C_T, as given by eq 3

$$C_T^{-1} = C_{mono}^{-1} + C_{dif}^{-1} \quad (3)$$

The film capacitance is given by

$$C_{mono} = \epsilon_0 \epsilon_{film}/d \quad (4)$$

where ϵ_0 is the permittivity of free space ϵ_{film} is the dielectric constant of the film, and d is the thickness of the monolayer

The differential capacitance as determined using cyclic voltammetry at a potential of −0 150 V is independent of the perchlorate concentration $0\ 2 \leq [LiClO_4] \leq 1\ 0$ M This result indicates that for high electrolyte concentrations the diffuse layer capacitance becomes sufficiently large so that it no longer contributes significantly to C_T Under these circumstances $C_T \approx C_{mono}$ and the limiting interfacial capacitance, 26 2 ± 3 6 μF cm^{-2}, can be used in conjunction with eq 4 to estimate the dielectric constant of the film Energy minimized molecular modeling indicates that a fully extended monolayer is approximately 17 Å thick yielding a monolayer dielectric constant of 50 3 ± 6 9 While this value is somewhat lower than that of bulk water, 78 5, it is consistent with a well-solvated monolayer that is permeable to electrolyte ions

Smith and White have further developed this model to describe the effects of monolayer protonation on the interfacial capacitance [28] This approach has been successfully used by Bryant and Crooks to determine the surface pK_a for pyridine derivatives adsorbed on gold electrodes [29] In this model, the total interfacial capacitance depends on the monolayer capacitance, the diffuse layer capacitance, and the degree of protonation of the monolayer, $C(f)$ according to eq 5

$$C_T^{-1} = C_{mono}^{-1} + [C_{dif} + C(f)]^{-1} \quad (5)$$

Assuming that C_{mono} remains constant, the term $[C_{dif} + C(f)]^{-1}$ varies with potential and with the solution pH As the pH of

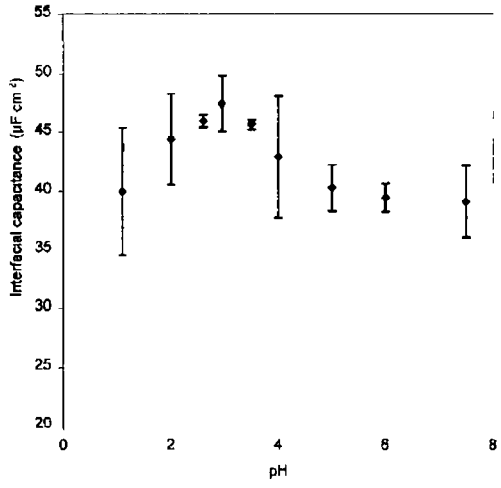

Figure 5 Dependence of the differential capacitance for a monolayer of $[Os(bpy)_2(4\text{ tet})Cl]ClO_4$ on the pH of the contacting electrolyte solution

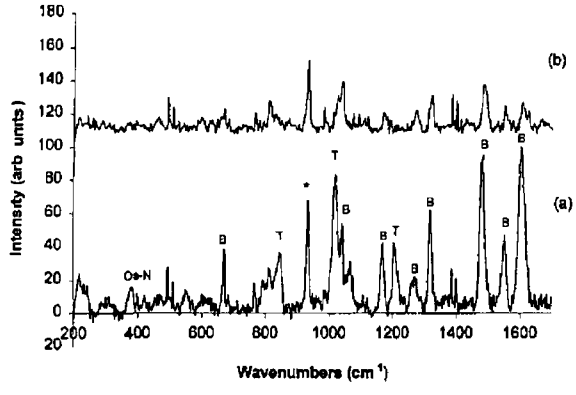

Figure 6 Potential controlled Raman spectra of $[Os(bpy)_2(4\text{ tet})Cl]ClO_4$ monolayers on a gold macrodisk electrode where the supporting electrolyte is 0 1 M $NaClO_4$ (a) −0 200 V (b) 0 500 V The wavelength of the exciting He−Ne laser is 632 8 nm

the contacting solution is altered, $C(f)$ reaches a local maximum near the pK_a, and a maximum is observed in the total interfacial capacitance Figure 5 shows the effect of systematically varying the pH of the contacting solution on the differential capacitance for $1\ 10 \leq pH \leq 7\ 50$ All changes in the capacitance were confirmed to be reversible by first decreasing and then increasing the pH of the supporting electrolyte The shape of the curve agrees with that predicted by theory[28] and yields a surface pK_a of $2\ 7 \pm 0\ 6$ Consistent with a highly solvated monolayer, this value agrees closely with pH induced changes in the metal-to-ligand charge-transfer (MLCT) band[11] observed for the complex dissolved in essentially aqueous media $2\ 7 \pm 0\ 2$

Potential-Dependent Raman Spectroscopy Potential dependent Raman spectroscopy was carried out in order to identify any structural changes that accompany redox switching of $[Os(bpy)_2(4\text{-tet})Cl]ClO_4$ monolayers Surface-enhanced Raman spectroscopy (SERS) is particularly useful as the enhanced sensitivity of this method allows a powerful insight into the monolayer structure, e g packing density and adsorbate orientation, to be obtained [30] The microscope Raman technique employed here allows the laser to be focused onto the modified surface eliminating any contribution from the supporting electrolyte or the electrode shroud Figure 6A,B shows the Raman spectra for $[Os(bpy)_2(4\text{-tet})Cl]ClO_4$ monolayers immobilized on a roughened gold macroelectrode at −0 200 and

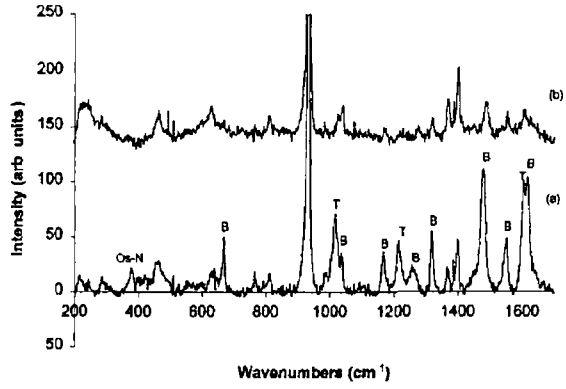

Figure 7 Potential controlled Raman spectra of $[Os(bpy)_2(4\text{ tet})Cl]ClO_4$ monolayers on a gold macrodisk electrode where the supporting electrolyte is 0 1 M $HClO_4$ (a) −0 200 V (b) 0 500 V The wavelength of the exciting He−Ne laser is 632 8 nm

0 500 V vs Ag/AgCl, respectively, where the supporting electrolyte is 0 1 M $LiClO_4$ The UV−visible spectrum of this complex indicates that the exciting HeNe laser (632 8 nm) is preresonant with the MLCT (Os(II)−bpy*) transition The resonance effect is confirmed through enhancement of features at 1605, 1553, 1482, 1320, 1268, 1170, 1015, and 669 cm^{-1}, all of which are associated with the bipyridyl moieties The features observed at 1206, 1042, and 848 cm^{-1} and a shoulder at 1607 cm^{-1} are associated with the 4-tet ligand A weaker feature at 380 cm^{-1} is associated with the Os−N stretch Oxidation results in quantitative loss of Os−N modes and 4-tet modes However, while oxidation significantly changes the relative intensities of the bipyridyl modes, they persist after the monolayer is oxidized

Figure 7A,B illustrates the Raman spectra of a dense monolayer at −0 200 and 0 500 V, respectively, where the supporting electrolyte is 0 1 M $HClO_4$ Vibrational features associate with $Os(bpy)_2$ remain relatively unperturbed by the presence of acid However, consistent with protonation, the 4-tet feature at 848 cm^{-1} disappears in low pH electrolyte and the band overlapping the bpy mode at 1606 cm^{-1} is resolved

Oxidizing the monolayer has a similar impact on the Raman spectra in both neutral and low pH electrolytes Specifically, the low-frequency Os(II)−N vibration collapses indicating efficient oxidation of all the metal centers and changes are observed in the relative intensities of all bpy modes Oxidation also results in loss of 4-tet modes Oxidation of the metal results in loss of MLCT, and one might expect that the resonance condition would be lost However, after oxidation the laser becomes preresonant with a bpy*−Os LMCT transition and the bpy-based bands continue to be observed even for the oxidized monolayers, albeit with different relative intensities In each instance all potential-controlled Raman responses are completely reversible

Heterogeneous Electron-Transfer Dynamics Redox-active bridging ligands are important in that they offer the possibility of significant virtual coupling (superexchange) depending on the difference between the redox potentials of the bridge and remote redox centers Electron transfer via superexchange may be the dominant mechanism if the LUMO of the bridge is similar in energy to the acceptor states of the remote redox center This pathway predominates because the closeness of the bridge and redox center energies acts to reduce the activation barrier to electron tunneling In contrast, if the $Os_{d\pi}$-HOMO separation is relatively smaller, then HOMO-mediated hole transfer will contribute significantly to the redox switching mechanism The

present system is particularly attractive for investigating this issue for two reasons First, the tetrazine ligand undergoes a reduction reaction within an electrochemically accessible potential window Second, the HOMO and LUMO levels of the bridging ligand can be altered by adjusting the pH of the supporting electrolyte, i e , protonation will decrease the electron density on the bridge simultaneously making it more difficult to oxidize but easier to reduce Therefore, unlike traditional alkanethiol monolayers in which bridge states can be modulated only by synthetically changing the structure, e g , by introducing a heteroatom,[31] this tetrazine offers the possibility of altering the proximity of bridge and metal states by a simple change in the chemical composition of the solution

The standard heterogeneous electron–transfer rate constant, k°, depends on both a frequency factor and a Franck–Condon barrier [32–34]

$$k^\circ = A_{et} \exp(-\Delta G^\ddagger/RT) \qquad (6)$$

Here A_{et} is the preexponential factor and $\Delta G^\ddagger$ is the electrochemical free energy of activation [35]

It is important to decouple the free energy and preexponential terms since the effect of changing bridge states will be reflected in A_{et} rather than $\Delta G^\ddagger$ One approach to decoupling these two contributions is to use classical temperature-resolved measurements of k° to measure the free energy of activation, $\Delta G^\ddagger$, allowing A_{et} to be determined In this way, information about the strength of electronic coupling can be obtained [26] A second method involves measuring electron-transfer rate constants at a single temperature over a broad range of reaction driving forces For example, Finklea,[36] Chidsey,[8] Creager,[37] and Murray[38] have assembled nonadiabatic electron-tunneling models that provide a good description of electron tunneling in monolayers of this kind [39,40] In this model, the cathodic rate constant is given by integral over energy (ϵ) of three functions (a) the Fermi function for the metal $n(\epsilon)$, (b) a Gaussian distribution of energy levels for acceptor states in the monolayer $D_{Ox}(\epsilon)$, (c) a probability factor for electron tunneling, P

$$k_{Ox}(\eta) = A\int_{-\infty}^{\infty} D_{Ox}(\epsilon)[n(\epsilon)]P \, d\epsilon \qquad (7)$$

The zero point of energy is defined as the Fermi level of the metal at the particular overpotential of interest The Fermi function describes the distribution of occupied states within the metal and is defined by

$$n(\epsilon) = \left(\frac{1}{1 + \exp[(\epsilon - \epsilon_F)/kT]}\right) \qquad (8)$$

where k_B is the Boltzmann constant The density of acceptor states is derived from the Marcus theory[41] and is represented by eq 9,

$$D_{Ox}(\epsilon) = \exp\left[-\frac{(\epsilon + \eta - \lambda)^2}{4k\lambda T}\right] \qquad (9)$$

where λ is the reorganization energy The distance dependent probability of electron tunneling is given by eq 10,

$$P = \exp(-\beta d) \qquad (10)$$

where d is the electron-transfer distance The distance-dependent tunneling parameter [14] β, is taken as 1 6 Å^{-1}

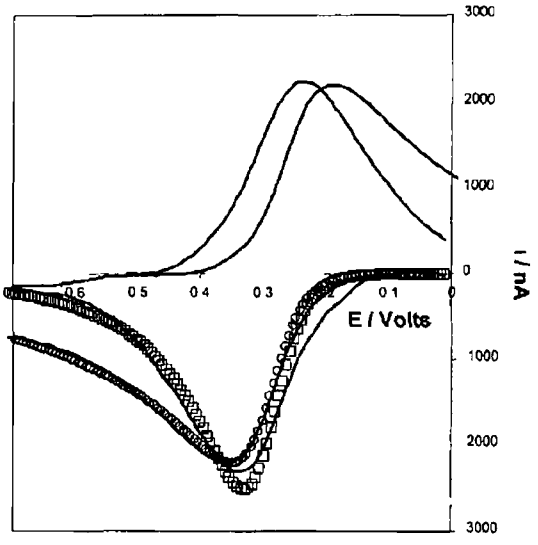

Figure 8 Cyclic voltammograms for a spontaneously adsorbed [Os(bpy)$_2$(4 tet)Cl]$^+$ monolayer on a 5 μm radius gold microdisk electrode where the scan rate is 1333 V s^{-1} Theoretical fits to the data using a nonadiabatic electron tunneling model at electrolyte pH values of 0 9 and 6 0 are denoted by O and □ respectively In both cases λ is 27 kJ mol^{-1} while k^o is 1 1 × 10^3 and 1 1 × 10^4 s^{-1} at pH values of 0 9 and 6 0 respectively

The current for the reaction of an immobilized redox center following first-order kinetics is[38]

$$i_F = nFA(k_{Ox}(\eta)\Gamma_{Red\,\eta} - k_{Red}(\eta)\Gamma_{Ox\,\eta}) \qquad (11)$$

where $\Gamma_{Red\,\eta}$ and $\Gamma_{Ox\,\eta}$ are the instantaneous surface coverages of the oxidized and reduced species and $k_{Ox}(\eta)$ and $k_{Red}(\eta)$ are the reaction rate constants given by eq 7 or its compliment in which $n(\epsilon)$ is replaced with $1 - n(\epsilon)$ and $-\lambda$ is replaced by $+\lambda$ in eq 9 Energy-minimized molecular modeling indicates that that the through-bond electron-transfer distance is approximately 12 6 Å Therefore, in using eq 11 to model the voltammetric response, there are only two freely adjustable parameters, k° and $\Delta G^\ddagger$ ($=\lambda/4$) To model the experimental cyclic voltammograms, we have used the Nelder and Mead Simplex[42] algorithm to find the values of k° and $\Delta G^\ddagger$ that minimize the sum square residuals between the theoretical and experimental currents observed in anodic branches of the linear sweep voltammo grams

Figure 8 shows the effect of changing the electrolyte pH from 6 0 to 0 9 on the experimental background corrected cyclic voltammograms for dense [Os(bpy)$_2$(4-tet)Cl]$^+$ monolayer deposited on a 5 μm radius gold microelectrode where the scan rate is 1333 V s^{-1} As discussed previously, by carefully selecting the electrode radius and by using concentrated electrolytes, it is possible to keep the iR drop to less than a couple of millivolts even at high scan rates [6,26]

Figure 8 shows that satisfactory agreement is observed between the experimental and theoretical anodic peak potentials and peak currents Significantly, for both pH values the optimum $\Delta G^\ddagger$ was 10 3 ± 1 1 kJ mol^{-1} indicating that the local microenvironment around the [Os(bpy)$_2$Cl]$^+$ moiety remains largely unchanged by protonating the tetrazine ligand However, the quality of the fit shown in Figure 8 is not particularly sensitive to $\Delta G^\ddagger$, e g increasing $\Delta G^\ddagger$ by 25% increases the residual sum of squares between the predicted and experimental peak currents by less than 10% Therefore, while fitting of the cyclic voltammograms can provide a convenient approach for

TABLE 2 Standard Heterogeneous Electron-Transfer Rate Constants, $k°$, Free Energies of Activation, $\Delta G^{\ddagger}$, and Preexponential Factors for the Metal-Based Redox Reaction within $[Os(bpy)_2(4\text{-tet})Cl]^{+/2+}$ Monolayers at Different Values of Electrolyte pH[a]

pH	$10^4 k°/s^{-1}$	$\Delta G^{\ddagger}$/kJ mol^{-1}	$10^{-5} A_{el}/s^{-1}$ [b]
6 01	1 15 ± 0 25	9 2 ± 0 4	4 7 ± 0 8
0 87	0 12 ± 0 02	11 4 + 0 3	1 2 ± 0 1

[a] Standard deviations are for at least three individual monolayers The supporting electrolyte is aqueous 1 0 M $LiClO_4$ [b] Preexponential factor extracted from the standard heterogeneous electron transfer rate constant using $\Delta G^{\ddagger}$

SCHEME 1

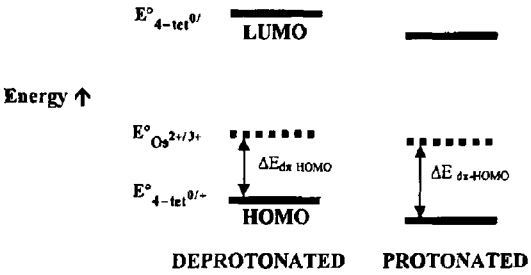

determining $k°$ for this system it appears to provide only an approximate value for $\Delta G^{\ddagger}$ In contrast, the quality of the fit is very sensitive to $k°$ which directly influences both the peak shape and half-wave potential

An important test of the reliability of the standard heterogeneous electron-transfer rate constants obtained is to investigate the scan rate dependence In this way, an insight into the dispersion in the kinetics can be obtained The best fits for voltammograms recorded at scan rates between 800 and 4000 V s^{-1} range from 0 9 × 10^4 to 1 4 × 10^4 s^{-1} and 1 0 × 10^3 to 1 4 × 10^3 s^{-1}, where the electrolyte pH is 6 01 and 0 87, respectively These results indicate that the monolayers are acceptably kinetically monodisperse The dispersion that is observed is most likely related to the concentration-dependent destabilizing lateral interactions found in the adsorption isotherm and rather broad peaks observed in slow scan rate voltammetry

Perhaps the most significant conclusion of Figure 8 is that heterogeneous electron transfer is slower for the protonated than for the deprotonated system The optimum value of $k°$ decreases by 1 order of magnitude from 1 1 × 10^4 s^{-1} to 1 2 × 10^3 s^{-1} (Table 2) when the tetrazine ligand is protonated In bridge-mediated redox reactions of this type, the electronic pathway is determined by the relative gaps between the metal $d\pi$ orbital involved in the redox step and the HOMO and LUMO of the bridge Protonation decreases the electron density on the tetrazine shifting both the bridge oxidation and reduction potentials in a positive potential direction, i e , simultaneously making it more difficult to oxidize but easier to reduce the bridge The fact that we observe a significant *decrease* in $k°$ indicates that it is the bridge HOMO that mediates the redox process, i e , the larger $d\pi$—HOMO separation in the protonated tetrazine causes $k°$ to decrease This HOMO-mediated hole transfer mechanism is consistent with studies on related mixed-valence complexes which suggest that electron-rich π-donating linkers of this type support hole superexchange reactions [43] As illustrated in Scheme 1, the hole is directed through the HOMO orbital of the bridge, creating a "virtual high-energy state In this tunneling pathway, the bridge is formally considered to oxidized by the traversing hole Therefore, the energy difference and degree of orbital mixing between the metal and bridge will directly impact the rate of electron transfer across the bridge

Conclusions

Stable close-packed monolayers of $[Os(bpy)_2(4\text{-tet})Cl]ClO_4$ have been formed on gold microelectrodes, bpy is 2,2′-bipyridyl, and 4-tet is 3 6-bis(4-pyridyl)-1,2,4,5-tetrazine The adsorbed monolayers exhibit well-defined voltammetric responses for 0 5 < pH < 8 0 Probing the pH dependence of the interfacial capacitance reveals that the tetrazine bridging ligand is capable of undergoing a protonation/deprotonation reaction with a pK_a of 2 7 ± 0 6 This value is indistinguishable from that found for the complex in solution This result, coupled with a monolayer dielectric constant of 50 3 ± 6 9, suggests that the film is highly solvated and permeable to electrolyte ions Cyclic voltammetry at scan rates up to 4000 V s^{-1} has been used to probe the rate of heterogeneous electron transfer across the monolayer/microelectrode interface Modeling the complete cyclic voltammogram suggests that redox switching proceeds via a nonadiabatic through-bond tunneling mechanism Significantly, protonating the tetrazine ligand decreases the standard heterogeneous electron-transfer rate constant by 1 order of magnitude from (1 15 ± 0 25) × 10^4 to (0 12 ± 0 02) × 10^4 s^{-1} This observation is consistent with mediating electronic states within the bridging ligand (superexchange) playing an important role in the redox switching process Specifically, the results suggest that hole transfer is mediated through the highest occupied molecular orbital (HOMO) of the tetrazine ligand Protonating the bridge increases the energy difference between the bridge states and the $Os^{2+/3+}$ redox reaction Therefore, protonation causes the standard rate constant to decrease

Acknowledgment Financial support from Enterprise Ireland, the Irish Science and Technology Agency, under the Basic Research Programme is gratefully acknowledged The generous loan of potassium hexachloroosmate(IV) by Johnson Matthey under the loan scheme is deeply appreciated

References and Notes

(1) Bixon M Jortner J Michel Beyerle M E *Biochim Biophys Acta* **1991** *301* 1056
(2) Wasielewski M R *Chem Rev* **1992** *92* 345
(3) Weaver M J *Chem Rev* **1992** *92* 463
(4) Forster, R J *J Electrochem Soc* **1997** *144* 1165
(5) McConnell H M *J Chem Phys* **1961**, *35* 508
(6) Forster R J *Inorg Chem* **1996** *35* 3394
(7) Keyes T E Forster R J Jayaweera P M Coates C G McGarvey J J Vos, J G *Inorg Chem* **1998** *22* 5925
(8) Chidsey C E D *Science* **1991** *251* 919
(9) Miller C Gratzel M *J Phys Chem* **1991**, *95* 5225
(10) Bixon M Jortner J *J Phys Chem* **2000** *104* 3906
(11) Forster R J Keyes T E Bond A M *J Phys Chem B* **2000**, *104* 6839
(12) Laviron, E *J Electroanal Chem* **1974** *52* 395
(13) Brown A P Anson F C *Anal Chem* **1977** *49* 1589
(14) Forster R J Faulkner L R *J Am Chem Soc* **1994** *116* 5444
(15) Forster R J Vos J G Keyes T E *Analyst* **1998** *123* 1905
(16) Feldberg S W Rubinstein I *J Electroanal Chem* **1988** *240* 1
(17) Trassati S *J Electroanal Chem* **1974** *53* 335
(18) Bard A J Faulkner L R *Electrochemical Methods Fundamentals and Applications* Wiley New York 1980
(19) Forster R J Keyes T E *J Phys Chem B* **1998** *102* 10004
(20) Forster R J O Kelly J P *J Electrochem Soc* in press
(21) Goodwin H A Kepert D L Patrick J M Skelton, B W White A H *Aust J Chem* **1984**, *37* 1817
(22) Ferguson J E Love, J L Robinson W T *Inorg Chem* **1972** *11*, 1662
(23) Creager S E Rowe G K *Anal Chim Acta* **1991** *246* 233
(24) Rowe G K Creager S E *Langmuir* **1991** *7* 2307
(25) Nagamura T Sakai K *J Chem Soc Faraday Trans* **1988**, *84* 3529
(26) Forster R J O Kelly J P *J Phys Chem* **1996** *100* 3695
(27) Smith, C P , White, H S *Anal Chem* **1992** *64* 2398
(28) Smith C P White H S *Langmuir* **1993** *9* 1

(29) Bryant M A Crooks R M *Langmuir* **1993** *9* 385
(30) Brolo A G Irish D E Szymanski G Lipkowski J *Langmuir* **1998** *14* 517
(31) Cheng J Saghi Szabo G Tossell J A Miller C J *J Am Chem Soc* **1996** *118*, 680
(32) Bagchi G *Annu Rev Chem* **1989** *40*, 115
(33) Sutin N *Acc Chem Res* **1982** *15* 275
(34) Barr S W Guyer K L Li T T T Liu H Y Weaver M J *J Electrochem Soc* **1984** *131* 1626
(35) Sutin N Brunschwig B S *ACS Symp Ser* **1982** *198* 105
(36) Finklea H O Hanshew D D *J Am Chem Soc* **1992**, *114* 3173
(37) Weber K Creager, S E *Anal Chem* **1994** *66* 3164
(38) Tender L Carter M T Murray R W *Anal Chem* **1994**, *66*, 3173
(39) Forster R J Loughman P J Figgemeier E Lees A C Hjelm J Vos J G *Langmuir* **2000** *16* 7871
(40) Forster R J Loughman P J Keyes T E *J Am Chem Soc* in press
(41) Marcus R A *J Phys Chem* **1963** *67* 853
(42) Ebert K Ederer H Isenhour T L *Computer Applications in Chemistry An Introduction for PC Users* VCH Publishers New York 1989
(43) Barigelletti, F De Cola L Balzani V Hage R Haasnoot J G Reedijk J Vos J G *Inorg Chem* **1989** *28* 4344

ARTICLE IN PRESS

ELSEVIER

Journal of Electroanalytical Chemistry

Journal of Electroanalytical Chemistry 00 (2002) 1–10

www elsevier com/locate/jelechem

Redox switching in solid deposits triazole bridged osmium dimers

Darren A Walsh [a], Tia E Keyes [b], Robert J Forster [a,*]

[a] National Centre for Sensor Research School of Chemical Sciences Dublin City University Dublin 9 Ireland
[b] School of Chemistry Dublin Institute of Technology Dublin 8 Ireland

Received 8 February 2002 received in revised form 18 June 2002 accepted 6 July 2002

Abstract

Solid deposits of the dimeric complex $[Os(bpy)_2Cl$ 4 bpt $Os(bpy)_2Cl]PF_6$ where bpy is 2,2′ bipyridyl and bpt is 3 5 bis(pyridin 4 yl) 1 2 4 triazole have been deposited onto platinum microelectrodes These layers exhibit unusually ideal electrochemical responses over a wide range of electrolyte compositions and *pH* values Scanning electron microscopy reveals that repeated switching of the redox composition of these layers does not induce any significant structural change within the deposits Cyclic voltammetry (CV) has been used to determine the apparent charge transport diffusion coefficient, D_{CT}, describing homogeneous charge transport through the deposit D_{CT} is independent of the electrolyte concentration suggesting that electron self exchange between adjacent redox centres limits the overall rate of charge transport through the solid In 1 0 M $LiClO_4$ and 1 0 M $HClO_4$ D_{CT} values of $2\,0 \pm 0\,1 \times 10^{-10}$ and $1\,7 \pm 0\,4 \times 10^{-10}$ $cm^2\ s^{-1}$ are observed, corresponding to second order electron transfer rate constants of $1\,8 \times 10^7$ and $3\,0 \times 10^7$ $M^{-1}\ s^{-1}$, respectively The rate of heterogeneous electron transfer across the electrode | deposit interface has been determined using fast scan CV The standard heterogeneous electron transfer rate constant, k°, is $1\,5 \pm 0\,1 \times 10^{-4}$ s^{-1} irrespective of the electrolyte pH Significantly this value is less than one order of magnitude smaller than that determined for a monomeric complex containing the same bridging ligand and redox active metal centre © 2002 Published by Elsevier Science B V

Keywords Solid state voltammetry Osmium dimers Charge transport Electron transfer dynamics Resistance

1 Introduction

The dynamics of electron transfer and mass transport processes within solids have been investigated only relatively recently [1,2] This situation is striking given the pivotal roles that solid-state redox active materials play in devices including optical detectors, energy storage, molecular electronics, catalysts and sensors [3–8] However, these applications demand that the redox composition of the solid can be switched rapidly in response to an applied potential, i e diffusion of charge compensating counterions through the solid must be rapid compared to electron self-exchange between adjacent centres Osmium complexes ought to be particularly useful in this regard because of their stability in numerous oxidation states and very large self-exchange rate constants [9 10] We recently demonstrated that the rate determining step for charge transport through solid deposits of $[Os(bpy)_2$ 4-bpt Cl] is limited by counterion diffusion rather than electron self-exchange [11] However using complexes with bulkier side groups appears to increase the free volume within the solid deposit facilitating rapid redox switching rates and electron self-exchange as the rate determining step [12] An alternative approach is to create dumb-bell shaped molecules by linking two redox active metal centres through an electrochemically innocent bridge Solid deposits of materials of this kind could then be used to investigate the relative contributions from both through-space and bridge mediated electron transfer processes

In this contribution, we report on solid-state deposits of the dimeric complex $[Os(bpy)_2Cl$ 4-bpt $Os(bpy)_2Cl]PF_6$ (Scheme 1) that are mechanically attached to a platinum microelectrode This complex is insoluble in water allowing the solid state redox properties to be

* Corresponding author Tel +353 1 7045943 fax +353 1 7045503
E mail address robert forster@dcu ie (R J Forster)

0022 0728/02/$ see front matter © 2002 Published by Elsevier Science B V
PII S0022 0728(02)01060 4

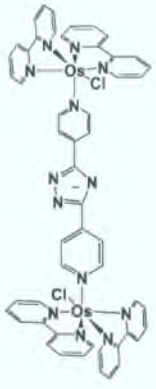

Scheme 1.

examined when the deposits are in contact with an aqueous electrolyte. These deposits exhibit unusually ideal voltammetric responses for the $Os^{2+/3+}$ redox reaction. Another attractive feature of these dimers is that the triazole bridge is capable of undergoing protonation/deprotonation reactions. In this way, the extent of electronic communication between the metal centres can be reversibly modulated. The remarkable ideality of the voltammetric response of these materials allows us to obtain an insight into charge transfer within the solid deposit as the concentration of the supporting electrolyte is systematically varied at both high and low pH values. Moreover, at high voltammetric scan rates, the rate of electron transfer across the deposit | electrode interface influences the observed response allowing the standard heterogeneous electron transfer rate constant, k°, to be determined. Significantly, the k° value obtained for mechanically attached solid deposits is approximately one order of magnitude smaller than that determined for monolayers in which $[Os(bpy)_2Cl]^+$ centres are linked to an electrode surface using the same bpt bridge [13]. These studies provide an insight into how the method of attachment of molecular materials onto metal substrates affects the rate of interfacial electron transfer.

2. Experimental

2.1. Synthesis and characterisation

2.1.1. $[Os(bpy)_2Cl$ 4-bpt $Os(bpy)_2Cl](PF_6)_2$

$[Os(bpy)_2$ 4-bpt Cl$]PF_6$ was synthesised as described previously [13]. $[Os(bpy)_2$ 4-bpt $Os(bpy)_2Cl_2](PF_6)_2$ was synthesized by dissolving $[Os(bpy)_2$ 4-bpt Cl$]PF_6$ (0.503 g, 0.56 mmol) in 50 cm^3 of EtOH and heating to reflux. A molar equivalent of $[Os(bpy)_2\ Cl_2]$ (0.314 g, 0.55 mmol) was dissolved in 30 cm^3 of EtOH and added in three lots to the refluxing solution. The solution was then refluxed for a further 36 h. After cooling, a concentrated solution of aqueous NH_4PF_6 was added to precipitate the dark purple–brown complex. The product was recrystallised by dissolving the complex in 50:50 C_3H_6O + water in the presence of a small amount of acid to ensure complete protonation of the 4-bpt bridge, followed by slow evaporation of the organic solvent. Yield: 0.724 g, 83%. The purity of the recrystallised product was confirmed using cation exchange HPLC (single peak, retention time 5.4 min) and elemental analysis (Calc. for $C_{52}H_{40}Cl_2F_{12}N_{13}Os_2P_2$: C, 39.3; H, 2.5; N, 11.4. Found: C, 39.2; H, 2.7; N, 11.3%). ^{1}H-NMR data (CD_3CN): bipyridyl, H3 (d), 8.47–8.52, H^4 (t), 7.84–7.89, H^6 (d), 7.62–7.64, H^5 (t), 7.28–7.32, 4bpt, H^2, 9.43 (d), H^3, 8.50 (dd), H^5 7.96–7.92 (dd), H^6 9.93, $H^{2''}$, 7.54 (dd) $H^{3''}$, 8.17 (d), $H^{5''}$, 8.23 (d), $H^{6''}$, 7.78.

2.2. Instrumentation

Microelectrodes were prepared using platinum microwires of radii between 1 and 25 μm sealed in a glass shroud that were mechanically polished as described previously [14]. Electrochemical cleaning of the electrodes was carried out by cycling in 0.1 M H_2SO_4 between potential limits chosen to oxidize initially and then to reduce the surface of the platinum electrode. Excessive cycling was avoided in order to minimize the extent of surface roughening.

Cyclic voltammetry (CV) was performed using a CH Instruments Model 660 electrochemical workstation and a conventional three electrode cell. All solutions were deoxygenated thoroughly using nitrogen, and a blanket of nitrogen was maintained over the solution during all experiments. Potentials are quoted with respect to a BAS Ag | AgCl gel-filled reference electrode in which the electrolyte concentration is 3.0 M NaCl. All experiments were performed at room temperature (22 ± 3 °C).

Two approaches were used to transfer the solid onto the surface of the working electrode. In the first method, the solid was transferred from a filter paper onto the surface of the electrode by mechanical abrasion. This process caused some of the complex to adhere to the surface as a random array of microparticles. In the second approach that was used to achieve high surface coverages, a drop of Milli-Q water was first added to the complex before applying the material to the electrode surface as a paste. Prior to electrochemical measurements the paste was allowed to dry. Deposits prepared by both methods give indistinguishable electrochemical responses. The stability of the solid deposits prepared by the two methods is comparable. After use, the electrode surface was renewed by polishing using aqueous slurry of 0.05 μm alumina.

Scanning electron microscopy (SEM) was performed using a Hitachi S-3000N system. For SEM investigations, deposits were formed on 3 mm radius graphite disks that were mounted directly in the microscope. In

electrochemical investigations, the modified disks were cycled electrochemically and then the layers were allowed to soak in electrolyte free Milli-Q water for at least 30 min before being washed copiously and then dried in a vacuum dessicator for several hours

UV–vis spectra for the solid state deposits were recorded using a Nikon Eclipse ME600 microscope equipped with both a 100W halogen lamp and a 100 W mercury arc source The films were deposited on conducting glass slides (ITO) and were positioned against a water-immersion objective (10 × magnification) and observed through the microscope An Ag | AgCl reference electrode and a large area platinum wire completed the three electrode electrochemical cell Spectra were recorded using an Andor Technology gated intensified CCD coupled to an Oriel model MS125 spectrograph fitted with a 600 lines/in grating Typically the gate width was 2 ms and for surface coverages less than 1×10^{-7} mol cm^{-2}, signal averaging was necessary The potential of the working ITO electrode was controlled using a CH Instruments Model 660 electrochemical workstation A Dell Dimension Pentium PC was used for data acquisition and analysis

3 Results and discussion

3 1 Break-in phenomena

Fig 1 illustrates the initial voltammetric response obtained when a solid deposit of [Os(bpy)$_2$Cl 4-bpt Os(bpy)$_2$Cl]PF$_6$ is first voltammetrically cycled in 80 20 H$_2$O + acetonitrile where the supporting electrolyte is 0 1 M LiClO$_4$ During these initial scans, the peak shape

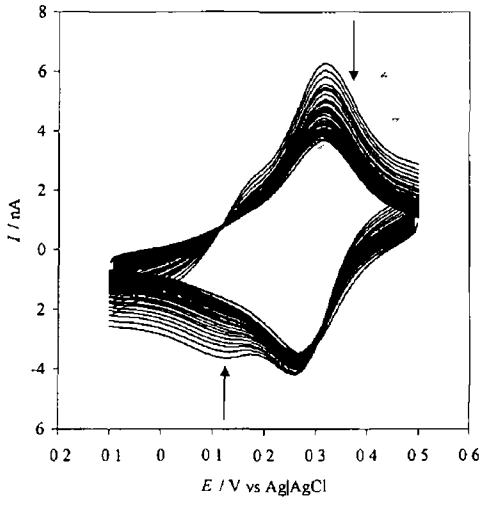

Fig 1 First 50 sweeps of a voltammetric cycle for a solid state [Os(bpy)$_2$ 4bpt Os(bpy)$_2$Cl$_2$](PF$_6$)$_3$ deposit attached to a 25 μm radius platinum microelectrode The supporting electrolyte is 0 1 M LiClO$_4$ containing 20% acetonitrile The scan rate is 0 2 V s^{-1}

changes and the anodic peak current, I_{pa}, decreases by approximately 40% while the cathodic peak current, I_{pc}, decreases by approximately 15% Significantly, after approximately 50 scans, the response no longer changes when the deposit is repeatedly cycled and remains stable for more than 24 h The observation that the greatest decrease is observed in I_{pa} suggests that the changes observed may be linked to transport of charge compensating perchlorate ions into the deposit However, differences in solubility of the oxidized and reduced forms, as well as redox driven structural changes may also contribute to the observed behaviour

SEM has been used to probe whether cycling the redox composition of the solid deposits changes their morphology SEM images have been obtained after solid deposits have been repeatedly cycled for up to 2000 scans at 0 1 V s^{-1} Fig 2A shows that, prior to voltammetric cycling, the deposits are unstructured and show no evidence of being macroscopically crystalline Fig 2B and C reveal that after cycling the layers in both neutral (1 0 M LiClO$_4$) and low pH electrolytes (1 0 M HClO$_4$) the deposits remain in a non-crystalline, amorphous state This behaviour contrasts sharply with that found for the corresponding monomer [Os(bpy)$_2$ 4-bpt Cl]PF$_6$, which electrocrystallised when cycled in 1 0 M HClO$_4$ [11] It is perhaps significant that the overall charge is significantly higher for the oxidised dimer, i e +3 at high pH and, because the triazole ligand can be protonated, +4 at low pH The corresponding charges for the monomer are +1 and +2 Therefore, greater electrostatic repulsion as well as the greater difficulty of achieving efficient close packing in the dimers may inhibit electrocrystallisation However, the most significant result of Fig 2 is that the changes observed in the voltammetry when the deposits are first cycled, do not correspond to a significant change in the morphology of the deposits

3 2 General electrochemical properties

Fig 3A illustrates the voltammetric response obtained for a 2 mM solution of [Os(bpy)$_2$Cl 4-bpt Os (bpy)$_2$Cl]$^+$ dissolved in acetonitrile where the supporting electrolyte is 0 1 M LiClO$_4$ For the dimer dissolved in solution, two, electrochemically reversible, waves are observed with formal potentials of 0 320 and 0 760 V These redox waves correspond to the metal based $Os^{2+/3+}$ redox reaction Since the dinuclear complex is highly symmetric, only electrostatic interactions, solvation energies and the extent of electronic coupling across the 4-bpt bridge are likely to be responsible for the relatively large separation between the two formal potentials [15]

Fig 3A also illustrates the voltammetric response observed for a solid deposit of the complex after approximately 50 repetitive scans Significantly, only a single redox process is observed even when the positive

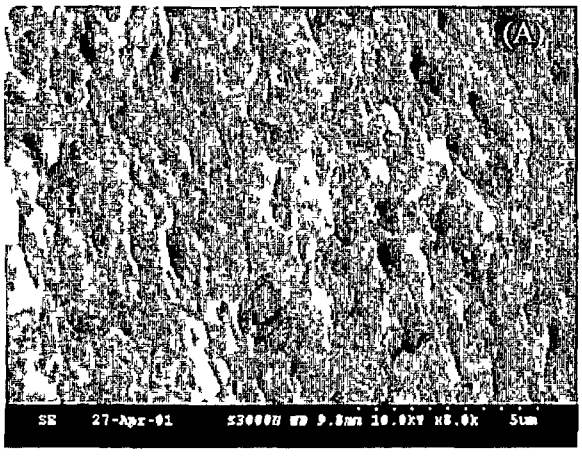

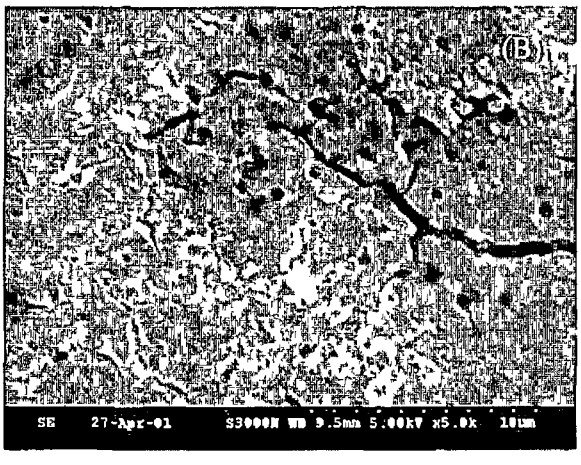

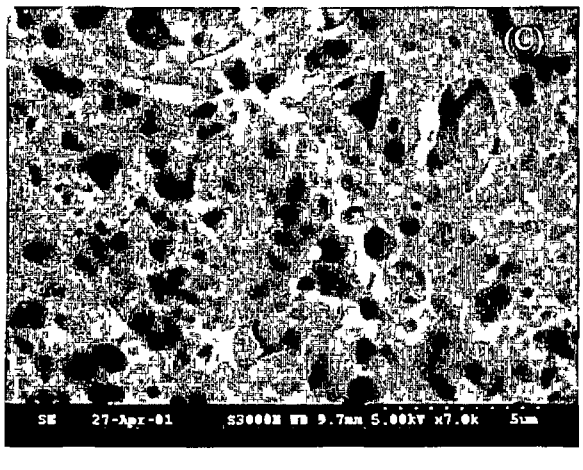

Fig 2 SEM images of a 3 mm radius graphite disk modified with a mechanically attached layer of $[Os(bpy)_2$ 4bpt $Os(bpy)_2Cl_2](PF_6)_3$ (A) is the deposit prior to voltammetric cycling (B) is after 2000 scans in 1 0 M $LiClO_4$ and (C) is after 2000 scans in 1 0 M $HClO_4$ Electrochemical scans were performed at 100 mV s^{-1} between −100 and +800 mV vs Ag | AgCl

potential limit is extended to 1 200 V However, the response observed is unusually ideal for a solid deposit and is similar to that found for the complex dissolved in acetonitrile For example, as expected for a reversible electrochemical process under semi-infinite diffusion control, the peak currents increase linearly with increasing square root of the scan rate, v Also, the peak-to-peak separation, ΔE_p, and the difference between the peak potential, E_P, and half-peak potential, $E_{p/2}$, are both 57 ± 3 mV Significantly, these values are consistent with a reversible electrochemical reaction involving the transfer of a single electron Therefore, it appears that only one of the osmium sites within the dimer can be oxidized when the complex is immobilized within a solid deposit This behaviour could arise because of increased electrostatic interactions due to the close proximity of adjacent redox centres in the solid deposit or from a relatively high Gibbs energy barrier to anion insertion into the solid The formal potential of the $Os^{2+/3+}$ couple is 40 ± 5 mV less positive for the solid deposit compared to the dimer dissolved in acetonitrile This result indicates that oxidizing the metal centre is thermodynamically more facile when the dimer is immobilised within a solid deposit However, while this behaviour suggests that the Gibbs energy barrier to anion insertion is not significant, the small differences in E° observed most likely reflect a higher dielectric constant within the solid deposit than that of acetonitrile This result suggests that redox centres within the deposit are at least partially solvated which is consistent with the nearly ideal voltammetry illustrated in Fig 3A

Fig 3B illustrates the electrochemical response of solid deposits of $[Os(bpy)_2Cl$ 4-bpt $Os(bpy)_2Cl]^+$ when they are cycled in either entirely aqueous 0 1 M $LiClO_4$ or 80 20 H_2O+ACN containing 0 1 M $LiClO_4$ as supporting electrolyte Even where the electrolyte solution contains 20% v/v acetonitrile, I_{p}, and I_{pc} change by less that 10% over an 8 h period suggesting that significant dissolution does not occur At this scan rate, the voltammetric response observed for the deposit in contact with the solution containing the organic solvent is sharper (FWHM is 135 ± 5 mV compared to 190 ± 10 mV in the absence of acetonitrile) and the peak shape is consistent with mixed semi-infinite linear diffusion and finite diffusion control These observations suggest that the rate of charge transport through the deposit is faster when the contacting solution contains acetonitrile

3 3 *Potential dependent UV–vis spectroscopy*

Since these deposits consist of discrete particles, not all of which may be in direct electrical contact with the electrode, it is important to determine what percentage of the deposit is electrochemically active In this way, an insight can be obtained into the extent to which

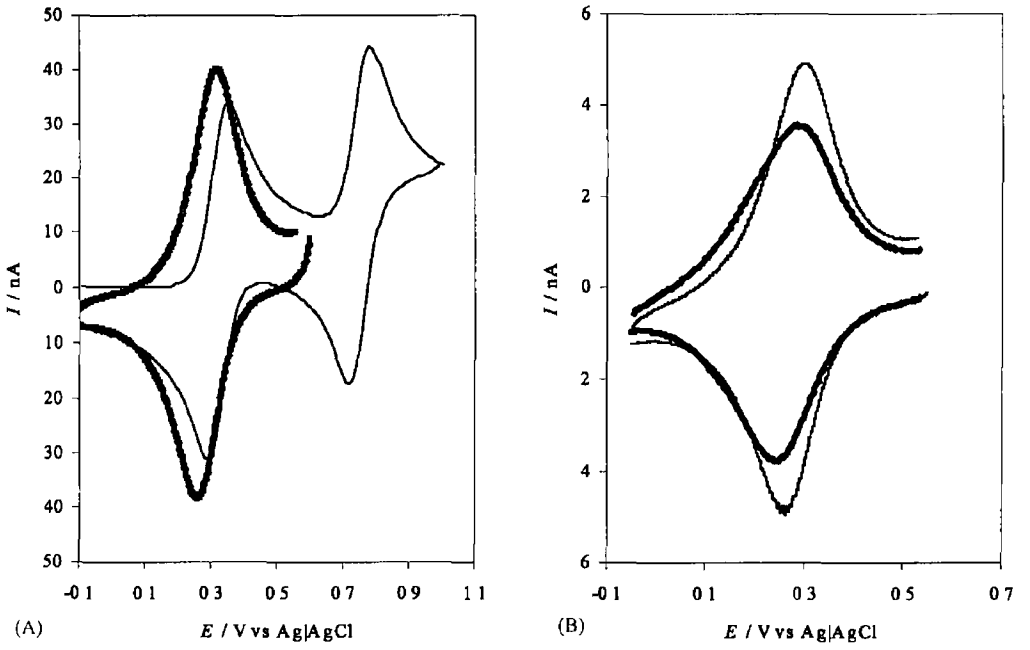

Fig 3 (A) Cyclic voltammograms for 1 2 mM solution (thin line) of $[Os(bpy)_2\ 4bpt\ Os(bpy)_2Cl_2]$ at a scan rate of 1 5 V s^{-1} (thin line) and a solid state layer of $[Os(bpy)_2\ 4bpt\ Os(bpy)_2Cl_2]$ (thick line) mechanically attached to a 25 μm radius Pt microelectrode at a scan rate of 2 V s^{-1} (B) Cyclic voltammograms for an $[Os(bpy)_2\ 4bpt\ Os(bpy)_2Cl_2]$ $(PF_6)_3$ deposit that is mechanically attached to a 25 μm radius platinum microelectrode in aqueous 0 1 M $LiClO_4$ (thick line) and in 0 1 M $LiClO_4$ containing 20% acetonitrile (thin line) The scan rate is 0 2 V s^{-1}

individual particles are interconnected Potential dependent UV–vis spectroscopy represents a convenient approach to probing this issue Fig 4 illustrates the changes in the UV–vis spectrum that occur during electrolysis of a solid state deposit in aqueous 1 0 M $LiClO_4$ at +0 600 V All changes are completely reversible, i e the peak intensities return to greater than 95% of their initial value when the deposit is oxidised and then re-reduced This behaviour persists over at least five potential cycles The surface coverage determined from the background corrected charge passed in the 5 mV s^{-1} anodic branch of the voltammogram is approximately 5×10^{-8} mol cm^{-2} Prior to oxidation, the deposit shows strong absorbances between 330 and 530 nm that are attributed to Os (dπ) to bpy and bpt (π*) MLCT transitions The dashed line of Fig 4 shows the spectrum obtained for the complex dissolved in acetomitrile and indicates that the spectroscopic transitions and relative peak intensities of the solid deposits are generally consistent with those observed for the complex in solution However, the absorption maxima are typically shifted to lower energy by approximately 10 nm for the solid deposits Consistent with oxidation of the Os^{2+} centres, the intensities of the MLCT bands decrease systematically with increasing electrolysis time Significantly, despite the fact that this deposit is less than a 1 μm thick, the spectrum changes continuously for periods up to 40 s suggesting that solid state charge transport is relatively slow in this system The inset of Fig 4 shows the absorbance (490 nm) versus time profile for the deposit and indicates that even for very long electrolysis times the absorbance at 490 nm never decays to zero This behaviour contrasts with previously reported systems where exhaustive electrolysis caused complete collapse

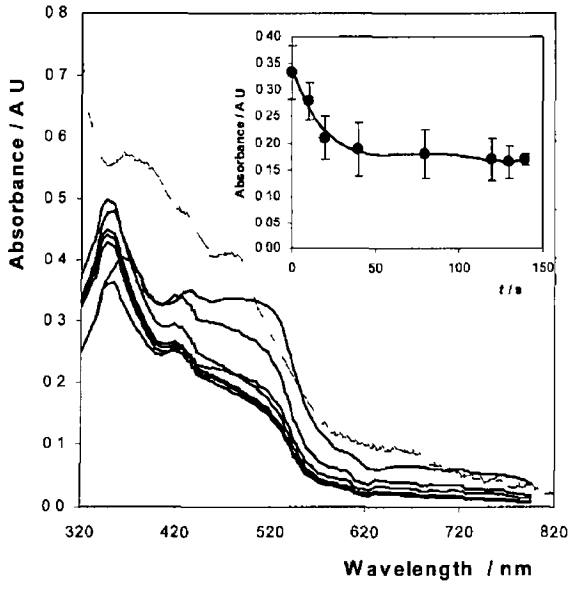

Fig 4 Time dependent changes in the UV–vis spectrum of a solid state $[Os(bpy)_2\ 4bpt\ Os(bpy)_2Cl_2](PF_6)_3$ deposit attached to an ITO electrode when electrolysed at +0 600 V in 1 0 M $LiClO_4$ From top to bottom the spectra represent electrolysis times of 0 10 20 40 80 120 and 140 s The inset shows a plot of the absorbance at 490 nm vs time

of the MLCT wave [11] The observation that exhaustive electrolysis decreases the absorbance to approximately 50% of its initial value is significant and supports the voltammetric data presented earlier which suggested that only one Os^{2+} site within the dimer is oxidized for the solid deposits Moreover, this observation suggests that the individual particles are highly interconnected and that close to 100% of the immobilised particles are electrochemically active, at least on a hundreds of seconds timescale

3 4 *Effect of electrolyte pH*

The 4-bpt bridge is capable of undergoing a protonation/deprotonation reaction which will influence both the strength of electronic coupling between the two metal centies and the overall charge on the complex There have been surprisingly few studies on the impact of protonation reactions on the structure of solid state materials This situation is striking because careful studies on biosystems have proven that both the secondary structure and hydrogen bonding play critical roles in dictating the efficiency of long-range electron transfer [16] Fig 5 illustrates the voltammetric response obtained for solid deposits of the dimers in 0 1 M $HClO_4$ and 0 1 M $LiClO_4$ where the solvent is 80 20 H_2O + ACN The peak shapes observed at each pH are similar and do not change significantly upon repetitive cycling in either electrolyte However, in low pH electrolyte, the formal potential is approximately 35 mV more positive than that found in near neutral electrolyte The observation that $E^{\circ\prime}$ is more positive in low pH electrolyte

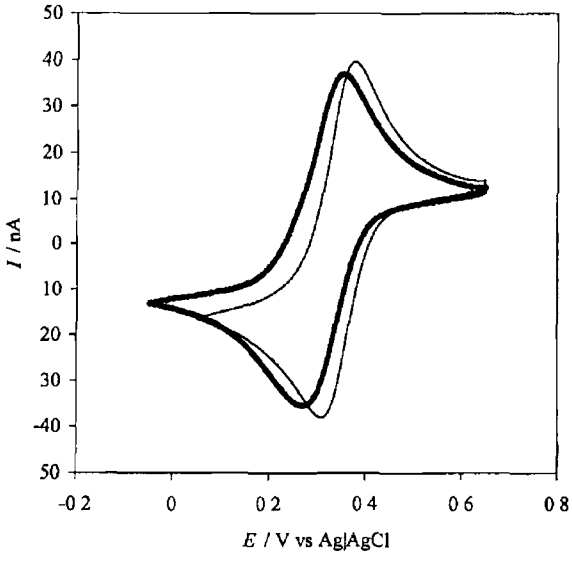

Fig 5 Cyclic voltammograms for an $[Os(bpy)_2$ 4bpt $Os(bpy)_2Cl_2](PF_6)_3$ deposit that is mechanically attached to a 12 5 μm radius platinum microelectrode in 0 1 M $LiClO_4$ containing 20% acetonitrile (thick line) and in 0 1 M $HClO_4$ containing 20% acetonitrile (thin line) The scan rate is 2 0 V s^{-1}

indicates that the Os^{2+} centres are thermodynamically more difficult to oxidise when the 4-bpt ligand is protonated A reduced electron donating ability of the protonated ligand and the higher overall positive charge within the layer are likely to contribute to this effect

3 5 *Resistance and interfacial capacitance*

When attempting to extract quantitative data from voltammetric data, e g formal potential, charge transport diffusion coefficients or heterogeneous electron transfer rate constants, it is important to consider the effects of both the electrode response time and ohmic effects Also, by examining the resistance as a function of the supporting electrolyte concentration, it ought to be possible to obtain a limited insight into the permeability of the deposit towards electrolyte ions When a polycationic deposit is placed in a dilute solution of a strong electrolyte, the concentration of counterions (PF_6 in this case) within the deposit is typically considerably larger than that found in the contacting solution For the deposits considered here, the anion concentration initially present in the deposit is expected to be between 1 5 and 3 M depending on the extent of protonation of the 4-bpt ligand Thus, under the influence of the concentration gradient, counterions may diffuse from the deposit into the solution until the concentrations become equal in the two phases However, if diffusion of charged counterions occurs, then electroneutrality within the deposit would be violated, and an electrical potential would develop at the interface This 'Donnan potential' would then increase until equilibrium was reached in which it completely opposes the tendency of the counterions to move down the concentration gradient Under these equilibrium conditions the net diffusion of counterions across the interface would be zero, and co-ions would be excluded from the solid deposit [17]

We have probed the existence of such a permselective response for these solid deposits by determining the contribution of the deposit resistance to the total cell resistance as the supporting electrolyte concentration is changed In the case of an ideally permselective response, ions would be effectively excluded from the membrane, and the deposit resistance would be independent of the supporting electrolyte concentration To determine the total cell resistance, we have performed short timescale, small amplitude, potential step chronoamperometry, in a potential region where no Faradaic response is observed In a typical experiment, the potential was stepped from −50 to 0 mV at both bare and modified microelectrodes, and the resulting current was recorded over the following 20 μs This capacitive current versus time transient can be described by Eq (1) [18]

$$I_c(t) = (\Delta E/R)\exp(-t/RC_{dl}) \quad (1)$$

where ΔE is the pulse amplitude, R is the total cell resistance, and C_{dl} is the integral double layer capacitance For both modified and bare electrodes, the current decays in time according to a single exponential, which is consistent with double layer charging alone [17] Fig 6 illustrates $I_c(t)$ versus t and semi-log current versus time plots for the solid deposits as the lithium perchlorate concentration is changed from 0 1 to 0 5 to 1 0 M The absolute slope of the semi-log plots represents the reciprocal of the cell time constant RC_{dl} Table 1 presents RC_{dl} values for an electrode before, and after modification with the dimer as a function of the perchlorate concentration This table shows that both the bare and the modified electrode cell time constants decrease with increasing electrolyte concentration as expected [17] However, the response time is considerably more sensitive to the supporting electrolyte concentration for the microelectrode coated with the solid deposit It is apparent from Eq (1) that R can be extracted from the intercepts of the semi-log plots shown in Fig 6 Fig 7 shows the total cell resistance for a bare and a coated electrode as the perchlorate concentration is changed from 0 1 to 1 0 M It is apparent that in both circumstances R is reduced at high electrolyte concentrations reflecting a reduced solution resistance Significantly, for perchlorate concentrations greater than about 0 5 M, the total cell resistance with and without the deposit are indistinguishable This result suggests that, for relatively high electrolyte concentrations, the deposit resistance is low probably because electrolyte can permeate the individual particles that exist on the microelectrode surface, vide infra

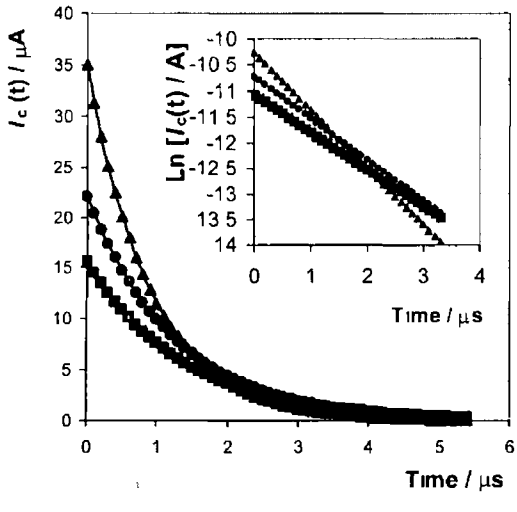

Fig 6 Current–time transients for a 25 μm radius platinum microelectrode modified with an $[Os(bpy)_2$ 4bpt $Os(bpy)_2Cl_2](PF_6)_3$ deposit following potential steps from −0 050 to 0 000 V From top to bottom the data correspond to aqueous 0 1 0 5 and 1 0 M $LiClO_4$ as supporting electrolyte The inset illustrates the corresponding semi log current vs time plots

3 6 Homogenous charge transport rates

The well-defined metal-based oxidation observed for this solid deposit makes them attractive systems for investigating the dynamics of charge transport in the solid state To achieve this objective, CV has been used to determine apparent diffusion coefficients as the concentration of supporting electrolyte is varied systematically Figs 8 and 9 show how the voltammetric responses obtained for solid deposits change as the scan rate is varied systematically from 200 to 800 mV s^{-1} in acidic and neutral electrolytes, respectively For this range of scan rates, as illustrated in the figure insets, the voltammetric peak currents increase as $v^{1/2}$ This behaviour is consistent with semi-infinite linear diffusion control in which the deposit is not exhaustively electrolysed and the depletion zones remain within individual microparticles Under these circumstances, the peak current, I_p, can be described in terms of the Randles–Sevçik equation

$$I_p = 2\,69\times10^5 n^{3/2} A D_{CT}^{1/2} c_{eff} v^{1/2} \quad (2)$$

where n is the number of electrons transferred, A is the area of the working electrode, D_{CT} is the apparent diffusion coefficient and c_{eff} is the effective fixed site concentration of the redox centre Previous studies on structurally related systems and crystallographic data suggest that the fixed site concentration is $1\,7\pm0\,05$ M [11,19] Analysing the data presented in Figs 8 and 9 using this approach, yields D_{CT} values of $2\,0\pm0\,6\times10^{-10}$ and $2\,0\pm0\,5\times10^{-10}$ cm^2 s^{-1} in 1 0 M $LiClO_4$ and 1 0 M $HClO_4$, respectively While these diffusion coefficients are large for solid deposits, they are still many orders of magnitude smaller than those found for the complex dissolved in solution, $5\,6\pm1\,1\times10^{-6}$ cm^2 s^{-1} These relatively small diffusion coefficients are likely to limit the technological exploitation of materials of this kind significantly For example, under semi-infinite linear diffusion conditions it would take approximately 15 s to switch a 1 μm thick film from one oxidation state to another

In this system, the physical structure of the deposit does not appear to change significantly as the oxidation state is switched Under these circumstances, homogenous charge transport through the deposit is limited either by electron self-exchange between the osmium sites or counterion diffusion through the solid If electron self-exchange is the rate determining step, charge compensating counterions must be freely available within the deposit and D_{CT} is expected to depend at best only weakly on the electrolyte concentration Significantly, Table 2 shows that D_{CT} does not depend

Table 1
Resistance R double layer capacitance C_{dl} and electrode response times RC for 25 μm radius platinum microelectrodes before and after modification with a solid deposit of $[Os(bpy)_2$ 4bpt $Os(bpy)_2Cl_2](PF_6)_3$ as the concentration of $LiClO_4$ is systematically varied [1]

$[LiClO_4]$/M	Bare			Modified		
	R/Ω	$C_{dl}/\mu F$	$RC_{dl}/\mu s$	R/Ω	$C_{dl}/\mu F$	$RC_{dl}/\mu s$
0 0	2400(192)	5 89(0 53)	1 41(0 25)	3169(253)	4 10(0 23)	1 29(0 18)
0 1	2200(188)	6 28(0 50)	1 38(0 23)	3212(198)	4 64(0 21)	1 49(0 17)
0 2	2056(132)	6 48(0 58)	1 33(0 21)	3034(215)	5 05(0 28)	1 53(0 19)
0 4	1877(140)	7 06(0 14)	1 32(0 12)	2800(184)	5 60(0 33)	1 56(0 20)
0 6	1700(119)	7 06(0 28)	1 20(0 13)	1890(195)	5 44(0 16)	1 02(0 14)
0 8	1550(15 5)	7 46(0 74)	1 15(0 12)	1636(156)	5 89(0 14)	0 95(0 10)
1 0	1400(70)	8 24(0 49)	1 15(0 13)	1475(35)	6 41(0 31)	0 94(0 07)

[1] The numbers in parentheses represent errors obtained from at least three independent experiments

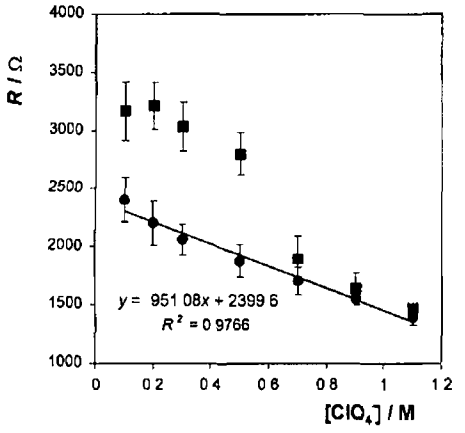

Fig 7 Dependence of the total cell resistance R on the concentration of $LiClO_4$ is supporting electrolyte Data for a bare 25 μm radius platinum microelectrode are shown on the lower curve (●) while the upper curve is for the same microelectrode modified with an $[Os(bpy)_2$ 4bpt $Os(bpy)_2Cl_2](PF_6)_3$ solid deposit (■)

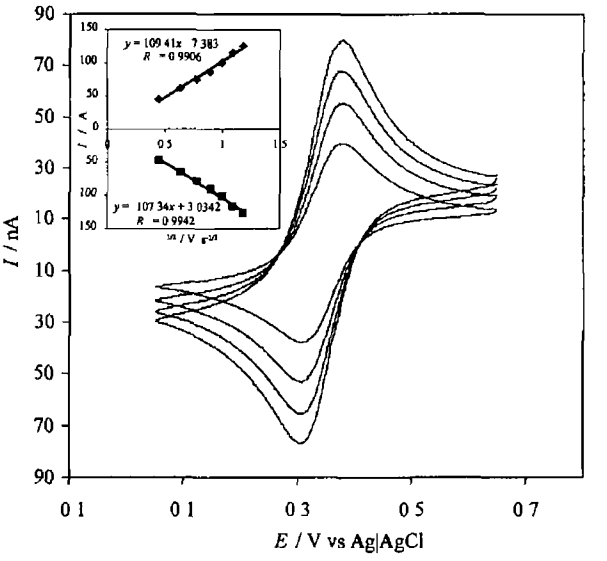

Fig 8 Scan rate dependence of the voltammetric response for a deposit of $[Os(bpy)_2$ 4bpt $Os(bpy)_2Cl_2](PF_6)_3$ formed on a 25 μm radius platinum microelectrode The supporting electrolyte is 0 1 M $HClO_4$ containing 20% acetonitrile From top to bottom the scan rates are 800 600 400 and 200 mV s^{-1} Inset I_p vs v for these deposits

on the concentration of electrolyte in either $LiClO_4$ or $HClO_4$ This observation suggests that ion transport is facile and that the rate of charge transport is limited by the rate of electron self-exchange between Os^{2+} and Os^{3+} couples within the deposit Moreover, the fact that D_{CT} is not influenced by the protonation state of the 4-bpt, suggests that the 'through-space' electronic communication between adjacent metal centres is substantially stronger than the 'through-bond' interaction occurring across the bridging ligand

The Dahms Ruff expression allows the second order rate constant, k_{SE}, describing the dynamics of self-exchange between adjacent $Os^{2+/3+}$ moieties, to be determined

$$D_{CT} = D_{phys} + 1/6k_{SE}\delta^2 c_{eff} \quad (3)$$

where D_{phys} described physical diffusion in the absence of electron hopping and δ is the inter-site separation between adjacent redox centres Given that the osmium redox centres are immobilised within a solid deposit, D_{phys} is assumed to be zero The inter-site separation is estimated from the X-ray crystal structure as a through-space distance of 13 4 Using these values, Eq (3) yields rate constants for electron self-exchange of $1\,8 \times 10^7$ and $3\,0 \times 10^7$ M^{-1} s^{-1} at pH 6 0 and 1 0, respectively These values are comparable with those reported for osmium poly-pyridyl complexes in solution [20] or within monolayers [21–23] It is perhaps important to note that the absolute values of these self-exchange rate constants depends on the accuracy of c_{eff} However, given the structural similarity of the present system and that investigated previously [11] where it was possible to estimate c_{eff}, experimentally uncertainty in c_{eff} will not change the order of magnitude of k_{SE}

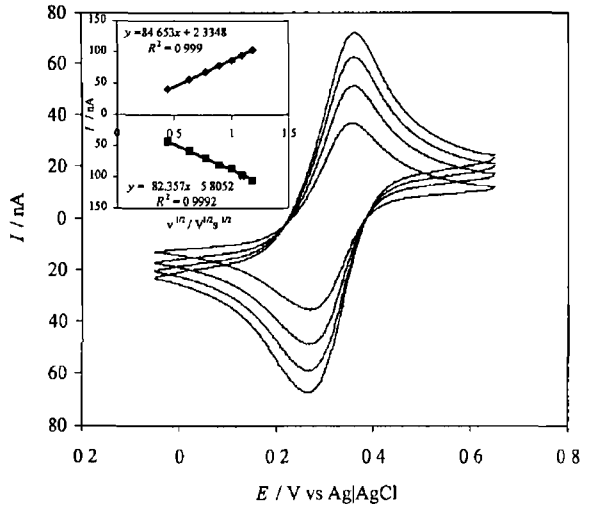

Fig 9 Scan rate dependence of the voltammetric response for a deposit of $[Os(bpy)_2$ 4bpt $Os(bpy)_2Cl_2](PF_6)_3$ formed on a 25 μm radius platinum microelectrode The supporting electrolyte is 0 1 M $LiClO_4$ containing 20% acetomtrile From top to bottom the scan rates are 800 600 400 and 200 mV s^{-1} Inset I_p vs v for these deposits

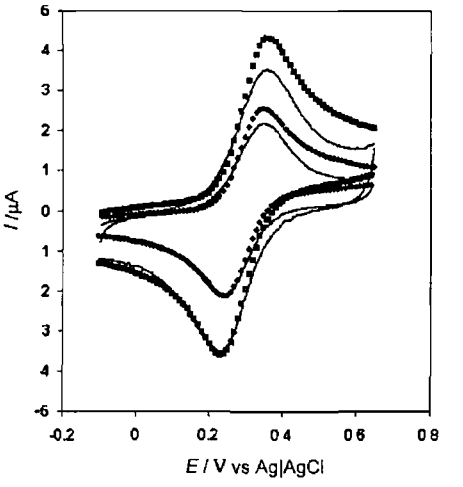

Fig 10 Cyclic voltammograms for a mechanically attached deposit of $[Os(bpy)_2$ 4bpt $Os(bpy)_2Cl_2](PF_6)_3$ formed on a 25 μm radius platinum microelectrode The scan rates are (from top to bottom) 571 and 200 V s^{-1} Theoretical voltammograms obtained generated according to the Butler–Volmer formalism of electrode kinetics are denoted by ■ and ★ at scan rates of 571 and 200 V s^{-1} respectively

Table 2
Effect of the identity and concentration of supporting electrolyte on the homogenous charge transport diffusion coefficient through solid state $[Os(bpy)_2$ Cl 4 bpt $Os(bpy)_2Cl](PF_6)_2$ deposits [a]

Concentration/M	10^{10} D_{CT}/cm^2 s^{-1} ($LiClO_4$)	10^{10} D_{CT}/cm^2 s^{-1} ($HClO_4$)
0 1	2 0 (0 6)	2 0 (0 5)
0 5	2 0 (0 4)	1 8 (0 3)
0 7	1 8 (0 6)	1 6 (0 3)
1 0	2 0 (0 1)	1 7 (0 4)
1 5	2 0 (0 4)	1 5 (0 1)
2 0	2 1 (0 3)	1 6 (0 3)

[a] Errors are in parentheses and represent the standard deviation on at least three independently formed deposits

3 7 *Heterogeneous electron transfer dynamics*

As discussed above the voltammograms shown in Figs 8 and 9 are controlled by electron self-exchange between adjacent osmium centres However, at higher scan rates the rate of heterogeneous electron transfer across the electrode | deposit interface influences the voltammetric response causing an increase in ΔE_p Fig 10 illustrates the voltammograms obtained for solid deposits of the dimer at scan rates of 200 and 571 V s^{-1} The resistance data illustrated in Fig 7 confirm that the ohmic drop expected under these conditions is less than 10 mV which is negligible compared to the ΔE_p observed Therefore, slow heterogeneous electron transfer is the dominant factor controlling the large peak to-peak separation observed at these high scan rates Fig 10 also illustrates theoretical fits to the experimental cyclic voltammograms generated according to the Butler–Volmer formalism of electrode kinetics [24] In fitting these voltammograms, the residual sum of squares between the experimental and theoretical oxidation currents were minimized and then the reduction branch of the voltammogram was predicted The satisfactory agreement observed between theory and experiment suggests that the voltammograms for the solid deposits can be described approximately by conventional solution phase models based on semi-infinite linear diffusion Moreover, the satisfactory fits suggest that the deposits are solvated and that the electrochemical double layer is established at the electrode | layer interface This conclusion is consistent with our observation that the formal potentials of solution phase and solid deposits are similar For $5 < v < 100$ V s^{-1}, the best fit simulated voltammogram is obtained where D_{CT} is $2\,0 \times 10^{-10}$ cm^2 s^{-1} and the standard heterogeneous electron transfer rate constant, $k°$, is $1\,08 \pm 0\,05 \times 10^{-3}$ cm s^{-1} The diffusion coefficient obtained by fitting the complete voltammogram is identical to that found using the Randle–Sevçik analysis to within 5% Significantly, the standard heterogeneous electron transfer rate constant is independent of the scan rate indicating that the layers are kinetically homogeneous The observation that the rate constants for all redox centres capable of undergoing heterogeneous electron transfer are experimentally indistinguishable suggests that the local microenvironments, electron transfer distances and reorganization energies are identical for individual redox centres An identical $k°$ value is obtained at both pH 1 0 and 6 0, indicating that protonating the bridging ligand does not affect the electron transfer rate

A challenging issue is to probe the effect of supramolecular order on the rate of heterogeneous electron transfer Previously, we reported on the heterogeneous electron transfer dynamics of spontaneously adsorbed monolayers of $[Os(bpy)_2Cl\ 4\text{-bpt}]^+$ [13] For these monolayers, apparent k° values of 1.6×10^5 and 4.4×10^4 s^{-1} were found for monolayer oxidation and reduction, corresponding to distance normalised heterogenous electron transfer rate constants of 1×10^{-2} and 4.4×10^{-3} cm s^{-1}, respectively Significantly these values are less than an order of magnitude larger than those found for the solid state layers described here This observation suggests that the 4-bpt bridge does not support strong electronic communication between the delocalised electronic states of an electrode and the localised redox orbitals of the $[Os(bpy)_2Cl]^+$ moiety

4 Conclusions

Solid deposits of $[Os(bpy)_2\ 4\text{-bpt}\ Os(bpy)_2Cl_2](PF_6)_2$ have been formed on platinum microelectrodes, bpy is 2,2′-bipyridyl and bpt is 3,5-bis(pyridin-4-yl)-1,2,4, triazole In both $LiClO_4$ and $HClO_4$ electrolytes the voltammetric response arising from the $Os^{2+/3+}$ redox couple is close to ideal and is reminiscent of that associated with an electrochemically reversible solution phase redox couple Significantly, while both metal centres can be oxidised within an experimentally accessible potential window when the dimer is dissolved in acetonitrile, only a single one electron transfer process is observed for the solid deposits Significantly, the dependence of the apparent diffusion coefficient on the concentration of the supporting electrolyte suggests that the rate of charge transport through the solid is controlled by electron hopping rather than charge compensating ion diffusion into the solid The rate constant of heterogeneous electron transfer across the electrode | deposit interface k°, is $1.08 \pm 0.05 \times 10^{-3}$ cm s^{-1} and is independent of the electrolyte pH This value is approximately one order of magnitude lower than that found for a similar monomeric complex in which the 4-bpt bridging ligand is attached directly to the electrode

References

[1] I Scholz L Nitschke G Henrion Electroanalysis 2 (1990) 85
[2] F Scholz B Lange Trends Res Anal Chem 11 (1992) 359
[3] C Yang G He R Wang Y Li J Electroanal Chem 471 (1999) 32
[4] M S Wrighton Science 231 (1986) 32
[5] C F D Chidsey R W Murray Science 231 (1986) 25
[6] L F Nazar G Goward M Leroux H Duncan T Kerr J Gaubicher Int J Inorg Mater 3 (2001) 191
[7] M J MacLachlan T Asefa G A Ozin Chem Eur J 6 (2000) 2507
[8] A Tredicucc C Gmachl F Capasso D L Sivco A L Hutchinson A Y Cho Nature 396 (1998) 350
[9] F Quaranta R Rella P Siciliano S Capone M Epifani L Vasanelli A Licciulli A Zocco Sensors Actuators B (1999) 350
[10] J Ni H Ju H Chen D Leech Anal Chim Acta 378 (1999) 151
[11] R J Forster T E Keyes Phys Chem Chem Phys 3 (2001) 1336
[12] L Keane C Hogan R J Forster Langmuir 18 (2002) 4826
[13] R J Forster J G Vos T E Keyes Analyst 123 (1998) 1905
[14] R J Forster L R Faulkner J Am Chem Soc 116 (1994) 5444
[15] K A Goldsby T J Meyer Inorg Chem 23 (1984) 3002
[16] H B Gray J R Winkler Ann Rev Biochem 65 (1996) 537
[17] A J Bard L R Faulkner Electrochemical Methods Fundamentals and Applications Wiley New York 1980
[18] R M Wightman D O Wipf in A J Bard (Ed) Electroanalytical Chemistry vol 15 Marcel Dekker New York 1989
[19] E Juris V Balzani F Barigelletti S Campagna P Belser A von Zelewsky Coord Chem Rev 82 (1988) 85
[20] M S Chan A C Wahl J Phys Chem 82 (1978) 2542
[21] D H Charych M Majda Thin Solid Films 210 (1992) 348
[22] D H Charych D J Anvar M Madja Thin Solid Films 242 (1994) 1
[23] W Y Lee M Majda G Brezesinski M Wittek D Mobius J Phys Chem Sect B 103 (1999) 6950
[24] F Garay V Solis M J Lovire Electroanal Chem 478 (1999) 17